Financial Modeling of Climate-related Risks

Théo Le Guenedal

INSTITUT POLYTECHNIQUE DE PARIS

NNT : 2022IPPAG009

Thèse de doctorat

ENSAE

IP PARIS

Financial Modeling of Climate-related Risks

Thèse de doctorat de l'Institut Polytechnique de Paris
préparée à École nationale de la statistique et de l'administration économique

École doctorale n°574 École doctorale de mathématiques Hadamard (EDMH)
Spécialité de doctorat : Mathématiques appliquées

Thèse présentée et soutenue à Paris, le 13/12/2022, par

THÉO LE GUENEDAL

Composition du Jury :

Christian Y. Robert Professeur de Statistique et sciences actuarielles à l'ENSAE (CREST)	Président
Antoine Mandel Professeur (section 26), Université Paris 1 Panthéon-Sorbonne	Rapporteur
Rüdiger Kiesel Professeur, University Duisburg-Essen, House of Energy Markets and Finance	Rapporteur
Ying Jiao Professeur, Claude Bernard University Lyon 1	Examinateur
Peter Tankov Professeur de finance quantititative à l'ENSAE (CREST)	Directeur de thèse
Thierry Roncalli Head of Quantitative Research at Amundi Asset Management, Professeur adjoint d'Economie à Evry-Paris-Saclay Université	Co-encadrant de thèse

Notice

The views expressed are the author's alone and do not necessarily correspond to those of Amundi Asset Management or Ecole doctorale de mathématique d'Hadamard.

Résumé

Ce projet de recherche est consacré à l'estimation des risques financiers liés au changement climatique. Au-delà des applications et des résultats quantitatifs, les chapitres de cette thèse ont pour principal objectif d'apporter des méthodologies générales utilisables par les praticiens. Le premier chapitre propose une méthode d'évaluation bottom-up du risque de transition adjointe aux modèles de risque classiques. Cette approche du risque opérationnel "*par les coûts*" engendrés par une taxe potentielle limite l'impact aux secteurs directement polluants, ce qui amène au deuxième chapitre, introduisant les tables d'entrée-sorties pour appréhender les effets indirects du risque de transition dans la chaîne d'approvisionnement. Ces approches offrent une structure statique permettant d'évaluer le risque dans un scénario donné, mais pas de déterminer le prix des obligations en considérant des scénarios hétérogènes et leur probabilité de réalisation. Pour ce faire, le troisième chapitre propose un modèle de pricing intégrant une approche bayésienne dans la mise à jours des probabilités de scénarios sur la base des sauts observés dans les mécanismes de tarification du carbone. Enfin, le dernier chapitre propose une méthodologie Monte-Carlo de simulation de dommages annuels causées par des cyclones tropicaux. La conversion des données climatiques brutes en base de données synthétique de sinistres est réalisée en couplant des relations statistiques et thermodynamiques. L'exposition des actifs physiques, les dynamiques des facteurs socio-économiques, les densités de populations locales et les vulnérabilités spécifiques aux différentes régions du monde sont empruntés à différents segments de la littérature. Ils sont combinés afin d'obtenir un modèle complet du triptyque classique nécessaire à l'étude des risques physiques : *intensité* x *exposition* x *vulnérabilité* généralisable et homogène sur l'ensemble des pays. Le signal résultant peut ensuite être inclus simplement dans des modèles de risque de crédit assimilant les dommages annualisés à de la dette additionnelle.

Abstract

This research project aims at estimating financial risks related to climate change. Beyond the applications and quantitative findings, the main objective of the chapters of this thesis is to provide a structural and methodological framework that is generalizable, in order to facilitate their integration by practitioners. The first chapter proposes a bottom-up measure of transition risk, which can be incorporated with classical risk models (Merton or credit risk model). This "*cost-based*" approach is limited to the directly polluting sectors, which leads to the second chapter, which allows for the diffusion of transition risk through the value chain. These approaches offer a static structure that allows for a fixed scenario stress-test but not for pricing the bonds by considering heterogeneous scenarios and the probability of realization. To this end, chapter three proposes a pricing model that integrates a Bayesian approach in updating scenario probabilities based on observed jumps in carbon pricing mechanisms. Finally, the last chapter proposes a Monte-Carlo methodology for simulating annual damages caused by tropical cyclones. The conversion of raw climatic data into a synthetic database of losses is achieved by coupling statistical and thermodynamic relationships. The exposure of physical assets, the dynamics of socio-economic factors, local population densities and specific vulnerabilities in different regions of the world are borrowed from different segments of the literature, and combined to obtain a complete model of the classical triptych necessary for the study of physical hazards : hazard intensity x exposure x vulnerability generalizable and homogeneous across countries. The resulting signal can then be simply included in credit risk models equating annualized damages with additional debt.

Table des matières

Chapitre 1

Introduction Générale

Cette thèse s'inscrit dans le cadre d'un projet de recherche portant sur l'intégration de critères extra-financiers et climatiques dans les stratégies d'allocation d'actifs. Elle est le résultat d'un partenariat de trois ans entre Amundi Asset Management et le Center for Research in Economics and Statistics (CREST) et a été élaborée à l'École Nationale de la Statistique et de l'Administration Economomique (ENSAE). Le projet de recherche, initié avec les travaux de Bennani *et al.* (2018), mesurant l'intégration des signaux Environnementaux, Sociaux et de Gouvernance (ESG) dans les marchés actions mondiaux, comprenait trois principaux axes : (i) étendre l'étude de l'effet des scores ESG au milieu obligataire ; (ii) développer des méthodologies quantitatives de mesure des risques liés au changement climatique et (iii) développer des outils d'alignement (stratégies de réduction des émissions de carbone) pour l'allocation de portefeuille. Tandis que le premier et le troisième thème ont donné lieu à plusieurs travaux opérationnels publiés par l'équipe de recherche quantitative d'Amundi (Ben Slimane *et al.*, 2019a ; Ben Slimane *et al.*, 2019b ; Drei *et al.*, 2019 ; Le Guenedal *et al.*, 2020 ; Le Guenedal, Lombard *et al.*, 2022 ; Le Guenedal & Roncalli, 2022 ; Lepetit, Le Guenedal *et al.*, 2021 ; Taleb *et al.*, 2020), cette thèse se concentre sur le deuxième aspect, c'est-à-dire sur le développement de méthodologies permettant de mieux quantifier le risque financier lié au climat. Ce risque se divise en deux catégories : le risque de transition, découlant d'un changement soudain de paradigme économique au profit d'un fonctionnement bas carbone, et le risque physique découlant de l'accroissement de la fréquence et de l'ampleur des événements climatiques et météorologiques entraînant la destruction du capital physique et le dysfonctionnement des infrastructures.

Le risque de transition est au centre de l'attention des acteurs de marchés car il est perçu comme plus susceptible d'impacter les portefeuilles d'investissement à moyen terme, en particulier dans la perspective du renforcement des politiques de transition (Fankhauser *et al.*, 2022). Toutefois, la matérialité de ces risques est restreinte par la faible probabilité que des réglementations aux retombées économiques néfastes à court et moyen terme soient implémentées (et maintenues) par les gouvernements (Alessi *et al.*, 2021 ; Campiglio *et al.*, 2022 ; Y.-X. Zhang *et al.*, 2017).

La littérature sur les risques physiques en finance est nettement moins mature et se limite principalement au marché de l'immobilier et de l'assurance. Bien qu'il existe de nombreux articles relatifs à l'évaluation des risques physiques locaux, le processus de définition du triptyque classique de '*intensité*' × '*exposition*' × '*vulnérabilité*', n'est pas généralisable à l'échelle mondiale, et donc aux portefeuilles d'investissements mondiaux. Depuis le discours historique '*Tragedy of the Hori-*

zons' de Mark Carney (2015), l'intérêt de la communauté financière pour le risque physique s'est sensiblement accru. Cependant, le fossé sémantique entre les mondes de la science du climat et de la finance (Bouchet *et al.*, 2022), rendant le dialogue et les interactions complexes entre deux communautés hautement spécialisées, reste un obstacle à une meilleure compréhension des répercussions financières des risques physiques. En conséquence, bien que toutes les études prévoient une augmentation des dommages futurs attendus, l'intégration des risques physiques dans les modèles d'évaluation des actifs reste faible. La multiplicité des aléas engendrant de potentiels dommages physiques complexifie leur agrégation et donc leur intégration dans les décisions d'allocation de portefeuille. Cependant, les progrès considérables en matière de modèles climatiques de circulation générale (en anglais, *general circulation models*, GCMs), et dans la modélisation la fine des dommages physiques nous poussent à remettre en question et à ajuster la quantification des conséquences économiques du changement climatique (Auffhammer, 2018), ainsi qu'à proposer de nouvelles méthodes prospectives pour prendre en compte les risques physiques dans l'évaluation des titres du marché.

Cette thèse est structurée comme suit. Les chapitres 2 à 4 se concentrent sur la transition. Le chapitre 2 explore la sensibilité du risque de crédit au prix du carbone. Le chapitre 3 présente une méthode structurelle et explicite permettant d'inclure les effets en cascade du prix du carbone dans la chaîne de valeur. Le chapitre 4 introduit un nouveau cadre d'évaluation des obligations d'entreprise permettant de prendre en compte l'incertitude des scénarios. Le chapitre 5 propose une approche structurelle globale afin de convertir les données de projection climatique des modèles de circulation générale en signaux matériels permettant l'intégration des risques physiques liés aux cyclones dans la modélisation des coûts de la dette souveraine. Dans cette introduction générale, nous fournissons une revue (non exhaustive) de la littérature sur les risques de transition et physique ainsi qu'une section résumant les principales contributions académiques de chacun des chapitres mentionnés.

1.1 Risque de transition

Les risques liés à la transition sont des risques commerciaux et opérationnels inhérents au basculement vers une économie plus verte. Ils ne sont pas directement causés par le changement climatique à proprement parler mais consécutifs aux politiques de régulation visant à limiter le réchauffement climatique. Par exemple, une entreprise industrielle s'appuyant sur un processus à forte intensité de carbone, court le risque de ne plus être rentable si la réglementation liée aux émissions de gaz à effet de serre se renforce. Ces risques peuvent également se manifester suite à un changement de la demande des consommateurs. Un constructeur automobile peut subir des pertes si son offre ne répond plus aux exigences environnementales de ses clients. L'évaluation des risques de transition repose sur l'analyse de scénarios. La première étape consiste donc à comprendre la construction de ces scénarios qui reposent sur des modèles d'évaluation intégrée (en anglais, *integrated assessment models*, IAM). Ces modèles permettent (aux universitaires ainsi qu'aux décideurs politiques, entre autres) de définir la, ou plutôt une trajectoire possible pour la principale variable de contrôle : le prix du carbone. Plusieurs études examinent les canaux de transmission du risque de transition à l'activité des entreprises et recherchent des preuves de son intégration dans les marchés des actions (Bolton & Kacperczyk, 2021 ; Görgen *et al.*, 2019),

des obligations d'entreprise (Duan *et al.*, 2021) ou des options (Ilhan *et al.*, 2019, 2021). En dehors des approches de marché, l'exposition au risque de transition est mesurée à l'aide de deux méthodologies complémentaires : les méthodologies *topdown* utilisant des modèles d'évaluation intégrée (Vermeulen *et al.*, 2018a ; Vermeulen *et al.*, 2019), et les approches *bottom-up* définissant le risque au niveau de l'entreprise (Monnin, 2018). En outre, l'impact systémique des risques liés au climat, importants et croissants tant pour l'économie réelle que pour le système financier, suscite de vives inquiétudes par ses effets amplificateurs. En effet, si l'impact direct du risque de transition sur les secteurs directement liés au climat (en anglais, *climate-relevant*), peut sembler limité (par exemple, 2 Investing Initiative, 2018 ; Aubert *et al.*, 2019 ; EIOPA, 2018 ; Schotten *et al.*, 2016 ; Vermeulen *et al.*, 2018a ; Vermeulen *et al.*, 2019 ; Weyzig *et al.*, 2014 suggérant une exposition moyenne d'environ 10% ; voir Bouchet et Le Guenedal, 2020a, Figure 2), les éventuels effets en cascade sur la chaîne d'approvisionnement (Cahen-Fourot *et al.*, 2019 ; Mardones & Mena, 2020) ainsi que la contagion des pertes financières – qui ont également mené à de nombreuses recherches (Battiston *et al.*, 2017 ; Roncoroni *et al.*, 2021) conduisant à de multiples méthodologies de stress-test – peuvent sensiblement augmenter les risques. Par ailleurs, plusieurs contributions mathématiques théorique ont permis de mieux comprendre les mécanismes de marché, expliquant la prise en compte des signaux de '*durabilité*' (Pástor *et al.*, 2021 ; Pedersen *et al.*, 2021), et depuis peu, des sauts incertains liés aux réglementations de réduction des émissions de GES dans la fixation du prix des titres de marché (Agliardi & Agliardi, 2021), permettant une intégration dynamique du risque de transition.

1.1.1 Conception de scénarios, politiques et risques effectifs

Modèles d'évaluation intégrée La plupart des méthodologies relatives aux risques de transition sont basées sur l'analyse de scénarios. Ces scénarios sont dérivés d'une modélisation économique déterministe du risque climatique réalisée par des modèles d'évaluation intégrée (IAM), qui introduisent ces considérations climatiques dans la modélisation macroéconomique classique. Le premier '*point de contact*' a été réalisé par William Nordhaus avec le modèle d'économie climatique intégrée dynamique (DICE) (W. D. Nordhaus *et al.*, 1992) et la littérature autour de ces modèles n'a cessé de croître depuis (Hourcade *et al.*, 2021). Les modèles intégrés les plus couramment utilisés par les praticiens et les institutions publiques se répartissent en deux grandes catégories : les modèles d'optimisation coûts-bénéfices et les modèles d'évaluation technico-économique. Les modèles d'optimisation coûts-bénéfices, tels que le modèle DICE, permettent essentiellement aux décideurs de tracer une trajectoire pour le coût social du carbone en maximisant la richesse ou bien-être social (en anglais *welfare*) dans le temps et en équilibrant les coûts des dommages (futurs) et ceux de l'atténuation (actuelle). Le taux optimal de réduction des émissions de GES est directement traduit en termes de coût social du carbone. Bien qu'ils soient encore populaires et largement utilisés dans les domaines de l'élaboration des politiques et de l'énergie, les modèles coûts-bénéfices reposent sur des hypothèses fonctionnelles et paramétriques fortes et ont des applications empiriques relativement faibles (Kohler *et al.*, 2006), notamment dans le domaine de la finance, nécessitant une granularité sectorielle et géographique plus fine. En revanche, la deuxième catégorie de modèles offre généralement un haut niveau de granularité dans leur représentation des secteurs, des pays et de leurs interactions et permet de déterminer le chemin optimal (ou le moins coûteux) pour atteindre un scénario de concentration donné sans calculer les dommages futurs.

Parmi ces modèles, on trouve par exemple le modèle EPPA (Babiker *et al.*, 2001 ; Y.-H. H. Chen *et al.*, 2022 ; Y.-H. Chen *et al.*, 2015) du MIT Joint Program ou le modèle IMACLIM-R (Hourcade *et al.*, 2010) développé par le Centre International de Recherche sur l'Environnement et le Développement (CIRED). Quel que soit leur type, les modèles peuvent être classés en fonction de trois caractéristiques principales : leur niveau de précision technologique, le niveau de complexité des rétroactions macroéconomiques, et le degré de réalisme de l'agent et des marchés. Par exemple, des modèles tels que REMIND/MERGE/IMAGE/MESSAGE/CGAM ont un niveau de précision technologique plus élevé avec une représentation plus simple de l'économie mondiale par rapport à EPPA, IMACLIM ou E3ME (Cambridge Econometrics, 2019) offrant une meilleure granularité sectorielle et des rétroactions macroéconomiques multisectorielles. Enfin, les approches *Stock-Flow Consistent* (SFC) (par exemple GEMMES, Giraud *et al.*, 2016) visent à mieux rendre compte du comportement des marchés en tenant compte des déséquilibres. Le meilleur modèle n'obtient pas nécessairement le meilleur score à chaque caractéristique, mais présente la meilleure configuration pour répondre à la question pour laquelle il a été conçu. Dans un rapport de l' Institut Louis Bachelier, Hourcade *et al.* (2021) décrit plus en détail les prérequis essentiels pour une bonne compréhension et donc l'utilisation de ces modèles intégrés.

Ces modèles offrent des représentations différentes et complémentaires de l'économie dans plusieurs scénarios avec des niveaux d'ambition variables en matière de transition. Un agent est soumis au risque de transition si les conditions suggérées par ces modèles (dans un scénario où la concentration de GES a été limitée avec succès) ne sont pas compatibles avec la rentabilité de son activité. Bien que ces modèles fournissent plusieurs variables de sortie à partir desquelles la probabilité conditionnelle de défaut pourrait être déduite, la représentation des secteurs autres que l'énergie (et dans une certaine mesure l'agriculture) est relativement limitée (Hourcade *et al.*, 2021). Par conséquent, en pratique, la plupart des études évaluant le risque de transition (sur l'économie réelle et les portefeuilles diversifiés) se concentrent encore exclusivement sur les chocs du prix du carbone. En effet, du point de vue de la gestion du risque financier, et en supposant que les prix du carbone produits par les IAM ne sont pas nécessairement explicites et peuvent intégrer d'autres mécanismes de transition, cette variable constitue une approximation correcte du risque réglementaire encouru par une entreprise. De plus, on peut souligner que les sauts erratiques et inattendus des prix du carbone sont plus susceptibles d'avoir un impact sur la valorisation des entreprises à forte intensité de carbone que d'autres mesures plus graduelles. En conséquence, les chapitres 2 à 4 considèrent cette variable comme la principale '*source*' et donc mesure du risque. Néanmoins, nous reconnaissons qu'il s'agit là d'une limite et qu'une meilleure compréhension du risque de transition nécessiterait l'utilisation de variables autres que le prix du carbone (Campiglio, 2016).

1.1.2 Canaux de transmission du risque de transition

Plusieurs études décrivent les canaux théoriques par lesquels le risque de transition peut avoir un impact sur le risque financier (Colas *et al.*, 2018 ; Monnin, 2018 ; TCFD, 2017 ; Thom & Ralite, 2019). Bien que le risque de transition puisse affecter les performances économiques et financières d'une entreprise à différents niveaux, il est généralement assimilable à un risque commercial ou opérationnel, qui sont d'ores et déjà gérés et intégrés aux modèles de risques bancaires. Par conséquent, il suffit de définir la sensibilité d'un (ou de plusieurs) indicateur(s) comptable(s)

de la performance économique et financière d'une entreprise au risque de transition (e.g. prix du carbone). Dès lors, la transmission de cette sensibilité aux risques de crédit, de liquidité ou de marché (Basel Committee on Banking Supervision, 2021, 2022) peuvent ensuite être quantifiés à l'aide de modèles financiers déjà existants.

Le changement de paradigme provoqué par la transition écologique se mesure dans la majorité des cas sur les flux de trésorerie futurs des entreprises. Celles-ci peuvent être affectées par une réduction des revenus (en raison d'une diminution de la demande de produits et services à forte intensité de carbone), ou au contraire, d'une demande accrue de produits et services compatibles ou indispensable à la transition. Les politiques de transition peuvent également affecter les charges d'exploitation : les coûts d'émission directs (prix du carbone) et les coûts d'émission indirects supplémentaires de la chaîne d'approvisionnement, représenteront des coûts supplémentaires pour les entreprises. On remarque par ailleurs que, d'un point de vue comptable, un exercice de stress-test utilisant un *prix effectif du carbone* permet d'impacter exclusivement les charges d'exploitation, tandis que la prise en compte d'un *coût social du carbone*[1], inclurait en théorie l'évolution de la demande des consommateurs et donc la transmission aux revenus de l'entreprise. D'autre part, l'adaptation des unités de production à un fonctionnement plus écologique, les dépenses de recherche et développement de nouvelles technologies doivent également être prises en compte pour évaluer l'exposition des entreprises aux risques de transition, par le biais de leurs dépenses d'investissement. En général, les coûts liés au climat se matérialisent par une taxe sur le carbone, une réduction de la demande ou d'investissements de l'entreprise, le cadre de modélisation du risque et de l'impact de la transition sera relativement similaire.

Les risques de transition peuvent également impacter le bilan comptable des entreprises. Tout d'abord, par le biais de la dépréciation des actifs circulant mais aussi immobilisés, principalement corporels. En effet, celles-ci peuvent subir des pertes dues à la dévaluation de leurs réserves (par exemple de combustibles fossiles) ou à l'obsolescence de leur capital de production (installations techniques) en raison d'une perte de compétitivité engendré, par le coût croissant du carbone. La littérature relative aux actifs concernés, dit '*échoués*' (en anglais, '*stranded assets*'), se concentre naturellement sur les sous-secteurs principalement concernés de l'énergie (e.g. charbon, les mines et les combustibles fossiles avec par exemple Caldecott, 2017 ; Caldecott, Harnett *et al.*, 2016 ; Caldecott *et al.*, 2013 ; Caldecott, Kruitwagen *et al.*, 2016). Le risque de transition peut également amplifier le risque de marché (i.e. dévalorisation des valeurs mobilières des titres émis par l'entreprise) et limiter la capacité de refinancement des plus polluantes par l'augmentation des coûts du capital. La mesure de la réaction des marchés boursiers au risque de transition a été largement abordée (Andersson *et al.*, 2016 ; Bolton & Kacperczyk, 2021 ; Engle *et al.*, 2020 ; Faccini *et al.*, 2021 ; Görgen *et al.*, 2019 ; Gurvich & Creamer, 2021 ; Harris, 2015 ; In *et al.*, 2018 ; Roncalli *et al.*, 2020 ; Roncalli *et al.*, 2021) ainsi que l'intégration de l'ESG et environnement dans la valorisation des obligations et coût de la dette (Apergis *et al.*, 2022 ; Baker *et al.*, 2018 ; Ben Slimane *et al.*, 2020 ; Duan *et al.*, 2021 ; Eliwa *et al.*, 2021 ; Hoepner *et al.*, 2018 ; Raimo *et al.*, 2021 ; Zerbib, 2019 ; R. L. Zhang, 2021). En réalité, tous les canaux de transmission énoncés ici sont imbriqués, notamment parce que sous l'hypothèse classique de l'efficience même partielle des marchés, la valorisation des valeurs mobilières reflète la perception des investisseurs des flux de trésorerie ou des

1. Défini dans les approches coûts-bénéfices comme la dérivé partielle de la consommation sur les émissions, voir Le Guenedal (2019a) pour une revue de la modélisation des risques climatique dans les modèles économiques classiques.

bilans futurs. Les acteurs de marché et les banques commencent d'ailleurs à prendre en compte ces risques. Par exemple, Delis *et al.* (2019) a montré que les banques tiennent compte du risque d'échouement dans le coût des prêts accordés aux entreprises du secteur énergie. L'imbrication des canaux peut également engendrer des effets rebonds, par exemple, Bolton et Kacperczyk (2021) suggèrent donc que les entreprises intensives offrent des rendements boursiers supérieurs afin de compenser le risque lié à leur émission de carbone. D'autre part, cet effet peut-être compensé, par des mécanismes de flux, avec par exemple une plus forte demande des investisseurs pour des titres émanant d'entité socialement responsables ayant un effet positive sur leur rendement. Cela complexifie l'analyse de causalité à partir des prix observés sur les marchés.

1.1.3 Les approches méthodologiques de quantification des risques de transition

Les mesures de marché En gestion d'actifs, une méthode traditionnelle de gestion du risque repose sur des modèles classiques d'évaluation de '*l'exposition*' des actifs financiers (Capital Asset Pricing Model, CAPM ; Sharpe, 1964), décomposant la performance des actifs entre l'*alpha*, propre à chaque actif, et le *beta*, rendant compte de sa sensibilité aux variations du marché et qui relève donc du risque dit '*systématique*'. L'approche fondamentale du CAPM a été étendue par plusieurs contributions introduisant de nouveaux facteurs de risque pour mesurer les primes de risque systématiques. Fama et French (1993) ont d'abord inclus des facteurs de risque de taille (SMB) et de valeur (HML), Carhart (1997) a ajouté le momentum (WML), Baker *et al.* (2011) la faible volatilité (VOL) et enfin Novy-Marx (2013) le facteur de risque de *qualité* (QMJ), reposant, entre autres (Lepetit, Cherief *et al.*, 2021), sur la rentabilité brute de l'entreprise. L' ensemble de ces facteurs constitue la configuration traditionnelle des stratégies factorielles d'investissement en actions (à 5 facteurs). Ces facteurs de risque de marché '*communs*' sont construits en classant les entreprises au sein d'un univers d'investissement suivant une caractéristique, respectivement la capitalisation boursière (SMB), le prix de l'action (HML), la performance récente (WML), la volatilité (VOL) et la rentabilité brute (QML), et en comparant les rendements des groupes les mieux classés par rapport aux groupes les moins bien classés. La différence de rendement définit les primes de risque associées à la caractéristique du sous-jacent. Par exemple, nous comparons les rendements portefeuille représentatif des grandes et des petites entreprises pour construire le facteur de risque SMB (small-minus-big). Cette méthode peut être appliquée au risque ESG (Bennani *et al.*, 2018 ; Drei *et al.*, 2019) et au risque de transition en utilisant les émissions de carbone (ou l'intensité) pour construire un facteur brun-moins-vert (Brown-minus-green, BMG, Görgen *et al.*, 2019 ; Roncalli *et al.*, 2021). L'avantage de cette approche est sa couverture, puisqu'elle permet de calculer l'exposition de n'importe quel titre coté (sans même connaître les émissions carbones de l'entreprise sous-jascente). Toutefois, elle repose sur l'hypothèse que la caractéristique utilisée, à l'origine la taille, la performance récente ou la volatilité, correspond à une stratégie d'investissement '*systématique*', ce qui n'est peut-être pas (encore) le cas pour les émissions de carbone. Du côté de l'investissement dit *passif*, il est également courant d'effectuer une optimisation en forçant un score total (ESG, émissions ou intensité carbone) à être supérieur ou inférieur à un certain seuil (Le Guenedal & Roncalli, 2022), tout en se rapprochant au maximum de la composition d'un indice de référence. Ainsi, il est possible de calculer la différence de performance obtenue par le portefeuille optimisé ou de construire des indices '*bas carbone*'. Ces approches empiriques du

marché sont largement utilisées pour contrôler l'intégration du risque de transition dans le prix des actifs. Cependant, elles sont rétrospectives et peuvent donc ne pas refléter pleinement l'étendue du risque de transition prospectif.

Choc d'évaluation direct Ce type d'approche considère une part fixe de pertes pour déterminer le montant global de l'exposition de différentes parties prenantes. Par exemple, Weyzig *et al.* (2014) considèrent un choc de 60% sur les stocks de combustibles fossiles et un choc de 30% sur la valeur des obligations de ce secteur, ce qui entraîne des pertes estimées entre 350 et 400 milliards d'euros pour l'ensemble des institutions financières européennes.

Les approches *top-down* Ces approches utilisent des variables macroéconomiques issues de modèles intégrés (IAM) pour estimer les pertes potentielles au niveau des portefeuilles. Par exemple, Vermeulen *et al.* (2018a), Vermeulen *et al.* (2019) étudient avec le modèle NiGEM l'impact d'un prix du carbone de 100 USD sur la valeur ajoutée sectorielle et les indices financiers [2]. En combinant un choc politique - reflété dans l'évolution du prix du carbone - et un choc technologique - qui modifie la fonction de production -, les pertes moyennes pour l'ensemble des institutions financières néerlandaises sont estimées entre 2,5 % et 11 % de la valeur initiale des actifs au cours des cinq prochaines années. Cette approche permet donc de définir le risque au niveau des régions et secteurs mais ne tient pas compte des facteurs idiosyncratiques des entreprises.

Les approches *bottom-up* Elles évaluent le risque de transition au niveau de l'émetteur. Par exemple, Howard et Patrascu (2017) étudient l'impact d'une hausse du prix mondial du carbone à 100 USD par CO_2e augmentant les coûts pour les entreprises proportionnellement à leurs émissions totales induites et évaluent une baisse de 14% de l'EBITDA agrégé de l'indice MSCI World. D'autres travaux, voir par exemple UNEP (2018) et Monnin (2018), s'appuient sur une méthodologie développée par le cabinet Carbon Delta qui inclut des avis d'experts. Pour la gestion d'actifs, les approches bottom-up sont plus adaptées à la construction de signaux utiles à la décision d'investissement. Par conséquent, nous avons cherché à répondre à la question suivante :

Question 1 ***Comment fournir une mesure structurelle de la sensibilité du risque de crédit idiosyncratique des entreprises en fonction du risque de transition évalué à partir des trajectoires de prix du carbone suggérées par les modèles intégrés (et sans recourir à des avis d'experts) ?***

1.1.4 Exposition directe et effets en cascade à travers la chaîne logistique

Le risque de transition découle d'un changement de paradigme sociétal majeur et ses répercussions sont systémiques. Si la première génération d'études se sont concentrées sur les actifs directement exposés, les universitaires et régulateurs s'intéressent désormais de plus en plus aux potentiels effets en cascade et aux conséquences sur l'ensemble de l'économie réelle et du système financier.

2. L'impact final sur les portefeuilles est ensuite évalué par des experts en fonction de leur sensibilité aux indices financiers.

Exposition directe Weyzig *et al.* (2014) analysent l'exposition des institutions financières de l'UE aux entreprises de combustibles fossiles et aux matières premières. À l'époque, les expositions (en pourcentage du total des actifs) se situaient entre 1,3 % pour les banques et 5 % pour les fonds de pension. Giuzio *et al.* (2019) actualisent ces résultats en étendant le champ d'application aux secteurs pertinents pour le climat, tels que définis par Battiston *et al.* (2017). Entre 2014 et 2019, les fonds de pension ont réduit leur exposition au risque de transition, tandis que les banques et les assureurs l'ont maintenue constante. L'EIOPA (2018) mesure également l'exposition au risque de transition des assureurs. Les secteurs liés au climat représentent 13% des portefeuilles d'investissement des assurances.

Un exercice régulièrement conduit consiste à mesurer l'exposition du système financier au risque de transition au niveau national. En France, l'exposition des banques aux secteurs intensifs en GES à été estimée à 12,7% en 2015 et a légèrement diminué en 2017 (Aubert *et al.*, 2019). Le secteur des combustibles fossiles représentait alors environ 20% des expositions aux risques majeurs en 2013 et 16,5% en 2018, ce qui suggère que ce risque est effectivement pris en considération par les banques. Bank of England (2015, 2017) et Batten *et al.* (2016) considèrent deux types d'actifs liés au climat : les titres d'entreprises susceptibles d'être directement impactées par des limites réglementaires de production ou d'utilisation de combustibles fossiles (10% des actifs) et les titres de secteurs à forte intensité de GES (20% des actifs). Aux Pays-Bas, Schotten *et al.* (2016) estiment que l'exposition des banques, des fonds de pension et des assureurs aux entreprises de combustibles fossiles se situe entre 2% (banques) et 5% (fonds de pension). Ils procèdent également à un examen de l'exposition de ces institutions aux secteurs à forte intensité de carbone, qui se situe entre 12,4% et 4,4%. Alors que la plupart des études se concentrent sur le système financier européen, 2 Investing Initiative (2018) mènent une analyse sur les portefeuilles des assureurs californiens (et souligne une exposition de 4 000 milliards de USD).

Récemment, Alessi et Battiston (2022) ont étudié l'exposition des institutions financières au risque de transition et l'ont mesuré, respectivement, à 12% pour les fonds d'investissement, 5% pour les banques et 15,1% pour les assureurs. D'autre part, ils ont également introduit un score de '*greenness*' (mesuré par la taxonomie de l'UE) et ont relevé des expositions beaucoup plus faibles, respectivement 3,2%, 0,8% et 4,8%. Bien que la région, les institutions, la classe d'actifs (actions, obligations, prêts, matières premières) et la définition des secteurs pertinents pour le climat diffèrent, la plupart des études convergent vers le même résultat : l'exposition directe moyenne des institutions financières aux secteurs pertinents pour le climat se situe entre 5 et 15%.

Effet en cascade Les risques de transition et physiques peuvent se propager en cascade à travers les pays et les secteurs et se répandre parmi les parties non affectées de l'économie (Naqvi & Monasterolo, 2021 ; Raymond *et al.*, 2020). Le premier '*stress-test*' climatique incluant un effet de cascade au sein du secteur financier a été proposé par Battiston *et al.* (2017) et récemment étendu par Roncoroni *et al.* (2021) en se concentrant sur les banques et les fonds d'investissement. Les auteurs se concentrent sur l'interconnexion interbancaire du système financier sans véritablement intégrer les interdépendances liées à la chaîne d'approvisionnement physique (par exemple, les matières premières, les produits chimiques, le carburant, etc.). Dans l'ensemble, plusieurs méthodologies de stress-tests financiers et bancaires ont été proposés (Allen *et al.*, 2020 ; Alogoskoufis *et al.*, 2021 ; Dunz *et al.*, 2021 ; Gourdel et Sydow, 2021 ; Grippa, Mann *et al.*, 2020 ;

Nguyen *et al.*, 2020 ; Reinders *et al.*, 2020a, etc.), examinés en détail dans Cartellier (2022). Plusieurs canaux de transmission sont étudiés pour les risques de transition et les risques physiques, incluant des effets de *second-tour* (en anglais, '*second round*') sur le plan financier, mais, avec une faible prise en compte des interdépendances avec l'économie réelle.

Économie réelle et table d'entrées-sorties Cahen-Fourot *et al.* (2019) utilisent un modèle d'entrées-sorties (IO) pour évaluer l'exposition des systèmes économiques aux effets d'obsolescence en cascade du capital, déclenchées par la réduction de la production et de l'utilisation des combustibles fossiles. Ils mesurent la propagation du choc à travers les secteurs et les pays via les demandes intermédiaires sectorielles et donc via les réseaux de production. D'autre part, Gemechu *et al.* (2014) et Muñoz-Zamponi et Mardones-Poblete (2016) ainsi que Mardones et Mena (2020) développent une méthode d'estimation des effets de cascade basée sur l'approche classique de Leontief (1970), permettant de mesurer les effets de la diffusion des coûts de la taxe carbone dans différents secteurs de l'économie. Par exemple, Mardones et Mena (2020) estiment l'impact des taxes environnementales sur les émissions de carbone et les polluants atmosphériques locaux introduites au Chili et utilisent l'extension environnementale du modèle de prix de Leontief (1970) et des micro-simulations pour analyser les principaux effets économiques, environnementaux et distributifs de cette politique. Cependant, ces exercices n'utilisent que des informations au niveau sectoriel, alors que l'application au stress-test des portefeuilles nécessite des informations au niveau des entreprises. La prise en compte du risque de la chaîne d'approvisionnement est encore limitée dans la littérature et les praticiens utilisent principalement les scopes d'émission 2 et 3 (dont les normes de calcul sont encore parfois incertaines) pour estimer ce risque. Sur la base de cette littérature déjà avancée, nous cherchons à répondre à la question suivante :

Question 2 ***Comment calculer les contributions au risque de transition entre les secteurs, en prenant mieux en compte les effets en cascade à travers la chaîne d'approvisionnement, mais aussi les émissions directes de carbone au niveau de l'entreprise ?***

1.1.5 Incertitude du scénario

Le climat futur, les politiques économiques menées pour faire face au changement climatique (Alessi *et al.*, 2021 ; Barradale, 2014 ; Campiglio *et al.*, 2022 ; Helm *et al.*, 2003 ; Nemet *et al.*, 2014 ; Y.-X. Zhang *et al.*, 2017), et les risques financiers potentiels, sont soumis à de profondes incertitudes (Bolton *et al.*, 2020 ; Chenet *et al.*, 2019 ; Monasterolo *et al.*, 2019 ; W. Nordhaus, 2018b). Sur les plans technologique et socioéconomique, on peut évoquer les incertitudes concernant la disponibilité future des technologies alternatives plus efficientes ou de capture des GES ou encore sur la possible coordination internationale autour de la transition écologique. Il existe aussi des incertitudes physiques relatives à la sensibilité du climat (i.e. *equilibrium climate sensitivity*) et au budget carbone mondial restant (Cox *et al.*, 2018 ; Meehl *et al.*, 2020), ainsi qu'aux points de basculement (en anglais '*tipping points*'), qui pourraient nécessiter des actions immédiates plus ambitieuses (Keen *et al.*, 2022 ; Weitzman, 2009) [3]. Dans ce contexte hautement incertain, il ne

3. Ces incertitudes sont bien décrites dans la littérature associée à la modélisation économique intégrant le climat et celle de l'énergie (Edenhofer *et al.*, 2006) qui distingue généralement les incertitudes de *paramètres* pour

semble pas réaliste de supposer, en amont, une connaissance parfaite du scénario en cours de réalisation (correspondant à un objectif climatique fixe). Bien que l'incertitude et l'imprévisibilité profonde des risques financiers liés au climat soient reconnues par la littérature, leur impact sur la dette des entreprises, sur les portefeuilles des banques et sur la résilience du système financier dans son ensemble, n'est pas suffisamment explicite. Il est donc nécessaire de prendre en compte les scénarios multiples et l'incertitude qui en découlent dans les modèles de valorisation.

Agliardi et Agliardi (2021) ont récemment développé un modèle intégrant l'incertitude liée aux risques climatiques s'ajoutant à celle relative aux bénéfices des entreprises pour les obligations perpétuelles. Dans leur description des flux de trésorerie, le choc politique aléatoire et le degré de compatibilité de l'activité avec une économie bas carbone (*degree of greeness*) déterminent l'amplitude des chocs sur la valeur de l'entreprise. Agliardi et Agliardi (2021) définissent la valeur seuil par la maximisation de la valeur des actions et explicitent la fonction de valeur du prix des obligations en résolvant l'équation différentielle partielle (EDP) caractéristique de la dynamique des prix. En se basant sur cet article récent, et en incluant des considérations de Leland (1994) et Leland et Toft (1996) où la firme peut initialement choisir sa structure de capital optimale et la maturité de ses dettes, nous cherchons à répondre à la question suivante :

Question 3 ***Comment prendre en compte l'incertitude du scénario, progressivement levée par l'observation de la trajectoire du prix du carbone, dans la fixation du prix de la dette de l'entreprise ?***

1.2 Risques physiques

En pratique atténué par la faible probabilité que des réglementations aux retombées économiques néfastes à court et moyen terme soient implémentées (et maintenues) par les gouvernements, le risque de transition demeure au centre de l'attention de la communauté financière, tandis que l'exposition de nos sociétés aux risques physiques ne cesse de croître. Ces risques météorologiques (sécheresses, inondations, tempêtes, etc.) effectivement attribuables au changement climatique (contrairement au risque de transition) sont bien plus complexes à prendre en compte au niveau des portefeuilles d'actifs, notamment car les canaux de transmission de ces risques sur les trésoreries ou les bilans comptables sont moins immédiats et transparents. Soulignons toutefois que les méthodologies d'analyse (Merz *et al.*, 2010), les causes principales de dommages (Merz *et al.*, 2021), le calcul de l'exposition (Jongman *et al.*, 2012 ; McGranahan *et al.*, 2007) et l'estimation des pertes attendues (Hallegatte *et al.*, 2013) y compris en termes d'impacts financiers (Mandel *et al.*, 2021), spécifiquement liés aux inondations fluviales et côtières, ont déjà fait l'objet de plusieurs travaux académiques.

1.2.1 Modélisation de l'intensité des événements extrêmes

Données climatiques La sensibilité de l'intensité des catastrophes naturelles au changement climatique se mesure à partir de données spécifiques caractéristiques des conditions environnementales localisées. Il existe trois principaux types de sources de données climatiques utiles à la concep-

les hypothèses, ou de *modèle*, pour le choix de la représentation mathématique du comportement des agents ou de leur utilité.

tion des modèles de risques physiques : les mesures météorologiques historiques, les réanalyses et les simulations par des modèles de circulation générale (*general circulation models*, GCM). Les premières sont des mesures précises et locales effectuées par des stations météorologiques ou lors d'évènements particuliers. Les réanalyses sont des données produites par des modèles de circulation calibrés avec des enregistrements météorologiques ; elles reflètent donc relativement précisément le climat passé. Enfin, les données produites à partir des modèles climatiques sont les seules qui permettent de décrire également le climat futur et leur intégration est donc indispensable aux modèles prospectifs d'évaluation des risques physiques. Ces modèles sont constamment améliorés lors des différentes phases du projet d'intercomparaison des modèles couplés (CMIP). Les derniers résultats utilisés par le Groupe d'experts intergouvernemental sur l'évolution du climat (GIEC) sont par exemple basés sur la sixième phase du projet (CMIP6). Il est donc essentiel pour les gestionnaires d'actifs d'être à jour dans l'intégration de ces informations, susceptibles de suggérer des révisions dans la tarification des actifs. Parmi les nombreuses variables disponibles en sortie de ces modèles, il s'agit ensuite de sélectionner les plus à même de caractériser l'intensité des aléas climatiques (ou la valorisation d'une classe d'actifs). Par exemple, l'estimation des dommages liés aux inondations et aux sécheresses nécessite des données relatives aux précipitations et à l'humidité [4], tandis que les tempêtes ou les tornades sont plus complexes à modéliser. L'approche la plus classique consiste donc à évaluer l'impact des conditions climatiques décrites par les modèles sur la *période de retour* soit la probabilité statistique de constater la récurrence d'un évènement d'une intensité donnée.

Modèles de circulation générale (GCMs) et traitement des données Les données produites par les modèles climatiques peuvent être biaisées. Il est donc nécessaire d'en utiliser plusieurs pour prendre en compte les erreurs propres à chacun d'eux. De plus, il est possible de corriger les biais des simulations par rapport aux observations et d'assumer que la fonction de correction sera la même dans le futur. Pour réduire l'incertitude causée par ces biais, il est possible d'utiliser la méthode dite '*cumulative distribution function-transform*' (CDF-t) développée dans Michelangeli *et al.* (2009) et Vrac *et al.* (2012) qui permet de corriger la distribution des variables climatiques. Ce type d'approche de correction de biais, similaire à un ajustement quantile-quantile, est utilisée de manière standard dans la communauté climatique (Navarro-Racines *et al.*, 2020) et des outils spécifiques sont développés pour faciliter la manipulation des données climatiques par les praticiens (Pérez-Zanón *et al.*, 2021).

Question 4.a ***Comment construire une base de donnée de cyclones tropicaux synthétiques, à partir de des données climatiques produite avec les GCMs, qui soit compatibles avec l'évaluation du risque financier ?***

1.2.2 Exposition des actifs

Inventaire d'actifs géolocalisés et approximation La géolocalisation des actifs exposés est une information indispensable pour l'évaluation des risques physiques. Une mesure à l'échelle de

4. En plus d'informations supplémentaires comme la topologie, les propriétés du sol, les coefficients de ruissellement, l'utilisation des terres, etc., ces données climatiques permettent de simuler la hauteur de crue intervenant par la suite dans les fonctions de dommages liés aux inondations

l'entreprise nécessite donc de connaître les coordonnées géographiques des sites dont dépend l'activité des émetteurs. Pour l'estimation de l'exposition d'un pays (d'une région ou d'une ville), certaines initiatives *open-source* permettent de constituer des inventaires d'actifs physiques pouvant permettre d'estimer le risque actuel. En effet, afin d'appréhender pleinement l'exposition d'un pays aux risques physiques à court et moyen terme, des indicateurs, pour chaque type d'aléa climatique, peuvent être définis selon plusieurs dimensions. En pratique, il faut donc estimer les coûts des infrastructures physiques dans les zones habitées (coûts de remplacement et d'adaptation potentielle), l'exposition du secteur de l'énergie, l'adaptabilité des secteurs des transports, de l'agriculture et de l'approvisionnement alimentaire, du système de distribution d'eau, etc., pour chaque type d'aléa climatiques, pour proposer une estimation des impacts économiques possibles ou des plans de résilience à moyen terme. Pour projeter l'exposition des actifs à plus long-terme, il est possible d'utiliser les éléments clés mentionnés ci-dessus et de faire l'hypothèse d'une distribution similaire dans le futur des actifs physiques qui leur est associés. Il est également possible, dans le cadre d'études portants sur différents scénarios climatiques (ce qui requiert des horizons de temps bien plus long) d'utiliser des méthodologies plus homogènes pour estimer la valeur des actifs physiques dans les différents pays (en utilisant par exemple l'intensité lumineuse nocturne capturée par satellite, voir Eberenz *et al.*, 2020). Néanmoins, nous notons que la littérature portant sur les risques physiques, traite généralement l'exposition des différentes catégories d'actifs indépendamment. Une littérature considérable traite notamment de l'exposition directe de la population, du secteur de l'énergie ou encore s'attache plus particulièrement aux systèmes de transport :

- **Population**. Plusieurs études portent sur l'exposition de la population et des infrastructures aux catastrophes naturelles et sur son évolution, offrant les principaux ordres de grandeur de l'exposition globale. Par exemple, McGranahan *et al.* (2007) constatent que 13% de la population urbaine mondiale est localisée dans des zones côtières de faible élévation (en anglais, *low elevation coastal zone*, LECZ). Suivant leur projection, les populations exposées dans ces zones devraient augmenter de plus de 50%, passant de 625 à 880 millions de personnes entre 2000 et 2030 à environ 1,4 milliard en 2060, soit 12% de la population mondiale dans le scénario envisagé (Neumann *et al.*, 2015). La croissance de la population n'est bien sûr pas le seul facteur à prendre en compte. Par exemple, sans tenir compte de l'expansion démographique, Geiger *et al.* (2021), suggèrent une augmentation de la population exposée aux cyclones tropicaux de 26% par an (33 millions de personnes) par degré d'augmentation de la température moyenne. Enfin l'exposition est très inégale suivant les différentes régions. On peut évoquer les pays insulaires du Pacifique (PIC) qui sont d'ores et déjà confrontés à des risques élevés, avec 57% de leur infrastructures situées près des côtes, ce qui représente une exposition de 21,9 milliards USD (Kumar & Taylor, 2015). Si l'exposition des infrastructures américaines a également été quantifiée, notamment par Bretz (2017) et Kousky *et al.* (2020) qui suggèrent que 1,8% du total des logements aux États-Unis seront inondés d'ici 2100, celle-ci demeurent bien inférieure à celle de l'Australie, dont 85% de la population serait exposée à des risques induits par le climat d'après Gurran *et al.* (2013).
- **Énergie**. Les impacts du changement climatique sur le secteur de l'énergie se mesurent selon deux principaux canaux de transmission : d'une part la perte d'efficacité et la baisse potentiel des rendements de la production, d'autre part les dommages directs subis par les infrastructures. Ces deux impacts peuvent entraîner une perte de valeur financière (réduction

des flux de trésorerie futurs, immobilisation du capital physique, etc.) et doivent être pris en compte pour la gestion d'actifs. En premier lieu, l'efficacité des centrales électriques est affectée. En effet, aux États-Unis et dans l'Union européenne, respectivement 91% et 78% de l'électricité est produite par des centrales thermoélectriques (nucléaires et à combustible fossile), qui sont sensibles à la fois à la température de l'air ambiant, ainsi qu'à la disponibilité et à la température de l'eau. Par conséquent, la production d'énergie est susceptible de subir une réduction d'efficacité estimée entre 4,4 et 16% en Europe et entre 6,3 et 19% aux États-Unis (Van Vliet *et al.*, 2012). Plusieurs études explorent cette réduction d'efficacité en détail (Linnerud *et al.*, 2011 ; Petrakopoulou *et al.*, 2020 ; Rübbelke & Vögele, 2011). D'autres études, prennent localement en compte les deux effets, par exemple, Sathaye *et al.* (2012) estiment l'impact du réchauffement sur l'efficacité de la production mais aussi sur le risque d'inondation des centrales électriques côtières et constatent que 25 d'entre elles ainsi que 86 sous-stations risquent d'être inondées en Californie. Pour mesurer ce risque en pratique, la base de données mondiale des centrales électriques (Byers *et al.*, 2018), met à disposition des données de géolocalisation pour un nombre croissant de centrales (cf. figure 1.4), ce qui devrait améliorer l'évaluation future de l'exposition physique [5].

- **Transport**. Des systèmes de transport efficaces sont essentiels à la prospérité et au bon fonctionnement des économies (Koks *et al.*, 2019) et nous constatons déjà que les évènements météorologiques sont la principale cause des surcoûts liés à la maintenance des réseaux et infrastructures. En effet, 30 à 50% des coûts d'entretien des routes en Europe sont associés aux conditions météorologiques, dont environ 10% (~ 0,9 milliard d'euros par an) sont générés par les seuls phénomènes météorologiques extrêmes (Nemry, Demirel *et al.*, 2012, p. 5). Koks *et al.* (2019), sur la base des données d'openstreetmap (OSM), ont estimé que les dommages annuels prévus au niveau mondial sur les actifs des infrastructures routières et ferroviaires pouvaient varier entre 3,1 et 22 milliards USD, et que l'investissement dans la protection contre les inondations devraient avoir un retour positif d'environ 60%. [6] La question de la résilience des systèmes de transport et des chaînes d'approvisionnement va au-delà des routes et des transports terrestres. Par exemple, Verschuur *et al.* (2020) évaluent les perturbations portuaires dues aux catastrophes naturelles sur 27 événements avec potentiellement une interruption de dix jours aux États-Unis associée à une vitesse de vent de 35 $m.s^{-1}$ ou une onde de tempête de 2,5 m. Selon la Banque mondiale, les pays à revenu faible ou intermédiaire devraient consacrer entre 0,5 et 3,3 % de leur PIB annuel (157 milliards à 1 000 milliards USD) à de nouvelles infrastructures de transport d'ici 2030, sans compter les coûts d'entretien non pris en compte dans ces chiffres estimatifs.

Exposition basée sur un scénario Il est donc clair que la définition de l'ensemble *intensité* × *exposition* × *vulnérabilité*, pour chaque évènement climatique par rapport à chaque type d'actif

5. Il convient de noter que les centrales peuvent être touchées, mais aussi le réseau ; certaines études se concentrent leur résilience et sur l'effet de cascade provoqué par les dommages infligés par les risques naturels (Albert *et al.*, 2004 ; Duenas-Osorio & Vemuru, 2009).

6. Les auteurs ont mesuré les dommages causés par les cyclones tropicaux, les tremblements de terre, les inondations de surface, les inondations fluviales et les inondations côtières, en utilisant des cartes de probabilité pour chaque danger sur différentes périodes de retour. Par exemple, ils introduisent cinq périodes de retour (entre 1/50 ans et 1/1000 ans) pour la distribution de la vitesse du vent pour les cyclones tropicaux.

Population (SSP2-2100)

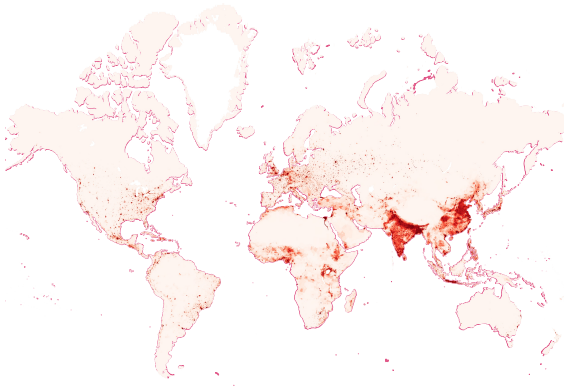

Centrales de production d'énergie

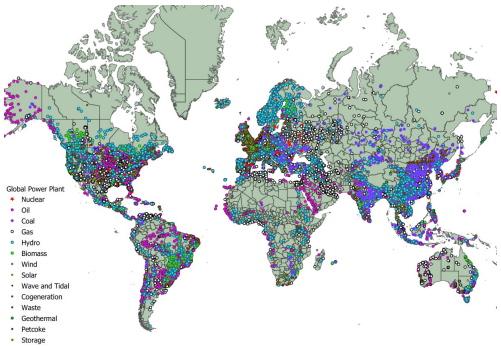

Inventaire mondial des routes

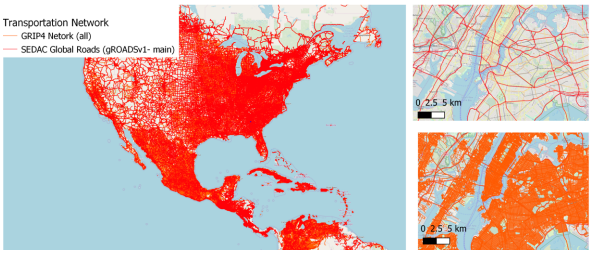

Terres cultivées de Earth stat (exemples)

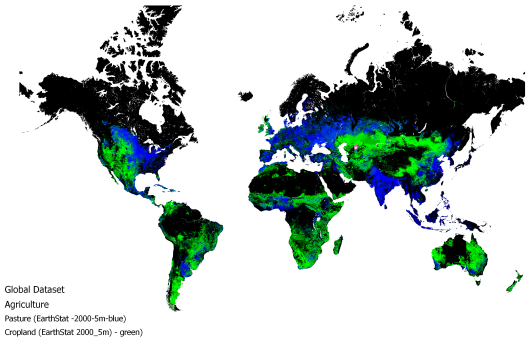

FIGURE 1.1 – Source de données à code open-source pour la représentation des actifs physiques : SEDAC (Jones & O'Neill, 2017), Base de données mondiale des centrales électriques (Byers *et al.*, 2018), Routes mondiales (Meijer *et al.*, 2018) vs. SEDAC (gROAD), Earth stat

clé est complexe en soit. Déterminer les expositions propres à chaque actif, l'exposition total d'un pays, ou même celle d'un portefeuille l'est plus encore, d'autant que cette tâche est sujette à des problématiques d'agrégation non triviales. L'évaluation à plus long terme des dommages nécessite la prise en considération de multiples facteurs socio-économiques. En effet, la littérature relative aux dommages causés par des cyclones tropicaux montre que ces facteurs socio-économiques sont en grande partie responsables de l'augmentation des dommages attendues dans le futur (Noy, 2016 ; Pielke Jr *et al.*, 2008 ; Weinkle *et al.*, 2018 ; Weinkle *et al.*, 2012 ; Ye *et al.*, 2020). Si la définition de l'exposition aux multiples risques des actifs locaux actuels est un défi, il est encore plus difficile, et pas nécessairement cohérent de projeter l'estimation de la valeur présente exposée, surtout à long terme. Il existe cependant des méthodes permettant de distribuer le capital physique et la population en fonction des trajectoires 'socio-économiques partagées' (en anglais, *shared socioeconomic pathways* ; SSP). Par exemple, Jones et O'Neill (2017) ont déployé des cartes haute résolution qui décrivent l'évolution de la population dans le cadre de chacun des cinq SSP utilisées par le GIEC [7], en intégrant les hypothèses de répartition des populations en zones

7. Une version allégée est disponible sur le site Socio-Economic Data and Application Center (SEDAC) et à 1km (accessible ici)

urbaines et rurales, relativement aux différents scénarios. Des projections plus agrégées du PIB et de la population globale (ou régionale) sont également largement disponibles dans les résultats des modèles d'évaluation intégrée utilisés par le GIEC. Cependant, il est clair que ces facteurs de projection à long terme ne peuvent pas être utilisés directement avec l'inventaire des infrastructures physiques. En effet, il n'apparaît pas pertinent de calculer la valeur future d'une centrale électrique en rapportant sa valeur actuelle à l'évolution de la population ou du PIB par habitant. Toutefois, la proposition d'Eberenz *et al.* (2019, 2020) permet de projeter la valeur des actifs physiques sur une grille fine en utilisant l'intensité lumineuse nocturne et la population. Bien que pour une estimation à moyen terme, les approches basées sur des inventaires restent à privilégier, ce type de méthodologie est adapté à l'estimation des dommages à plus long terme.

Question 4.b ***Comment définir une mesure de l'exposition des actifs physiques de manière à ce que (i) elle soit suffisamment représentative de la valeur réelle des actifs locaux (ii) elle puisse être projetée dans des scénarios socio-économiques partagés ?***

1.2.3 Modélisation de la vulnérabilité et des dommages

Au-delà de la sensibilité du PIB à la température moyenne mondiale Des fonctions de dommages sont utilisées par les modèles intégrés de type coûts-bénéfices afin de modéliser l'impact de l'augmentation de la température moyenne mondiale sur le produit intérieur mondial (Hanemann, 2008 ; W. Nordhaus, 1993, 2018a ; Weitzman, 2009, 2010, 2012). L'utilisation de ce type de fonction dans les modèles économiques, visant à estimer la politique de taxation optimale qui permettrait l'atténuation des dommages futurs, est largement remise en question (Auffhammer, 2018 ; Pindyck, 2017). En pratique les modèles d'évaluation technico-économiques sont d'ailleurs largement privilégiés (Hourcade *et al.*, 2021). Cependant, l'utilisation d'une fonction de dommage demeure justifiée pour l'évaluation des risques physiques avec des aléas et des actifs particuliers.

Les fonctions de dommages $\Omega_j(I) \in [0,1]$ sont définies comme la fraction de la perte d'un actif par rapport à l'intensité d'un évènement I. Elles sont calibrées sur les dommages rapportés dans le passé (sinistres, pertes économiques, etc.) en utilisant une grandeur appropriée représentative de l'intensité de l'événement. Dans le cas des tempêtes (cyclone tropical, tempêtes hivernales européennes, tornades, etc.), les dommages sont généralement définis à partir des vents maximums ($m.s^{-1}$) ou de la pression centrale (hPa). Les dommages directs liés aux inondations sont généralement définis à partir de la hauteur de crue (en anglais *flood depth*, en m) par classe d'occupation des sols (voir figure 1.5, Huizinga *et al.*, 2017). L'intensité d'une sécheresse peut être représentée par l'indice de précipitation standard et l'évaporation (Bachmair *et al.*, 2017 ; McKee *et al.*, 1993 ; Vicente Serrano *et al.*, 2010) et ils sont plus susceptibles d'affecter les secteurs de l'énergie (par la réduction de l'efficacité) ou de l'agriculture. Dans le cas du risque agricole, le nombre maximum de jours consécutifs de gel, de jours humides ou de jours secs et la plage de température du jour ou d'autres indicateurs agroclimatiques peuvent être utilisés pour définir des fonctions de dommages paramétriques.

Littérature sur les fonctions de dommage Un grand nombre de travaux académiques décrivent les spécifications mathématiques de différentes fonctions de dommages physiques. Par

Inondations européennes (Huizinga *et al.*, 2017) Vent paramétrique (K. A. Emanuel, 2011)

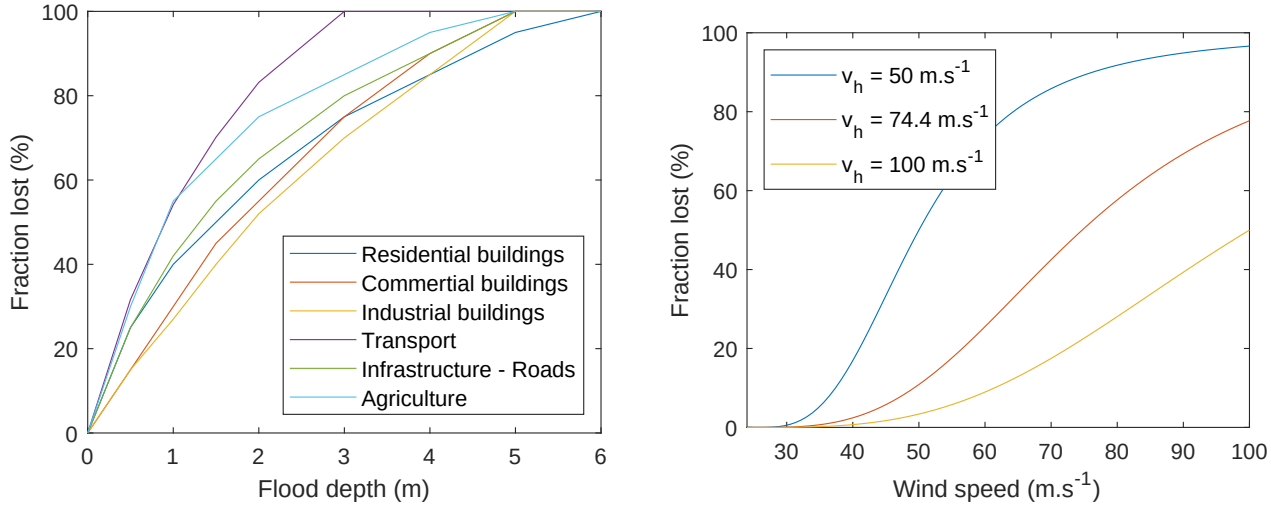

FIGURE 1.2 – Exemple de fonction de dommage physique appliquée

exemple, Prahl *et al.* (2015) proposent plusieurs approches afin de mesurer la fraction de propriété détruite lors des tempêtes. Ces fonctions sont calibrées sur des sinistres observés sur des bâtiments résidentiels en Allemagne. [8] Pour les inondations, les fonctions de dommages les plus utilisées sont celles définies par Huizinga *et al.* (2017). En plus de dépendre du type d'évènement, ces fonctions peuvent (et doivent) être calibrées pour différents types d'actif. Par exemple, les fonctions pour différentes catégories de bâtiments en Europe sont représentées dans la figure 1.5 [9].

Alors qu'un grand nombre de travaux relatifs aux dommages causés par le vent sur des bâtiments résidentiels soit disponibles (aussi bien en Amérique, en Australie, qu'en Europe ou au Japon ; Crompton et McAneney, 2008 ; Ginger *et al.*, 2010 ; Hart, 1976 ; Pita *et al.*, 2015 ; Prahl *et al.*, 2015), les études visant à estimer la vulnérabilité des bâtiments commerciaux, industriels, transports, ou autre, sont moins nombreuses [10]. Afin de proposer des fonctions pour les autres type de bâtiments, Unanwa *et al.* (2000) ont développé une méthodologie reposant sur des arbres de décision, utilisant diverses informations relatives à la structure des bâtiments et en distinguant leurs fonctions [11]. Il suggère donc que les bâtiments commerciaux et institutionnels sont respectivement légèrement et significativement plus vulnérables que les bâtiments résidentiels de hauteur moyenne. En outre, cette étude révèle qu'un vent supérieur à 43-60m.s^{-1} génère des dommages généralisés et qu'un régime de vent soutenu supérieur à 73m.s^{-1} peut entraîner la destruction totale de la plupart des bâtiments (sauf pour les immeubles de moyenne et faible hauteur). Des descriptions plus précises de la vulnérabilité des bâtiments sont fournies dans les rapports de l'Agence

8. Il explore également les fonctions relatives à d'autres aléas Prahl *et al.*, 2016.
9. Aussi disponible pour l'Amérique du Nord, l'Asie, l'Amérique centrale et du Sud, l'Afrique et l'Océanie.
10. La période de construction peut être utilisée comme paramètre pivot car la résistance de ces bâtiments devraient être similaires lorsqu'ils sont construits à la même période, Unanwa *et al.* (2000).
11. Notons que les méthodologies d'évaluation par arbres de décision ou autre forme de procédure conditionnelles conviennent également lorsqu'aucune fonction explicite ne peut être calibrée. Par exemple, pour les routes, Koks *et al.* (2019) supposent que les vents extrêmes entraînent le coût de nettoyage des arbres tombés (lorsque les vents cycloniques dépassent 42 m.s^{-1} (~151 km.h^{-1}, Virot *et al.*, 2016) et si la densité d'arbres autour du bien est d'au moins 10/km^2 (Crowther *et al.*, 2015).

fédérale de gestion de crise Américaine (*Federal Emergency Management Agency*, FEMA) qui définissent notamment une méthodologie à laquelle est adossée le logiciel standardisé Hazus. Les méthodes d'évaluation sous-jacentes pour estimer les pertes potentielles dues aux tremblements de terre, aux inondations, aux ouragans et aux tsunamis sont décrites dans le rapport FEMA (2009).

Une autre difficulté pour l'évaluation de la vulnérabilité des biens aux tempêtes, et en particulier aux cyclones tropicaux, est que les dommages totaux peuvent être causés par de multiples sous-périls, et les pertes inhérentes à chacun d'entre eux ne sont pas clairement rapportées dans les bases de données accessibles et utilisables pour la calibration des fonctions. Néanmoins, la vitesse du vent, également utilisée dans l'échelle de Saffir-Simpson, reste un bon indicateur des dommages potentiels pour les différents types de tempêtes. Enfin, dans le cadre d'une évaluation prospective et à long terme, l'introduction d'une représentation de l'exposition des actifs physiques compatible avec une projection dans les SSP (et donc s'éloignant potentiellement d'un inventaire d'infrastructures réelles), nécessite, par souci de cohérence, que la fonction de dommage soit re-calibrée à partir de la représentation utilisée pour l'actif considéré.

Les travaux de Aznar Siguan et Bresch (2019), Bresch (2017) et Lüthi (2019), avec la plateforme d'estimation des risques physiques (CLIMADA) couplée à une représentation des valeurs estimées des actifs physique pertinentes (Eberenz *et al.*, 2019, 2020), sont des contributions importantes dans le domaine de l'estimation des dommages. Au lieu d'une approche de la vulnerabilité '*bottom-up*' basée sur l'ingénierie (et la résistance des bâtiments à certaines conditions), Eberenz *et al.* (2021) a opté pour une fonctionnelle paramétrique (cf. Figure 1.5) initalement introduite par K. A. Emanuel (2011), introduisant un hyper-paramètre v_h dont dépend le niveau de vulnérabilité de la région considérée. Plus la valeur de $v_h(j)$ est élevé, plus la vitesse du vent doit être importante pour engendrer de réels dommages dans la région j. Nous notons que les efforts et investissements d'adaptation peuvent être reflétés par des changements dans ce paramètre.

Question 4.c ***Comment calculer les dommages liés à un cyclone tropical le long de trajectoires synthétiques sur la base des diverses contributions existantes ?***

Du dommage physique à la perte économique ou financière Une fois les dommages physiques directs calculés, il faut définir leur canaux de transmission, et potentiels facteurs d'amplification, menant à des pertes économiques. En effet, les dommages liés aux catastrophes incluent les pertes physiques directes éventuellement assurées, et les conséquences économiques à plus long terme de l'événement [12]. La propagation et l'amplification des dommages rend les impacts économiques à plus long terme plus complexes à estimer. Pour répondre à cette question, Hallegatte (2008) a introduit un cadre d'entrée-sortie et défini le ratio d'amplification économique comme le multiplicateur entre le coût direct et les pertes économiques totales [13]. Pour Katrina,

12. Par exemple, les coûts directs de l'ouragan Katrina sont estimés à 125 milliards USD (2005), dont 80 milliards couverts par les assurances (EMDAT et Swiss Re Group (2020)). Les conséquences du cyclone sur sur la production pétrolière américaine par exemple (dont 19 % a été endommagée) ont encore augmenté ce coût. Il est parfois complexe de définir l'impact économique à long terme du cyclone. Par exemple, les cyclones impactent les secteurs agricoles et alimentaires, ce qui pénalise l'économie sur une plus longue période. Par exemple, les ouragans Irma et Maria en 2017 en Dominique ont détruit 100 % des plantations agricoles, tandis que Yassi en Australie en 2011 a détruit 75% des plantations agricoles dans les zones touchées.

13. Il convient de noter que ce coefficient d'amplification peut déjà être pris en compte dans les dommages rapportés dans certaine base de données (par exemple, Guha-Sapir *et al.*, 2018).

ce coefficient a été estimé à 1,39 par exemple (Hallegatte, 2008). En général, l'auteur suggère que l'impact économique d'événements dont les pertes directes dépassent 200 milliards USD pourraient impliquer un coût total deux fois plus important. Dans ce cas, l'augmentation du coût due au changement climatique pourrait dépasser la capacité de reconstruction des pays les plus pauvres. De plus, les pertes subies par un pays pourraient affecter les actifs financiers à l'échelle mondiale. Pour estimer l'effet de cascade du risque physique, il faudrait combiner les effets de la chaîne d'approvisionnement physique et la contagion financière (Bressan *et al.*, 2022 ; Mandel *et al.*, 2021).

Quelques résultats sur les dommages attendus Pour divers type de risques, d'actifs et de fonctions de dommages, plusieurs études ont estimé les pertes futures induites par les catastrophes naturelles ou le changement climatique. Cela permet de fixer l'ordre de grandeur de l'impact du changement climatique, en particulier pour les risques d'inondations. Par exemple, Hallegatte *et al.* (2013) quantifient les pertes potentielles dues aux inondations dans les 136 plus grandes villes côtières, et estiment que les pertes actuelles (6 milliards USD par an en 2005) devraient atteindre 52 milliards de USD par an en 2050, sans tenir compte des changements socio-économiques. Dans le scénario de référence, c'est-à-dire sans investissements d'adaptation, les impacts sur ces villes devraient atteindre 1 000 milliards USD. Vousdoukas *et al.* (2018) suggèrent que sans investissements d'adaptation supplémentaires, les dommages annuels attendus (EAD) actuels des pertes côtières de 1,35 milliard d'euros pourraient varier entre 93 et 961 milliards d'euros en Europe. Dans l'ensemble, la plupart constatent des dommages importants en claire augmentation induite par le changement climatique. La problématique suivante concerne l'intégration des informations du risque par les marchés (dans le passé), et de mesurer l'ampleur de l'augmentation des coûts qui se fera ressentir (dans le futur).

1.2.4 Risque financier et réponse des marchés

Bien que l'intégration des risques physiques par les marchés financiers dans leur ensemble n'ai pas été clairement mise en évidence empiriquement (ni explicitée théoriquement), il existe des marchés spécifiques qui reflète certaines expositions locales. Par exemple, le risque de cyclones tropicaux est naturellement intégré aux prix des produits financiers destinés à assurer des couvertures en cas d'évènement extrême sur le marché dédié des *cat-bonds* (Bantwal & Kunreuther, 2000 ; Morana & Sbrana, 2019) [14], ainsi que dans le coût de la dette des États et des émetteurs locaux sur les marchés des obligations municipales [15]. Sur le marché des actions, des travaux plus opérationnels (Dimov & Parsons, 2021) observent à la fois un impact négatif (et statistiquement significatif) avant la tempête et un retour positif après des cyclones sur la performance des actions des industrie possédant des infrastructures dans la région touchée aux État-Unis [16]. À l'aide d'une approche plus académique d'étude d'évènements, Lanfear *et al.* (2019) ont également montré que les marchés actions répondaient aux informations sur les tempêtes. Dans l'ensemble, ces études

14. Et ces marchés répondent aux évenements, par exemple, Harvey et Irma ont clairement impacté le prix des cat-bonds lorsqu'ils sont arrivé sur les cotes des États-Unis en 2017.

15. Sur ce marché particulier, l'étude de Rizzi (2022) suggère par exemple que préserver le capital naturel permet de réduire le coût la dette.

16. Ces possibles renversements de tendances découlent de la plus grande liquidité de ce marché.

suggèrent que l'étude des cyclones tropicaux constitue un axe de recherche pertinent pour mesurer l'impact du changement climatique sur les portefeuilles, d'autant plus que leur impact sur les pays, et leur capacité d'endettement à long terme n'a pas été clairement établi.

Par ailleurs, au-delà des risques liés aux cyclones tropicaux, il est important de souligner que la prise en compte du changement climatique par les marchés financiers n'est pas clairement établie. Sur le marché action, Hong *et al.* (2019) constate par exemple que les prix des titres émis par les entreprises des secteurs liés à l'alimentation *sous réagissent* aux risques de changement climatique, et, en particulier, n'actualisent pas efficacement l'augmentation des risques de sécheresses dans le futur. De même, Gostlow (2019), en utilisant une approche factorielle, souligne que le risque climatique physique n'explique pas les rendements boursiers. Avec le même type d'approche, introduisant un facteur construit à partir de données textuelles, Faccini *et al.* (2021) n'observent pas de réponse significative des prix de marché par rapport aux signaux construits à partir des mentions et de l'actualité relatives aux catastrophes naturelles.

Cependant, de plus en plus d'articles traitent de l'impact du changement climatique sur le risque de défaut souverain (Beirne *et al.*, 2020 ; Klusak *et al.*, 2021 ; Volz *et al.*, 2020), ou encore, démontrent l'impact d'évènements, comme les inondations côtières, sur des instruments financiers, comme les *credit default swap* (CDS) souverains (Dey, 2022). Plus précisément, Beirne *et al.* (2020), montrent, par le biais d'une analyse économétrique, que la vulnérabilité et la résilience au risque climatique sont déjà des déterminants significatifs des spreads des obligations souveraines. Klusak *et al.* (2021) simulent l'effet du changement climatique sur les notations de crédit souverain dans des scénarios de réchauffement alternatifs. Leur méthodologie est basée sur un modèle statistique de prédiction de notation, combiné à un modèle de croissance macroéconomique pour projeter les impacts du réchauffement climatique sur le PIB.

Sur le plan théorique, Mallucci (2020) propose une approche du risque climatique encouru par les îles souveraines des Caraïbes par le modèle d'équilibre général dynamique d' Eaton et Gersovitz (1981) permettant de décrire largement les relations créancier-emprunteur au niveau des pays, et en particulier de prendre en compte les mécanismes menant au remboursement, au défaut ou à d'éventuelles renégociations. Il démontre que le risque accru de catastrophe réduit la capacité de ces îles souveraines à émettre de la dette et que le changement climatique restreint encore plus l'accès de ces gouvernements insulaires aux marchés financiers. L'inconvénient de l'utilisation de ce type d'approche est qu'elles complexifient la transposition des mesures du risque au niveau des portefeuilles. D'autre contributions incontournables formalisent les implications des risques de catastrophes sur les actifs (Tsai & Wachter, 2015 ; Wachter, 2013). A partir de ces concepts, Karydas et Xepapadeas (2019, 2021) développent d'ailleurs un modèle d'inclusion théorique du risque physique reliant l'émission de carbone, les investissements d'atténuation et la composition du portefeuille. Ils proposent une modélisation de l'impact de catastrophes rares sur la prime des actions et les taux d'intérêt souverains [17].

Bien que la littérature mentionnée permette de comprendre et d'intuiter certains effets liés aux risques physiques, il n'existe pas, à l'heure actuelle, de méthodologie intégrée efficiente. En effet, il s'agit de décrire plus clairement les canaux de transmission, à partir des variables climatiques

17. Leur modèle suppose que le choc lié aux régulations visant à limitant les émissions de GES est endogène (augmente en probabilité avec l'augmentation de la fréquence de catastrophes naturelles), ainsi que la relation entre l'augmentation de la température et la probabilité de la catastrophe est connue

brutes, jusqu'aux prix des actifs, afin d'évaluer le risque physique au niveau des portefeuilles (en bottom-up). Ce qui nous amène à la question suivante :

Question 4.d ***Quel est l'impact des dommages annualisés liés aux cyclones tropicaux sur le coût de la dette des pays émergents ?***

1.3 Contributions principales

1.3.1 Sensibilité du risque de crédit au prix du carbone [18]

L'un des leviers permettant d'atteindre les objectifs fixés par l'accord de Paris consiste à donner un prix aux émissions de gaz à effet de serre. En pratique, il existe deux principaux mécanismes de tarification du carbone : les taxes sur le carbone et les systèmes d'échange de quotas d'émission (ETS), qui couvrent ensemble un nombre croissant d'émetteurs [19]. Des fluctuations rapides des prix effectifs du carbone peuvent représenter un risque pour les activités des entreprises et avoir un impact sur leur solvabilité. En s'appuyant sur des scénarios tendanciels à moyen terme (2024) et du Groupe d'experts intergouvernemental sur l'évolution du climat (GIEC) à long terme (2060), cette étude analyse la sensibilité du risque de crédit de 763 entreprises internationales. Les secteurs '*Énergies fossiles*', '*Eau, électricité, gaz*' et '*Matériaux*' sont les plus sensibles. Toutefois, le risque ne devient significatif qu'à long terme. Un renforcement des mécanismes de tarification des émissions de gaz à effet de serre semble donc envisageable à moyen terme sans compromettre la stabilité financière.

Mesure de la probabilité de défaut scénarisée avec le modèle de Merton, 1974 Soit $\boldsymbol{\mathcal{CE}}_{1,i}$ l'émission annuelle directe de carbone (Scope 1) de l'entreprise i avec des bénéfices avant intérêts, impôts, dépréciations et amortissements constants (EBITDA_i) et $\text{CP}(\text{k},\text{t})$ le prix du carbone dans le scénario k à l'année t. Nous définissons le choc direct lié au coût du carbone comme suit :

$$\xi(i,k,t) = \frac{\boldsymbol{\mathcal{CE}}_{1,i} \times \text{CP}(\text{k},\text{t})}{\text{EBITDA}_i} \tag{1.1}$$

Avec le modèle de Merton (1974) nous obtenons la distance au défaut pour chaque scénario de prix :

$$\text{DD}(i,k,t) = \frac{\ln\left(\frac{(1-\xi(i,k,t)) \times V(i,k=0,t=0)}{D(i)}\right) + \left(r + \frac{1}{2}\left(\sigma_V(i)\right)^2\right)T}{\sigma_V(i)\sqrt{T}} \tag{1.2}$$

18. Ce chapitre est issu de Bouchet et Le Guenedal (2020b) qui a reçu le prix du meilleur article du GRASFI pour la recherche sur la finance climatique (sponsorisé par l'Imperial College London) en 2020. Cette version révisée est publiée dans le *Revue Economique* numéro spécial de mars 2022 sur les risques de transition, 73(2), Bouchet et Le Guenedal (2022).

19. Les informations sur l'état de l'art des mécanismes de tarification du carbone sont mises à disposition par la Banque mondiale, I4CE et les taux effectifs de carbone (2021) ont été calculés par la OCDE. Les entreprises devront soit payer la taxe correspondant à leurs émissions, soit acheter des quotas de carbone sur un marché de plafonnement et d'échange en fonction de la réglementation à laquelle elles sont soumises

où σ_V est la volatilité de la valeur de l'actif V, r le taux sans risque, T la maturité (1 an) et D la dette totale. La probabilité théorique de défaut PD d'un émetteur est :

$$\mathrm{PD}(i,k,t) = \Phi(-\mathrm{DD}(i,k,t))$$

Ces mesures sont définies pour chaque émetteur i dans chaque scénario k à chaque année t.[20] Nous comparons le nombre d'entreprises dont la probabilité de défaut dépasse 20% dans le scénario de transition futur aux niveaux historiques. Par exemple, nous pouvons voir dans la figure 1.6, que le risque de crédit auquel est confronté le secteur des services publics devient plus élevé qu'il ne l'était lors de la crise financière mondiale avant 2030 dans le scénario SSP2-19 (1,5°C), et augmente au-delà du niveau de 2007/2008 quel que soit le scénario après 2040. En revanche, le nombre d'entreprises à risque dans d'autres secteurs (y compris les secteurs intensifs comme l'énergie ou les matériaux) reste inférieur au niveau de la crise financière dans le scénario SSP2-26 1,8°C.

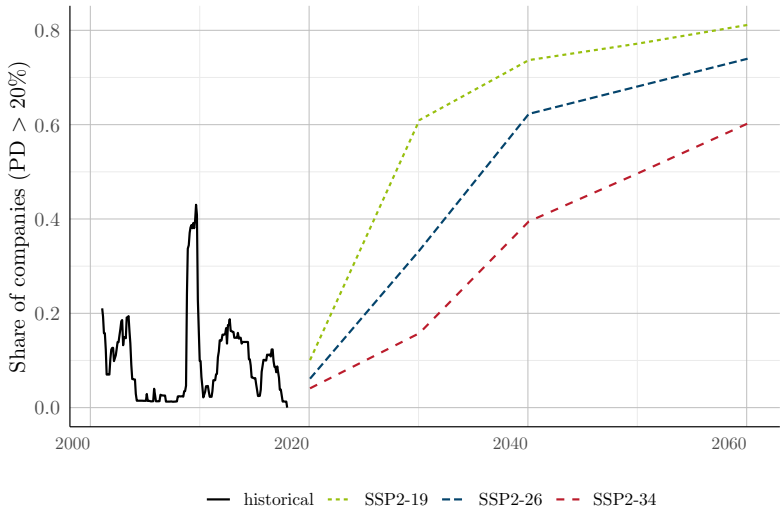

FIGURE 1.3 – Share of Utilities companies whose Merton's probability of default exceeds 20%

Le prix du carbone seuil Nous proposons également d'identifier pour chaque entreprise un *prix du carbone seuil* ($\boldsymbol{\mathcal{CPM}}$) qui correspond au prix à partir duquel la probabilité de défaut atteint une certain valeur S :

$$\boldsymbol{\mathcal{CPM}}_i := \max\{\mathrm{CP} : \mathrm{PD}(i) \leq S\}$$

20. Le ratio de choc ainsi défini peut également être introduit dans un modèle de notation de crédit (par exemple Pineau *et al.*, 2022) et inclure d'autres paramètres dans des approches de flux de trésorerie actualisés avec des mesures prospectives ou utilisé pour établir des probabilités de transition de notation.

Dans un cadre statique (c'est-à-dire dette à constante D_i, et émission de carbone $\boldsymbol{\mathcal{CE}}_{1,i}$) et pour des caractéristiques de valeur d'actif fixe (σ_i et V_i) [21], nous obtenons :

$$\boldsymbol{\mathcal{CPM}}_i = \left[1 - \exp\left(\sigma_V(i)\sqrt{T}\Phi\left(-S\right) - \left(r + \frac{1}{2}\sigma_V(i)^2\right)T\right) \cdot \frac{D(i)}{V(i)}\right] \cdot \frac{\text{EBITDA(i)}}{\mathcal{CE}_1(i)}$$

Une faible valeur de $\boldsymbol{\mathcal{CPM}}$ signifie que la structure du capital de l'entreprise la rend vulnérable à un changement mineur du prix du carbone. Dans cet article, nous étudions la distribution de l'indice $\boldsymbol{\mathcal{CPM}}$ en fonction de l'intensité de carbone (Trucost scope 1) en utilisant une valeur seuil de $S = 50\%$. Nous constatons une dépendance relativement faible du $\boldsymbol{\mathcal{CPM}}$ sur l'intensité carbone, par conséquent, une grande partie du risque de transition dépend de la structure du capital idiosyncratique des entreprises. Cette métrique a plusieurs applications. Pour les entreprises, cette mesure peut être utilisée pour évaluer le risque d'un projet dans des environnements fiscaux variables. Pour les gestionnaires de portefeuille, cette méthode permet d'évaluer le risque de défaut au niveau de l'émetteur en fonction des variations des prix locaux du carbone. Cependant, la disponibilité des données sur la repartitions des émissions au sein des différentes régions et l'absence d'effet de diffusion des secteurs intensifs au reste de l'économie, limitent l'intérêt de cet exercice sur un portefeuille diversifié. La prochaine question est donc de savoir comment prendre en compte le risque de transition associé aux émissions de GES dans un portefeuille diversifié, en tenant compte des effets en cascade dans l'économie réelle.

1.3.2 Effets en cascade du prix du carbone dans la chaîne de valeur

Nous évaluons l'impact de la tarification du carbone globale prenant en compte à la fois le coût des émissions idiosyncratiques des entreprises et leur diffusion intersectorielle. L'impact sur la valorisation des entreprises est partagé entre les entreprises intensives et les entreprises moins intensives grâce à l'introduction d'une répercussion du coût du carbone dans un modèle de diffusion sectoriel, basé sur une base de données mondiale d'entrées-sorties (en anglais, *world input output database*, WIOD). En nous concentrant sur les composants de l'indice MSCI World, nous montrons qu'en dehors des secteurs habituels à forte intensité de carbone, tels que l'énergie, les services publics et les matériaux, les secteurs moins intensifs en carbone, tels que l'industrie, la consommation de base, la consommation discrétionnaire et les technologies de l'information, peuvent contribuer de manière significative au risque global, en raison de la répercussion attendue du coût du carbone dans la chaîne de valeur. Les indices mondiaux pourraient connaître des changements significatifs dans leur univers d'investissement et leur composition sectorielle.

L'approche entrée-sortie de Leontief (1970) appliquée aux externalités environnementales Soit M le vecteur des émissions directes et indirectes (en amont) par secteur × pays (55 x 44). En notant $G = \boldsymbol{\mathcal{CI}}_1$ le vecteur des intensités directes (scope 1) du secteur × pays, CP le prix mondial du carbone et $\mathcal{E} = (\varepsilon_i, .., \varepsilon_n)^T$ le vecteur des montants en USD payé par émission directe ou indirecte, nous avons les relations suivantes :

$$M = \left(I - A^T\right)^{-1} \times G \quad \text{et} \quad \mathcal{E} = \text{CP} \times M \tag{1.3}$$

21. Obtenu en résolvant le système classique de Merton avec une valeur d'équité observable E_i et une volatilité $\sigma_E(i)$.

Les mesures d'intensité de carbone G sont construites à partir de l'intensité Scope 1 d'Exiobase (disponible sur 163 secteurs) et la matrice A des coefficients d'exigence directe (a_{ij}) est extraite de WIOD (mise à jour en 2015).

Estimation au niveau de l'entreprise Nous affinons ensuite la définition de M et de $\mathcal{E}$ en incluant les données au niveau de l'émetteur. Ainsi, nous résolvons ce problème pour chaque émetteur k faisant partie du i-ième secteur avec une intensité d'émission directe de scope 1 g^k (provenant de Trucost). Le vecteur des intensités d'émissions directes et indirectes m^k est défini au niveau de l'émetteur comme suit :

$$m^k = \underbrace{m_i}_{\text{intensité directe et indirecte sectorielle}} + \underbrace{\left(g^k - g_i\right)}_{\text{Écart relatif de l'intensité d'un émetteur par rapport à son secteur}} \tag{1.4}$$

Impact de l'introduction du prix du carbone Nous comparons ensuite les prix unitaires avant (p_i) et après $(p_i^{\varepsilon^k})$ l'introduction d'un prix mondial du carbone en supposant que le coût du travail et du capital (et donc la valeur ajoutée) sont les mêmes avant et après l'introduction du prix du carbone :

— Le **prix sectoriel de base (avant la tarification du carbone)**, comprenant la taxe *add-valorem*, le coût des intrants et la valeur ajoutée, peut être écrit comme suit :

$$p_i = (1+\tau_i)\left[\sum_{j=1}^{n} p_j a_{ij} + v_i\right] \quad \text{ou} \quad P = \left[(I - A_\tau)^{-1}\right]^T V \tag{1.5}$$

où la valeur ajoutée peut s'écrire $v_i = wl_i + rk_i$ avec w le prix du travail, l_i le coefficient d'intensité du travail, r le coût du capital et k_i le coefficient d'intensité du capital.

— Le **prix du secteur après l'introduction d'un prix du carbone**, le prix unitaire de l'émetteur k, tenant compte de ses coûts directs et de ceux liés au carbone dans la chaîne d'approvisionnement devient :

$$p_i^{\varepsilon^k} = (1+\varepsilon_i^k)(1+\tau_i)\left[\sum_{j=1}^{n} p_j^{\varepsilon^k} a_{ij} + v_i\right] \quad \text{ou} \quad P(\varepsilon^k) = \left[(I - A_\tau^{\varepsilon^k})^{-1}\right]^T V \tag{1.6}$$

La matrice A_τ^ε des exigences directes rend compte de l'impact du prix du carbone suivant Mardones et Mena (2020). En vertu des hypothèses susmentionnées et en normalisant à 1 les prix unitaires avant le choc, nous définissons l'impact de l'intensité de carbone directe plus celle en amont au niveau de l'émetteur à l'aide des équations (1.31) et (1.32) :

$$P(\varepsilon^k) = \left[(I - A_\tau^{\varepsilon^k})^{-1}\right]^T \times (I - A_\tau^T) \times P \tag{1.7}$$

$$\xi_i^k(\varepsilon^k) = \frac{x_i^{\varepsilon^k}}{x_i} = \frac{1}{p_i^{\varepsilon^k}} \tag{1.8}$$

$\xi_i^k(\varepsilon^k)$ est le ratio d'impact mesurant la réduction de la demande due à l'introduction du prix du carbone sur l'émetteur k. Cette approche donne une mesure complémentaire du risque lié au

carbone auquel sont confrontées les entreprises, du point de vue de la chaîne d'approvisionnement. Ensuite, nous comparons l'impact d'un choc direct uniquement avec celui de la diffusion complète du prix. Nous constatons par exemple que certains secteurs, tels que la fabrication d'ordinateurs, d'appareils électroniques et d'optiques, présentent une contribution importante au risque lorsque nous tenons compte des émissions de carbone en amont.

Impact sur l'indice de référence Nous illustrons l'impact sur l'indice MSCI World. Nous faisons l'hypothèse simplificatrice que le choc est entièrement transmis sur le prix des actions, de sorte que :

$$\Delta E_k(\mathrm{CP}) = (\xi_i^k(\varepsilon^k) - 1) \times \mathrm{EV}_k(0) \tag{1.9}$$

Pour chaque entreprise, son nouveau poids dans l'indice dépend du choc de bénéfice subi, ce qui entraîne un choc de sa capitalisation boursière.

$$E_k(\mathrm{CP}) = E_{k,0} - ES_k \times \mathrm{EV}_k(0) \quad \text{et} \quad w_k(\mathrm{CP}) = \frac{E_k(\mathrm{CP})}{\sum_k^N E_k(\mathrm{CP})} \tag{1.10}$$

où $E_k(\mathrm{CP})$ est l'estimation de la capitalisation boursière ajustée au flottant de l'entreprise k après l'introduction d'un prix du carbone CP, et $w_k(\mathrm{CP})$ est le poids correspondant dans l'indice. Nous montrons qu'en dehors des secteurs habituels à forte intensité de carbone, tels que l'énergie, les services publics et les matériaux, les secteurs moins intensifs en carbone, tels que l'industrie, la consommation de base, la consommation discrétionnaire et les technologies de l'information, peuvent contribuer de manière significative au risque global, en raison de la répercussion attendue du coût du carbone dans la chaîne de valeur. L'introduction d'un choc de 50 USD/tonne réduirait le poids des secteurs des services publics, de l'énergie et des matériaux de respectivement 18,8%, 8,6% et 4,7% en termes relatifs. Au contraire, les secteurs de la finance et de l'immobilier bénéficient du choc carbone en raison de leur intensité carbone directe relativement faible et de leurs émissions indirectes limitées de premier niveau (en amont) (augmentation relative de leur poids de 3,3% et 2,5%, respectivement).

1.3.3 Valeur de la dette des entreprises sous incertitude liée au scénario de transition

Nous proposons un modèle adapté à la gestion dynamique du risque de défaut lié à la transition en tenant compte de l'incertitude des scénarios. En particulier, nous élaborons un modèle pour la tarification et la couverture dynamiques des obligations d'entreprise sensibles aux risques de transition. Nous partons d'un ensemble de scénarios possibles et supposons que l'agent ne connaît pas le scénario à priori, mais déduit les probabilités de scénario postérieures à partir de l'observation des chocs de prix du carbone, qui sont modélisés par un processus de saut. Nous utilisons un modèle inspiré de Leland et Toft (1996) et de la littérature ultérieure sur le sujet, où le moment du défaut (ou de la restructuration) est déterminé de manière endogène par les actionnaires afin de maximiser la valeur des capitaux propres. Une hausse du prix du carbone déclenche donc une mise à jour des probabilités du scénario, ce qui entraîne une réévaluation instantanée de la valeur de l'entreprise et peut déclencher l'événement de défaut ou modifier la probabilité de défaut.

Dynamique de la valeur de l'entreprise Nous considérons une entreprise générant un flux de trésorerie continu stochastique V_t par unité de temps, qui est affecté par les réglementations visant à réduire les émissions de GES. Ces réglementations climatiques sont caractérisées par un processus de prix du carbone croissant $C_t = \sum_{i=1}^{N_t} \widetilde{Y}_i$, où N est un processus de Poisson doublement stochastique, dont l'intensité dépend du scénario de transition, et $(\widetilde{Y}_i)_{i\geq 1}$ est une séquence de variables aléatoires i.i.d. , indépendantes de N, représentant les ajustements du prix du carbone. Nous supposons qu'il existe n scénarios d'ambition environnementale croissante, et désignons par $\lambda_1, \ldots, \lambda_n$ les intensités de prix respectives, où $0 < \lambda_1 < \cdots < \lambda_n$.

La dynamique des flux de trésorerie de l'entreprise sous la mesure de probabilité risque-neutre est donnée par

$$\frac{dV_t}{V_{t-}} = \mu dt + \sigma dW_t - dL_t, \quad \text{avec} \quad L_t = \sum_{i=1}^{N_t} Y_i, \tag{1.11}$$

où W est un mouvement brownien standard indépendant de I et N, et $(Y_i)_{i\geq 1}$ est une séquence de variables aléatoires i.i.d. , indépendantes de W, N et I, qui déterminent l'impact du prix du carbone sur le flux de trésorerie. Par exemple, si l'entreprise a une intensité d'émission constante par unité de revenu, désignée par α, alors $Y_i = \alpha \widetilde{Y}_i$. Soit ν être la distribution de Y_1, $e := \mathbb{E}[Y_1]$, nous supposons que ν a un support borné appartenant à $(-\infty, 1)$ et tel que :

$$r + e\lambda_i - \mu > 0 \tag{1.12}$$

pour tous les scénarios i, où r est le taux sans risque.

Nous notons $\mathcal{F}_t = \sigma(W_s, N_s, s \leq t)$ le filtrage des observations, qui contient les revenus de l'entreprise ainsi que la trajectoire du prix du carbone mais ne contient pas le véritable scénario I, et $\hat{p}_t^i = \mathbb{E}[I = i|\mathcal{F}_t]$, la probabilité postérieure d'être dans le scénario i étant donné les observations disponibles au temps t. Alors l'intensité de N est donnée par $\hat{\lambda}_t = \sum_{i=1}^n \lambda_i \hat{p}_t^i$, et les probabilités filtrées sont données par

$$\hat{p}_t^i = \frac{e^{-\lambda_i t} \lambda_i^{N_t} \hat{p}_0^i}{\sum_j e^{-\lambda_j t} \lambda_j^{N_t} \hat{p}_0^j}. \tag{1.13}$$

Ainsi dans la filtration $(\mathcal{F}_t)$ le couple (V_t, N_t) est un processus de Markov non-homogène dans le temps. Nous introduisons également la notation pour l'intensité et les probabilités de saut avec une dépendance explicite sur N :

$$\hat{\lambda}^N(t) := \frac{\sum_i e^{-\lambda_i t} \lambda_i^{N+1} \hat{p}_0^i}{\sum_j e^{-\lambda_j t} \lambda_j^N \hat{p}_0^j}, \qquad \hat{p}_t^{i,N} = \frac{e^{-\lambda_i t} \lambda_i^N \hat{p}_0^i}{\sum_j e^{-\lambda_j t} \lambda_j^N \hat{p}_0^j} \tag{1.14}$$

Calcul de la valeur de l'entreprise et du prix de l'obligation L'entreprise paie un coupon continu b correspondant à une dette de valeur nominale K et de maturité T. À tout instant $\tau < T$, les actionnaires peuvent prendre l'une des deux décisions suivantes, en fonction de la valeur des flux de trésorerie futurs de l'entreprise. Tout d'abord, si la valeur des flux de trésorerie futurs est supérieure à la valeur notionnelle K de la dette, les actionnaires peuvent décider de rembourser la dette à la valeur notionnelle (événement de restructuration). Tandis que si la valeur des flux de trésorerie futurs est inférieure à la valeur notionnelle K de la dette, les actionnaires peuvent décider de déclencher l'événement de défaut, auquel cas les détenteurs d'obligations reçoivent la valeur des flux de trésorerie futurs. La date de défaut/restructuration est déterminée par les actionnaires

de l'entreprise afin de maximiser la valeur des capitaux propres. La valeur des flux de trésorerie futurs à l'instant t s'écrit :

$$\begin{aligned}\widehat{V}_t &= \mathbb{E}\Big[\int_t^\infty e^{-r(s-t)}V_s\Big|\mathcal{F}_t\Big] = \sum_{i=1}^n \mathbb{P}[I=i|\mathcal{F}_t]\,\mathbb{E}\Big[\int_t^\infty e^{-r(s-t)}V_s\Big|\mathcal{F}_t, I=i\Big]\\ &= V_t\sum_{i=1}^n \frac{\hat{p}_t^i}{r+e\lambda_i-\mu} = V_t\,\alpha_t^{N_t},\end{aligned}$$

où

$$\alpha_t^N := \sum_{i=1}^n \frac{1}{r+e\lambda_i-\mu}\,\frac{e^{-\lambda_i t}\lambda_i^N\hat{p}_0^i}{\sum_j e^{-\lambda_j t}\lambda_j^N\hat{p}_0^j}.$$

Le prix de l'obligation peut alors être écrit comme une solution à un problème d'optimisation :

$$B^N(t,V) = \inf_{\tau\in\mathcal{T}([t,T])}\mathbb{E}\Big[\int_t^{\tau\wedge T} e^{-r(s-t)}b\,ds + e^{-r(T\wedge\tau-t)}\widehat{V}_{T\wedge\tau}^{t,V,N}\wedge K\Big]. \tag{1.15}$$

Nous établissons théoriquement l'existence de seuils de défaut et de restructuration et étudions leurs propriétés. Notre résultat principal fournit une méthode d'approximation numérique du prix des obligations $B^N(t,V)$.

Proposition 1. *Soit $B^{N,M}(t,V):[0,T]\times\mathbb{R}_+\mapsto\mathbb{R}$, pour $N\le M$, défini comme suit :*

$$B^{M,M}(t,V) := G^M(t,V),$$

où pour chaque M, G^M est borné et continu de Lipschitz dans V et pour $N<M$, $B^{N,M}(t,V)$ et $\mathcal{T}^*([t,T])$ est l'ensemble des temps d'arrêt à valeurs dans $[t,T]$ adapté à la filtration du mouvement brownien $(W_s-W_t)_{s\ge t}$ est la solution de l' inégalité variationnelle

$$\min\{b-rB^{N,M}+\mathcal{L}^{N,M}B^{N,M},\alpha_t^N V\wedge K-B^{N,M}\}=0, \tag{1.16}$$

sur $(t,V)\in[0,T]\times\mathbb{R}_+$ avec $B^{N,M}(T,V)=\alpha_T^N V\wedge K$, où

$$\mathcal{L}^{N,M}f = \frac{\partial f}{\partial t}+\mu V\frac{\partial f}{\partial V}+\frac{1}{2}\sigma^2V^2\frac{\partial^2 f}{\partial V^2}N+\hat{\lambda}^N(t)\int_{-\infty}^1\big\{B^{N+1,M}(t,V(1-x))-f(t,V)\big\}\,\nu(dx). \tag{1.17}$$

Alors,

$$\lim_{M\to\infty}B^{N,M}(t,V)=B^N(t,V)$$

pour $N=0,1,\dots$ et $(t,V)\in[0,T]\times\mathbb{R}_+$, où la convergence a lieu à une vitesse plus rapide qu'exponentielle.

Cette proposition nous permet de développer un algorithme pour calculer le prix des obligations $B^N(t,V)$, en contrôlant l'erreur d'estimation. Le modèle est ensuite illustré par une étude de cas utilisant des données financières et d'émission de plusieurs entreprises et des scénarios de transition du NGFS. Nos résultats montrent que dans un contexte ou le scénario est incertain, les ajustements du prix du carbone sont plus susceptibles de déclencher un défaut que lorsque le véritable scénario est explicitement connu, car après chaque ajustement, le scénario le plus ambitieux sur le plan environnemental devient plus probable. Nous quantifions également l'impact de la vitesse à laquelle

les agents découvrent les informations sur le scénario sur le niveau des *spreads* de crédit et nous constatons qu'une découverte plus rapide des informations conduit à des *spreads* plus élevés car de meilleures informations permettent aux actionnaires d'optimiser le moment du défaut, ce qui augmente la valeur de l'option de défaut et diminue le prix de l'obligation. Notre modèle illustre donc l'importance de l'information sur les scénarios pour la fixation du prix des obligations dans un contexte de la transition environnementale. En particulier, nous constatons qu'une information insuffisante sur les prix futurs du carbone et une découverte lente de l'information peuvent conduire à une surévaluation des obligations susceptibles de faire défaut et à des événements potentiellement douloureux de défaut ou de réévaluation à l'échelle du marché lorsque l'information est finalement découverte.

1.3.4 Modélisation des risques physiques : le cas des cyclones tropicaux

Les cyclones tropicaux sont responsables d'une grande partie des dégâts résultant des catastrophes naturelles. L'estimation des dommages liés aux cyclones à l'échelle nationale est un défi suscitant un intérêt croissant dans le contexte de l'adaptation aux changements climatiques. Les modèles climatiques mondiaux, dont les sorties sont disponibles du projet de comparaison des modèles couplés (CMIP), ne résolvent pas les cyclones tropicaux. Nous introduisons donc un algorithme de génération de cyclones comprenant un module thermodynamique pour l'évaluation nationale intégrée des dommages (en anglais, *Cyclone generation Algorithm including a THERmodynamic module for Integrated National damage Assessment*, CATHERINA), couplant les relations statistiques et thermodynamiques pour générer des trajectoires synthétiques sensibles aux conditions climatiques locales et estimant les dommages induits par les cyclones tropicaux au niveau national. Cet algorithme est conçu pour être compatible avec les données des modèles CMIP offrant une solution fiable pour intégrer les cyclones tropicaux dans les projections climatiques. Nous l'illustrons en produisant des projections de dommages dans des scénarios de concentration représentatives (en anglais, *representative concentration pathways*, RCP) au niveau mondial et pour des pays individuels. L'algorithme contient un module permettant de corriger les biais des modèles climatiques en fonction des distributions des variables climatiques dans les réanalyses. Ce modèle a été développé en premier lieu pour répondre au besoin de la communauté économique et financière qui recherche des signaux quantitatifs permettant une meilleure évaluation des risques physiques à long terme, pour estimer, par exemple, leur impact sur la dette souveraine.

Intensité des cyclones tropicaux Les cyclones sont initiés avec distribution spatiale et saisonnière estimée sur la base de données IBTrACS de manière similaire à Bloemendaal *et al.* (2020). Soit $[t_1, t_2]$ une période de temps (de pas annuels) suffisamment large pour refléter le climat (et pas seulement la variation météorologique). Le nombre de cyclones pour chaque année $t \in [t_1, t_2]$ suit la distribution de Poisson avec un paramètre dépendant de la région : $N_t \sim \mathcal{P}(\hat{\lambda}_B)$. Nous utilisons les paramètres λ_B donnés dans Bloemendaal *et al.* (2020) et contrôlons le nombre de cyclones intenses qui touchent terre. La longitude et la latitude initiales sont attribuées en rééchantillonnant aléatoirement les coordonnées des genèses passées puis l'évolution temporelle de la latitude et de la longitude du centre du cyclone est décrite par un processus autorégressif (Bloemendaal *et al.*, 2020 ; James & Mason, 2005).

Le vent (utilisé dans la fonction de dommage) et la pression centrale (modélisée avec des variables climatiques) sont liés en utilisant la relation vent-pression (WPR), qui est calibrée séparément pour chaque bassin. L'intensité potentielle maximale, variable instrumentale utilisée dans le processus d'intensification, est définie le long de la trajectoire en suivant le cadre résumé dans Holland (1997) :

$$\mathrm{MPI}_t = \mathrm{MSLP}(x_t, y_t, t) \cdot \exp^{-X_t}, \tag{1.18}$$

$$X_t = \frac{\mathcal{E}_t \cdot \mathrm{SST}(x_t, y_t, t) \cdot \Delta S_t^m - \frac{f(y_t)^2 r_{env}^2}{4}}{R_d \cdot \mathrm{SST}(x_t, y_t, t)}, \tag{1.19}$$

$$\mathcal{E}_t = \frac{\mathrm{SST}(x_t, y_t, t) - T_{\mathrm{tropo}}(x_t, y_t, t)}{\mathrm{SST}(x_t, y_t, t)}, \tag{1.20}$$

$$\Delta S_t^m = R_d \ln\left(\frac{\mathrm{MSLP}(x_t, y_t, t)}{P_{t-1}^c}\right) + \frac{L_v(q_{c\,t}^\star - q_t^{env})}{\mathrm{SST}(x_t, y_t, t)}, \tag{1.21}$$

où (x_t, y_t, t) sont les coordonnées de l'oeil du cyclone, $\mathrm{SST}(x_t, y_t, t)$ et $T_{\mathrm{tropo}}(x_t, y_t, t)$ sont respectivement les températures de la surface de la mer et de la tropopause, $R_d = 287,058$ J.kg^{-1}.K^{-1} est la constante spécifique des gaz pour l'air sec, $\mathrm{MSLP}(x_t, y_t, t)$ est la pression locale moyenne au niveau de la mer, $\mathrm{RH}(x_t, y_t, t)$ est l'humidité relative proche de la surface à 2 mètres extraite du jeu de données mensuel d'ERA-5 (ou des modèles climatiques CMIP). $f(y_t) = 2\omega \sin(y_t)$ est un paramètre de Coriolis dépendant de la latitude, r_{env} est la distance entre l'œil et la zone dans des conditions régulières (fixée à 500 km). La différence de potentiel d'entropie humide ΔS^m est définie le long de la trajectoire en utilisant l'humidité spécifique dans l'œil (en considèrent une humidité relative à saturation) par rapport aux conditions environnementales ($q_c^\star$ et $q_{env}(\mathcal{RH})$) et L_v est la chaleur latente de vaporisation. Certains contrôles, tels que la chute de pression maximale observée pour la température correspondante et la relation de décroissance pour les cyclones évoluant au-dessus des terres, sont également ajustés pour chaque bassin et appliqués dans l'algorithme de génération de pistes synthétiques. L'extraction des variables climatiques de différents modèles nous permet de corriger les biais et d'évaluer l'incertitude des modèles. L'évolution de la pression centrale en fonction du MPI est décrite par l'équation stochastique autorégressive suivante (James & Mason, 2005) :

$$\Delta P_t^c = c_0 + c_1 \Delta P_{t-1}^c + c_2 e^{-c_3[P_t^c - \mathrm{MPI}_t]} + \varepsilon_t^P, \quad \text{avec} \quad \varepsilon_t^P \sim \mathcal{N}(0, \sigma_{P^c}) \tag{1.22}$$

Après trois itérations sur terre (i.e. pour $t > 12h$), nous appliquons la fonction de décroissance pour éviter de générer des dommages irréalistes trop loin de la côte (Bloemendaal *et al.*, 2020 ; Kaplan & DeMaria, 1995).

Exposition (SSP) et projections scénarisées Pour estimer les expositions futures le long des trajectoires des cyclones dans chaque scénario, nous utilisons l'estimation de la valeur du bien physique exposé (Eberenz *et al.*, 2020) et les coefficients représentant le changement entre l'état actuel et le scénario futur dans le cadre des voies socio-économiques partagées (Jones & O'Neill, 2020 ; O'Neill *et al.*, 2017 ; O'Neill *et al.*, 2014). L'exposition physique locale aux coordonnées (x, y) au temps t dans une région j dans le scénario k est définie comme suit :

$$\Phi(x, y, j, k, t) = \underbrace{(F_{\mathrm{GDP}}^{cap}(j, k, t))^{\alpha_1}}_{\text{Facteur macroéconomique}} \cdot \underbrace{(F_{pop}(x, y, k, t))^{\alpha_2} \cdot \mathcal{L}_P(x, y)}_{\text{Facteur local}}. \tag{1.23}$$

où $\mathcal{L}_P(x, y)$ est la densité de population locale provenant de Eberenz *et al.* (2020), le facteur F_{GDP}^{cap} est la croissance projetée du PIB par habitant pour chaque région à partir de base de données du SSP (Riahi *et al.*, 2017), et F_{pop} est le facteur de croissance de l'exposition de la population basé sur les projections locales de population (Jones & O'Neill, 2020). Nous introduisons les exposants α_1 et α_2 pour démêler les effets de l'augmentation de l'intensité des cyclones, de la croissance du PIB et de la croissance de la population sur les dommages futurs, ainsi que pour prendre en compte de manière simple une éventuelle adaptation future au risque de cyclone tropical.

Vulnérabilité (CLIMADA) et calcul des dommages Pour estimer la fraction des pertes dues à une tempête avec une vitesse de vent soutenue V, K. A. Emanuel (2011) a introduit la formule suivante :

$$f(V, v_h^j) = \frac{\left(\max(V - v_0, 0)\right)^3}{(v_h^j - v_0)^3 + \left(\max(V - v_0, 0)\right)^3}, \tag{1.24}$$

où f est la fraction de la valeur de la propriété perdue, $v_0 = 25,7$ m.s^{-1} et v_h^j un paramètre qui doit être calibré pour chaque région j récupéré dans Eberenz *et al.* (2021). Nous calculons les dommages causés le long des trajectoires synthétiques comme suit. Tout d'abord, une grille uniforme de valeurs de biens physiques avec un pas proportionnel au rayon moyen d'un cyclone est définie sur la carte du pays affecté. La trajectoire du cyclone est interpolée linéairement, et les carrés de quadrillage affectées par le cyclone sont identifiées. Ensuite, nous calculons la proportion de perte $f(V, v_h^j)$ à partir de la vitesse maximale du vent simulée. Puis nous calculons le dommage total en agrégeant sur chaque carré de quadrillage traversé par le cyclone, l'exposition des biens physiques locale multipliée par la proportion de richesse perdue. À la suite de cette procédure, nous obtenons le dommage total simulé $\text{SED}_i(j, t)$ causés par le i-ième cyclone dans la région j, simulé avec les variables climatiques de l'année t. Le coût des dommages causés par les cyclones dans la région j et l'année t est le suivant : $\mathcal{D}(j, t) = \sum_i \text{SED}_i(j, t)$, en sommant donc tous les cyclones survenant dans une année donnée. Cette procédure peut ensuite être répétée de nombreuses fois pour obtenir la distribution des dommages annuels causés par les cyclones et calculer d'autres statistiques telles que la moyenne et les quantiles de cette distribution.

Application financière Nous produisons des projections de dommages dans les scénarios de concentration représentatives (RCP) au niveau mondial et pour les pays individuels en utilisant les données du projet d'intercomparaison des modèles couplés (CMIP5). Nous proposons ensuite d'appliquer une spécification économétrique Hilscher et Nosbusch (2010) pour estimer comment le risque physique affecte les spreads ajustés de'option (OAS) des pays à travers l'impact des dommages directs sur le ratio dette/PIB. En raison de la plus grande vulnérabilité des pays émergents, nous décidons de nous concentrer sur les composants de l'indice JP Morgan EMBI. Contrairement à la littérature existante (Beirne *et al.*, 2020 ; Klusak *et al.*, 2021 ; Volz *et al.*, 2020), notre objectif est d'analyser l'impact des risques physiques sur les spreads des obligations souveraines de manière directe, en évaluant les dommages économiques de futurs cyclones synthétiques, sans passer par des modèles d'évaluation intégrée (IAMs). En effet, l'utilisation de tels modèles pour évaluer les dommages climatiques futurs est encore parfois perçue comme controversée dans la littérature (Auffhammer, 2018 ; Pindyck, 2017). Nous calibrons un modèle économétrique transversal pour le

spread (ajusté de l'option) sur la base de données annuelles de fin d'année :

$$\mathrm{OAS}_t = \alpha \quad + \quad \beta_6 \frac{L_t}{\mathrm{GDP}_t} + \sum_j C_j + \epsilon_t. \tag{1.25}$$

ici, l'OAS est le spread ajusté en fin d'année, issu du rapport de position de JP Morgan EMBI dans BarraOne et C_j sont des variables de contrôle qui permettent de construire un modèle expliquant plus de 70 % du spread des titres de l'indice JP Morgan EMBI. Le modèle couvre 74 pays entre 2010 et 2020. Pour chaque pays j de l'indice JP Morgan EMBI, nous évaluons la variation annuelle du spread des obligations due aux dégâts des cyclones, dans le scénario k pour l'année t en utilisant la formule suivante :

$$\Delta_{k,t}\mathrm{OAS}(j,k,t) = \beta_6 \times \frac{\mathcal{D}(j,k,t)}{F_{\mathrm{PIB}}(j,k,t)\mathrm{PIB}(j,2020)}, \tag{1.26}$$

où nous rappelons que $\mathcal{D}$ représente les dommages cycloniques annualisés, et F_{GDP} est le facteur de croissance du PIB pour le pays/scénario spécifié. Nos résultats suggèrent que les pays les plus pauvres peuvent subir des sauts de spread de crédit représentant un coût d'emprunt écrasant et inhibant leur capacité de reconstruction. En effet, nous avons constaté que les cinq plus grands événements observés dans le passé (y compris les inondations et les tremblements de terre) ont entraîné une hausse d'environ 20 points de base de l'écart de taux à 10 ans pour tous les pays considérés. En termes relatifs (c'est-à-dire en normalisant par le PIB des pays touchés), les 55 événements ayant générés le plus de dommage (dans EM-DAT) entraînent en moyenne une hausse de 5 points de base dans la fenêtre de 30 jours suivant la fin de l'événement signalé dans EM-DAT. En revanche, en termes d'impact prospectif des cyclones tropicaux, nous avons constaté que certains États peuvent être soumis à des chocs de spreads allant jusqu'à 200 points de base.

General Introduction

This thesis is part of a research project dealing with the integration of extra-financial and climate criteria in asset allocation strategies. It is the result of a three-year partnership between Amundi Asset Management and the Center for Research in Economics and Statistics (CREST). The research project initiated by Bennani *et al.* (2018) included several questions: (i) Investigating the impact of Environmental, Social and Governance (ESG) scores on bonds pricing; (ii) developing methodologies for climate-related risk measurement and management and (iii) developing alignment tools (carbon emission reduction strategies) for portfolio allocation. While the first and third objectives lead to several operational working papers published by Amundi Quantitative Research team (Ben Slimane *et al.*, 2019a; Ben Slimane *et al.*, 2019b; Drei *et al.*, 2019; Le Guenedal *et al.*, 2020; Le Guenedal, Lombard, *et al.*, 2022; Le Guenedal & Roncalli, 2022; Lepetit, Le Guenedal, *et al.*, 2021; Taleb *et al.*, 2020), this thesis focuses on the second aspect, that is on the development of methodologies to better quantify climate-related financial risk. This risk falls in two categories: the transition risk, arising from a sudden shift toward low-carbon economy, and the physical risk stemming from the increased frequency and severity of climate and weather events causing physical capital destruction and infrastructure malfunction. Transition risk is the center of attention in financial markets and is more likely to impact investment portfolios in the medium-term, in particular in the perspective of strengthening transition policies (Fankhauser *et al.*, 2022). However, transition risks are mitigated by the limited likelihood of governments implementing and maintaining regulations (potentially) harmful for their economy (Alessi *et al.*, 2021; Campiglio *et al.*, 2022; Y.-X. Zhang *et al.*, 2017).

On the other hand, the literature on physical risks is still relatively scarce in the field of finance, and mostly limited to the housing, real estate and insurance market. In particular, although there are numerous papers relative to local physical risks assessment, the process to define the classical triad of '*hazard*' × '*exposure*' × '*vulnerability*', is not generalizable to a global scale, and therefore to global investment portfolios. Since the landmark speech *Tragedy of the Horizons* by Mark Carney (2015), the interest of the financial community to physical risk has grown. However, the semantic gap between the worlds of climate science and finance (Bouchet *et al.*, 2022), making dialogue and interactions complex between two highly specialized communities remains an obstacle to a better understanding of physical risks. As a result, although the expected future damages are projected to grow in all studies, the integration of the physical risks in asset pricing models remains weak. In addition, the multi-hazards aspect of physical risk is another puzzle for their aggregation and easy integration in portfolio allocation decisions. However, the advances in climate science and physical damage modeling push us to adjust the quantification of the economic consequences of climate change (Auffhammer, 2018), and to propose forward looking methods to account for physical risks in the pricing of market securities.

This thesis is structured as follows. Chapters 2 to 4 focus on the transition risk dimension. Chapter 2 explores the sensitivity of credit risk to carbon price. Chapter 3 presents a structural method to include cascading effects of the carbon price in the value-chain. Chapter 4 introduces a novel bond pricing framework allowing to account for scenario uncertainty. Chapter 5 proposes a global structural approach for converting general circulation model (CGMs) climate projection data into material signals for pricing cyclone-related physical risks. In this general introduction we provide a (non-exhaustive) review of the literature on transition and physical risks and a section summarizing the main academic contributions of each of the aforementioned chapters.

1.4 Transition risks

Transition risks are business risks that arise from the shift to a greener economy. They are not directly caused by climate change but rather by policies to reduce global warming. For example, an industrial company relying on a carbon intensive process is at risk if the regulation strengthen. They can also come from a change in consumer demand. A car manufacturer can suffer losses if its offer does not meet the customers' expectations in terms of environmental requirements. Transition risk assessments are based on scenario analysis. The first step is therefore to understand the construction of these scenarios, that rely on integrated assessment models (IAMs). These models allow academics and policy makers, among other things, to derive the trajectory of the main control variable: the carbon price. Several studies investigate the transmission channels of the transition risk to firms' business and look for evidence of its integration in the equity (Bolton & Kacperczyk, 2021; Görgen *et al.*, 2019), corporate bond (Duan *et al.*, 2021) or option markets (Ilhan *et al.*, 2019, 2021). Apart from market approaches, the exposure to transition risk is measured with two main complementary methodologies: top-down methodologies using integrated assessment models (Vermeulen *et al.*, 2018a; Vermeulen *et al.*, 2019), and bottom-up approaches defining the risk at the company level (Monnin, 2018). In addition, there is a major concern about the systemic impact of climate-related risks, that are material for both the real economy and the financial system. Indeed, while the direct impact of transition risk on climate-relevant sectors can appear limited (e.g. 2 Investing Initiative, 2018; Aubert *et al.*, 2019; EIOPA, 2018; Schotten *et al.*, 2016; Vermeulen *et al.*, 2018a; Vermeulen *et al.*, 2019; Weyzig *et al.*, 2014 suggesting an average exposure around 10%; see Bouchet and Le Guenedal, 2020a, Figure 2), the possible cascading effects on the supply-chain (Cahen-Fourot *et al.*, 2019; Mardones & Mena, 2020) as well as the contagion of financial losses has also attracted much research (Battiston *et al.*, 2017; Roncoroni *et al.*, 2021) leading to multiple stress-test methodologies. In addition, several mathematical contributions have allowed a better understanding of the risks and market mechanisms in place (Pástor *et al.*, 2021; Pedersen *et al.*, 2021), or since recently, to account for uncertain jumps related to climate policy in the pricing of market securities (Agliardi & Agliardi, 2021), allowing a dynamic integration of transition risk.

1.4.1 Scenario design, policies and effective risk

Integrated assessment models Most transition risks methodologies are based on scenario analysis. Scenarios are derived from deterministic economic modeling of climate risk made by integrated assessment models (IAMs), introducing climate considerations in classic macroeconomic

modeling. The first '*point of contact*' was made by William Nordhaus' with the dynamic integrated climate economy (DICE) model (W. D. Nordhaus *et al.*, 1992) and the literature around these models has been growing ever since (Hourcade *et al.*, 2021). The integrated models most commonly used by practitioners and public institutions fall in two main categories: cost-benefit and technico-economic evaluation models. Cost-benefit optimisation models, such as the seminal DICE (W. D. Nordhaus *et al.*, 1992), essentially allow policy makers to draw a path for the social cost of carbon maximizing the welfare over time balancing the costs of (future) damage against those of (present) mitigation. The optimal GHG emission reduction rate is directly translated in terms of social cost of carbon. Although they are still popular and widely used in the fields of policy making and energy, cost-benefit models are based on strong functional and parameter assumptions and have relatively weak empirical applications (Kohler *et al.*, 2006), in particular in the field of finance, requiring finer sector (× country) granularity. On the other hand, the second category of models generally offers a high level of granularity in their representation of sectors, countries and their interactions and allows to determine the optimal (or least cost) path to reach a given concentration scenario without computing future damages. Among these models we can find for example, the EPPA model (Babiker *et al.*, 2001; Y.-H. H. Chen *et al.*, 2022; Y.-H. Chen *et al.*, 2015) from the MIT Joint Program or the IMACLIM-R model (Hourcade *et al.*, 2010) developed by the Centre International de Recherche sur l'Environnement et le Développement (CIRED). Regardless of their type, models can be sorted using three major characteristics: *(i)* their level of technological precision, *(ii)* the level of complexity of macroeconomic feedbacks, and *(iii)* the degree of realism of agent and markets. For example, models such as REMIND/MERGE/IMAGE/MESSAGE/CGAM have higher level of technological precision with a simpler representation of the world economy compared to EPPA, IMACLIM or E3ME (Cambridge Econometrics, 2019) offering better sector granularity and macroeconomic multi-sectoral feedbacks. Finally, the Stock-Flow Consistent (SFC) approaches (e.g. GEMMES, Giraud *et al.*, 2016) aim at better capturing market behavior accounting for imbalances. The best model does not necessarily obtain the best score for each characteristic, but has the best configuration to answer the question it was designed to address. In a report of Institut Louis Bachelier, Hourcade *et al.* (2021) further describe the essential prerequisites for a clear understanding and therefore use of integrated models and Le Guenedal (2019a) reviews the main mathematical representations used in the economic modeling of climate risks.

Cost of carbon These models offer different and complementary representations of the economy in several scenarios with varying levels of ambition in terms of transition. An agent is subject to transition risk if the conditions suggested by these models (in a scenario where the concentration of GHG have been successfully limited) are not compatible with its activity. Although these models provide several output variables from which the conditional probability of default could be deduced, the representation of sectors other than energy (and to some extent agriculture) is relatively limited (Hourcade *et al.*, 2021). Therefore, in practice, most of the studies assessing transition risk (on real economy and diversified portfolios) still focus on carbon price shocks exclusively. Indeed, from a financial risk management perspective, and assuming that carbon prices produced by IAMs are not necessarily explicit and may represent other transition mechanisms, this variable constitutes a suitable proxy of the regulatory risk incurred by a company. Moreover, unexpected jumps in carbon prices are more likely to impact the valuation of carbon intensive

companies than other more gradual measures. Nevertheless, we acknowledge that this is a limitation and that a better understanding of transition risk requires using variables beyond the price of carbon (Campiglio, 2016).

Transmission channels Several studies detail the theoretical channels through which transition risk may have an impact on financial risk (Colas *et al.*, 2018; Monnin, 2018; TCFD, 2017; Thom & Ralite, 2019). Transition risk may affect the economic and financial performance of a company at different levels. Once the first transmission channel to financial performance is defined, the impact on credit, liquidity or market risk (Basel Committee on Banking Supervision, 2021, 2022) can be quantified using already existing financial models.

First, the company's future cash flows may be affected by the transition through reduced revenues (due to reduced demand for carbon-intensive products and services), or growth in demand for transition-friendly products and services. Transition policies can also affect operating expenditure: the direct emission costs (carbon price) and incremental indirect emissions costs from the supply-chain, will represent additional costs for the companies. In practice, in a stress-test, using an *effective carbon price* allows us to shock exclusively the operating expenditure, while considering the *social cost of carbon*, would include the shift in demand (and transmission to revenues). On the other hand, the adaptation of production units to greener functioning, the research and development expenditures to develop new technologies must also be taken into account to assess company exposure to transition risks, through their capital expenditures. To some extent, whether the climate-related cost materialize through a carbon tax, reduction in demand or company investments, the modeling framework of transition risk and impact will be relatively similar.

A second axis of impact of the transition on valuation or risk is through the balance sheet and several studies empirically investigate these effects. A company can suffer losses due to the devaluation of its reserves (e.g. fossil fuel) or the *stranding* of its production capital due to loss of competitiveness in the context of higher cost of carbon for example. Literature on stranding assets particularly focuses on energy (e.g. coal, mining and fossil fuel) sectors (Caldecott, 2017; Caldecott, Harnett, *et al.*, 2016; Caldecott *et al.*, 2013; Caldecott, Kruitwagen, *et al.*, 2016). Transition risk may also amplify market risk and limit the refinancing capacity of companies. The measure of stock market response to transition risk has been extensively addressed (Andersson *et al.*, 2016; Bolton & Kacperczyk, 2021; Engle *et al.*, 2020; Faccini *et al.*, 2021; Görgen *et al.*, 2019; Gurvich & Creamer, 2021; Harris, 2015; In *et al.*, 2018; Roncalli *et al.*, 2020; Roncalli *et al.*, 2021) as well as the integration of ESG and environmental concerns in bond pricing and cost of debt (Apergis *et al.*, 2022; Baker *et al.*, 2018; Ben Slimane *et al.*, 2020; Duan *et al.*, 2021; Eliwa *et al.*, 2021; Hoepner *et al.*, 2018; Raimo *et al.*, 2021; Zerbib, 2019; R. L. Zhang, 2021). These transmission channels are nested as today's *market risk* is derived from investors perception of future cash-flow or balance sheet repricing. For example, Delis *et al.* (2019) showed that banks account for stranding risk in the cost of loans issued to energy companies and Bolton and Kacperczyk (2021) more recently found that intensive US companies stock returns were higher, suggesting that investors have started to expect a compensation for their risk relative to their carbon emission.

1.4.2 Methodological approaches

We distinguish several methodological approaches to measure transition risk (Bouchet & Le Guenedal, 2022).

Market measures In the field of asset management, a traditional method for risk management relies on the Capital Asset Pricing Model (Sharpe, 1964). This seminal framework was extended by several contributions introducing new risk factors to capture systematic risk premia: Fama and French (1993) first included size (SMB) and value (HML) risk factors. Then, Carhart (1997) added the momentum (WML), Baker *et al.* (2011) the low volatility (VOL) and finally Novy-Marx (2013) included the quality (QMJ) risk factors. Together, they form the traditional configuration in factorial equity investment strategies of the 5-factor model. These common market risk factors are constructed sorting companies within an investment universe by the corresponding characteristic (respectively market cap, share price, recent performance, volatility and gross profitability), and comparing the returns of higher vs. lower ranked groups. The difference of returns defines the market risk premia associated to the characteristic of the underlying. For example, we compare the returns of large and small businesses to construct the SMB (small-minus-big) risk factor. This method can be applied to ESG (Bennani *et al.*, 2018; Drei *et al.*, 2019) and transition risk using carbon emissions (or intensity) to build a brown-minus-green factor (Görgen *et al.*, 2019; Roncalli *et al.*, 2021). The advantage of this approach is its coverage, as we can compute the exposure of any stock (even without knowing its emissions). However, this approach is based on the assumption that the characteristic used, originally size, value momentum or low volatility, corresponds to a '*systematic*' investment strategy, which may not be the case for carbon emissions (yet). In the passive investment space, it is also common to perform minimum variance optimization by forcing a total score, ESG or emissions, to be above (or below) a certain threshold (Le Guenedal & Roncalli, 2022). This way we can both compute the difference of performance obtained by the optimized portfolio and construct low carbon indices. These empirical market approaches are widely used to monitor transition risk integration in asset prices, however, they are backward looking and therefore may not fully reflect the extent of the transition risk.

Direct valuation shock approaches consider a fixed share of losses to determine the global amount of exposure of different stakeholders. For instance, Weyzig *et al.* (2014) consider a 60% shock on fossil fuel stocks and a 30% shock to the value of bonds in this sector, which leads to estimated losses of between EUR 350 and 400 billion for all European financial institutions.

Top-down approaches include economic variables from IAM to estimate potential losses at the portfolio level. For example, Vermeulen *et al.* (2018a), Vermeulen *et al.* (2019) study the impact of a carbon price of USD 100 on sectoral value-added and financial indices with the NiGEM model. When a policy shock - reflected in the evolution of the carbon price - and a technological shock - which changes the production function - are combined, the average losses for all Dutch financial institutions are estimated to be between 2.5% and 11% of the initial value of assets over the next five years. This approach thus allows for geographic and sectoral specification in the measurement of transition risk, but does not account for firms' idiosyncratic factors.

Bottom-up approaches essentially assess transition risk at the issuer level. For example, Howard and Patrascu (2017) study the impact of a rise in the global carbon price to USD 100 per CO_2e increasing the costs for companies proportionally to their total induced emissions and find a 14% decrease in the aggregate EBITDA of the MSCI World Index. Other works, see for example UNEP (2018) and Monnin (2018), rely on a methodology developed by the firm Carbon Delta which includes expert opinions.

In the field of asset management, bottom-up approaches are more suited to the investment decision-making process. Therefore, we aim at answering the following question:

Question 1 ***How to compute a structural measure of firms' idiosyncratic credit risk sensitivity to transition risk, that does not use expert opinions but rather carbon price trajectories suggested by integrated assessment models?***

1.4.3 Direct exposure and cascading effects through supply-chain

Transition risk is systemic. While the first studies focused on the total amount of assets directly at risk, academics now increasingly consider the cascading effects of this risk on the financial system and the real economy.

Direct exposure Weyzig *et al.* (2014) analyze the exposure of EU financial institutions to fossil fuel companies and commodities. By then, the exposures (as a percentage of total assets) ranged between 1.3% for banks and 5% for pension funds. Giuzio *et al.* (2019) update these results by extending the scope to climate-relevant sectors, as defined by Battiston *et al.* (2017). Between 2014 and 2019, pension funds reduced their exposure to transition risk while banks and insurers have kept it constant. EIOPA (2018) also measures the transition risk exposure of insurers. Climate-relevant sectors account for 13% of insurance investment portfolios.

Supervisors also measure the financial system's exposure to transition risk at a national level. In France, banks' exposure to GHG-intensive sectors reached 12.7% of total credit risk exposure in 2015 and decreased slightly in 2017 (Aubert *et al.*, 2019). The fossil fuel sector accounted for approximately 20% of major risk exposures in 2013 and 16.5% in 2018, suggesting that the risk is taken into consideration by banks. Bank of England (2015, 2017) and Batten *et al.* (2016) consider two types of climate-related assets: securities of companies that may be directly impacted by regulatory limits to produce or use fossil fuels (10% of assets) and securities of GHG-intensive sectors (20% of assets). In the Netherlands, Schotten *et al.* (2016) estimate that the exposure of banks, pension funds and insurers to fossil fuel companies is between 2% (banks) and 5% (pension funds). They also conduct an review of exposure to carbon-intensive sectors, which is between 12.4% and 4.4%. While most studies focus on the EU financial system, 2 Investing Initiative (2018) conduct an analysis on Californian insurers' portfolios (and find an exposure of USD 4 000 billion).

Recently, Alessi and Battiston (2022) surveyed the exposure of financial institutions to transition risk and found, respectively 12% for investment funds, at 5% for banks and at 15.1% for insurers. On the other and they also introduce a greenness score (measured through the EU taxonomy), and found much lower exposures, i.e. 3.2%, 0.8% and 4.8% respectively. Although

the region, institutions, asset class (equity, bond, loan, commodity), and the definition of climate-relevant sectors varies, most studies converge toward the same result: financial institutions' average direct exposure to climate-relevant sectors ranges between 5 and 15%.

Cascading effect The transition (and physical) risk(s) can cascade through countries and sectors and spread among unaffected parts of the economy (Naqvi & Monasterolo, 2021; Raymond *et al.*, 2020). The first financial *climate stress-test* including cascading effect (within the banking sector) was proposed by Battiston *et al.* (2017) and recently extended by Roncoroni *et al.* (2021) with a focus on banks and investment funds. In these papers, authors focus on the financial system interconnectedness rather than on the physical supply-chain interdepencies (e.g. materials, resources, chemicals, fuel, etc.). Overall, several stress-testing frameworks for the financial and banking system have been proposed (Allen *et al.*, 2020; Alogoskoufis *et al.*, 2021; Dunz *et al.*, 2021; Gourdel and Sydow, 2021; Grippa, Mann, *et al.*, 2020; Nguyen *et al.*, 2020; Reinders *et al.*, 2020a, etc.), that are reviewed and classified in details in Cartellier (2022). Several transmission channels are investigated for both transition and physical risks including second round effects on the financial side, but again, with a minor inclusion of interdependencies related to the real economy.

Focusing on the sector diffusion of transition risks, Cahen-Fourot *et al.* (2019) use an Input-Output (IO) model to assess the exposure of economic systems to capital stranding cascades triggered by the reduction of fossil fuel production and use. They estimate how supply-side capital stranding propagates across sectors and countries via production networks. In particular, they provide sector-level estimates of the exposure of capital stocks to the risk of becoming unusable due to a marginal loss of primary inputs employed in a country's fossil fuel sector. Gemechu *et al.* (2014), Mardones and Mena (2020), and Muñoz-Zamponi and Mardones-Poblete (2016) develop a sector-level stress testing method based on the Leontief (1970) approach, allowing the effects of the diffusion of carbon tax costs to be measured across various sectors in the economy. For example, Mardones and Mena (2020) estimate the impact of environmental taxes on carbon emissions and local air pollutants introduced in Chile, and use the environmental extension of the Leontief (1970) price model and micro-simulations to analyze the main economic, environmental, and distributive effects of this policy. However, these exercises use sector-level information only, while application to portfolio stress-testing requires company level information. To our knowledge the consideration of the supply-chain risk is still limited in the literature and practitioners use exclusively emission scopes 2 and 3 (whose calculation standards are still sometimes uncertain) to estimate this risk. Based on these observations, we aim at answering the following question:

Question 2 ***How to compute the transition risk contributions among sectors with a better consideration of cascading effects through supply-chain but also firm-level direct carbon emissions?***

1.4.4 Scenario uncertainty

The future climate, climate-related economic policies (Alessi *et al.*, 2021; Barradale, 2014; Campiglio *et al.*, 2022; Helm *et al.*, 2003; Nemet *et al.*, 2014; Y.-X. Zhang *et al.*, 2017), and therefore climate-related financial risks are subject to deep uncertainties (Bolton *et al.*, 2020; Chenet *et al.*, 2019; Monasterolo *et al.*, 2019; W. Nordhaus, 2018b). They are related, among other factors,

to uncertainty about future availability of mitigation technologies and international cooperation (Edenhofer *et al.*, 2006); uncertainty of climate sensitivity and remaining global carbon budget (Cox *et al.*, 2018; Meehl *et al.*, 2020), uncertainty about tipping points, which may require bold immediate actions (Keen *et al.*, 2022; Weitzman, 2009), etc. In this context, perfect knowledge of the scenario corresponding to a fixed climate objective is clearly not a valid assumption. Although the deep uncertainty and unpredictability of climate-related financial risks is recognized by the literature, its impact on corporate debt, on banks' portfolios and on the resiliency of the financial system as a whole, is not sufficiently well understood. Accounting for multiple scenarios and scenario uncertainty in pricing procedures is therefore necessary.

Agliardi and Agliardi (2021) recently developed a model for defaultable perpetual bonds - incorporating uncertainty due to climate-related risks in addition to the uncertainty about corporate earnings. In their specification, the random policy shock and *degree of greenness* determine downward jumps in the firm value. Agliardi and Agliardi (2021) found the threshold value by equity value maximization and explicit the bond price value function solving the partial differential equation (PDE) characteristic of the price dynamics. Based on this recent paper, and including considerations from Leland (1994) and Leland and Toft (1996) where the firm can originally chose its optimal capital structure and the maturity if its debts, we aim at answering the following question:

Question 3 ***How to account for scenario uncertainty, gradually lifted by the observation of carbon price trajectory, in the pricing of the corporate debt?***

1.5 Physical risks

Transition risk has been the focus of the attention of the financial community. On the other hand, whereas the transition risk is in practice mitigated by the limited likelihood of governments implementing regulations harmful for their economy (Alessi *et al.*, 2021; Campiglio *et al.*, 2022), the exposure of our societies to physical risk does not cease to grow. These risks concern the financial losses that effectively come from climate change, and not from the mitigation measures aiming to prevent it. Causes of climate-related physical risks includes droughts, floods, storms, etc. Physical risks are far more difficult to quantify, as their evaluation requires multidisciplinary methodologies: climate modeling, physical asset geolocation, financial loss estimation, etc. We remark that the methodologies of analysis (Merz *et al.*, 2010), the main causes and drivers of damages (Merz *et al.*, 2021), the calculation of exposure (Jongman *et al.*, 2012; McGranahan *et al.*, 2007) and estimation of expected losses (Hallegatte *et al.*, 2013), including financial effects (Mandel *et al.*, 2021), related to both river and coastal floods are already addressed in several studies.

1.5.1 Modeling the intensity of extreme events

Climate data To measure the change in the intensity of a natural disaster, it is necessary to use climate data. There are three types of climate data sources from which we can design physical risk models: meteorological records, reanalysis and simulations by climate general circulation models (GCMs) whose outputs are becoming increasingly available (Tankov & Tantet, 2019). The first

corresponds to physical measures made in space and time, but these measures do not necessarily cover the entire grid. The second collects the outputs of a model that has been calibrated with meteorological records and gives the best estimates of past climate. Climate models are constantly improved and the different phases of the coupled model intercomparison project (CMIP) provide outputs of climate variables. For instance, the latest results used by the intergovernmental panel on climate change (IPCC) are based on the sixth phase of the project (CMIP6). Then, we must extract the climate variables required to model each hazard. Floods and droughts-related damage estimation mainly requires precipitations and humidity-related variables from climate models, [22] while storms or tornadoes [23] are much more complex to model.

General Circulation models (GCMs) and data treatment Climate models produce biased climate data. It is therefore necessary to use several models to take these biases into account. Moreover, it is possible to correct biases with respect to observations, on the basis of historical meteorological data or reanalysis, assuming that the correction function will be the same in the future. For example the *cumulative distribution function-transform* (CDF-t) method developed in Michelangeli *et al.* (2009) and Vrac *et al.* (2012) allows to correct the distribution of climate variables. This type of bias correction approach similar to a quantile-quantile adjustment, is standard in the climate community (Navarro-Racines *et al.*, 2020) and toolboxes are being developed to ease climate data handling by practitioners (Pérez-Zanón *et al.*, 2021).

Hazard modeling and sensitivity to climate change A key step is to define the sensitivity of the intensity of extreme events to change in raw climate variables. For floods or droughts, this step can be relatively direct from precipitation and humidity variables from GCMs and hydrological and water balance models such as PCR-GLOBWB (Sutanudjaja *et al.*, 2018) or NOAH-MP (Niu *et al.*, 2011; Yang *et al.*, 2011), [24] LISFLOOD (Sosa *et al.*, 2020; Van Der Knijff *et al.*, 2010), or specific to coastal risk with DIVA (Hinkel & Klein, 2009), etc. For example, using the CGMs of CMIP5, Tabari (2020) reports that approximately 72% of the global land is likely to go through aridification in the future. They also found flood intensity increases with global warming at the rates of 5.07%/K for humid, 3.63%/K for semi-humid and 3.12%/K for semi-arid climate regions. Most of the uncertainty about future floods comes from uncertainty in precipitation, which is relatively low (CMIP5 planetary sensitivity in extreme precipitation is below 6 %/°C, Kharin *et al.*, 2013).

Concerning tropical cyclones, the thermodynamic theory is developed in several seminal contributions by K. A. Emanuel (1988, 1999) and Holland (1997). The rise of sea surface temperatures (Pachauri *et al.*, 2014; Solomon *et al.*, 2007) increases the amount of energy available for cyclones to grow in intensity (K. A. Emanuel, 1991), which is already measurable. Indeed, K. A. Emanuel

22. In addition to multiple additional data, mainly *static*: topology, soil properties, runoff coefficients, land-use, etc.

23. Tornadoes arise from severe thunderstorms in warm, moist, unstable air along and ahead of cold fronts; they are more likely to form with large values of both convective available potential energy (CAPE) and deep-tropospheric wind shear. Climate change should increase the CAPE but decrease wind shear (Brooks, 2013). Therefore, the global response of tornadoes to climate change remains limited (J. Elsner & Guishard, 2014).

24. Note that pre-processed bias corrected data for "*Water sector indicators of hydrological change across Europe from 2011 to 2095 derived from climate simulations*" is available on the Copernicus climate data store.

(2005) demonstrated an increase of the intensity index of tropical cyclones over the 30-year period since the mid-1970s. The current scientific consensus projects intensity increases of 2 to 11% by 2100 with lowering frequency by 6 to 34%, but an increase of most intense cyclones and associated precipitations(T. R. Knutson *et al.*, 2010). Concerning extra-tropical storms or European winter-storms, the literature also suggests significant increase of intensity and potential losses increasing by 25% on average in Germany for example (Donat *et al.*, 2011). Recently, Kossin *et al.* (2020) also demonstrated the increasing trend of major tropical cyclone threshold exceedance probability and this trend is clearly observable in the Atlantic basin (J. B. Elsner *et al.*, 2008). However, to our knowledge there are no integrated tools allowing to produce future cyclone tracks from climate data as for floods.

Question 4.a ***How to build a database of depressions (tropical cyclone 'candidates') that would be compatible with Monte-Carlo financial risk assessment, from widely available climate data?***

1.5.2 Asset exposure

The geolocation of the exposed assets is an important data in the context of physical risks. Corporate level assessment requires to have the geolocated facilities on which the business of the issuers depends. For country exposure estimation some open-source initiatives allow to both estimate the current risk at the country level and to generate some projection factors. To fully apprehend a country physical risk exposure in short and medium term, (multi-hazard) indicators can be defined following multiple dimensions: physical infrastructure costs in populated areas including the replacement costs and potential adaptation, energy sector exposure, transports resiliency, agriculture and food supply, water distribution system, (etc.) to properly measure economic impacts. To project asset exposure in the long-term, we could use the aforementioned breakdown of key elements and assume a similar distribution in the future. However, in the context of long term assessments or for comparability reasons, it may be interesting to use a more aggregated view of global physical asset value distribution (using for example nightlight intensity, see Eberenz *et al.*, 2020). Nevertheless, the relevant literature on physical exposure generally treats these key elements independently. For example a considerable literature addresses the direct exposure of population, energy or transportation systems:

- **Population**. Several studies measure the exposure of population and infrastructure to natural disasters. McGranahan *et al.* (2007) reported that 13% of the world urban population lived in the Low Elevation Coastal Zone (LECZ). The exposed populations in the LECZ are projected to increase by more than 50%; from 625-880 million in 2000-2030 to approximately 1.4 billion, given the population density in exposed area of 534 people/km^2, in 2060 representing 12% of the world population in the scenario considered (Neumann *et al.*, 2015). Concerning tropical cyclones, Geiger *et al.* (2021) finds that the population exposure grows by 26% per year (33 million people) for each degree increase in global mean surface temperature without considering population expansion. Kumar and Taylor (2015) focus on South Pacific and demonstrate that Pacific island countries (PICs) are facing high risks with 57% of the infrastructures near coast (500 km), which represents an exposure of USD 21.9 billion. Bretz (2017) and Kousky *et al.* (2020) suggest that 1.8% of total housing in the United states

will be inundated by 2100. Gurran *et al.* (2013) focusing on Australian exposure found that 85% of this country population were exposed to climate-induced risks.

- **Energy**. The impacts of climate change on the power sector have been estimated through two main channels: loss in energy production efficiency and infrastructure damage. Both impacts can potentially result in financial value loss (reduced future cash flows, physical capital stranding, etc.). First, the efficiency of power plants will be affected. Indeed, in the United States and European Union 91% and 78% of electricity, respectively, is produced with thermoelectric (nuclear and fossil-fuel) power plants, which are sensitive to both ambient air temperature and water availability and temperature. Therefore, energy production is likely to suffer efficiency reduction estimated to range between 4.4 to 16% and in Europe and 6.3 to 19% in the United States (Van Vliet *et al.*, 2012). Several studies (Linnerud *et al.*, 2011; Petrakopoulou *et al.*, 2020; Rübbelke & Vögele, 2011) explore this reduction of efficiency. Sathaye *et al.* (2012) estimate the impact of expected warming on energy production efficiency but also on risk of flooding and find that 25 coastal power plants and 86 substations are at risk of flooding in California. To measure this risk in practice, the Global Power Plant Database (Byers *et al.*, 2018), is making available geolocation data for an increasing number of plants (c.f. Figure 1.4), which could ease future physical exposure assessment. Note that the power plants can be affected but also the network. Some studies therefore focus on energy network resiliency and the cascading effect caused by damage inflicted by natural hazards (Albert *et al.*, 2004; Duenas-Osorio & Vemuru, 2009).
- **Transport**. Efficient transportation systems are key for prosperous economies (Koks *et al.*, 2019) and weather is already the main cause of additional cost in the transportation system maintenance. Indeed, 30% to 50% of maintenance costs of roads in Europe are associated with weather and approximately 10% of these costs (EUR 0.9 billion /year) are generated by extreme weather events alone (Nemry, Demirel, *et al.*, 2012, p. 5). Koks *et al.* (2019), based on openstreetmap (OSM) data, found that, the global expected annual damage on road and railway infrastructure assets ranges from 3.1 to 22 billion US dollars, and that investing in flood protection would have a positive return around 60%. [25] The question of resiliency of transportation systems and supply-chains goes beyond roads and terrestrial transportation. For example, Verschuur *et al.* (2020) assesses the port disruptions due to natural disasters across 27 events. For instance, there is potentially a ten day disruption in U.S.A. associated with a 35 $m.s^{-1}$ wind speed and/or 2.5 m storm surge. The World Bank suggests that low- and middle-income countries would need to spend between 0.5-3.3% of their GDP annually (US 157 billion to 1 trillion) on new transport infrastructure by 2030, plus the maintenance cost non accounted for in these figures (Rozenberg *et al.*, 2019; Rozenberg & Fay, 2019).

Scenario-based exposure The definition of the *hazard* × *exposure* × *vulnerability* for each hazard and each key element is complex and risk contributions are even more difficult to aggregate at a country or a portfolio level. In addition, the assessment of future damages requires to take into consideration multiple socioeconomic factors. Literature on tropical cyclone-related damage

25. Authors measured the damage caused by tropical cyclones, earthquakes, surface flooding, river flooding, and coastal flooding. Authors use probability maps for each hazard on different return periods. For example, they use five return periods (between 1/50 years and 1/1000 years) for wind speed distribution for tropical cyclones.

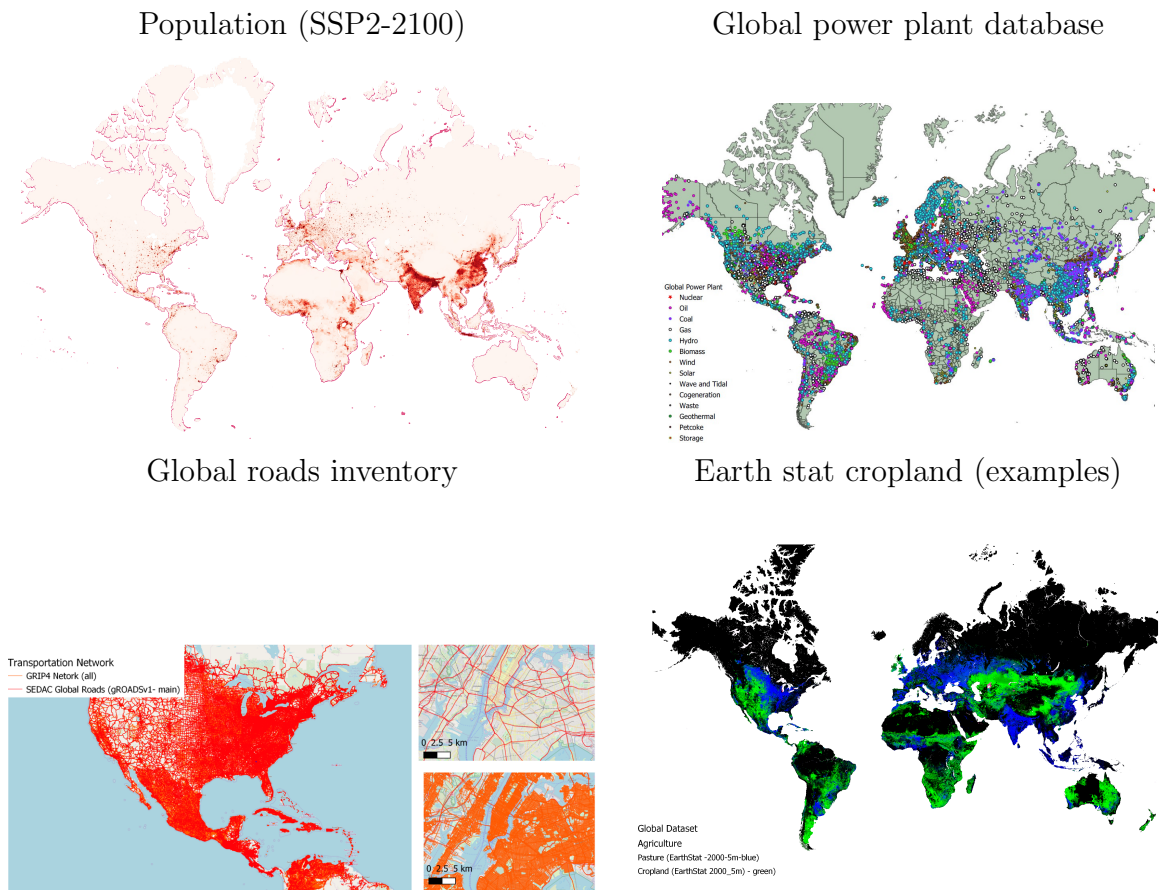

Figure 1.4 – Some open-source data source for physical asset representation: SEDAC (Jones & O'Neill, 2017), Global power plant database (Byers *et al.*, 2018), Global roads (Meijer *et al.*, 2018) vs. SEDAC global Roads (gROAD), Earth stat

shows that the projection of these socioeconomic factors is responsible for a large share of change in expected damage (Noy, 2016; Pielke Jr *et al.*, 2008; Weinkle *et al.*, 2018; Weinkle *et al.*, 2012; Ye *et al.*, 2020). If the definition of local asset value is a challenge, it is even more challenging to project this estimate into the future. Nevertheless, there are some initiative to distribute physical capital and population in the shared-socioeconomic pathways (SSP). For example, Jones and O'Neill (2017) deployed high quality raster data under each of the five shared socio-economic pathways (SSPs) used by the IPCC [26] to project population in the long-term including rural- vs. urbanisation assumptions. In addition, more aggregated projection of GDP and population are also broadly available outputs of the IAMs used by the IPCC. However, these long-term projection factors cannot be used directly with physical infrastructure inventory (as it would not be relevant to multiply the value of a power plant today by the change in population and or GDP/per capita, to compute its future value). However, Eberenz *et al.* (2019, 2020) downscale physical asset value on 32 arc-second grid using nightlight and population to spread the global physical asset index on a thinner grid. Although for mid-term estimation, the inventory approach is to be preferred, this

26. A light version available on the Socio-Economic Data and Application Center (SEDAC) website and at 1km (here)

approach is suited for longer term projections.

Question 4.b ***How to define physical asset exposure in such a way that (i) it represents sufficiently well real local asset value (ii) it can be projected in shared-socioeconomic scenarios?***

1.5.3 Vulnerability and damage modeling

Beyond GDP sensitivity to global average temperature Damage functions are introduced in the cost-benefits IAMs to model the impact of the increase of global average temperature on the global domestic product (Hanemann, 2008; W. Nordhaus, 1993, 2018a; Weitzman, 2009, 2010, 2012). The use of this function to determine the optimal policy mitigating future damage has been largely criticized (Auffhammer, 2018; Pindyck, 2017). However, their use is justified in physical risks assessment when considering particular hazards and assets.

Damage functions $\Omega_j(I) \in [0,1]$ are defined from historical records as the fraction of loss of an asset with respect to the hazard intensity I. They are calibrated on past reported damages (insurance claims, economic loss, etc.) using the appropriate indicator representing the event intensity. In the case of storms (tropical cyclone, European winter storms, tornadoes etc.), the damages are generally defined from maximum winds ($m.s^{-1}$) or central pressure (hPa). Concerning floods, direct flood damage is commonly done using flood depth (m). The functions return the fraction of losses that would occur at specific water depths per asset or per land-use class (see European floods damage functions in Figure 1.5, Huizinga *et al.*, 2017). Drought intensity can be represented with standard precipitation index and evaporation (Bachmair *et al.*, 2017; McKee *et al.*, 1993; Vicente Serrano *et al.*, 2010) but they are more likely to affect energy (through reduction in efficiency) or agriculture sectors. In the case of agriculture risk, the maximum number of consecutive frost/wet or dry days and duirnal temperature range or other agroclimatic indicators can be used to define parametric damage functions.

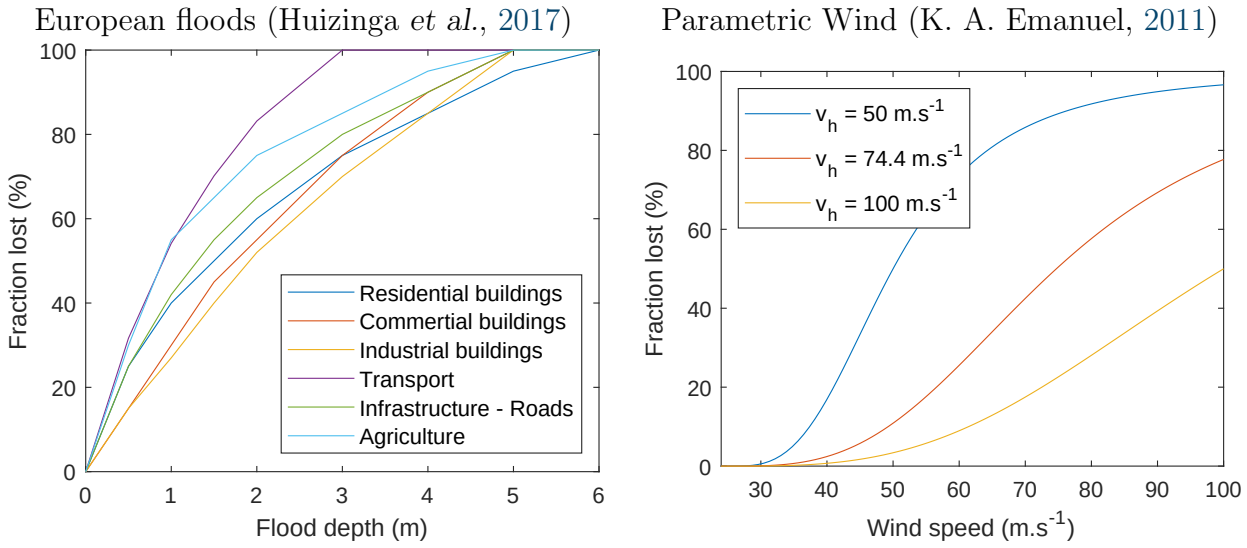

Figure 1.5 – Example of applied physical damage function

Literature on damage functions There is a rich literature on physical damage functions. For example, Prahl *et al.* (2015) describe mathematical specification (and calibration on insurance data) of damage functions for storms and other natural hazards on residential buildings in Germany Prahl *et al.* (2016). In flood risk assessments, the damage functions used are generally those defined in Huizinga *et al.* (2017). In addition to depending on the peril, these functions can be calibrated to different types of asset. For example, the functions for various building types in Europe are represented in Figure 1.5. [27]

For storm-related damages, there are several studies on wind damage functions for residential buildings in America, Australia, Europe or Japan (Crompton & McAneney, 2008; Ginger *et al.*, 2010; Hart, 1976; Pita *et al.*, 2015; Prahl *et al.*, 2015), but less research is available for other building types (commercial, industrial, transport, etc). [28] Nevertheless, Unanwa *et al.* (2000) developed a decision tree framework to assess wind vulnerability of varying building types based on their structure, distinguishing commercial, institutional and residential buildings. Decision-tree or purely conditional frameworks are also suited when no explicit functions can be fitted. For example, for roads, Koks *et al.* (2019) assume that extreme winds result in the clean-up cost of falling trees (when the cyclone winds exceed 42 $m.s^{-1}$ (~151 $km.h^{-1}$, Virot *et al.*, 2016) and if the tree density around the asset is at least $10/km^2$ (Crowther *et al.*, 2015).

For buildings vulnerability, Unanwa *et al.* (2000) suggest that the commercial and institutional buildings are respectively slightly and significantly more vulnerable than residential and mid-rise buildings. This study reveals that wind above 43-60 $m.s^{-1}$ generates generalized damage and sustained wind regime above 73 $m.s^{-1}$ could lead to the destruction of most buildings entirely (expect for mid and low-rise). More precise descriptions of building vulnerability are provided in the Federal Emergency Management Agency (FEMA) reports setting a standardized methodology and software (Hazus). The underlying assessment methods for estimating potential losses from earthquakes, floods, hurricanes, and tsunamis are described in FEMA (2009).

A remaining pitfall to assess assets vulnerability to storms, and particularly tropical cyclones, is that damages can be caused in practice by multiple sub-perils, which are not always perfectly reported in a harmonized way (i.e. not in EMDAT for example). Nevertheless, the wind speed remains a good indicator of potential damages. Finally, in the particular context of our forward looking and long-term assessment we do not use real infrastructure inventory, but a proxy of downscaled physical asset value. Therefore, the damage function must be defined for this specific data set.

Aznar Siguan and Bresch (2019), Bresch (2017), and Lüthi (2019) set up a platform for physical risk estimation (CLIMADA), coupled with a database of estimated values of local assets (Eberenz *et al.*, 2019, 2020). Instead of engineering-based approach, Eberenz *et al.* (2021) opted for a parametric functional (c.f Figure 1.5). They use the specification introduced by K. A. Emanuel (2011), depending on a hyper-parameter v_h setting the level of vulnerability of the considered asset group (region), to the considered intensity indicator (wind). The higher $v_h(j)$, the lower the region j is impacted by the wind. We note that the adaptation effort can be reflected by changes in this parameter or determined to mitigate the expected damages. [29]

27. Also available for North America, Asia, center and south America, Africa and Oceania.

28. The construction period can be used as pivot parameter as the performance of these buildings should be similar when constructed at the same period, Unanwa *et al.* (2000).

29. For example, focusing on coastal flood damages Prahl *et al.* (2018), also determined urban protection cost.

Question 4.c ***How to compute the damage related to tropical cyclone along synthetic tracks?***

From physical damage to economic or financial loss Once physical damages are computed, one must define the transmission channels from the direct damage to economic losses. Indeed, the damages related to disasters fall in two categories (Le Guenedal *et al.*, 2021b): the direct physical losses, possibly insured, and the longer-term economic consequences of the event. [30] The propagation of damages in the economic system makes the longer-term economic impacts more complex to estimate. To address this difficulty, Hallegatte (2008) introduced an input-output framework and defined the economic amplification ratio (EAR) as the multiplier between direct cost and the total economic damage. Note that this amplification ratio may already be accounted for in reported damages (e.g. Guha-Sapir *et al.*, 2018). Finally, the losses suffered by a country might affect financial assets globally. Estimating the cascading effect of physical risk would require to combine the physical supply-chain effects and financial contagion (Bressan *et al.*, 2022; Mandel *et al.*, 2021).

For various hazards, assets and damage functions, several studies assessed the (potential) future expected losses induced by natural disasters or climate change, with a greater focus on flood risk. For example, Hallegatte *et al.* (2013) provide an economic quantification of potential flood losses in the 136 largest coastal cities. In their estimations the flood losses (USD 6 billion/year in 2005) are expected to reach USD 52 billion/year in 2050 only projecting socio-economic change. [31] In the baseline scenario, i.e. with no adaptation investments, the impacts on these cities are projected to USD 1 trillion. Vousdoukas *et al.* (2018) suggest that without further adaptation investments, [32] the present expected annual damage (EAD) of coastal losses of EUR 1.35 billion could range between EUR 93 and 961 billion in Europe. In all, most find significant damage and expected increase with climate change. The next question becomes does the market integrate this information? Has it in the past, and should it in the future?

1.5.4 Financial risk

The question of pricing of physical risks by the financial markets has not been fully addressed in the academic literature. However, practitioners have started to take some physical risks into consideration. In particular, local exposures to tropical cyclones are already priced, through the cat-bond market (Bantwal & Kunreuther, 2000; Morana & Sbrana, 2019) and/or relative spread of

30. For instance, the direct costs of hurricane Katrina are estimated to USD 125 billion (2005), among which USD 80 billion were covered by insurance (EMDAT and Swiss Re Group (2020)). The consequences of the cyclone on the U.S. economic growth, which went down from 4.1% in the third quarter of 2005 to 1.7% in the fourth quarter before bouncing back to 5.4% in the first quarter of 2006, and on U.S. oil production (19% of which was damaged) increased this cost further. It is sometimes hard to define long-term economic impact of the cyclone. For instance, cyclones often destroy agriculture and live stock, which affects the economy during a longer period. For instance, hurricanes Irma and Maria in 2017 in Dominica destroyed 100% of agricultural plantations, while Yassi in Australia in 2011 destroyed 75% of agricultural plantations in the affected areas.

31. For instance, the population in massive coastal cities is projected to grow by 25% by 2050 (Aerts *et al.*, 2014).

32. On the other hand, most of these studies do not account for adaption. For example Prahl *et al.* (2018) includes the protection cost curve. This study also offers (Fig. 5) some comparative analysis with Hallegatte *et al.* (2013) (and Hallegatte *et al.* (2011) for Copenhagen) of Expected loss per meter of height inundated per cities.

the states and local issuers in the municipal bonds markets. Recently, Rizzi (2022) suggested that adaptation (more precisely natural capital protection) is priced in the municipal bond market. Similarly, Harvey and Irma clearly impacted the price of the cat-bonds when they made landfall in the United States in 2017. Dimov and Parsons (2021) studied the impact of historical cyclone landfall on the equity performance of manufacturers owning facilities located in the region affected by a given storm. For U.S. companies, they observed both "*a statistically significant negative pre-landfall drift and a significant positive post-landfall drift*". On the academic side, Lanfear *et al.* (2019) also showed that stock markets responded to storm information using an event study approach. These studies suggest that tropical cyclones are good candidates for measuring the impact of climate change on portfolios. However, the impact on countries has not been clearly established.

Beyond tropical-cyclone related risks, it is unclear if the financial markets fully price changing climate conditions. For example, on the equity side, Hong *et al.* (2019) investigate if food stocks efficiently discount the long term drought risk and find that food stock prices are *underreacting* to climate change risks. Gostlow (2019) using a factor approach finds that physical climate risk do not explain stock returns. Using text-based factor approach, Faccini *et al.* (2021) did not find evidence of significant integration of the news related to natural disasters.

On the other hand, Dey (2022) finds evidence of the impact of coastal floods on sovereign credit default swap (CDS) spread. A number of recent articles and reports address the impact of climate change on sovereign default risk (Beirne *et al.*, 2020; Klusak *et al.*, 2021; Volz *et al.*, 2020). In particular, the report (Volz *et al.*, 2020) (see Table 4 therein) identifies multiple transmission channels through which physical and transition climate risks may impact sovereign bond spreads and default probabilities. Beirne *et al.* (2020), show, through econometric analysis, that climate risk vulnerability and resilience are already significant determinants of the sovereign bond spreads. The article (Klusak *et al.*, 2021) simulates the effect of climate change on sovereign credit ratings under alternative warming scenarios. Their methodology is based on a statistical rating prediction model, combined with a macroeconomic growth model to project the impacts of global warming on GDP. These results are consistent as it makes sense for the corporate market to be mainly concerned by transition risk and for sovereign bonds or CDS to reflect issuing countries' exposure to longer term risks.

From a more theoretical perspective, Mallucci (2020) assessed the impact of disasters on Caribbean sovereign islands using dynamic general equilibrium models approach (Eaton & Gersovitz, 1981) and found that disaster risk reduces government's ability to issue debt and that climate change further restricts government's access to financial markets. The downside of the use of dynamic general equilibrium modeling framework is that it makes the assessments complex to transpose at a portfolio level. Tsai and Wachter (2015) and Wachter (2013) also formalize the pricing of assets subject to disaster risk. Karydas and Xepapadeas (2019, 2021) develop a framework to price physical risk linking carbon emission, mitigation investments and portfolio composition. They model the impact of rare disasters on equity premium (global aggregate) and sovereign interest rates.

To our knowledge, there is no integrated methodology describing the full transmission channel of the physical risk (from raw climate variables) to asset prices and allowing to evaluate the physical risk at a portfolio level in a bottom-up fashion. This leads us to this final question of this thesis:

Question 4.d ***What might be the impact of the annualized tropical cyclone-related damages on emerging countries spread?***

1.6 Main contributions

1.6.1 Credit risk Sensitivity to Carbon Price [33]

One of the ways to achieve the goals set by the Paris climate agreement is to set an effective price on carbon. In practice, there exist two main carbon pricing systems: carbon taxes and the emissions trading systems (ETS), which together cover an increasing number of issuers. [34] Rapid fluctuations in the effective carbon price can represent a risk for companies' businesses and impact their creditworthiness. Using the Intergovernmental Panel on Climate Change (IPCC) scenarios, this study analyses the credit risk sensitivity of 763 international companies in the medium (2024) and long term (2060). The Energy, Utilities, and Materials sectors are the most affected, with a higher and more heterogeneous risk for the Utilities. However, this risk is only significant in the 1.5°C and 1.8°C scenarios and materializes in the long term. A strengthening of greenhouse gas emission pricing mechanisms therefore seems achievable in the medium term without compromising financial stability.

Measuring the scenario-based probability of default with Merton (1974) framework
Let $\boldsymbol{\mathcal{CE}}_{1,i}$ be the direct annual carbon emission (scope 1) of company i with constant earnings before interest, taxes, depreciation, and amortization (EBITDA_i) and $\text{CP}(\text{k},\text{t})$ be the carbon price in the scenario k at year t. We define the direct carbon cost-related shock as:

$$\xi(i,k,t) = \frac{\boldsymbol{\mathcal{CE}}_{1,i} \times \text{CP}(\text{k},\text{t})}{\text{EBITDA}_i} \tag{1.27}$$

Introducing this direct shock in the Merton (1974) model gives the scenario-based distance to default:

$$\text{DD}(i,k,t) = \frac{\ln\left(\frac{(1-\xi(i,k,t)) \times V(i,k=0,t=0)}{D(i)}\right) + \left(r + \frac{1}{2}\left(\sigma_V(i)\right)^2\right)T}{\sigma_V(i)\sqrt{T}} \tag{1.28}$$

where σ_V is the volatility of the asset value V, r the risk free rate, T the maturity (1 year) and D the total debt. The theoretical probability of default PD of an issuer is:

$$\text{PD}(i,k,t) = \Phi(-\text{DD}(i,k,t))$$

33. This chapter is derived from Bouchet and Le Guenedal (2020b) that received the GRASFI Best Paper Prize for Research on Climate Finance (sponsored by Imperial College London) in 2020. This revised version is published in the *Revue Economique* special issue of march 2022 on transition risks, 73(2), Bouchet and Le Guenedal (2022).

34. Information about state-of-art of carbon pricing mechanisms are made available by the World Bank, I4CE and effective carbon rates (2021) were computed by the OECD. Companies will either have to pay the tax corresponding to their emissions, or buy carbon allowance on a cap-and-trade market depending on the regulation to which they are subject

These two metrics are defined for each issuer i in each scenario k at each year t.[35] We compare the number of companies whose probability of default exceeds 20% in future transition scenario to historical levels. For example, we can see in Figure 1.6, that the credit risk faced by the Utilities sector becomes higher than it was in the global financial crisis before 2030 in the SSP2-19 (1.5°C) scenario, and increases beyond the 2007/2008 level regardless of the scenario after 2040. On the other hand, the number of companies at risk in other sectors (including intensive ones such as Energy or Materials) remains below the financial crisis level in the scenario 1.8°C.

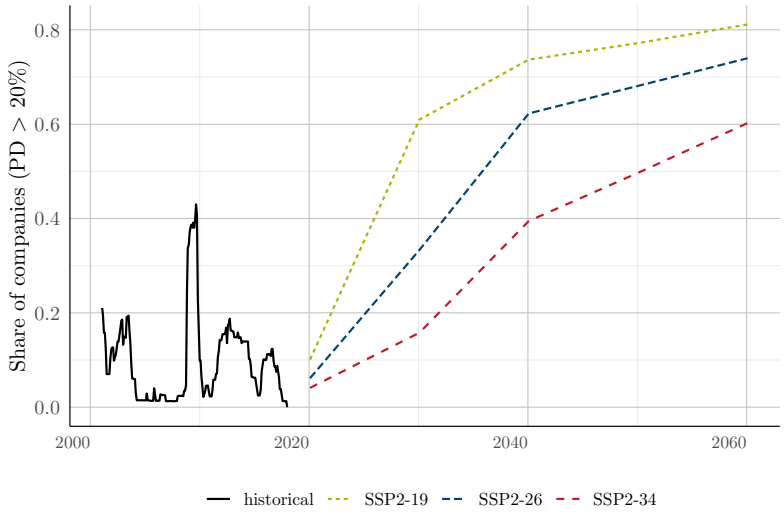

Figure 1.6 – Share of Utilities companies whose Merton's probability of default exceeds 20%

The carbon price margin We also suggest identifying for each company the *carbon price margin* ($\mathcal{CPM}$) which corresponds to the price at which the probability of default reaches a certain threshold S:

$$\mathcal{CPM}_i := \max\{\text{CP} : \text{PD}(i) \leq S\}$$

In a static framework (i.e. constant debt D_i, carbon emission $\mathcal{CE}_{1,i}$) and for fixed asset value characteristics (σ_i and V_i)[36], we obtain:

$$\mathcal{CPM}_i = \left[1 - \exp\left(\sigma_V(i)\sqrt{T}\Phi\left(-S\right) - \left(r + \frac{1}{2}\sigma_V(i)^2\right)T\right) \cdot \frac{D(i)}{V(i)}\right] \cdot \frac{\text{EBITDA(i)}}{\mathcal{CE}_1(i)}$$

A low value of $\mathcal{CPM}$ means that company's capital structure leaves it vulnerable to a minor change in the carbon price. In this paper we study the distribution of $\mathcal{CPM}$ as function of the (Trucost scope 1) carbon intensity $\mathcal{CI}$ using a threshold value of $S = 50\%$. We note a relatively low dependence of the $\mathcal{CPM}$ on $\mathcal{CI}$, therefore, a large share of the transition risk still depends

35. Note that the shock ratio thus defined can also be introduced in a standard credit rating models and include other scope (e.g. Pineau *et al.*, 2022), in discounted cash flow approaches with forward looking metrics or used to establish rating transition probabilities.

36. Obtained solving the classical Merton system with observable equity E_i value and volatility $\sigma_E(i)$.

on corporate idiosyncratic capital structure. This metric has several applications. For companies, this measure can be used to assess the riskiness of a project in varying taxation environments. For portfolio managers, this method makes it possible to assess the default risk at the issuer level subject to changes in local carbon prices. However, data availability on the breakdown of regional emissions and the lack of diffusion effect from intensive sectors to the rest of the economy, limits the interest of this exercise on a diversified portfolio. The next question is therefore how to account for carbon risk in a diversified portfolio, taking into consideration cascading effects in the real economy.

1.6.2 Cascading effects of carbon price through value chain

In this chapter, we assess the impact of carbon pricing in a global framework considering both the cost of idiosyncratic corporate emissions and their cross-sector diffusion. The impact on corporate valuation is shared among intensive firms and less intensive ones through the introduction of a carbon cost pass-through in a sector diffusion model, based on a World Input-Output Database (WIOD). Focusing on the constituents of the MSCI World Index, we show that apart from the usual carbon-intensive sectors, such as Energy, Utilities and Materials, less carbon-intensive ones, such as Industrials, Consumer Staples, Consumer Discretionary and Information Technology can contribute significantly to the global risk, due to the expected pass-through of the carbon cost in the value chain. World indices could experience significant changes in their investment universe and sector composition.

Leontief (1970) Input-output approach applied to environmental externalities Let $M = \boldsymbol{\mathcal{CI}}_{1+\text{upstream}}$ be the vector of direct and indirect (upstream, first-tier) emissions per sector × country (55 x 44). Noting $G = \boldsymbol{\mathcal{CI}}_1$ the vector of sector × country direct (scope 1) emission, CP the global carbon price and $\mathcal{E} = (\varepsilon_i, .., \varepsilon_n)^T$ the amount in dollars paid per direct or indirect emission, we have the following relations:

$$M = \left(I - A^T\right)^{-1} \times G \quad \text{and} \quad \mathcal{E} = \text{CP} \times M \tag{1.29}$$

The carbon intensity measures G are constructed using Exiobase scope 1 intensity (available over 163 sectors) and the matrix A of direct requirement coefficients (a_{ij}) are retrieved from WIOD (updated in 2015).

A firm-level estimation We then refine the definition of M and $\mathcal{E}$ including issuer level data. Thus, we solve this problem for each issuer k part of the i-th sector, with a direct scope 1 emission intensity g^k (from Trucost). The vector of direct plus indirect emission intensities m^k is defined at the issuer level as follows:

$$m^k = \underbrace{m_i}_{\text{Sector direct + indirect intensity}} + \underbrace{\left(g^k - g_i\right)}_{\text{Issuer direct intensity relative to its sector}} \tag{1.30}$$

Impact of carbon price introduction Then, we compare the unitary prices before (p_i) and after ($p_i^{\varepsilon^k}$) the introduction of a global carbon price under the assumption that the cost of labor and capital (and thus the value added) are the same before and after the introduction of the carbon price:

— The **baseline sector price (before carbon pricing)**, including add-valorem tax, cost of input and value-added, can be written as follows:

$$p_i = (1+\tau_i)\left[\sum_{j=1}^{n} p_j a_{ij} + v_i\right] \quad \text{or} \quad P = \left[(I - A_\tau)^{-1}\right]^T V \tag{1.31}$$

where the value added can be written as $v_i = wl_i + rk_i$ with w the price of labor, l_i the coefficient of labor intensity, r the cost of capital and k_i the coefficient of capital intensity.

— The **sector price after the introduction of a carbon price**, the unitary price of issuer k, accounting for its direct and supply-chain carbon-related costs becomes:

$$p_i^{\varepsilon^k} = (1+\varepsilon_i^k)(1+\tau_i)\left[\sum_{j=1}^{n} p_j^{\varepsilon^k} a_{ij} + v_i\right] \quad \text{or} \quad P(\varepsilon^k) = \left[(I - A_\tau^{\varepsilon^k})^{-1}\right]^T V \tag{1.32}$$

The matrix A_τ^ε of direct requirements accounts for the carbon price impact following Mardones and Mena (2020). Under the aforementioned assumptions and normalizing unitary prices before shock to 1, we define the impact of direct plus first-tier upstream carbon intensity at the issuer level using Equations (1.31) and (1.32):

$$P(\varepsilon^k) = \left[(I - A_\tau^{\varepsilon^k})^{-1}\right]^T \times (I - A_\tau^T) \times P \tag{1.33}$$

$$\xi_i^k(\varepsilon^k) = \frac{x_i^{\varepsilon^k}}{x_i} = \frac{1}{p_i^{\varepsilon^k}} \tag{1.34}$$

$\xi_i^k(\varepsilon^k)$ is the impact ratio measuring the reduction in demand due to the introduction of the carbon price on the issuer k. This approach gives a complementary measure of the carbon-related risk faced by companies, from a supply chain perspective. Then we compare the impact of a direct shock only with that of the full price diffusion. We find for example that some sectors, such as Manufacture of computer, electronic and optic have a large risk contribution when we account for the (first-tier) upstream carbon emissions.

Market impact We illustrate the impact on the MSCI World Index. We make the simplifying assumption that the shock is fully passed on the equity price so that:

$$\Delta E_k(\text{CP}) = (\xi_i^k(\varepsilon^k) - 1) \times \text{EV}_k(0) \tag{1.35}$$

For each firm, its new weight in the index depends on the experienced earning shock, leading to a shock to its market capitalization.

$$E_k(\text{CP}) = E_{k,0} - ES_k \times \text{EV}_k(0) \quad \text{and} \quad w_k(\text{CP}) = \frac{E_k(\text{CP})}{\sum_k^N E_k(\text{CP})} \tag{1.36}$$

where $E_k(\text{CP})$ is the estimation of float-adjusted market capitalization of the firm k after the introduction of a carbon price CP, and $w_k(\text{CP})$ is the corresponding weight in the index. We show that apart from the usual carbon-intensive sectors, such as Energy, Utilities and Materials, less carbon-intensive ones, such as Industrials, Consumer Staples, Consumer Discretionary and Information Technology can contribute significantly to the global risk, due to the expected pass-through of the carbon cost in the value chain. Introducing a USD 50/ton shock would reduce the weight of the Utilities, Energy and Materials sectors by respectively 18.8%, 8.6% and 4.7% in relative terms. On the contrary, the Financial and Real Estate sectors benefit substantially from the carbon shock because of their relatively low direct carbon intensity and limited first tier (upstream) indirect emissions (3.3% and 2.5% relative increase in their weight, respectively).

1.6.3 Bond pricing under transition scenario uncertainty

In this chapter, we propose a framework for the dynamic management of transition-related default risk accounting for scenario uncertainty, and in particular, for dynamic pricing and hedging of defaultable bonds sensitive to transition risks. We start with a set of possible scenarios and assume that the agent does not know the scenario a priori, but deduces posterior scenario probabilities from the observation of carbon price shocks, which are modelled with a jump process. We use a model inspired by Leland and Toft (1996) and subsequent literature on the topic, where the default (or restructuring) time is endogenously determined by the shareholders to maximize the equity value. A jump in the carbon price therefore triggers an update of scenario probabilities, which in turn leads to an instant re-evaluation of the firm value and may trigger the default event or change the probability of default.

Firm value dynamics We consider a company generating a stochastic continuous cash flow V_t per unit time, which is affected by the climate policy. The climate policy is characterized by an increasing carbon price process $C_t = \sum_{i=1}^{N_t} \widetilde{Y}_i$, where N is a doubly stochastic Poisson process, whose intensity depends on the transition scenario, and $(\widetilde{Y}_i)_{i\geq 1}$ is a sequence of i.i.d. random variables, independent from N, representing the adjustments of the carbon price. We assume that there are n scenarios with increasing environmental stringency, and denote by $\lambda_1, \dots, \lambda_n$ the respective price intensities, where $0 < \lambda_1 < \cdots < \lambda_n$.

The cash flow dynamics of the company under the risk-neutral probability measure is given by

$$\frac{dV_t}{V_{t-}} = \mu dt + \sigma dW_t - dL_t, \quad L_t = \sum_{i=1}^{N_t} Y_i, \tag{1.37}$$

where W is a standard Brownian motion independent from I and N, and $(Y_i)_{i\geq 1}$ is a sequence of i.i.d. random variables, independent from W, N and I, which determine how the carbon price affects the cash flow. For example, if the firm has constant emission intensity per unit of revenue, denoted by α, then $Y_i = \alpha \widetilde{Y}_i$. We let ν be the distribution of Y_1, $e := \mathbb{E}[Y_1]$ and assume that ν has bounded support belonging to $(-\infty, 1)$ and

$$r + e\lambda_i - \mu > 0 \tag{1.38}$$

for all i, where r is the risk-free rate.

Denote by $\mathcal{F}_t = \sigma(W_s, N_s, s \le t)$ the observation filtration, which contains the firm's revenues and the carbon price trajectory but does not contain the true scenario I, and let $\hat{p}_t^i = \mathbb{E}[I = i|\mathcal{F}_t]$ be the posterior probability of being in scenario i given the available observations at time t. Then the intensity of N is given by $\hat{\lambda}_t = \sum_{i=1}^n \lambda_i \hat{p}_t^i$, and the filtered probabilities are given by

$$\hat{p}_t^i = \frac{e^{-\lambda_i t}\lambda_i^{N_t}\hat{p}_0^i}{\sum_j e^{-\lambda_j t}\lambda_j^{N_t}\hat{p}_0^j}, \tag{1.39}$$

which means that in the filtration $(\mathcal{F}_t)$, the couple (V_t, N_t) is a time-inhomogeneous Markov process. We also introduce the notation for the jump intensity and probabilities with explicit dependence on N:

$$\hat{\lambda}^N(t) := \frac{\sum_i e^{-\lambda_i t}\lambda_i^{N+1}\hat{p}_0^i}{\sum_j e^{-\lambda_j t}\lambda_j^{N}\hat{p}_0^j}, \qquad \hat{p}_t^{i,N} = \frac{e^{-\lambda_i t}\lambda_i^{N}\hat{p}_0^i}{\sum_j e^{-\lambda_j t}\lambda_j^{N}\hat{p}_0^j}$$

Computing the firm value and the bond price The company pays a continuous coupon b corresponding to a debt with notional value K and maturity T. At any time $\tau < T$, the shareholders may make one of the following two decisions, depending on the value of the company's future cash flows:

— If the value of the future cash flows is greater than the notional value K of the debt, the shareholders may decide to redeem the debt at notional value (restructuring event).

— If the value of the future cash flows is smaller than the notional value K of the debt, the shareholders may decide to trigger the default event, in which case the bondholders receive the value of the future cash flows.

The default/restructuring date is determined by the company's owners to maximize equity value. The value of the future cash flows at time t is given by

$$\begin{aligned}\widehat{V}_t &= \mathbb{E}\left[\int_t^\infty e^{-r(s-t)}V_s\Big|\mathcal{F}_t\right] = \sum_{i=1}^n \mathbb{P}[I=i|\mathcal{F}_t]\,\mathbb{E}\left[\int_t^\infty e^{-r(s-t)}V_s\Big|\mathcal{F}_t, I=i\right]\\ &= V_t\sum_{i=1}^n \frac{\hat{p}_t^i}{r+e\lambda_i-\mu} = V_t\,\alpha_t^{N_t},\end{aligned}$$

where we denote

$$\alpha_t^N := \sum_{i=1}^n \frac{1}{r+e\lambda_i-\mu}\,\frac{e^{-\lambda_i t}\lambda_i^N\hat{p}_0^i}{\sum_j e^{-\lambda_j t}\lambda_j^N\hat{p}_0^j}.$$

The bond price can then be written as a solution to an optimization problem:

$$B^N(t,V) = \inf_{\tau\in\mathcal{T}([t,T])}\mathbb{E}\Big[\int_t^{\tau\wedge T} e^{-r(s-t)}b\,ds + e^{-r(T\wedge\tau-t)}\widehat{V}_{T\wedge\tau}^{t,V,N}\wedge K\Big]. \tag{1.40}$$

We establish theoretically the existence of default and restructuring thresholds and study their properties. Our main result provides a method for the numerical approximation of the bond price $B^N(t,V)$.

Proposition 2. *Let $B^{N,M}(t,V):[0,T]\times\mathbb{R}_+\mapsto\mathbb{R}$, for $N\le M$ be defined as follows:*

$$B^{M,M}(t,V):=G^M(t,V),$$

where for each M, G^M is bounded and Lipschitz continuous in V and and for $N<M$, $B^{N,M}(t,V)$ is the solution of the variational inequality

$$\min\{b-rB^{N,M}+\mathcal{L}^{N,M}B^{N,M},\alpha_t^NV\wedge K-B^{N,M}\}=0, \tag{1.41}$$

on $(t,V)\in[0,T]\times\mathbb{R}_+$ with $B^{N,M}(T,V)=\alpha_T^NV\wedge K$, where

$$\mathcal{L}^{N,M}f=\frac{\partial f}{\partial t}+\mu V\frac{\partial f}{\partial V}+\frac{1}{2}\sigma^2V^2\frac{\partial^2f}{\partial V^2}+\hat{\lambda}^N(t)\int_{-\infty}^{1}\left\{B^{N+1,M}(t,V(1-x))-f(t,V)\right\}\nu(dx). \tag{1.42}$$

Then,

$$\lim_{M\to\infty}B^{N,M}(t,V)=B^N(t,V)$$

for $N=0,1,\dots$ and $(t,V)\in[0,T]\times\mathbb{R}_+$, where the convergence takes place at faster than exponential rate.

This proposition allows us to develop an algorithm for computing the bond price $B^N(t,V)$, controlling the estimation error. The model is then illustrated with a case study using financial and emission data of several companies and NGFS transition scenarios. Our results show that under transition scenario uncertainty, carbon price adjustments are more likely to trigger a default than when the true scenario is known because after each adjustment the more environmentally stringent scenario becomes more likely. We use our model to quantify the impact of the speed at which scenario information is discovered by the agents on the credit spread level and find that faster information discovery leads to higher spreads since better information allows the shareholders to optimize the timing of default, increasing the value of default option and decreasing the bond price. Our model therefore illustrates the importance of scenario information for bond pricing in the context of environmental transition: we find that insufficient information about future carbon prices and slow information discovery may lead to overpricing of defaultable bonds and potentially painful market-wide default or repricing events when information is finally discovered.

1.6.4 Modeling physical risks: the case of tropical cyclones

Tropical cyclones are responsible for a large share of global damage resulting from natural disasters and estimating cyclone-related damage at a national level is a challenge attracting growing interest in the context of climate change. The global climate models, whose outputs are available from the Coupled Model Intercomparison Project (CMIP), do not resolve tropical cyclones. The Cyclone generation Algorithm including a THERmodynamic module for Integrated National damage Assessment (CATHERINA) presented in this paper, couples statistical and thermodynamic relationships to generate synthetic tracks sensitive to local climate conditions and estimates the damage induced by tropical cyclones at a national level. The framework is designed to be compatible with the data from CMIP models offering a reliable solution to resolve tropical cyclones in climate projections. We illustrate this by producing damage projections in Representative Concentration Pathways (RCP) at the global level and for individual countries. The algorithm

contains a module to correct biases in climate models based on the distributions of the climate variables in the reanalyses. This model was primary developed to answer the need of the economic and financial community that is seeking quantitative signals that would allow for a better quantification of physical risks in the long term, to estimate, for example, the impact on sovereign debt.

Tropical cyclone intensity The cyclones are initiated with spatial and seasonal distribution estimated on the IBTrACS database similarly to Bloemendaal *et al.* (2020). Let $[t_1, t_2]$ be a period of time with annual steps large enough to reflect climate (and not only meteorological variation). The number of cyclones for each year $t \in [t_1, t_2]$ follows the Poisson distribution with parameter depending on the region: $N_t \sim \mathcal{P}(\hat{\lambda}_B)$. We use the parameters λ_B given in Bloemendaal *et al.* (2020) and controled the number of intense cyclones making landfall. The initial longitude and latitude are attributed resampling randomly the coordinates of past genesis and for each initialized cyclone, then the time evolution of the latitude and longitude of the cyclone center is described with an autoregressive process (Bloemendaal *et al.*, 2020; James & Mason, 2005).

The wind (used in the damage function) and the central pressure (modeled with climate variables) are related using the wind-pressure relationship (WPR), which is calibrated separately for each basin. The maximum potential intensity, instrumental variable used in the intensification process, is defined along track following the framework summarized in Holland (1997):

$$\mathrm{MPI}_t = \mathrm{MSLP}(x_t, y_t, t) \cdot \exp^{-X_t}, \tag{1.43}$$

$$X_t = \frac{\mathcal{E}_t \cdot \mathrm{SST}(x_t, y_t, t) \cdot \Delta S_t^m - \frac{f(y_t)^2 r_{env}^2}{4}}{R_d \cdot \mathrm{SST}(x_t, y_t, t)}, \tag{1.44}$$

$$\mathcal{E}_t = \frac{\mathrm{SST}(x_t, y_t, t) - T_{\mathrm{tropo}}(x_t, y_t, t)}{\mathrm{SST}(x_t, y_t, t)}, \tag{1.45}$$

$$\Delta S_t^m = R_d \ln\left(\frac{\mathrm{MSLP}(x_t, y_t, t)}{P_{t-1}^c}\right) + \frac{L_v(q_{c\,t}^\star - q_t^{env})}{\mathrm{SST}(x_t, y_t, t)}, \tag{1.46}$$

where (x_t, y_t, t) are the coordinates of the eye, $\mathrm{SST}(x_t, y_t, t)$ and $T_{\mathrm{tropo}}(x_t, y_t, t)$ are respectively the sea-surface and tropopause temperatures, $R_d = 287.058$ J.kg^{-1}.K^{-1} is the specific gas constant for dry air, $\mathrm{MSLP}(x_t, y_t, t)$ is the mean local sea-level pressure, $\mathrm{RH}(x_t, y_t, t)$ is the near surface relative humidity at 2 meters extracted from the monthly dataset of ERA-5 climate reanalysis or CMIP climate models. $f(y_t) = 2\omega \sin(y_t)$ is a Coriolis parameter depending on the latitude, r_{env} is the distance between the eye and the area under regular conditions (fixed at 500 km). The difference of moist entropy potential ΔS^m is defined along track using specific humidity in the eye vs. at environmental conditions (q_{env} and $q_c^\star$) and L_v is the latent heat of vaporization. Some controls such as the maximum pressure drop observed for the corresponding temperature and the decay relationship for cyclones evolving over land are also fitted for each basin and applied in the synthetic tracks generation algorithm. Extracting the climate variables from different models allows us to correct the biases and evaluate model uncertainty. The evolution of the central pressure depending on the MPI is described by the following autoregressive stochastic equation

(James & Mason, 2005):

$$\Delta P_t^c = c_0 + c_1 \Delta P_{t-1}^c + c_2 e^{-c_3[P_t^c - \mathrm{MPI}_t]} + \varepsilon_t^P, \tag{1.47}$$

$$\varepsilon_t^P \sim \mathcal{N}(0, \sigma_{P^c}), \tag{1.48}$$

After three steps on land we apply the decay function to avoid generating unrealistic damages too far inside the coast similarly to Bloemendaal *et al.* (2020) and Kaplan and DeMaria (1995).

Exposure (SSP) To estimate future exposures along the cyclone tracks in each scenario, we use the downscaled estimation for the exposed physical asset value (Eberenz *et al.*, 2020) and the coefficients representing the change between the current state and the future scenario in the framework of the shared socioeconmic pathways (Jones & O'Neill, 2020; O'Neill *et al.*, 2017; O'Neill *et al.*, 2014). The local physical exposure at the coordinates (x, y) at time t in a region j in scenario k is defined as follows:

$$\Phi(x, y, j, k, t) = \underbrace{(F_{\mathrm{GDP}}^{cap}(j, k, t))^{\alpha_1}}_{\text{Global macro factor}} \cdot \underbrace{(F_{pop}(x, y, k, t))^{\alpha_2} \cdot \mathcal{L}_P(x, y)}_{\text{Local factor}}. \tag{1.49}$$

where $\mathcal{L}_P(x, y)$ is the local population density from Eberenz *et al.* (2020), the factor F_{GDP}^{cap} is the projected GDP per capita growth for each region from SSP database (Riahi *et al.*, 2017), and F_{pop} is the population exposure growth factor based on the local projections of population (Jones & O'Neill, 2020). We introduce the exponents α_1 and α_2 to disentangle the effects of increased cyclone intensity, GDP growth and population growth on the future damages, as well as to account in a simple manner for possible future adaptation to tropical cyclone risk.

Vulnerability (CLIMADA) To estimate the fraction of loss from a storm with sustained wind speed V, K. A. Emanuel (2011) introduced the following formula:

$$f(V, v_h^j) = \frac{\left(\max(V - v_0, 0)\right)^3}{(v_h^j - v_0)^3 + \left(\max(V - v_0, 0)\right)^3}, \tag{1.50}$$

where f is the fraction of the property value lost, $v_0 = 25.7$ m.s^{-1} and v_h^j a parameter that needs to be calibrated for each region j retrieved from Eberenz *et al.* (2021). We compute the damage caused by these synthetic tracks, using the following simplified process. First, a uniform grid of physical asset values with step given by the average cyclone radius is defined on the map of affected area. The cyclone track is linearly interpolated, and the tiles affected by the cyclone (containing a part of the interpolated path) are identified. Second, for each tile identified in the previous step, we retrieve the maximum wind speed V, and compute the proportion of wealth lost $f(V, v_h^j)$. Then, we compute the total simulated damage by aggregating the physical asset exposure multiplied by the proportion of wealth lost on each tile over all tiles affected by the cyclone. As a result of this procedure, we obtain the total simulated damage $\mathrm{SED}_i(j, t)$ caused by the i-th cyclone in region j, simulated with climate variables for year t. Finally, the cyclone damage cost in region j and year t follows: $\mathcal{D}(j, t) = \sum_i \mathrm{SED}_i(j, t)$, where the sum is taken over all cyclones occurring in a given year. This procedure can then be repeated many times to obtain the distribution of annual cyclone damages and compute other statistics such as the mean and quantiles of this distribution.

Financial application We produce damage projections in representative concentration pathways (RCP) at the global level and for individual countries using the coupled model intercomparison project data (CMIP5). We then propose to apply Hilscher and Nosbusch (2010) econometric specification to estimate how physical risk affects the option-adjusted-spreads (OAS) of emerging countries through the impact of direct damage on the debt-to-GDP ratio. Because of the higher vulnerability of emerging countries, we decide to focus on the constituents of the JP Morgan EMBI Index. In contrast to the existing literature (Beirne *et al.*, 2020; Klusak *et al.*, 2021; Volz *et al.*, 2020), our aim is to analyze the impact of physical risks on sovereign bond spreads directly, by evaluating economic damage from synthetic future cyclones, without making reference to integrated assessment models. We calibrate a cross-sectional econometric model for the option-adjusted spread based on annual end-of-year data:

$$\mathrm{OAS}_t = \alpha \quad + \quad \beta_6 \frac{L_t}{\mathrm{GDP}_t} + \sum_j C_j + \epsilon_t. \tag{1.51}$$

where the OAS is the end-of-year option adjusted spread, from JP Morgan EMBI position report in BarraOne and C_j are control variables that allow to construct a model explaining more than 70% of the spread of the securities in the JP Morgan EMBI index. The model covers 74 countries between 2010 and 2020. For each country j in the JP Morgan EMBI index, we assess the annual bond spread variation due to cyclone damage, in scenario k for the year t using the following formula:

$$\Delta_{k,t}\mathrm{OAS}(j,k,t) = \beta_6 \times \frac{\mathcal{D}(j,k,t)}{F_{\mathrm{GDP}}(j,k,t)\mathrm{GDP}(j,2020)}, \tag{1.52}$$

where we recall that $\mathcal{D}$ stands for annualized cyclone damage, and F_{GDP} is the GDP growth factor for the specified country/scenario. Our results suggest that poorest countries may suffer jumps in credit spread representing overwhelming borrowing cost and inhibiting their reconstruction capacity. Indeed, quantitatively, we noted that the 5 biggest events observed in the past (including flood and earthquake) have lead to about 20bps rise of 10Y spread for all countries considered. In relative terms (i.e. normalizing by the GDP of affected countries), the 55 most damaging events lead on average to 5 bps rise in the 30 days window following the end of the event reported in EM-DAT. By contrast, in terms of forward looking impact of tropical-cyclones, we found that some states can be subject to shock in spreads up to 200 bps.

Chapter 2

Credit risk Sensitivity to Carbon Price [1]

Climate change impacts the functioning of human societies and global economic activity (Pachauri *et al.*, 2014; Tol, 2018). To prevent its unfavorable consequences, the international community has committed to reduce its global greenhouse gas (GHG) emissions [2] to keep global average warming below 2℃, along with a more ambitious objective of 1.5℃. These international agreements include nationally determined contributions (NDC), which set targets at a national level. NDCs can be achieved through different mechanisms. Currently, 81 countries have committed to implement a carbon price in their NDC. Figure 2.1 shows that the number of carbon pricing initiatives has increased in recent years and now covers 20% of global GHG emissions (World Bank, 2019a).

This transition towards a low-carbon economy generates a *transition risk* for the financial system. This risk has already been flagged by regulators and financial institutions (Campiglio *et al.*, 2018). Following the warning of Carney (2015), various regulators have first estimated market exposure to the transition risk and the related potential systemic risk. Although more research is needed in this area, these studies highlight significant financial losses for *climate-relevant* sectors and the need to focus on credit risk (Monnin, 2018; NGFS, 2018).

Financial institutions have to develop methodologies applicable to their balance sheets and portfolios in order to manage transition risk. According to the Financial Stability Board Task force on Climate-related Financial Disclosures (TCFD, 2017), transition risk can come from changes in policy and regulation, markets, technology or consumer behavior. As pointed by Campiglio *et al.* (2018), the assessment of climate-related financial risks is hampered by various challenges. First, the data required is often deficient or is provided with excessively low granularity. In addition, the evaluation of climate-related financial risks requires modeling the dynamic interactions between the macroeconomy, the financial system, climate change and environmental policies. These models are subject to deep uncertainty. In this study, we focus on the rise of the carbon price. This is one of the main regulatory risks and its assessment requires that data be available with acceptable coverage.

The issue of carbon pricing has been tackled by two branches of literature through two distinct

1. This chapter is derived from Bouchet and Le Guenedal (2020b) that received the GRASFI Best Paper Prize for Research on Climate Finance (sponsored by Imperial College London) in 2020. This revised version is published in the *Revue Economique* special issue of march 2022 on transition risks, 73(2), Bouchet and Le Guenedal (2022).

2. First with the Kyoto protocol (1997) and more recently with the Paris agreement (2016).

research questions. On the one hand, some investigated what the optimal price of carbon would be. Many economists have estimated the *social cost* of carbon (SCC), i.e. the optimal cost of additional emissions, minimizing both future damages and the impact on current economy. They generally rely on cost-benefit or cost-efficiency approaches, using assessment models and underlying damage functions. [3] While most researchers agree on the need for a carbon price, the results vary widely, depending on models, discount rates and countries (Tol, 2018).

On the other hand, an emerging field of research in finance aims to answer the following question: what are the financial risks associated with a carbon price rise? Indeed, regardless of the optimal value of the price over time, it is observable that an increasing share of GHG emissions is subject to an effective carbon price (see Figure 2.1). It is therefore possible to study the financial consequences of this trend. Some studies have measured the impact of the observed carbon price on financial performance (Oestreich & Tsiakas, 2015; Scholtens & van der Goot, 2014). However, multi-variate regressions or variance decomposition methods used in finance seem to have limits in forecasting the impact of a potential carbon price on credit risk. The observed carbon prices on which they rely are not comparable with the projections of carbon price from transition scenarios (UNEP, 2018). A second stream of research has investigated the extent to which market prices already integrate carbon risk, approximated by the carbon emissions of issuers (Andersson *et al.*, 2016; Görgen *et al.*, 2019; Ilhan *et al.*, 2019; J. Jung *et al.*, 2018). Heterogeneous results emphasize the need to better understand the financial risks associated with carbon price.

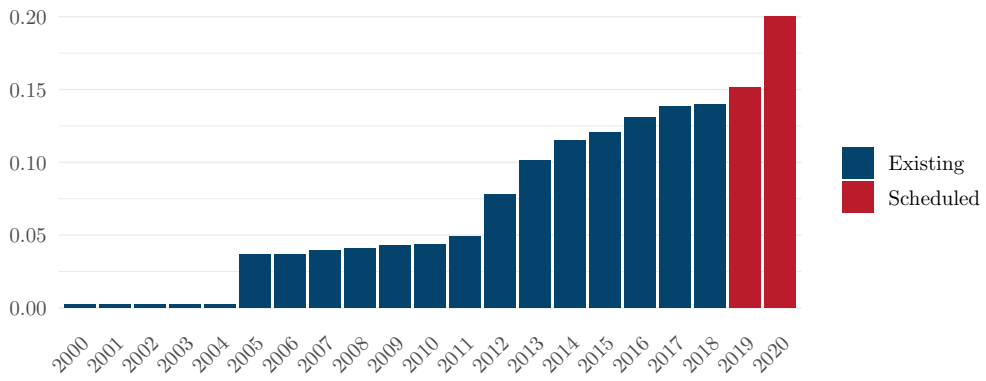

Figure 2.1 – Share of GHG emissions covered by an effective carbon price. Source: World Bank (2019a)

Few research works address the credit risk associated with future carbon prices from a bottom-up perspective (Howard & Patrascu, 2017; Monnin, 2018; UNEP, 2019). Our study aims to answer the following research question: how does carbon price variation impact sectoral credit risk across scenarios and time? Our contribution to the literature is threefold. First, we conduct a bottom-up analysis of a global reference portfolio, based on corporate emissions by countries. Secondly, we address the "tragedy of the horizons" by using both medium-term (five-year) and long-term (40-year) scenarios. Medium-term analyses are based on current effective carbon prices for each sector in each country (OCDE, 2018; World Bank, 2019a). Long-term scenarios are based on the

3. For a review of methodologies, see Le Guenedal (2019b).

social carbon price scenarios of Intergovernmental Panel on Climate Change (2018). Finally, we propose a new indicator, the *carbon price margin*, which takes the economic and capital structure of the firm into account to measure carbon risk.

This chapter is structured as follows. Section 2.1 develops the theoretical model and describes the data. Section 2.2 presents the main results, which are discussed in Section 2.3.

2.1 Methodology and data

2.1.1 Structural transmission model

From carbon price to total asset value shock The carbon price transmission channel to income statements is described in Table 2.1. In practice, there are many ways a change in carbon price can affect firms; this methodology covers one of them. We recall that emission quotas are considered as commodities and included in cost of goods sold. On the other hand, carbon taxes are mostly associated with the cost of fuels. The acquisition cost of fuels consists of the purchase price, including customs duties and other non-recoverable taxes. [4] We consider the carbon tax as a non-recoverable tax.

Table 2.1 – Transmission channel of the carbon price

Variable	Step	Formula
Revenue*	(1)	
Cost of goods sold – **quotas or carbon tax**	(2)	
Gross profit	(3)	(1)-(2)
Operating expense excluding deprec. and amort.	(4)	
EBITDA	(5)	(3)-(4)
Depreciation and amortization**	(6)	
EBIT	(7)	(5)-(6)
Interest expense	(8)	
Tax expense	(9)	
Net income	(10)	(7)-(8)-(9)

Notes:
* Reduced demand effect would affect revenues
** Asset stranding effects would imply depreciations

Let $\mathcal{CE}(i,j,t)$ be the emissions in tons of CO2 equivalent emitted by the company i in a given region j at year t. Each region j has a representative carbon price CP for each date t in each scenario k. [5] This price is based on the mechanisms in region j. The reference scenario $k = 0$, is the baseline where current carbon prices remain unchanged:

$$\mathrm{CP}(j, k = 0, t) = \mathrm{CP}(j, k = 0, t = 0)$$

4. According to Article 213–31 from Autorité des normes comptables, entreprises industrielles et commerciales, Dispositions générales.

5. The notations are summarized in Appendix 3..1 on page 101.

Each year, each company has carbon cost CC derived from the company activity in each region j in the set $\mathcal{M}$ of regions where the company has reported direct emissions:

$$\mathrm{CC}(i,k,t) = \sum_{j\in\mathcal{M}} \mathcal{CE}(i,j,t) \times \mathrm{CP}(j,k,t)$$

Integrating this carbon cost leads to a shock to EBITDA defined as: [6]

$$\xi(i,k,t) = \frac{\mathrm{CC}(i,k,t)}{\mathrm{EBITDA}(i,k=0,t=0)}$$

The impact of the variation of EBITDA on total asset value V can be computed through two approaches. The first option is to compute, for each year, the new asset value as the sum of discounted future cash flows. This approach requires defining the discount rate for each company and therefore adds parameters to our model. As our study focuses on the comparability of different companies, we used a second approach that relies on the assumption that the financial ratio between the enterprise value and the EBITDA remains constant over time. [7] In this case, the shock is directly transmitted to the enterprise value. The economic shock transmission to the financial valuation of each company i, in each scenario k and at each date t writes:

$$V(i,k,t) = (1-\xi(i,k,t)) \times V(i,k=0,t=0)$$

From total asset value shock to probability of default The probability of default is derived from total asset value shock through the framework developed by Merton (1974). The initial total asset value $V(i,k=0,t=0)$ of the company i and total asset volatility $\sigma_V(i)$, which are not observable, are determined by solving equations (2.1) below. [8] In our study, this system is resolved solely to determine initial values for $V(i,k=0,t=0)$ and $\sigma_V(i)$ and is independent of scenario k and future date t:

$$\begin{cases} E(i) = V(i)\Phi(\mathrm{d}_1) - D(i)e^{-rT}\Phi(\mathrm{d}_2) \\ \\ E(i) = \dfrac{\sigma_V(i)}{\sigma_E(i)}\Phi(\mathrm{d}_1)V(i) \end{cases} \tag{2.1}$$

where $E(i)$ is the observable equity value, σ_E is the observable equity volatility, D is the total debt, Φ is the cumulative normal distribution function and:

$$\begin{aligned} d_1 &= \frac{\ln\left(\dfrac{V(i)}{D(i)}\right) + \left(r + \dfrac{1}{2}\left(\sigma_V(i)\right)^2\right) \times T}{\sigma_V(i)\sqrt{T}} \\ \\ d_2 &= d_1 - \sigma_V(i)\sqrt{T} \end{aligned}$$

6. Reinders *et al.* (2020b) presented a similar stress-test methodology at the Global Research Alliance for Sustainable Finance (2019). However, there are multiple differences in the two methodologies: the definition of the shock (EBITDA and not discounted cash flows), the bottom-up configuration and multiple scenario and horizons in this study.

7. In this case, we can write $V(i,t) = \mathcal{R}_i \times \mathrm{EBITDA}(i,t)$ where $\mathcal{R}_i$ is a constant financial ratio neutral in this study. The assumption is that $\mathcal{R}_i$ is *stable* over time for each company, which is verified in this study.

8. Note that companies' value is also disclosed by providers and we used several values for robustness check. This system is solved using Newton's method.

where r is the risk-free rate and T the maturity. Once the initial total asset value and total asset volatility are determined, we can compute the distance to default DD by incorporating the shock ($\xi \in [0,1]$). Then, the distance to default is given by:

$$\mathrm{DD}(i,k,t) = \frac{\ln\left(\frac{(1-\xi(i,k,t)) \times V(i,k=0,t=0)}{D(i)}\right) + \left(r + \frac{1}{2}\left(\sigma_V(i)\right)^2\right)T}{\sigma_V(i)\sqrt{T}}$$

and the theoretical probability of default PD of an issuer is:

$$\mathrm{PD}(i,k,t) = \Phi(-\mathrm{DD}(i,k,t))$$

The distance and probability of default are defined for each issuer i in each scenario k at each date t. In a situation where parameters such as asset volatility, risk-free rate, total debt or financial ratio, are not assumed to be fixed, the System (2.1) would have to be solved at each date in each scenario.

The carbon price margin To measure the transition risk of a company, the existing literature essentially uses carbon intensity, i.e. scope 1 and 2 emissions with respect to the revenues. While carbon intensity allows us to take into account the size of the company, it does not take into account its capital structure. This study proposes to calculate for each company the *carbon price margin* $\boldsymbol{\mathcal{CPM}}$ which corresponds to the price at which the probability of the company's default reaches a certain threshold S: the *carbon price margin* ($\boldsymbol{\mathcal{CPM}}$) which corresponds to the price at which the probability of default reaches a certain threshold S:

$$\boldsymbol{\mathcal{CPM}}_i := \max\{\mathrm{CP} : \mathrm{PD}(i) \leq S\}$$

In this study, the threshold was calibrated to 50%. In a static framework (i.e. constant debt D_i, carbon emission $\boldsymbol{\mathcal{CE}}_{1,i}$) and for fixed asset value characteristics (σ_i and V_i) [9], we obtain:

$$\boldsymbol{\mathcal{CPM}}_i = \left[1 - \exp\left(\sigma_V(i)\sqrt{T}\Phi\left(-S\right) - \left(r + \frac{1}{2}\sigma_V(i)^2\right)T\right) \cdot \frac{D(i)}{V(i)}\right] \cdot \frac{\mathrm{EBITDA(i)}}{\mathcal{CE}_1(i)}$$

2.1.2 Scenario definition

One of the obstacle pointed out by Carney (2015) to address climate-related financial risk is the mismatch between the long-term horizon of climate change and the short-term horizon of finance, known as the *tragedy of the horizons*. In order to address this issue, our study includes a medium-term (five-year) and a long-term (40-year) analysis.

Medium-term scenarios The medium-term analysis focuses on the period from 2019 to 2023 and relies on current carbon prices in four regions. We distinguish the countries belonging to the EU-ETS, Japan, United States and the rest of the world. To estimate the average effective prices in each region, we compute the carbon revenues in 2018 and divide them by the GHG emissions in the corresponding region. This estimation is based on following data:

9. Obtained solving the classical Merton system with observable equity E_i value and volatility $\sigma_E(i)$.

— The World Bank publishes an annual report on the state and trends of carbon pricing mechanisms (World Bank, 2019a). Moreover, since May 2017, it has provided an interactive online platform, the *carbon pricing dashboard*, with open access to the underlying data. This database covers 57 carbon-pricing initiatives, covering 11 gigatons of CO2 emissions accounting for 20.1% of global GHG emissions and provides information on GHG coverage, prices and global value from 1990. [10]

— The International Carbon Action Partnership (ICAP) is an international forum for more than 35 jurisdictions, which have implemented, or are planning to implement, emissions trading systems (ETS). The ICAP ETS map, an interactive tool with open data, provides factsheets on ETS initiatives. [11]

— The Institute for Climate Economics (I4CE) (Postic & Métivier, 2019) provides an overview of carbon price mechanisms by region around the world.

Our first scenario (*trend*) extends the current linear trajectory in the evolution of revenues from carbon price mechanisms. The second (*acceleration*) considers a 40% increase of the carbon price each year over the next five years.

Long-term scenarios For the long-term analysis, carbon prices are retrieved from the Intergovernmental Panel on Climate Change (IPCC) database. [12] This database provides 598 variables associated with 177 scenarios generated by 25 models. Data is generally available until 2100 with a 5- or 10-year step (Huppmann *et al.*, 2018). The carbon prices provided by these models are global. Figure 2.2 shows that future trajectories for carbon prices vary widely depending on scenarios and models. We therefore selected three scenarios, which cover the range of carbon prices in the database. Medium and long term scenarios are illustrated in Figure 2.2 and Table 2.2).

Table 2.2 – Scenario selection

Scenario	IPCC Ref.	Temperature 2100	Carbon price 2024 (EU)	Carbon price 2060
Acceleration	–	–	27	–
Trend	–	–	15	–
1.5°C	SSP2-19	1.5°C with ~ 66% probability	–	781
1.8°C	SSP2-26	1.8°C	–	152
2.2°C	SSP2-34	2.2°C	–	54
3.8°C	SSP2-Baseline	3.8°C	–	0

2.1.3 Companies data

The medium- and long-term analyses are performed on the MSCI World Index, composed of 1 644 large and mid cap companies across 23 developed markets countries. To calculate the impact

10. Source: https://carbonpricingdashboard.worldbank.org/map_data, data extracted on September 16th, 2019.
11. Source: https://icapcarbonaction.com/en/ets-map, data extracted on September 16th, 2019.
12. Source: https://data.ene.iiasa.ac.at/iamc-1.5c-explorer/ visited on September 16th, 2019.

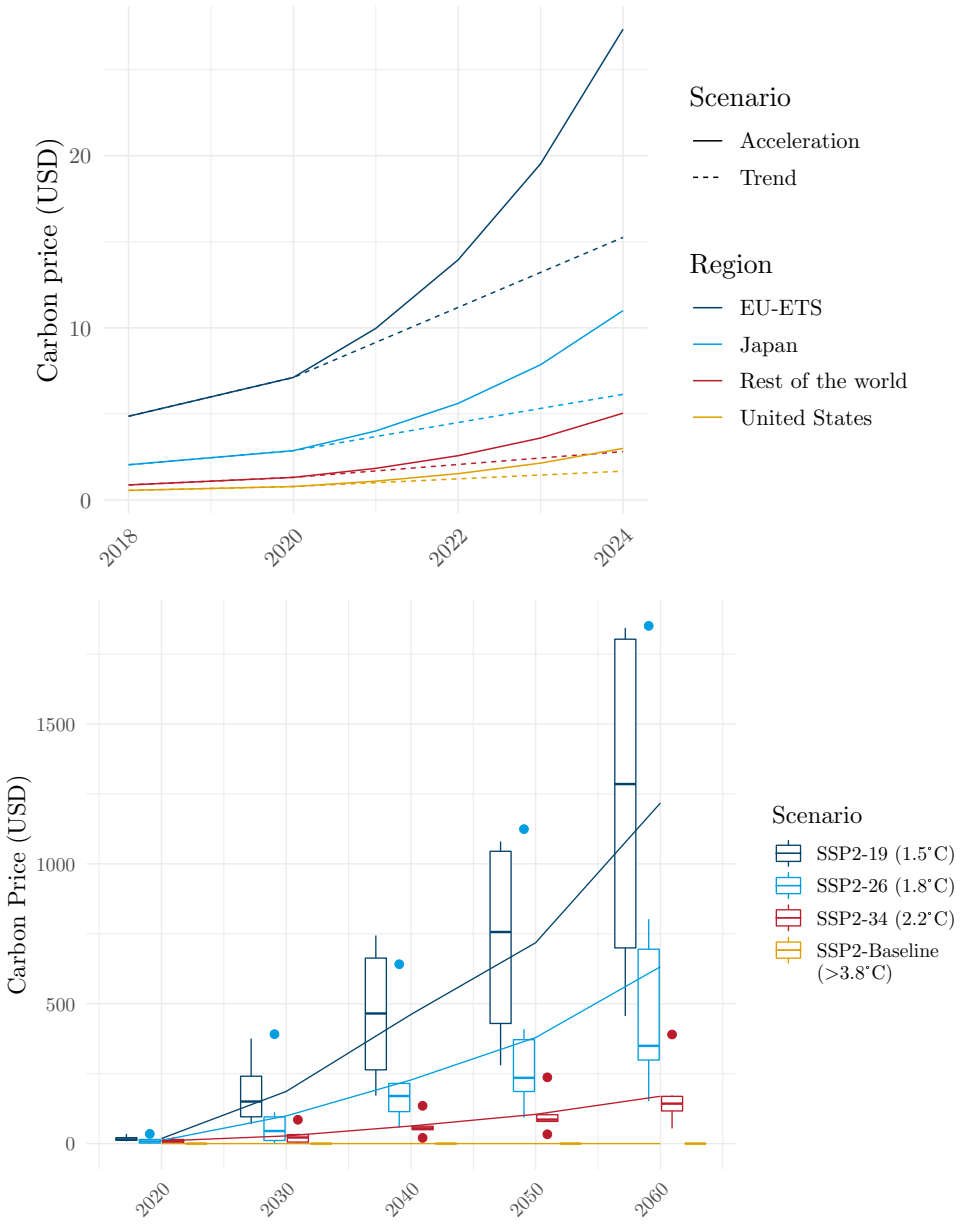

Figure 2.2 – Scenario selection and global distribution of carbon price (all models and scenarios). Above: medium-term; Below: long-term carbon price scenarios*

* Note: The box-plot (25-75 percentile and median) illustrates the cross-sectional dispersion of the suggested carbon price across models (dots are outliers) and the line is the mean carbon price. (Source: IASAA SSP database version 2.0)

of each scenario on EBITDA and probability of default, we need the GHG emissions as well as the financial data of each company.

GHG Emissions To avoid double counting, only direct emissions - i.e. from sources owned or controlled by the company (GHG Protocol) - (scope 1) are taken into account. The data comes from the Carbon Disclosure Project (CDP) database, which each year centralizes environmental data communicated by more than 7,000 companies. The database provides, for each company, a breakdown of its emissions by country.

Financial Data EBITDA, equity value, equity volatility and face value of debt are retrieved from Bloomberg and Orbis Datastream as of December 31, 2018.

Coverage and data quality As carbon accounting is not as mature as financial accounting, the use of data related to GHG emissions is limited by the coverage and quality of this data. To limit the risk of low coverage, this study focuses on the MSCI World Index, which is made up of large and medium-sized companies with greater incentives to disclose and audit their non-financial information. To take into account data quality issues, a second database providing GHG emissions by company (Trucost) is used to test the robustness of the results.

Financial companies have limited direct GHG emissions and specific financial situations, and are excluded from the sample (which leaves us with 1,395 remaining companies), as are companies with missing financial data in 2018 (1,199 remaining companies), and companies with missing GHG emissions data (763 remaining companies, Figure 2.3).

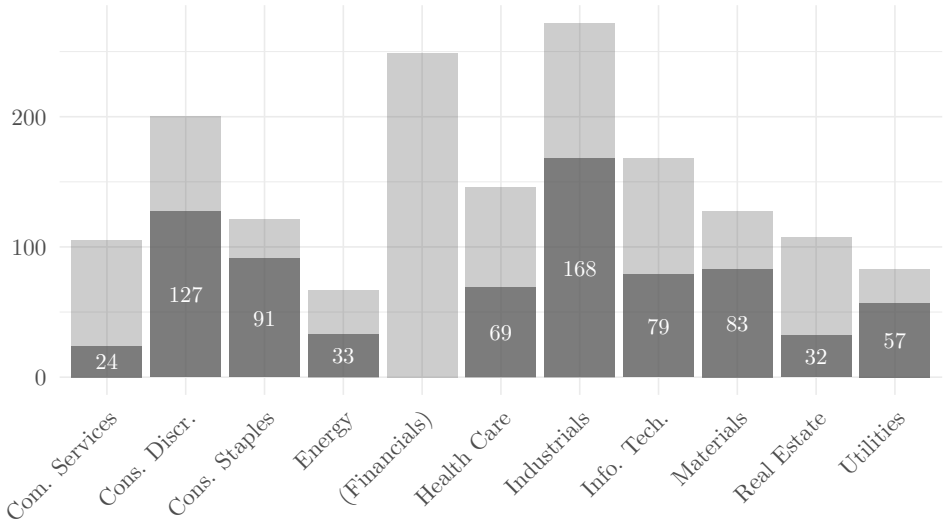

Figure 2.3 – Sectoral coverage (companies in the MSCI World Index)

2.2 Results

The analysis of medium and long term scenarios allows us to identify the most sensitive sectors (2.2.1), but also those for which the risk is the most heterogeneous (2.2.2). The sensitivity analysis

shows the importance of the interactions between variables in the model (2.2.3).

2.2.1 A limited medium-term risk becoming significant in the long term

The impact of an increase in the carbon price on each firm's credit risk is reflected by its probability of default. This should not be interpreted in absolute terms, but in comparison with the historical data or with other similar firms. First, the percentage of firms whose probability of default reaches a certain threshold within each sector is used to analyze the heterogeneity of credit risk across sectors. Two threshold values determined based on the historical default probabilities are tested: 10% and 20%. In the medium term, the percentage of companies whose probability of default exceeds the 10% threshold changes only for the Utilities sector. In the *trend* scenario, this percentage rises from 7% in 2019 to 8.8% in 2024, while in the *acceleration* scenario it reaches 11 % in 2024. Within this sector, the companies concerned by this increase belong to the power generation industry, which is characterized by a high carbon intensity.

In the long term, the threshold of 20% is used to better differentiate between sectors (c.f. Figure 2.4). The percentage of companies whose probability of default exceeds this threshold changes significantly for three sectors: i) Utilities, ii) Materials and iii) Energy. In scenario 1.5°C, credit risk reaches levels above the 2007/2008 crisis for all of these sectors. In line with the results obtained in the medium term, the Utilities sector experiences the fastest and largest increase in transition-related credit risk, reaching a percentage twice as high as in 2007/2008. For this sector, the percentage of companies at risk in 2060 reaches a level higher than in 2007/2008 regardless of the scenario adopted (between 60% for the 2.2°C scenario and 80 % for the 1.5°C). Conversely, in the Energy and Materials sectors, under the scenario of 1.8°C there are 40% less companies at risk in 2060 than during the 2007/2008 financial crisis and under the scenario of 2.2°C there are 80% less companies at risk than during the financial crisis. In other words, the number of companies at risk in other sectors than Utilities (including intensive ones such as Energy or Materials) remains below the financial crisis level in the scenario 1.8°C.

2.2.2 Sectoral heterogenity

The three most intensive GICS sectors Utilities, Materials and Energy are the most sensitive to an increase in the carbon price. The threshold value of the carbon price – at which the probability of a company's default reaches 50% – allows us to analyze the heterogeneity within these sectors. We recall that in this study, this threshold is set arbitrarily at 50%. This parameter could be calibrated with historical data, to reflect, for example, the change of solvency corresponding to a downgrade in credit rating or the transition from investment grade to high-yield.

The median threshold carbon price for the entire universe studied is very high (nearly 10,000 USD), with the 1st quartile at 1,480 USD, i.e. a price twice as high as that envisaged by the 1.5C scenario in 2060. For the three sectors identified as the most sensitive to carbon price increases, this threshold price ranges from USD 662 (Fossil fuels) to USD 80 (Utilities), which confirms that the Utilities sector is the most sensitive to carbon price increases.

However, the risk is very heterogeneous within sectors. The ratio of the 3rd to 1st quartile of the threshold carbon price is 5.6 for the Utilities sector, while it is only 2.4 for the Materials sector

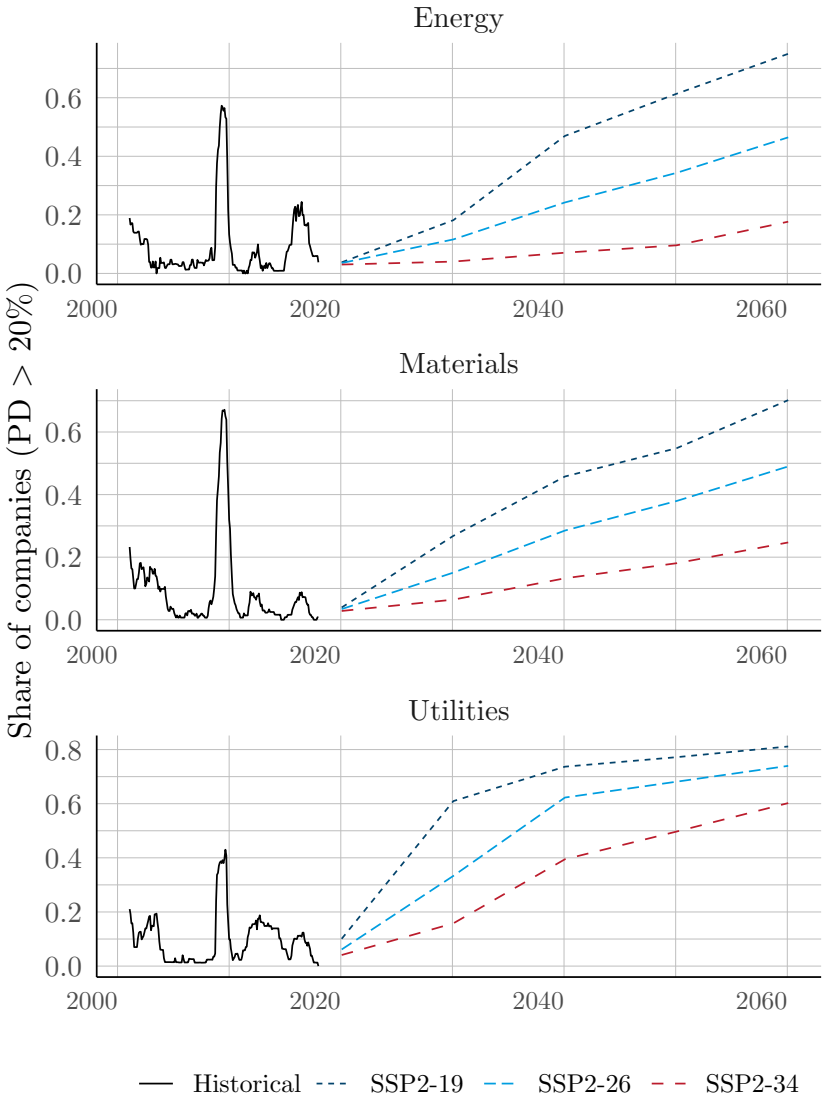

Figure 2.4 – Credit risk long term impact

Note: To compare the evolution of credit risk between sectors, we project the share of companies whose probability of default becomes greater than 20%, for each sector, according to the three long-term scenarios, and with respect to historical levels (in particular the 2007/2008 financial crisis).

and 1.5 for the Fossil Energy sector. The Utilities sector is therefore both the most sensitive, but also the one where (relative) heterogeneity between firms is greatest.

2.2.3 Sensitivity analysis

The Merton model used to calculate the probability of default for each issuer is based on extra-financial (GHG emissions), economic (EBITDA) and financial (debt ratio, volatility) variables. As

Table 2.3 – Sector statistics for variables of interest

Variable	Median	1rst Quartile	3rd Quartile
All sectors			
Scope 1	0.2	0.0	1.3
EBITDA	1.9	1.0	4.2
Debt	4.3	1.7	10.3
Market Capitalization	16.1	9.6	35.2
Volatility (1 year)	19.9	16.9	24.1
CPT	9977.5	1480.3	37979.7
Energy			
Scope 1	3.5	1.0	14.9
EBITDA	2.8	1.4	6.6
Debt	8.0	4.0	12.8
Market Capitalization	17.8	9.3	46.8
Volatility (1 year)	23.6	18.5	26.9
CPT	662.3	377.3	1392.7
Scope 1	2.2	0.5	8.6
Materials			
EBITDA	1.6	0.9	2.5
Debt	3.4	1.5	6.9
Market Capitalization	12.1	6.9	18.7
Volatility (1 year)	22.4	18.5	25.9
CPT	609.5	213.1	1673.2
Utilties			
Scope 1	20.2	4.9	35.7
EBITDA	2.8	1.7	4.2
Debt	14.1	7.5	22.6
Market Capitalization	13.7	9.2	23.9
Volatility (1 year)	17.3	12.9	19.9
CPT	80.0	43.8	489.3

Note: Scope 1 in tCO2, EBITDA, Debt and Market Capitalization (in 2021) are in billion, volatility is given in percent and the threshold carbon price in USD per ton of CO2.

the interactions between these variables are not linear, the sensitivity of the probability of default with respect to each variable depends on the values taken by the others. The relationship between the economic shock caused by an increase in the carbon price thus depends strongly on volatility: the lower the volatility, the greater the sensitivity of the probability of default to an increase in the carbon price (Figure 2.6 (a)). Conversely, the debt ratio sets the tipping point towards default but has little effect on the relationship between the probability of default and the economic shock caused by a price increase (Figure 2.6 (b)).

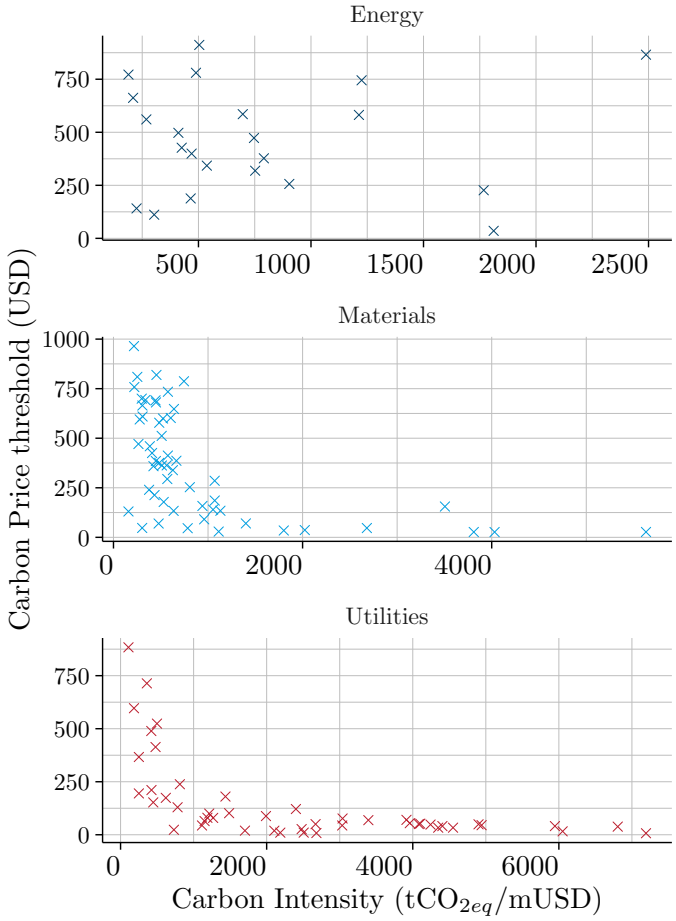

Figure 2.5 – Carbon intensity and threshold carbon price

Note: The "threshold carbon price" corresponds to the price at which the probability of the company's default reaches 50%. The carbon intensity corresponds to the company's GHG emissions in relation to its turnover. There is a decreasing relationship between the two, but it is not linear.

Empirically, the carbon price margin is correlated with carbon intensity – GHG emissions relative to sales – but the absolute value of the correlation coefficient decreases with carbon intensity. In other words, the higher the carbon price, the less impact its increase will have on the number of companies at risk. Moreover, this correlation is not homogeneous across sectors. Other economic (margin) and financial (debt ratio, volatility) variables partially compensate for a high carbon intensity. In the Fossil Energy sector, for example, the most intensive company also has one of the highest threshold carbon prices (*i.e.* lower credit risk).

(a) Sensitivity to volatility and carbon shock at constant leverage

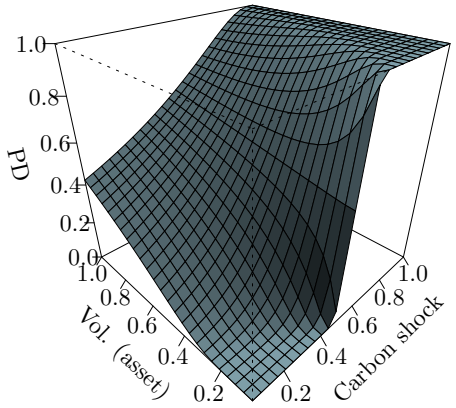

(b) Sensitivity to debt and carbon shock at constant volatility

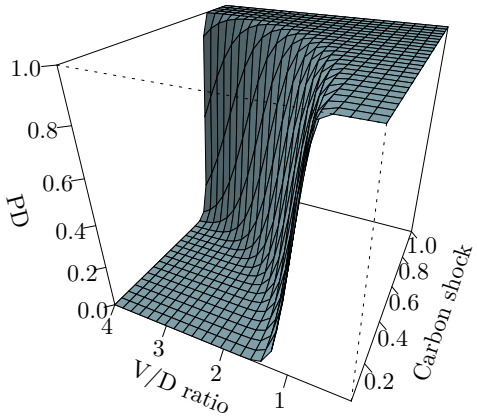

Figure 2.6 – Sensitivity of the probability of default to key variables

2.3 Discussion

This study contributes to the literature on three levels. First, the results provide a better understanding of the heterogeneity of transition risk across and within economic sectors (2.3.1). Second, these results contribute to the debate on the overall financial impact of different transition scenarios in the medium and long term (2.3.2). Finally, this study proposes a methodology and a simple indicator for measuring transition risk at the level of each counterparty (2.3.3). However, the significance of these results is limited by several factors (2.3.4).

2.3.1 A heterogeneous impact within the intensive sectors

Our results confirm that some sectors are more sensitive than others to changes in the carbon price. These sectors have already been identified in the literature as being *climate-relevant*: Utilities, Materials and Fossil fuels [13] (Battiston *et al.*, 2017; Howard & Patrascu, 2017; Vermeulen *et al.*, 2018a). However, this study contributes to a better understanding of the heterogeneity of credit risk within these sectors. For example, firms in the Utilities sector have a higher average risk, but also more heterogeneity. However, this sector deserves special attention. It provides essential services to the economy and is characterized by high concentration as well as high government intervention (through equity or subsidies). As the increase in the carbon price is a risk generated by public policy instruments (tax or emission permits), it is likely that governments will adapt price levels or provide specific measures for the sector so as not to compromise energy security.

2.3.2 Limited impact of enhanced carbon pricing mechanisms

The results of this study suggest that the 1.5C and 1.8C scenarios generate significant long-term credit risk in only three sectors (in the SSP2-34 scenario, the risk is concentrated in the Utilities sector). The carbon price associated with these scenarios (USD 780 in 2060 in scenario 1.5°C) is significantly higher than the current price (USD 1.24 on average in 2018). In the medium term, the credit risk associated with a *trend* or *acceleration* scenario is concentrated in the utilities sector and concerns less than 11% of companies in 2024 in a scenario that nevertheless foresees an annual increase in the carbon price of 40%. In the short term, this increase is necessary in order to reinforce the price signal sent to agents and to change their production and consumption patterns. In France, for example, the value of action for the climate, which serves as a reference for cost-benefit approaches, is estimated at EUR 90 in 2020 and EUR 250 in 2030. This study suggests that this strengthening of carbon pricing mechanisms could be considered without generating a significant increase in credit risk compared to historical trends.

2.3.3 A new indicator to measure carbon risk

Financial institutions are increasingly encouraged to assess, manage and communicate the climate risks associated with their financial assets. In France, for example, Article 173 of the Energy Transition Act establishes an obligation to communicate on the integration of climate

13. The transport sector does not appear explicitly because it is considered in the GICS classification as an industrial group in the "Industry" sector.

issues. Today, carbon intensity is the indicator most frequently used to measure the transition risk (ACPR-AMF, 2020). However, its value is difficult to interpret (tons of carbon dioxide equivalent per unit of sales) and the results of this study show that its relationship with credit risk is not linear and is weakly correlated for certain sectors. Although it only integrates a component of transition risk, the *carbon price margin* presented in this study makes it possible to integrate economic and financial variables into the measurement of risk, and to have an indicator expressed in monetary units, comparable to the prices observed – or implied in the case of taxes – in the regions where the production assets are located.

2.3.4 Limits

Given the quality of the extra-financial data, the multidimensional nature and indirect effects of transition risk, and the modeling assumptions used, the results of this study should be interpreted with caution and could be extended in different directions.

The first set of limitations is related to the lack of maturity of non-financial accounting. The number of standardized indicators available to assess transition risk is limited, as is the reliability and coverage of the data. By limiting itself to greenhouse gas emissions (an indicator common to all sectors), the study focuses on the impact of policy incentives, but does not take into account regulatory, technological or demand changes. To analyze transition risk, the threshold carbon price could, for example, be complemented by an analysis of assets likely to be devalued, research and development efforts (e.g., number of *green* patents) that allow for rapid adaptation to technological changes and disruptions, the market power of companies (particularly in concentrated energy sectors), and their liability risk [14] (Bolton *et al.*, 2020). In addition, missing data may introduce a downward bias, as companies that are behind in their transition may also be more reluctant to provide this information.

The second set of limitations is related to the indirect effects of an increase in the carbon price and the projection assumptions used. The increase in costs associated with an increase in the carbon price can be passed on in the price of sold product, particularly in sectors where price elasticity is low (Howard & Patrascu, 2017). This effect was observed, for example, in the electricity market during the first phase of the European permit trading system (Scholtens & van der Goot, 2014). Furthermore, the study makes the conservative assumption that GHG emissions will remain stable. However, the increase in carbon prices should be accompanied by a change in production methods that will allow firms to reduce their GHG emissions. The potential for reduction depends on both the sector and individual strategies: two companies producing electricity with the same GHG emissions today may experience different reduction trajectories depending on their ability to adapt quickly to the energy transition, in particular by investing in new, "greener" sources of energy (Bolton *et al.*, 2020).

14. The database " Climate Change Litigation database", jointly developed by the Sabin Center for Climate Change Law and Arnold & Porter, for example, provides information on more than 1,800 climate change-related corporate proceedings.

2.4 Conclusion

This article aims to answer the question: how sensitive is a firm's credit risk to the carbon price? Since 2015, a growing body of work has focused on transition risk (Campiglio *et al.*, 2018). However, few of these studies are conducted at the micro level to analyze the heterogeneity of risk within sectors (Monnin, 2018; UNEP, 2019). This study uses the GHG emissions of more than 1,000 international companies and medium (5 years) and long-term (41 years) carbon price projections to analyze the impact of an increase in the carbon price on the credit risk of companies, using the Merton model. The results confirm that three particularly intensive sectors (Utilities, Fossil Energy and Materials) are considerably impacted by a significant increase in the carbon price (several hundred dollars), but that the risk is very heterogeneous within these sectors. The results suggest, however, that this risk is limited to the most ambitious scenarios (1.5°C and 1.8°C) in the long run, and that a strengthening of current GHG pricing mechanisms is possible without compromising financial stability. The scope of the results is limited by the quality of the extra-financial data, as well as by some strong modeling assumptions (no anticipation of firms, no pass-through of emissions-related costs in the sales price). Given the acceleration in 2021 of the carbon price in the European ETS and the ongoing discussion on the implementation of a carbon adjustment mechanism at the borders, the study could be extended by focusing on the EU and by taking into account the indirect effects of an increase in the carbon price (increase in prices and decrease in quantities) as well as the mitigation potential of GHG emissions of firms.

Appendix

Indices	
$i \in \mathcal{U}$	Company
$j \in \mathcal{M}$	Country
k	Scenario
t	Date
Variables	
CC_i	Total carbon expense (cost) of an entity
CP	Local representative carbon price
D_i	Total dept
DD_i	Distance to default
PD_i	Probability of default
E_i	Equity value
EBITDA_i	Earnings before interest, taxes, depreciation, and amortization
r	risk free rate
$\mathcal{CE}_i$	Direct reported emissions
T	Maturity (Merton)
$\sigma_{v,i}$	Asset volatility
$\sigma_{e,i}$	Equity volatility
V_i	Total asset value
ξ_i	Regulatory shock on EBITDA

Chapter 3

Cascading Effects of Carbon Price through the Value Chain [1]

In 2021, the Intergovernmental Panel on Climate Change (IPCC) released the First Chapter of its Sixth Assessment Report (AR6), highlighting the need to reach net-zero emissions as soon as possible to avoid the disastrous effects of climate change. At COP26 in November 2021, governments shared the need to take concrete and radical measures to cut global GHG emissions and reach this objective. Many countries, including members of the European Union, the United States and China, strengthened their carbon reduction targets prior to or during COP26.

The understanding of the need to transition towards a low-carbon economy is now shared among governments and there is no doubt that this will affect all economic agents. Among the tools available to governments, investors and corporations to achieve those pledges, carbon pricing schemes are likely to play a key role, whether they take the form of direct carbon taxes, emissions trading systems [2], or the use of internal carbon pricing models by corporations and by financial analysts who evaluate them (Postic & Fetet, 2021; Ramstein *et al.*, 2019). By placing an adequate price on GHG emissions, carbon pricing will help decision makers internalize the external cost of climate change and set economic incentives to develop clean technology. In particular, investors can use carbon pricing to analyze the potential impact of climate change on their investment portfolios and efficiently reallocate capital towards low-carbon or climate-resilient activities.

In this chapter, we focus on assessing the effect of carbon pricing on corporate income statements. Although the cost of carbon could be incorporated by firms through different mechanisms, we consider the case of introducing a carbon pricing mechanism that would impact the operating cost of emitting corporations. We study the cross-sector diffusion of this cost through the value chain and its impact on consumers' demand and firms' earnings.

A significant amount of research has been conducted on climate stress testing frameworks and methodologies (Alogoskoufis *et al.*, 2021; Battiston *et al.*, 2017; H. Jung *et al.*, 2021). Among the few papers assessing the climate risk impact at the firm level, Bouchet and Le Guenedal (2020b)

1. This chapter is available on SSRN (Adenot *et al.*, 2022) and is the result of a partnership with Amundi Technology and Amundi Institute to build carbon stress-testing environment for portfolio managners.

2. In 2021, the price of the European Union Emissions Trading System (EU-ETS) passed the symbolic threshold of EUR 50 per tCO_{2eq}, demonstrating that market participants anticipate more stringent regulations on corporate carbon emissions.

(previous chapter) develop a methodology to assess the credit risk sensitivity of debt issuers to a carbon tax. Based on Scope 1 emissions, they estimate the impact of a carbon tax on firms' EBITDA [3], and its medium and long-term impact on corporate issuers credit risk. Berner *et al.* (2021) introduce a measure of systemic climate risk, which is a financial institution's expected capital shortfall in a climate stress scenario and develop a stress testing procedure to measure the resilience of financial institutions. A limitation of the above-mentioned approaches, however, is that they only tackle direct impacts of carbon taxation on issuers and do not consider how this tax is diffused in the economy through indirect costs via a firm's suppliers. We propose to go further and to introduce a cross-sector diffusion methodology.

It is widely acknowledged that transition and physical risks can cascade through countries and sectors and spread among unaffected parts of the economy (Naqvi & Monasterolo, 2021; Raymond *et al.*, 2020). Focusing on the sector diffusion of transition risks, Cahen-Fourot *et al.* (2019) use an Input-Output (IO) model to assess the exposure of economic systems to capital stranding cascades triggered by the reduction of fossil fuel production and use. They estimate how supply-side capital stranding might propagate across sectors and countries via production networks. In particular, they provide sector-level estimates of the exposure of capital stocks to the risk of becoming unusable due to a marginal loss of primary inputs employed in a country's fossil fuel sector. Gemechu *et al.* (2014), Mardones and Mena (2020), and Muñoz-Zamponi and Mardones-Poblete (2016) develop a sector-level stress testing method based on the Leontief (1970) approach, allowing the effects of the diffusion of carbon tax costs to be measured across various sectors in the economy. For example, Mardones and Mena (2020) estimate the impact of environmental taxes on carbon emissions and local air pollutants introduced in Chile, and use the environmental extension of the Leontief (1970) price model and micro-simulations to analyze the main economic, environmental, and distributive effects of this policy.

In these applications, however, the sector-level results cannot be used to evaluate the heterogeneous impact of the introduction of a carbon price on each specific firm. In this chapter, we propose an extension of the above-mentioned framework to estimate the shock suffered by a given firm, considering both the costs of (1) firm-level direct carbon emissions and (2) indirect emissions, whose costs propagate through the various sectors and countries because of their trading links. These costs have a price impact on the goods and services produced, and affect the final consumers' demand (Calvet & Marical, 2012), which in turn affects the firms' revenues and their earnings. Our empirical investigation derives the impact of the introduction of a carbon price on firms' earnings on the universe of firms belonging to the MSCI World Index. We consider three distinct scenarios for the carbon price, set to be equal to USD 50, 100 or 300 per ton of CO_{2eq}. This corresponds broadly to the suggested values for the SSP2-26 (1.8°C) in 2030, SSP2-19 (1.5°C) in 2030 and SSP2-19 (1.5°C) in 2040.

Our contribution to literature is twofold. First, our research is, to our knowledge, the first to apply an Input-Output framework to estimate the effect of a carbon price diffusion at the firm level. Second, while most of the Input-Output analyses are conducted for a single country, (Gemechu *et al.*, 2014; Mardones & Mena, 2020; Muñoz-Zamponi & Mardones-Poblete, 2016), we assess the impact of carbon price on firms across a large set of countries, both developed and emerging, which requires us to incorporate cross-country dependencies between sectors. We find

3. Earnings Before Interest, Taxes, Depreciation and Amortization

that apart from the high carbon-intensive sectors, such as Energy, Utilities and Materials, several low carbon-intensive sectors could be significantly impacted by the introduction of a carbon price, because of its cascading effect through the firms' supply chain. The three most carbon intensive sectors, Energy, Utilities and Materials could suffer an earnings shock of between than 7% and 12%, with the introduction of a carbon price at USD 50. However, less intensive sectors such as Information Technology, Consumer Discretionary or Consumer Staples could also incur a non-negligible shock, close to 4%.

If we consider two alternative scenarios of a carbon price at USD 100 or USD 300, in line with temperature scenarios of 1.5°C in 2030 and in 2040, respectively, these effects could be exacerbated. The average earnings shocks for carbon-intensive firms could reach 22% and 47%, respectively, for the most impacted sector (Utilities). In these two scenarios, less intensive sectors would also be heavily impacted. For example, Information Technology could be subject to earnings shocks of 8% and 23% respectively. With simple hypotheses on the relationship between earnings and the firm's value, we derive a plausible scenario for the evolution of each sector's market share in the MSCI World index. The introduction of a carbon price could have a substantial impact on the investment universe, distorting its sector composition towards less carbon intensive sectors such as Financials and Health Care.

This chapter is structured as follows. Section 3.1 presents the model, Section 5.1.1 the data used and Section 3.3 our results. Section 3.4 provides some concluding remarks.

3.1 Model

We aim to measure the impact of carbon pricing on firms' value. Carbon pricing will change consumer behavior by incentivising the consumption of low-carbon alternatives of more carbon-intensive products. The model derives the impact of carbon pricing on firms' value by computing the change in demand for a product resulting from a higher selling price. Indeed, firms are likely to increase their selling prices in order to absorb the rising marginal costs due to the introduction of a carbon price. These carbon costs are likely to diffuse across the economy. Our model estimates the carbon cost pass-through across various sectors and countries of the world economy.

3.1.1 Cross-sector diffusion model

Leontief (1970) introduced Input-Output models to quantify and represent the interdependencies between various sectors in an economy or different regional economies. In what follows, we present the way production functions are modeled in the original framework and the way this framework can be applied to estimate environmental externalities.

Leontief production function and intermediary sector consumption Following Leontief (1970), we consider a fixed-proportions production function. This means that the factors of production used to produce a given good or service are supposed to be fixed and constant, as there is no substitutability between factors. In this framework, each sector j makes use of the inputs from sector i in the fixed proportion:

$$a_{ij} = \frac{x_{ij}}{x_j} \quad 1 \leq i \leq n \quad 1 \leq j \leq n \tag{3.1}$$

where x_j is the production of the j-th sector and $x_{i,j}$ denotes the quantity sold by the i-th sector to the j-th sector. [4]

Based on the assumption that the final demand net of imports for sector i y_i is exogenous and that the production of sector i, x_i and its demand for inputs x_{ij} are endogenous, the Input-Output model can be represented in a matrix form as:

$$X = AX + Y \quad X \in \mathbf{R}^{n\times 1} \quad A \in \mathbf{R}^{n\times n} \quad Y \in \mathbf{R}^{n\times 1} \tag{3.2}$$

where:

$$X \equiv \begin{pmatrix} x_1 \\ \vdots \\ x_n \end{pmatrix} \quad A \equiv \begin{pmatrix} a_{11} & \cdots & a_{1n} \\ \vdots & \ddots & \vdots \\ a_{n1} & \cdots & a_{nn} \end{pmatrix} \quad Y \equiv \begin{pmatrix} y_1 \\ \vdots \\ y_n \end{pmatrix} \tag{3.3}$$

Equation (3.2) can be written as:

$$X = (I - A)^{-1}Y \tag{3.4}$$

The matrix $(I - A)^{-1}$ is called the Leontief inverse. The element in position ij of this matrix represents the impact of a change in final demand in the j-th sector on the i-th sector. These constant proportion parameters are retrieved from an Input-Output table (in our case, the World Input-Output database, WIOD) in the form provided in Table 3.1.1.

Table 3.1.1 – Illustration of WIOD dataset (normalized in %)

		USA			
	Sectors	(1) Crop and animal production	(2) Forestry and logging	(3) Fishing and aquaculture	···
USA	(1) Crop and animal production	0.159	0.018	0.018	···
	(2) Forestry and logging	0.025	0.041	0.041	···
	···	...	...	... ...	

Source: World Input-Output database (WIOD)

Table 3.1.1 should be understood as follows: to produce 1 dollar of output, the crop and animal production sector in the United-States buys 0.159 cents of products from itself and 0.018 cents of products from the forestry and logging (in the United States). Figure 3..1 on page 102 illustrates some sector dependencies in the United-States. The data source used to represent these dependencies is further described in section 3.2.1.

4. Depending on the data source, these tables can be found in quantity ratios or monetary value ratios. In practice, it is easier to find data in monetary value as they are easier to measure than quantities. When in monetary value, the matrix A components (a_{ij}) becomes: $\frac{x_{ij}p_i}{x_j p_j}$. In this chapter, we develop the theory using tables in quantity ratios. Fortunately, under certain assumptions described below, it is possible to use the more common monetary tables.

Application to the estimation of environmental externalities The Leontief (1970) approach can be applied to estimate environmental externalities, and in particular GHG emissions. Each sector's total attributable emissions include direct (Scope 1) and indirect emissions related to the required inputs for its activity from other sectors (i.e. upstream emissions: Scope 2 and, to some extent, Scope 3). At a sector level, the direct emission intensities are defined by $g_i = \frac{c_i}{x_i p_i}$, where c_i represents the direct absolute carbon emissions and g_i the direct emissions intensity (expressed in tCO_{2e}/mUSD) of the i-th sector. The vector of total (direct and indirect) upstream emission intensities M can be calculated using the Leontief inverse (Mardones & Mena, 2020). Noting $G = (g_1, .., g_n)^T$ the vector of sector direct GHG emission intensities (scope 1), we have:

$$M = (I - A^T)^{-1} \times G \tag{3.5}$$

Let CP be the carbon price in USD/tCO_{2e}, which is supposed to be fixed. By multiplying M by the scalar CP we obtain the vector of carbon price rate representing the amount paid per dollar of output in each sector. Letting $\mathcal{E} = (\varepsilon_1, ...\varepsilon_n)^T$ denote this carbon price rate vector, we have:

$$\mathcal{E} = \text{CP} \times M \tag{3.6}$$

where the coefficient ε_i represents the mean carbon cost of a dollar unit of production from the sector i.

Leontief price model The Input-Output approach allows to analyze the price structure of goods and services offered in each sector of the economy. Leontief (1970) assumes that firms in a given sector set their price by taking into account their marginal costs and not the variation of demand ('cost-push' price model). When there is no carbon price, and following Mardones and Mena (2020) and Mardones and Muñoz (2018) the unitary price of the i-th sector can be defined as a function of the other sector's unitary prices, of its ad valorem taxation rate: τ_i and of its value-added produced

$$v_i = wl_i + rk_i$$

where w is the price of labor, l_i is the coefficient of labor intensity, r is the cost of capital, k_i is the coefficient of capital intensity:

$$p_i = (1 + \tau_i)\left[\sum_{j=1}^{n} p_j a_{ij} + wl_i + rk_i\right] = (1 + \tau_i)\left[\sum_{j=1}^{n} p_j a_{ij} + v_i\right] \tag{3.7}$$

Note that because our analysis is run at the World level, a slight difference with Mardones and Mena (2020) is that we do not have to consider the price of imports, the coefficient of imported inputs intensity and the tariff on imports (supposed to be comprised in the tax rate at the country/sector level). In matrix form, Equation (3.7) can be rewritten:

$$P = (I - (A_\tau)^T)^{-1} V \tag{3.8}$$

with $V = (v_1, .., v_n)^T$ the vector of value added in each sector, and the matrix A_τ^T, is the transpose of the matrix of *direct requirements*, reporting the proportion in which an input from a given sector is demanded to generate a product unit of another sector:

$$(A_\tau)^T \equiv \begin{pmatrix} a_{11} + (1 - \frac{1}{(1+\tau_1)}) & \cdots & a_{1n} \\ \vdots & \ddots & \vdots \\ a_{n1} & \cdots & a_{nn} + (1 - \frac{1}{(1+\tau_n)}) \end{pmatrix} \tag{3.9}$$

The implementation of a carbon pricing mechanism modifies unitary prices. Under these new assumptions, sector prices will be equal to the average costs of production, which encompass the carbon cost. Let p_i^ε denote the new unitary price of sector i affected by carbon pricing. Under the assumption that the cost of labor and capital (and thus the value added) are the same before and after the introduction of the carbon price, p_i^ε can be written:

$$p_i^\varepsilon = (1+\varepsilon_i)(1+\tau_i)\left[\sum_{j=1}^{n} p_j^\varepsilon a_{ij} + v_i\right] \tag{3.10}$$

In matrix form, this Equation can be rewritten:

$$P(\varepsilon) = \left[(I - A_\tau^\varepsilon)^{-1}\right]^T V \tag{3.11}$$

The matrix A_τ^ε of *direct requirements* is thus slightly modified to account for the carbon price impact. It includes both carbon price and ad-valorem tax rates (respectively noted ε and τ). Its expression thus becomes (Mardones & Mena, 2020):

$$(A_\tau^\varepsilon)^T \equiv \begin{pmatrix} a_{11} + (1 - \frac{1}{(1+\tau_1)(1+\varepsilon_1)}) & \cdots & a_{1n} \\ \vdots & \ddots & \vdots \\ a_{n1} & \cdots & a_{nn} + (1 - \frac{1}{(1+\tau_n)(1+\varepsilon_n)}) \end{pmatrix} \tag{3.12}$$

Using Equation (3.8) to express the exogenous value added V as a function of the price vector $P = (p_1, .., p_n)$ when there is no carbon pricing mechanism in place, the vector of sector prices accounting for carbon pricing follows from Equation (3.11):

$$P(\varepsilon) = \left[(I - A_\tau^\varepsilon)^{-1}\right]^T (I - (A_\tau)^T)P \tag{3.13}$$

The introduction of a carbon price affects prices for consumers. If we further assume that the monetary value of what is purchased by consumers at the sector level remains constant before and after the introduction of the carbon price, [5] – i.e. the price elasticity of demand of all sectors is constant and equal to one – we derive from $P(\varepsilon)$ and P a *sector impact ratio* defined as the ratio of the production after environmental taxation to the original production. The impact ratio of the i-th sector (x_i^ε) can be calculated as:

$$\mathcal{R}_i = \frac{x_i^\varepsilon}{x_i} = \frac{p_i}{p_i^\varepsilon} \tag{3.14}$$

By further assuming that equilibrium sector prices before the introduction of carbon pricing are normalized and equal to 1 [6] (i.e. $\forall i \in [1; n], p_i = 1$), we get that:

$$\mathcal{R}_i = \frac{1}{p_i^\varepsilon} \tag{3.15}$$

5. This is a strong assumption. It would be possible to calculate empirically the elasticity of substitution i.e. a price elasticity of demand for each sector, or even for each issuer by taking into account its market power. We leave this development for further applied research.

6. This assumption also allows us to use IOTs in monetary value because then: $\frac{x_{ij}}{x_j} = \frac{x_{ij}p_i}{x_i p_j}$

3.1.2 Firm-level estimation

Our objective is to calculate an impact ratio for each firm We have granular information on firms' specific direct carbon intensities. The carbon indirect exposure of each firm however (i.e. the upstream impact of the carbon price on the firm's suppliers) can only be defined at the sector level.

Considering an issuer k part of the i-th sector, with a direct emission intensity g^k, we hypothesize that the vector of direct plus indirect emission intensities m^k is defined as the sum of an indirect carbon intensity estimated at the sector level and a direct carbon intensity. It can be written as follows:

$$m^k = \underbrace{m_i}_{\text{Sector direct + indirect intensity}} + \underbrace{\left(g^k - g_i\right)}_{\text{Issuer direct intensity relative to its sector}} \tag{3.16}$$

where m_i is the sector direct and indirect (upstream) intensity and g_i is the direct emission intensity of sector i. We then calculate an adapted carbon pricing rate vector $\mathcal{E}^k$ at the issuer level:

$$\mathcal{E}^k = \text{CP} \times m^k \tag{3.17}$$

Then, Equations (3.13) and (3.14) become respectively:

$$P(\mathcal{E}^k) = \left[(I - A_\tau^{\mathcal{E}^k})^{-1}\right]^T \times (I - A_\tau^T) \times P \tag{3.18}$$

$$\mathcal{R}_i^k(\mathcal{E}^k) = \frac{x_i^{\mathcal{E}^k}}{x_i} = \frac{p_i}{p_i^{\mathcal{E}^k}} \tag{3.19}$$

where $\mathcal{R}_i^k(\mathcal{E}^k)$ is the impact ratio measuring the reduction in demand due to the introduction of the carbon price on the issuer k.

Finally, let $\text{EBITDA}^k(0)$ be the firms' earnings before the introduction of the carbon price (we suppose the carbon price to be equal to 0 à that time) and $\text{EBITDA}^k(\text{CP})$ the earnings impacted by the introduction of a carbon price CP through the value chain (3.19). We make the hypothesis that the firms' EBITDA depends linearly on the demand for the goods and services it sells and that this relationship does not change through time or with the introduction of the carbon price. Thus, for a given value of the carbon price CP we can estimate for each issuer the percentage change in earnings due to the introduction of carbon pricing, i.e. the earnings' shock ES^k:

$$ES^k = \frac{\text{EBITDA}^k(0) - \text{EBITDA}^k(\text{CP})}{\text{EBITDA}^k(0)} = 1 - \mathcal{R}_i^k(\mathcal{E}^k) \tag{3.20}$$

In what follows, we will focus on the earnings shock due to the carbon price introduction relative to its 2019 level.

3.2 Data

3.2.1 Input-Output table

As previously discussed, an Input-Output table describes the sale and purchase relationships between producers and consumers within an economy. Our worldwide Input-Output table is provided by the World Input-Output Database (WIOD), and was last updated in 2015. [7] It covers 43 countries plus the 'rest of the world' region. [8] Our universe of firms is split between 55 private sectors within each country. We are thus dealing with a $(44 \times 55) \times (44 \times 55)$ matrix.

Figure 3.2.1 represents the direction of the main Input-Output relationships between sectors in the United States in a Kamada Kawai forced-directed graph. Interestingly, we notice that some sectors have unidirectional relationships. For example, "mining and quarrying" (4) is a clear sector input for "manufacture of basic metals" (15). On the other hand, others have bi-directional relationships, for example "motion picture video programming" (38) and "telecommunications" (39). This representation allows us to visualize potential clusters, also called communities. For examples, sub-sectors 7, 10, 12, 14, 17, 18 (all belonging to the GICS manufacturing sector), 45 ("legal and accounting activities") and 51 ("public administration and defense") have closed relationships in the United States. We can expect a similar response to a variation of carbon price between firms in this community.

Each WIOD sub-sector was mapped to a GICS sector. [9] In practice, we mapped the GICS (sub-industry) level 3 to WIOD sectors.

3.2.2 Firm characteristics

In our empirical estimation, we focus on the 1 552 firms that compose the MSCI World Index.

Financial data Firm-level Earnings before Interest, Taxes and Depreciation (EBITDA) are provided by FactSet.

Emission data We use two types of emission data:

— **Sector-level GHG emissions**: Sector-level average intensities of GHG emissions (Scope 1) are provided by Exiobase 3 [10] (see Stadler *et al.* (2018) for more detail). It covers 43 countries and 5 rest of the World regions split up between 163 sectors.

7. The World Input–Output Database (WIOD) is the outcome of a project that was funded by the European Commission from 2009 to 2012 (Timmer *et al.*, 2015). It is available at: http://www.wiod.org/database/wiots16. WIOD data has been widely used by scholars to measure global value chains (see for example Timmer *et al.*, 2014; Wang *et al.*, 2013). Among its main advantages, it offers a reasonable (but not too granular) decomposition in 55 sectors and a relatively recent update of the data. Alternative Input-Output tables are currently available, the most popular one being Exiobase: https://www.exiobase.eu/index.php/about-exiobase, but its last update is from 2012.

8. Some countries in investment universe have no direct match in WIOD sectors (e.g. Bermudas, Cayman Island, Singapore), we therefore associated in the Rest of the world cluster in this first exercise.

9. Figure 3..1 on page 102 represents (a symmetrical version) of the sector interconnections within the United States, as available in WIOD Input-Output table. Note that a slightly different representation has been adopted, allowing us to represent in the same graph the carbon intensities of each sector.

10. Available at: https://zenodo.org/record/4588235#.YQQJwqgzabg.

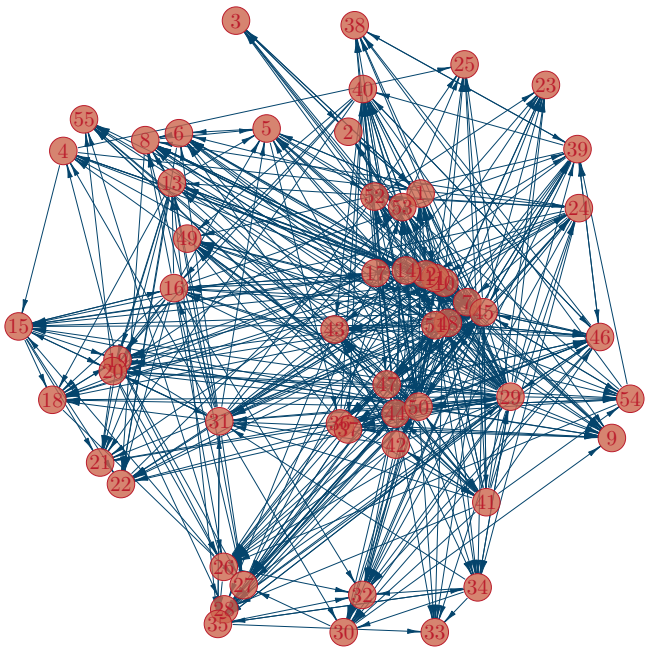

Figure 3.2.1 – Force-directed (Kamada Kawai) graph representation of the sector Input-Output relationships (WIOD table) in the United States

Note: Kamada Kawai drawing algorithm takes binary graphs as input. This chart was built taking in consideration only relations exceeding 1%.

— **Issuer-level GHG emission:** Data are provided by Trucost. We retrieve Scope 1 emissions intensity for all firms in our investment universe.

Financial data and carbon intensities are retrieved as of December 2019. Based on the data available, we can provide an estimate of the earning shock for 94% of the firms belonging to the MSCI world Index (covering 96% of the total market capitalization of the index). Table 3..2 in the same Appendix provides more detail about this coverage, in terms of number of stocks and market capitalization, for each GICS Sector.

3.2.3 Carbon price scenarios

To make realistic assumptions about carbon price evolution, we collect carbon prices corresponding to different climate scenarios as per the Shared Socioeconomic Pathways (SSP) of the IPCC. In these scenarios, the carbon price increases over time - along with the model uncertainty

- and is directly linked to the ambition of the scenario expressed in temperatures - the lower the temperature, the higher the carbon price. Whether these pathways are optimal is still an open debate and some would argue that a consistent trajectory would be setting a higher price today (Daniel *et al.*, 2019). In this chapter, we consider three different scenarios for the carbon price: USD 50, USD 100 and USD 300 per tCO_{2eq}, which correspond broadly to the suggested carbon prices for the SSP2-26 (1.8°C) in 2030, SSP2-19 (1.5°C) in 2030 and SSP2-19 (1.5°C) in 2040.

3.3 Results

3.3.1 Impact of a carbon price introduction

Figure 3.3.1 shows the dispersion of the firms' shocks to EBITDA within each GICS sector, when a carbon price of USD 50, USD 100 and USD 300 is introduced. To facilitate the representation of our results, the 56 sectors have been mapped into the 11 GICS sectors. Table 3.3.1 provides the corresponding statistics. In yellow, we also present the direct impact of the introduction of a USD 50 carbon price on EBITDA, when there is no sector diffusion of the carbon tax i.e. when only direct costs are considered, as in Bouchet and Le Guenedal (2020b) (c.f. Chapter 2). In dark blue, light blue and red, we present the results of our estimation considering the sector propagation of the carbon price impact on demand, when the carbon price is set at USD 50, USD 100 and USD 300 per tCO_{2eq} respectively.

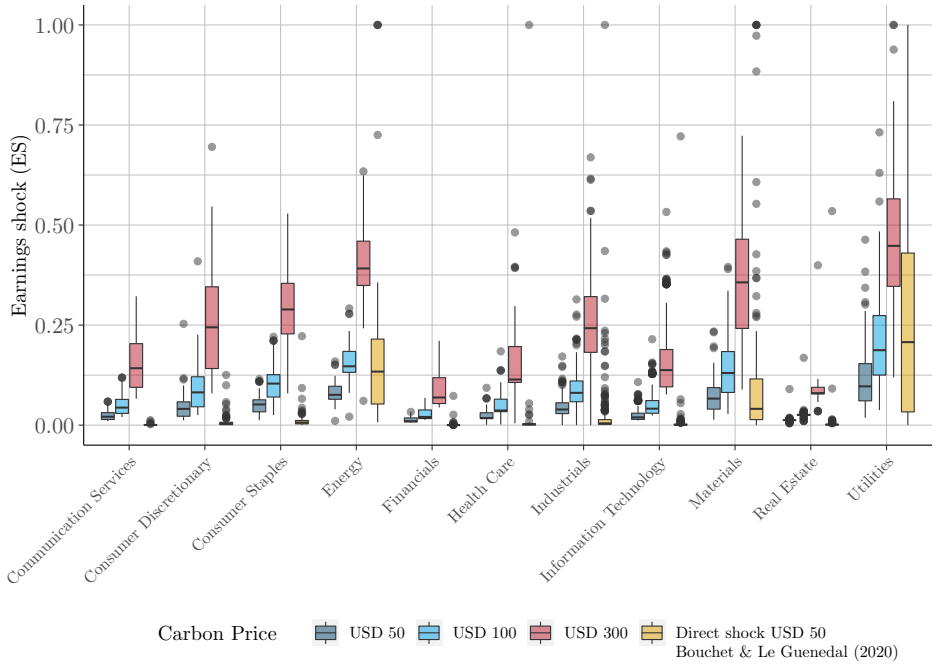

Figure 3.3.1 – Earnings shock due to the introduction of a carbon price of USD 50, 100 and 300 per tCO_{2eq} on firms belonging to the MSCI World Index, by sector

When only direct emissions are considered, only three (carbon intensive) sectors are significantly impacted: Utilities, Energy and Materials, with an average percentage change in earnings

of 28.1%, 20.4% and 13.4% respectively. All other sectors see their earnings change by less than 3% with the introduction of a carbon price of USD 50. When considering the cross-sector diffusion of the carbon price, the picture changes dramatically. The most impacted sectors, Energy, Materials and Utilities remain largely hit by a carbon price introduction, but their impact ratio is on average twice smaller than with direct costs. The percentage change in EBITDA is 11.6% vs 28.1% for Utilities, 8.2% (vs 20.4%) for the Energy sector, and 7.2% vs 13.4% for Materials (see Table 3.3.1). This is because firms in these sectors are selling their products across sectors and worldwide, thus disseminating their carbon costs.

For a carbon price level at USD 50, the least impacted sectors are Real Estate (1.3% reduction in EBITDA), Financials (1.4%) and Health Care (2.5%). The most impacted sectors (Utilities, Energy and Materials) are closely followed by Consumer Staples, Industrials and Consumer Discretionary (5.1%, 4.4% and 4.2% decrease in earnings respectively). The shock to EBITDA rises rapidly with the carbon price. For example, for the Energy sector, it goes from 8.2% to 15.7% and 40.1% when the carbon price goes from USD 50 to USD 100 and USD 300. Strikingly, for a small number of firms belonging to the Energy, Health Care, Industrials, Materials and Utilities sectors, the firm's earnings go to zero when a carbon price is set at USD 300. These firms will likely have to adapt before a large carbon price is set, lest they become completely unprofitable.

By aggregating the firms' earnings shocks at the sector level, we derive transition risk exposures for each sector. We define the market capitalization weighted *sector risk contribution* as:

$$C_i = \sum_k w_k \times \mathcal{R}_i^k(\mathcal{E}^k)$$

where w_k is the weight in the MSCI World index computed from the free-float Equity value the in December 2021. We find a total direct shock $C_{ind} = \sum_i C_i$ of 2.37% for the MSCI World Equity Index after a rise of USD 50 in the carbon price. When diffusion of carbon cost is present, the shock becomes 3.16% (See Figure 3.3.2a). The sector breakdown shows that the contribution of sectors such as Information Technology or Consumer Discretionary is not negligible, because of the large share of the index they currently represent. This suggests that sector exclusions of the most intensive sectors (Utilities, Energy and Materials) will not allow us to mitigate transition risk at the index level because of the cascading effects in the real economy. Figure 3.3.2b includes the thinner breakdown of relative risk contribution in WIOD sectors. Interestingly, we observe that for sub-industries such as computer programming or manufacture of computer components, contribution to global risk is clearly not negligible.

Figure 3.3.2 – Sector decomposition of the MSCI World total earnings shock due to the introduction of a carbon price of USD 50 per tCO_{2eq}

(a) Relative contributions of GICS sectors earning shocks

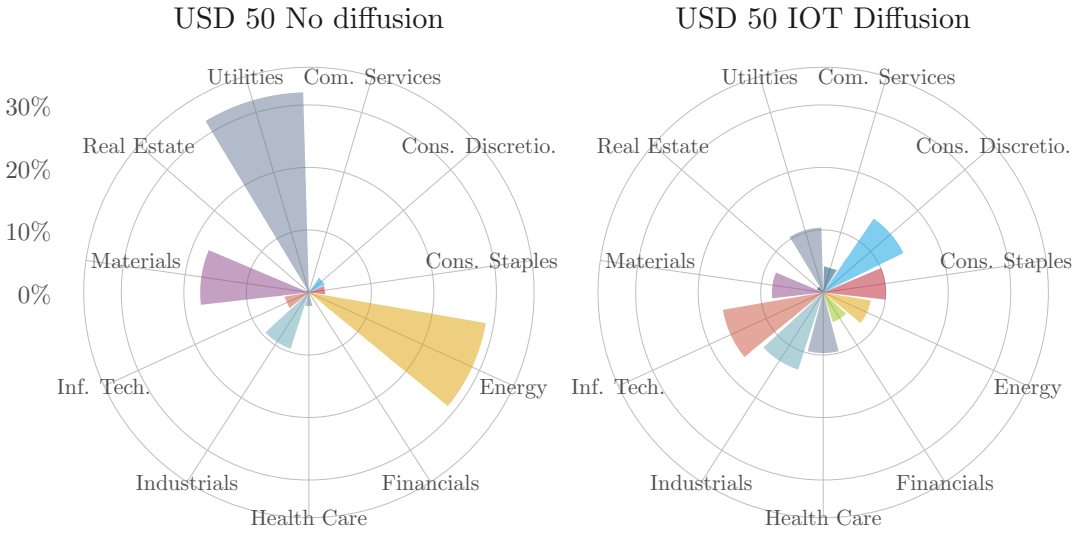

Note: the total risk contribution is respectively 2,37% in the simulation with no diffusion and 3.16 % in the simulation with USD 50 IOT diffusion. The contribution in the chart above are rebased i.e. we display $C_i / \sum(C_i)$.

(b) 35 largest relative contributions of WIOD sectors earning shocks

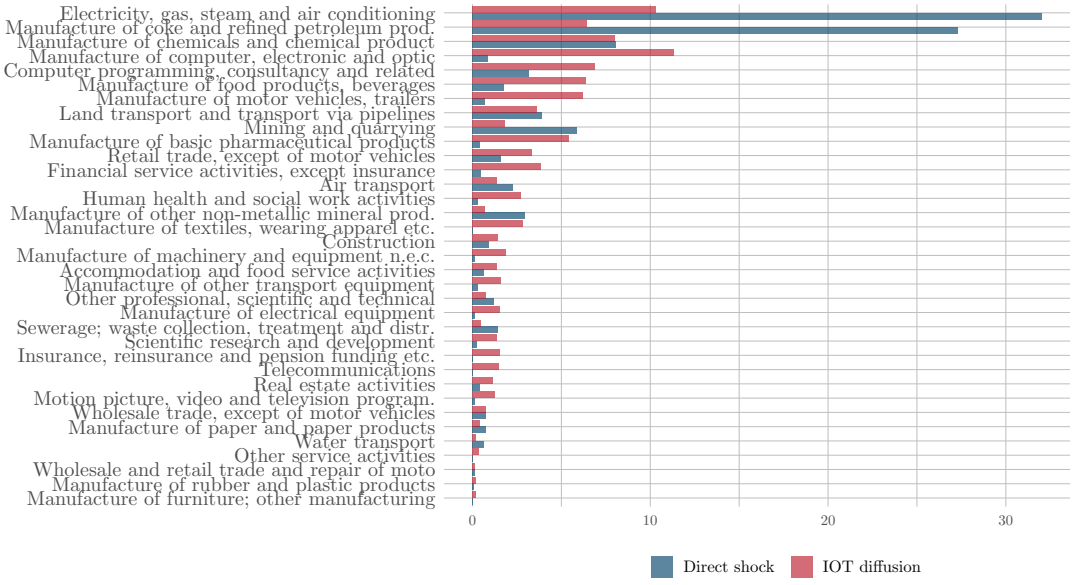

Table 3.3.1 – Earnings shock distribution by sector

	Carbon price	Sector.name	Mean	St. dev.	Q1	Median	Q3
Direct chock	$ 50.00	Communication Services	0.09%	0.17%	0.02%	0.04%	0.09%
		Consumer Discretionary	0.74%	1.54%	0.12%	0.38%	0.71%
		Consumer Staples	1.18%	2.37%	0.32%	0.65%	1.16%
		Energy	20.42%	24.92%	5.28%	13.37%	21.49%
		Financials	0.22%	1.00%	0.00%	0.01%	0.02%
		Health Care	1.07%	8.60%	0.06%	0.17%	0.37%
		Industrials	2.72%	8.45%	0.20%	0.45%	1.37%
		Information Technology	0.75%	5.71%	0.02%	0.08%	0.25%
		Materials	13.45%	23.18%	1.38%	4.07%	11.54%
		Real Estate	0.91%	5.63%	0.07%	0.12%	0.21%
		Utilities	28.13%	29.64%	3.31%	20.74%	43.00%
IOT shock diffusion	$ 50.00	Communication Services	2.49%	1.34%	1.41%	2.11%	3.12%
		Consumer Discretionary	4.19%	2.75%	2.22%	4.06%	5.82%
		Consumer Staples	5.07%	2.49%	3.32%	5.17%	6.32%
		Energy	8.16%	2.77%	6.46%	7.56%	9.71%
		Financials	1.38%	0.69%	0.80%	0.99%	1.80%
		Health Care	2.50%	1.44%	1.63%	1.77%	3.10%
		Industrials	4.40%	2.44%	2.88%	3.91%	5.58%
		Information Technology	2.67%	1.84%	1.43%	1.94%	2.98%
		Materials	7.24%	4.14%	3.99%	6.63%	9.37%
		Real Estate	1.32%	0.83%	1.19%	1.24%	1.29%
		Utilities	11.59%	8.53%	6.07%	9.69%	15.36%
IOT shock diffusion	$ 100.00	Communication Services	5.12%	2.69%	2.93%	4.37%	6.43%
		Consumer Discretionary	8.60%	5.17%	4.58%	8.18%	12.09%
		Consumer Staples	10.19%	4.86%	7.02%	10.38%	12.62%
		Energy	15.71%	4.99%	13.19%	14.70%	18.43%
		Financials	2.86%	1.45%	1.64%	2.04%	3.80%
		Health Care	5.17%	2.94%	3.36%	3.65%	6.48%
		Industrials	8.95%	4.66%	5.84%	8.06%	11.03%
		Information Technology	5.57%	3.81%	2.97%	4.12%	6.13%
		Materials	14.07%	7.24%	8.16%	13.03%	18.38%
		Real Estate	2.71%	1.54%	2.47%	2.55%	2.68%
		Utilities	20.76%	13.45%	12.51%	18.73%	27.38%
IOT shock diffusion	$ 300.00	Communication Services	15.82%	7.23%	9.45%	14.22%	20.36%
		Consumer Discretionary	24.50%	11.97%	14.14%	24.44%	34.56%
		Consumer Staples	28.16%	11.41%	22.80%	28.90%	35.44%
		Energy	40.09%	10.12%	34.90%	39.16%	45.97%
		Financials	9.24%	4.48%	5.39%	6.90%	11.85%
		Health Care	15.71%	7.88%	10.66%	11.40%	19.63%
		Industrials	25.47%	10.78%	18.19%	24.23%	32.12%
		Information Technology	16.92%	9.91%	9.56%	13.75%	18.89%
		Materials	36.07%	13.73%	24.17%	35.67%	46.46%
		Real Estate	8.69%	3.63%	7.80%	7.99%	9.45%
		Utilities	45.10%	19.86%	34.68%	44.80%	56.55%

3.3.2 Sensitivity analysis

Sensitivity to firms' direct emissions The large cross-sectional dispersion observed at the firm level within sectors, should reflect (at least partly) firms' dispersion in their levels of direct emissions. Figure 3.3.3 plots the firms' carbon price impact on earnings (for a carbon price set to USD 50 / tCO_{2e}) as a function of their Scope 1 carbon intensity [11]. There is a global positive relationship between firm level carbon intensity and the carbon price impact on earnings. However, at a global level, the relationship is not linear. To measure the sensitivity of the earnings' shock ES (our transition risk metric) to the firms' direct emissions (Scope 1 carbon intensity $\mathcal{CI}_1$), we perform the following regression:

$$ES = a + \beta \mathcal{CI}_1 \tag{3.21}$$

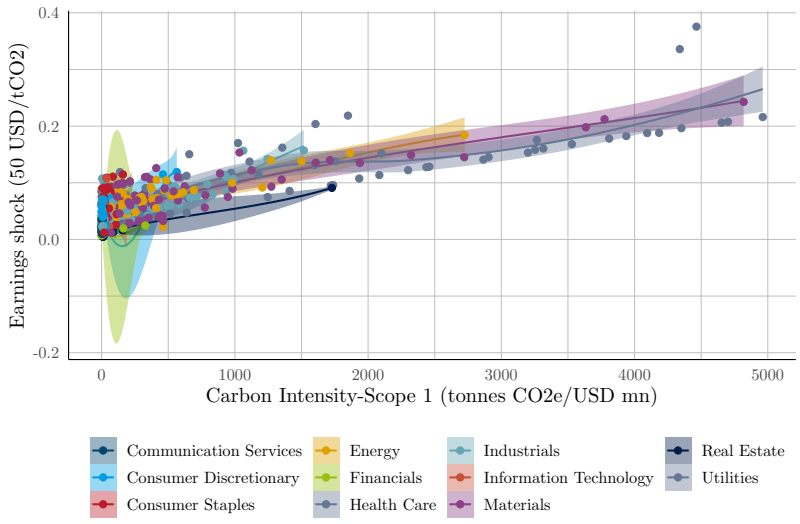

Figure 3.3.3 – Firms' earnings shock due to the introduction of a carbon price of USD 50, depending on their carbon intensity, MSCI World

For directly intensive sectors, such as Energy, Utilities, Materials, but also for Real Estate, the level of emissions is the main factor explaining the earnings shocks. Table 3.3.2 shows that the explanatory power of the single factor regression is high for intensive sectors (R-square higher than 64%). Results are consistent with the fact that the carbon risk of intensive actors should be proportional to their level of emission while we expect non-intensive actors to be impacted by other indirect effects. Note that removing one outlier firm (Swire Pacific) classified by GICS in the Real Estate sector, while its activity involves many other activities such as aviation, beverages and food chain, marine services, and trading and industrial, reduces the R-square of the Real Estate Sector to 12.6%.

Sensitivity to indirect sector intensity Firms belonging to less carbon intensive sectors should have a lower correlation between their transition risk measure and their idiosyncratic Scope 1 direct emissions intensity. Table 3.3.2 confirms that for sectors such as Health Care, Financials,

11. firms' sector can be visualized through the colors of the dots.

Table 3.3.2 – Descriptive statistics of single factor linear regressions of earnings shocks (due to a USD 50 carbon price introduction) and Carbon Intensity, for each sector - Equation (3.21)

Sector	β	R^2_{adj}	N obs
Health Care	0.0799	0.3 %	146
Financials	0.0385**	1.33 %	218
Industrials	0.0638***	48.60 %	240
Consumer Staples	0.190**	6.48 %	113
Consumer Discretionary	0.0363***	42.69 %	159
Information Technology	0.184**	4.97 %	177
Utilities	0.0392***	75.58 %	84
Materials	0.0405***	64.78 %	111
Real Estate	0.0459***	94.70 %	94
Energy	0.0485***	69.50 %	49
Communication Services	0.0232	-0.92 %	89

Signif. codes: $\star\star\star$ 0.01 $\star\star$ 0.05 $\star$ 0.1
Note: firm carbon intensities (Scope 1 emissions) are in $GtCO_{2e}$/USD mn.

Information Technology, or Communication Services, the relationship is weak. This is consistent with the idea that for firms belonging to these low carbon-intensive sectors, profitability will not be affected by the direct pricing on the relatively low emissions implied by their activity, but rather by the change of prices in their supply-chain [12]. Our methodology allows to encompass both idiosyncratic and sector-level or country-level systematic risk implied by a shift in carbon price.

Because our model is based on sector × country level indicators, we should be able to capture the influence of this supply-chain indirect intensity by considering for each firm the indirect carbon intensity of its sector and country. Thus, we will measure the sensitivity of the firms' earning shock to issuer direct ($\mathcal{CI}_1$) and indirect emission intensity, by estimating the following relationship:

$$ES = a + \beta_{\text{direct}}\mathcal{CI}_1 + \beta_{\text{indirect}}\left(m_{i,c} - g_{i,c}\right) + \epsilon_{i,c} \tag{3.22}$$

where $m_{i,c}$ denotes upstream direct and indirect intensities at the WIOD sector i and country c level. To account only for indirect upstream emissions, we subtract the average sector intensity $g_{i,c}$ from the $m_{i,c}$ (containing both direct and indirect emission by construction).

Table 3.3.3 presents the descriptive statistics of the regression corresponding respectively to the impact of the variation of USD 50 in the world carbon price for intensive and non-intensive sectors. We note that for non-intensive sectors, the scope 1 emission intensity is less significant (Consumer stable, discretionary, and communication services). In general, the above two-factor model explains well the earnings shock obtained with the diffusion methodology for a given value of carbon price variation but the betas and intercept both depend on the carbon price [13]. Figure

12. In fact, these sectors risk arise from their scope 3. In this study, we focus on upstream component of the scope 3. We leave the downstream emission for further research, as data on the matter in not mature.

13. However, the relative sector exposures ($\frac{\beta}{\sum_{i=1}^{11}\beta_i}$) is stable although there are slight non-linear effect at a GICS level because the diffusion is performed using the WIOD mapping. Also, the value of the betas are hard to interpret because of the very different possible values (and scales) of variables $\mathcal{CI}_1$, $m_{i,c}$ and $g_{i,c}$.

Table 3.3.3 – Descriptive statistics of multi-factor linear regressions of earnings shocks (due to a USD 50 carbon price introduction) on firm's direct Carbon Intensity and sector indirect emissions, for each sector - Equation (3.22)

Sector	β_{direct}	β_{indirect}	R^2_{adj}	N obs
Health Care	$0.0656^{\star\star\star}$	$0.157^{\star\star\star}$	98.3%	142
Financials	$0.0550^{\star\star\star}$	$0.154^{\star\star\star}$	94.2 %	200
Industrials	$0.0386^{\star\star\star}$	$0.167^{\star\star\star}$	97.2 %	223
Consumer Staples	0.0153	$0.146^{\star\star\star}$	95.6 %	108
Consumer Discretionary	$0.0391^{\star\star\star}$	$0.172^{\star\star\star}$	97.5 %	149
Information Technology	$0.0543^{\star\star\star}$	$0.169^{\star\star\star}$	99.7 %	81
Utilities	$0.037^{\star\star\star}$	$0.102^{\star\star\star}$	94.8 %	76
Materials	$0.044^{\star\star\star}$	$0.162^{\star\star\star}$	98.1 %	106
Real Estate	$0.0486^{\star\star\star}$	$0.0974^{\star\star\star}$	72.1 %	76
Energy	$0.0470^{\star\star\star}$	$0.124^{\star\star\star}$	92.7 %	46
Communication Services	$0.0466^{\star\star\star}$	$0.139^{\star\star\star}$	95.4 %	38

Signif. codes: $\star\star\star$ 0.01 $\star\star$ 0.05 $\star$ 0.1
Note: firm carbon intensities (Scope 1 emissions) are in $GtCO_{2e}$/USD mn. The difference between the number of observation is related to issuer in countries not in the WIOD tables. To increase the coverage in the stress-test however, we mapped these issuer to the rest of the world aggregate.

3.3.4 illustrates the relationship between the earning shock *ES*, the carbon intensities and the indirect carbon intensity $m_{i,c}$ when introducing a carbon price of USD 50 [14].

Using a proxy of firms' indirect carbon emissions at the sector × country level significantly improves the explanatory power of the regressions. In particular, the dispersion of firms' transition risk, for firms belonging to the Information Technology sector, and to a lesser extent non directly intensive sectors such as Communication Services and Financials, is relatively well explained by the linear supply-chain multi-factor model. For these sectors, non-negligible residual errors remain and estimating the firms' earning shock requires the full network analysis and cannot be captured by linear effects.

3.3.3 Impact on index composition

The transition risk estimated in the previous section may have important consequences on the composition of the investment universe. Assuming that earning shocks will translate into firm value and thus market capitalization shocks, we can estimate the potential impact of a carbon price introduction on index constituents and measure the resulting distortion in the index composition.

Let us assume that the firms' value (EV_k) is proportional to its earnings (Bouchet & Le

14. Direct and indirect contributions axis are in logarithm scale for visualisation reasons. Similar figures can be obtained when considering a higher carbon price at USD 100 or USD 300. The *height* of the plot, characterizing the intercept of the regression, depends mostly on the carbon price. The higher the price, the higher the global impact.

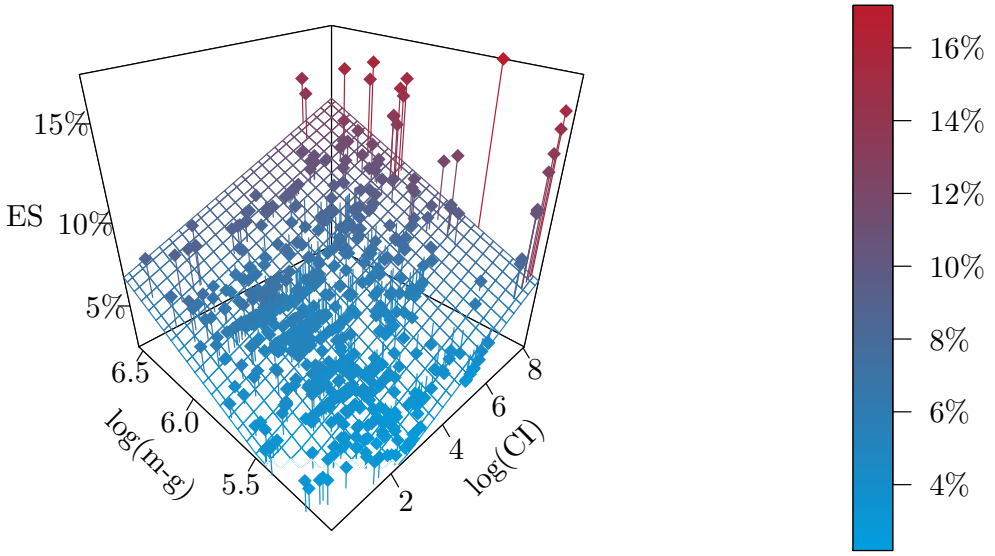

Figure 3.3.4 – Firms' earnings shock due to the introduction of a carbon price of USD 50, depending on their idiosyncratic carbon intensity and indirect upstream sector×country emission intensities, MSCI World

Guenedal, 2020b), we can write:

$$\mathrm{EV}_k(t) = r_k \times \mathrm{EBITDA}^k(t) \tag{3.23}$$

where r_k is a corporate-specific ratio that is supposed to be constant through time [15]. This implies that:

$$\frac{(\mathrm{EV}_k(\mathrm{CP}) - \mathrm{EV}_k(0))}{\mathrm{EV}_k(0)} = \frac{(\mathrm{EBITDA}^k(\mathrm{CP}) - \mathrm{EBITDA}^k(0)) \times r_k}{\mathrm{EBITDA}^k(0) \times r_k} = -ES^k \tag{3.24}$$

The enterprise value represents the total asset summing over the free-float market capitalization (Equity) and total debt:

$$EV_k = E_k + D_k \tag{3.25}$$

Assuming that the debt remains constant we have:

$$\Delta EV_k(\mathrm{CP}) = \Delta E_k(\mathrm{CP}) \tag{3.26}$$

15. In practice, this ratio can be subject to non negligible variations when considering long time periods.

and, using Equation (3.24) the shock is fully passed on the equity price such as:

$$\Delta E_k(\mathrm{CP}) = (\mathcal{R}_i^k(\mathcal{E}^k) - 1) \times \mathrm{EV}_k(0) \tag{3.27}$$

We can now estimate the changes in firms' weights in the index due to the carbon price introduction. For each firm, its new weight in the index depends on the experienced earning shock, leading to a shock to its market capitalization.

$$E_k(\mathrm{CP}) = E_{k,0} - ES_k \times \mathrm{EV}_k(0) \quad \text{and} \quad w_k(\mathrm{CP}) = \frac{E_k(\mathrm{CP})}{\sum_k^N E_k(\mathrm{CP})} \tag{3.28}$$

where $E_k(\mathrm{CP})$ is the estimation of float-adjusted market capitalization of the firm k after the introduction of a carbon price CP, and $w_k(\mathrm{CP})$ is the corresponding weight in the index [16].

We aggregate firms' weights shocked by the carbon price at the sector level and obtain a new sector composition of the MSCI World index (for each carbon price scenario: USD 50, 100 or 300). We can then compare this projected sector composition of the MSCI World to the current composition of the index as displayed in Table 3.3.4 and Figure 3.3.5.

Table 3.3.4 – Sector composition of the MSCI World before and after a carbon price introduction at USD 50, 100 and 300

		USD 50		USD 100		USD 300	
	MSCI World*(%)	weight (%)	relative change	weight (%)	relative change	weight (%)	relative change
Communication Services	7.4	7.5	1.6%	7.6	3.0%	7.9	7.6%
Consumer Discretionary	12.9	12.8	-0.8%	12.6	-1.9%	11.9	-7.5%
Consumer Staples	6.9	6.8	-1.8%	6.7	-3.9%	6.0	-13.2%
Energy	3.1	2.8	-8.6%	2.6	-16.9%	1.6	-49.8%
Financials	13.0	13.5	3.3%	13.9	6.7%	15.9	21.6%
Health Care	12.7	12.9	1.5%	13.1	3.0%	13.7	8.4%
Industrials	10.0	9.9	-1.3%	9.7	-3.0%	8.9	-10.9%
Information Technology	24.4	25.0	2.2%	25.5	4.3%	27.5	12.5%
Materials	4.0	3.8	-4.7%	3.6	-9.3%	2.9	-26.6%
Real Estate	2.8	2.9	2.5%	2.9	5.0%	3.2	15.4%
Utilities	2.8	2.3	-18.8%	1.8	-34.5%	0.4	-84.6%

* The original MSCI World index composition has been rebased to account for missing data on firms' carbon emissions. We cover 96% of the original index.

We find that the introduction of a carbon price has a non-negligible impact on the investment universe, distorting the sector composition of the MSCI World index. Introducing a USD 50/ton

16. Note that for financial firms, we apply the ratio directly to market cap at at t=0: $E_k(\mathrm{CP}) = E_{k,0} - \mathcal{R}_i^k(\varepsilon^k) \times \mathrm{E}_k(0)$, so we do not introduce irrelevant debt for this sector. Applying a similar methodology for all sectors would provide similar results with lower amplitude impacts.

Figure 3.3.5 – Carbon price adjusted indices

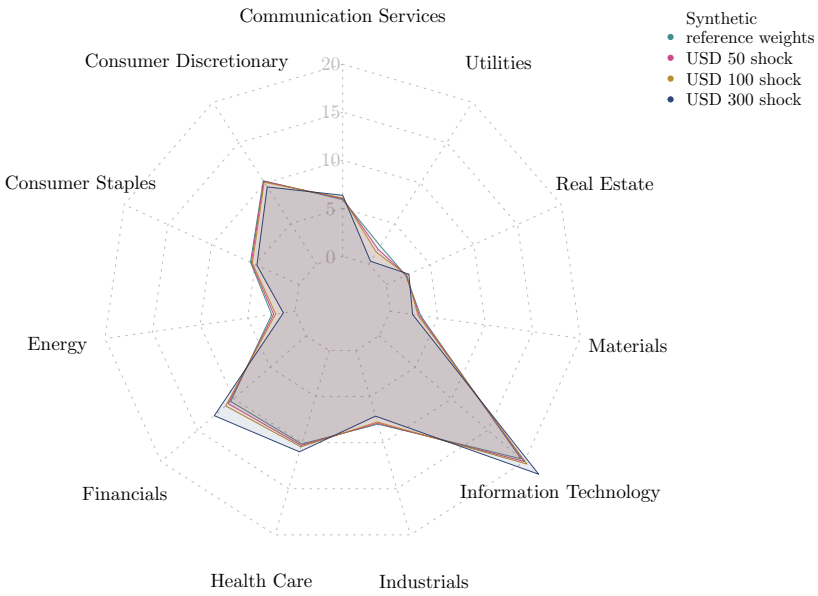

shock would reduce the weight of the Utilities, Energy and Materials sectors by respectively 18.8%, 8.6% and 4.7% in relative terms. On the contrary, the Financial and Real Estate sectors benefit substantially from the carbon shock because of their relatively low direct carbon intensity and limited first tier (upstream) indirect emissions (3.3% and 2.5% relative increase in their weight, respectively). These results should however be interpreted with caution because the impact on the Financial sector could most likely derive from other channels (downstream impact and financial contagion to other sectors) than the ones investigated in this analysis. The Information Technology, which is currently the largest sector in the index, sees its weight increase by 2.2% in relative terms. When considering the introduction of a carbon price at USD 100 or 300, the sector deviations in the index become very large, with a relative sector weight reduction up to 84.6% for Utilities, 49.8% for the Energy sector and 26.6% for Materials. The Financial sector benefits the most. Its sector weight in the index increases by 21.6% in relative terms for a carbon price at USD 300.

3.4 Conclusion

Central bankers are now used to conduct stress testing exercises of banks' exposures to climate risk (see for example Allen *et al.* (2020), Alogoskoufis *et al.* (2021)). A number of supervisors already considered the extension of climate stress tests to investors, such as insurance companies

and pension funds (Vermeulen *et al.* (2018b), EIOPA (2022)). However, climate stress tests are still not widespread in the investment management industry, despite the recent recommendation by ESMA (2022). Our study offers a methodological step in that direction, that could hopefully be useful for investors willing to implement simple stress testing exercises at their portfolio level.

An important insight from our analysis is that even low carbon-intensive sectors could be substantially impacted by the introduction of a carbon price, because of its cascading effect on firms' supply chains. Although carbon intensive sectors, such as Utilities, Energy and Materials, could suffer earnings shocks between 7% and 12%, with the introduction of a carbon price at USD 50, less intensive sectors such as Information Technology, Consumer Discretionary and Consumer Staples could also incur non negligible shocks, close to 3-4%. In the case of a higher carbon price, these effects could be exacerbated. The earnings shock for carbon-intensive firms could reach 21% (and even 45%) on average for the most impacted sector (Utilities), with a carbon price of USD 100 and USD 300 respectively. In these two scenarios, less intensive sectors would also be heavily impacted. For example, the Information Technology sector could be subject to earnings shocks of 6% and 17% in these two carbon price scenarios, respectively. Interestingly, the introduction of a carbon price will have a substantial impact on the investment universe, distorting the sector composition of the main indices. Our exercise based on the MSCI World index shows that introducing a USD 50/ton shock would significantly lower the weight of the Utilities, Energy and Materials sectors, while the Financials and Real Estate sectors would benefit the most.

Our results should be put into perspective as they rely on simplifying model assumptions and data limitations. On the data side, the Input-Output tables of direct requirements provide static information about flows between sectors. In the past, the supply-chain relationships between sectors remained relatively stable over time. However, in the context of a rapidly evolving environment, such as the one triggered by the shift in climate change, this assumption might no longer be valid. Firms in our analysis, even if they are dealing with multiple activities, have been assigned to one unique sector, which might bias the estimates for highly diversified firms. Moreover, the Input-Output tables describe broad supply chain relationships between sectors, but there might be considerable dispersion at the firm level within a given sector. The same limit applies to the firm's country classification. Issuers are only associated with their country of incorporation, attached to their ISIN. Firm-level supply chain data, allowing us to establish precise relationships between a given supplier and its clients, could be used to improve the framework. But, like Input-Output data, supply-chain data provide little information on the nature, strength or substitutability of the supply-chain relationships.

On the methodological side, we made several strong assumptions that could probably be relaxed. Prices before the introduction of carbon pricing are normalized to 1. In practice, elasticities of substitution are likely to be specific to products, sectors and countries and depend on exogenous factors. Additionally, we considered a global carbon price that would be imposed on all sectors and countries uniformly. This does not factor in existing carbon pricing mechanisms and their plurality. Carbon pricing initiatives are local, and taxes or allowance prices are sometimes fixed at a sector level. Finally, we assumed cost pass-through to be equal to 1, meaning that the entire cost would be passed on by firms to their customers. In practice, firms may choose to absorb part of this cost by reducing their margins. More complex methods could be designed to assess the impact of a carbon price. For example, Xie (2000) developed an environmentally extended social accounting matrix, which describes in a more comprehensive way the relationships between

production activities, production factors, income, consumption and capital accumulation in an accounting framework. Other alternative approaches would involve using a General Equilibrium model (Guo *et al.*, 2014; Siriwardana *et al.*, 2011) to simulate the effect of the carbon price on firms' profits, while making assumptions on economic agents' behavior.

Appendix

Table 3..1 – Notations

Indices	
i, j	Sectors
k	Issuer
Variables	
y_i	Final demand net of imports for the i-th sector
x_i	Initial production level of the i-th sector
x_i^{ε}	Production level of the j-th sector after carbon price introduction
$x_i^{\varepsilon^k}$	Production level of firm k after carbon price introduction
x_{ij}	Production sold by the i-th sector to the j-th sector
a_{ij}	Technical coefficient: Input-Output matrix element
g_i	Direct emissions intensity of the i-th sector
m_i	Direct and indirect emissions intensity of the i-th sector
e^k	Direct emissions intensity of firm c
m_i^k	(Cie k not in the i-th sector) Direct and indirect emissions intensity of the i-th sector
m_i^k	(Cie k in the i-th sector) Direct emissions intensity of firm c and indirect emissions intensity of the j-th sector
CP	Carbon price ($\$/tCO_2e$)
ε_i	Carbon price rate ($ taxed/$ output)
τ_i	Ad valorem tax in the i-th sector
p_i	Initial unitary price in the i-th sector
p_i^{ε}	Unitary price in the i-th sector after carbon price introduction
$p_i^{\varepsilon^k}$	Unitary price of firm k carbon price
w	Price of labor
l_i	Coefficient of labor intensity in the i-th sector
r	Cost of capital
k_i	Coefficient of capital intensity in the i-th sector
t_i^m	Tariff on imports in the i-th sector
p_i^m	Unitary price of imports in the i-th sector
q_i	Coefficient of imported inputs intensity in the i-th sector
EBITDA^k	Initial EBITDA of firm k
EBITDA$^{\varepsilon^k}$	EBITDA of firm k after carbon price introduction
$\mathcal{R}^k$	Enterprise Value to EBITDA ratio
EV^k	Enterprise Value of firm k

Table 3..2 – Investment universe covered in our analysis

GICS	Cov. (N stocks)	Mkt cap (MSCI World)	Mkt cap (study)	Cov. (Mkt cap)
Communication Services	88,00%	8,58%	7,09%	82,61%
Consumer Discretionary	93,49%	12,64%	12,36%	97,77%
Consumer Staples	94,07%	6,78%	6,66%	98,24%
Energy	96,00%	3,09%	2,96%	95,79%
Financials	96,89%	13,27%	12,51%	94,28%
Health Care	92,90%	12,32%	12,17%	98,72%
Industrials	94,07%	10,03%	9,59%	95,57%
Information Technology	94,12%	23,88%	23,44%	98,14%
Materials	93,91%	4,01%	3,84%	95,61%
Real Estate	95,83%	2,70%	2,67%	99,04%
Utilities	98,81%	2,68%	2,68%	100,00%
Total	94,3%	100,00%	95,97%	95,98%

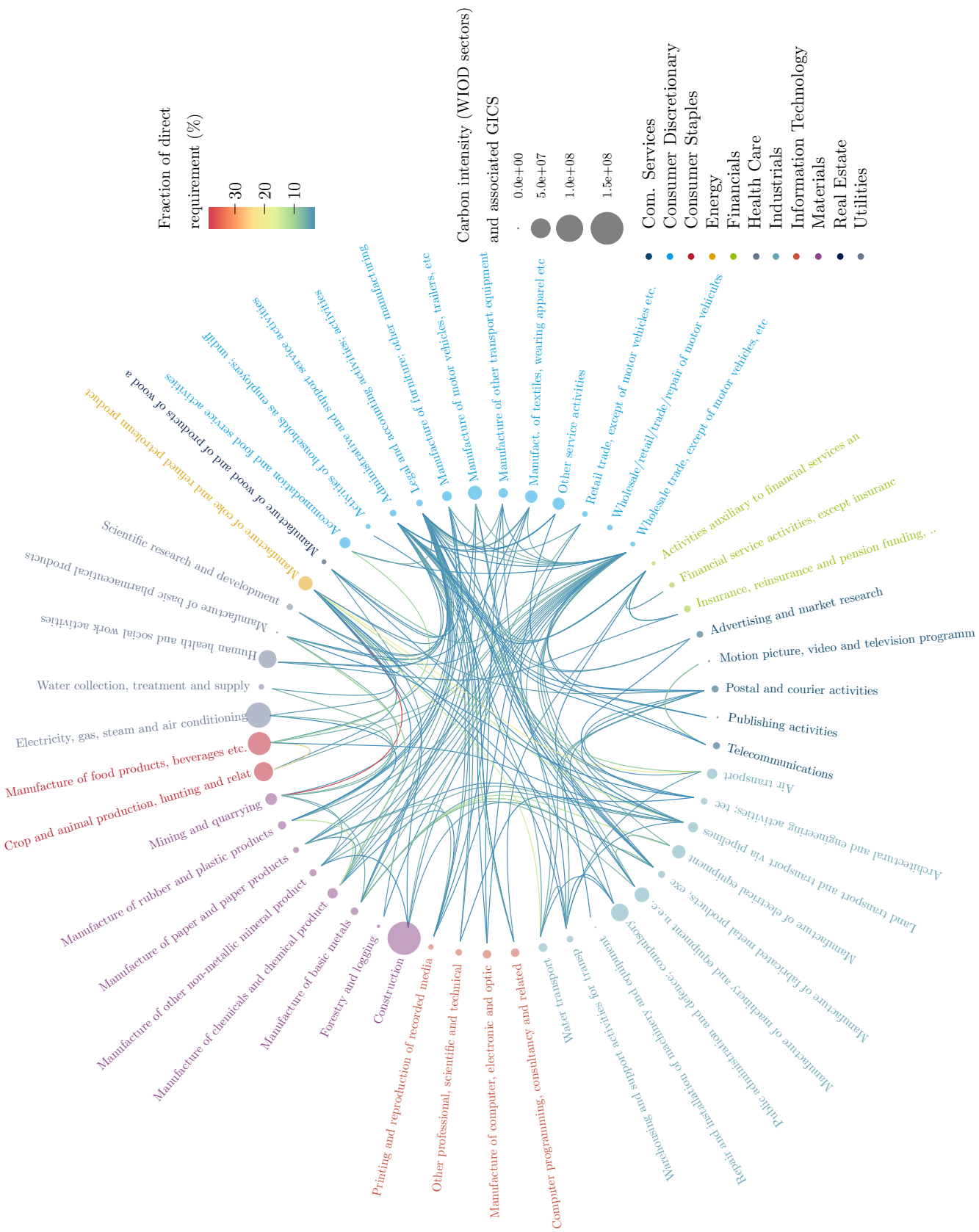

Figure 3..1 – Connection between WIOD sectors (within the US) mapped in GICS categories

Chapter 4

Corporate Debt Value under Transition Scenario Uncertainty [1]

4.1 Introduction

Since the landmark "*Tragedy of the horizons*" speech by Mark Carney (2015), the understanding that climate change creates both threats and opportunities for the financial sector became common knowledge. Among the climate-related risks, transition risks are likely to be the most material in the short-term. These risks are not directly related to climate events but rather to asset stranding, policy changes and shifts in consumer and investment sentiment related to climate change adaptation and mitigation (Bank of England, 2017; TCFD, 2017). The Basel committee in its recent publications (Basel Committee on Banking Supervision, 2021, 2022) emphasizes that banks should identify, monitor and manage all material climate-related financial risks and in particular understand the impact of climate-related risk drivers on their credit risk profiles. This paper therefore focuses on the impact of transition risk and transition scenario uncertainty on the credit risk of corporate bonds.

The modern approach to transition risk measurement and management is based on scenario analysis. A scenario describes a possible future by specifying the evolution of a range of economic variables. Climate-economy scenarios are produced by integrated assessment models (IAMs), and describe the evolution of the economy under given climate conditions (1.5°C scenario) or climate policy assumptions. These scenarios are developed and published by international organizations (Network for Greening the Financial System, NGFS; International Energy Agency, IEA), research institutes, governments or multinational companies. To each scenario corresponds a series of variables evolving in time (GDP, energy demand CO2 emissions, carbon price). Among them, we use the price of carbon as primary indicator of greenhouse gas (GHG) regulation risk. We acknowledge the limitations of this approach, as carbon price cannot be the only tool to ensure transition (Campiglio, 2016). However, from a financial risk management perspective, and assuming that carbon prices produced by IAMs are not necessarily explicit and may represent other transition mechanisms, this variable constitutes a suitable proxy of the regulatory risk incurred by a company. Moreover, unexpected jumps in carbon prices are more likely to impact the creditworthiness of carbon intensive companies than other more gradual measures.

1. This chapter is available on SSRN (Le Guenedal & Tankov, 2022).

While the scenario approach is an important tool to understand the sensitivity of the financial system to climate risks, it does suffer from a number of drawbacks. The most important one is probably the inherently static nature of the scenarios, which are assumed to be completely known at the time of the stress testing exercise, and are only rarely updated. In practice, the worst-case situation in terms of transition risks (disorderly transition) involves sudden variations in the price of carbon leading to direct defaults by companies that did not anticipate the magnitude of the variation, fire sales and contagion effects, as outlined in Roncoroni *et al.* (2021). In this context, the methods based on fully deterministic trajectories are clearly not suitable for dynamic financial risk management, which requires computing the sensitivity of portfolios to carbon price changes, and developing dynamic hedging strategies.

To fill this gap, we propose a framework for the dynamic management of transition-related default risk accounting for scenario uncertainty. We start with a set of possible scenarios and assume that the agent does not know the scenario a priori, but deduces posterior scenario probabilities from the observation of carbon price shocks, which are modelled with a jump process. We use a model inspired by Leland and Toft (1996) and subsequent literature on the topic, where the default (or restructuring) time is endogenously determined by the shareholders to maximize the equity value. A jump in the carbon price therefore triggers an update of scenario probabilities, which in turn leads to an instant re-evaluation of the firm value and may trigger the default event or change the probability of default.

Our model allows for dynamic pricing and hedging of defaultable bonds sensitive to transition risks. We establish theoretically the existence of default and restructuring thresholds and study their properties. An efficient numerical method to compute the bond price and the thresholds is then presented and its convergence is analyzed. The model is illustrated with a case study using financial and emission data of several companies and NGFS transition scenarios. Our results show that under transition scenario uncertainty, carbon price adjustments are more likely to trigger a default than when the true scenario is known because after each adjustment the more environmentally stringent scenario becomes more likely. We use our model to quantify the impact of the speed at which scenario information is discovered by the agents on the credit spread level and find that faster information discovery leads to higher spreads since better information allows the shareholders to optimize the timing of default, increasing the value of default option and decreasing the bond price.

This paper is structured as follows. The rest of the introduction reviews the relevant literature. Section 2 presents our bond pricing model and characterizes the optimal default and restructuring thresholds. Section 3 describes a fast iterative algorithm for computing the bond price. So as not to perturb the flow of the paper, the technical proof of Proposition 4 in this section has been moved to the Appendix. Details of the implementation are given in Section 4. Section 5 discusses model calibration and provides bond pricing examples. Section 6 concludes the paper by analyzing the implications of our model for practitioners and regulators.

Literature review Many authors have recently investigated the impact of climate transition risks on corporate and sovereign debt (Battiston *et al.*, 2019; Monnin, 2018). In particular, Bouchet and Le Guenedal (2020b) introduced a structural methodology to measure the credit risk related to the increase of emission related costs at the level of individual firms. Like many other papers in this field, this approach uses Merton (1974) distance to default and shows that credit

risk generated by an increase in carbon price is concentrated on carbon intensive sectors. At the same time, Adenot *et al.* (2022) show that taking into account sectoral interdependencies allows to quantify the impact of transition risks on bond portfolios beyond utilities, materials and energy sectors.

An even wider literature explores, using the scenario approach, the exposure of banks' portfolios to transition risks, either as a final goal (Nguyen *et al.*, 2020) or in the wider context of stress-testing the resiliency of financial institutions or the entire financial system (Battiston *et al.*, 2017; Dietz *et al.*, 2016; Roncoroni *et al.*, 2021; Vermeulen *et al.*, 2021). These studies typically compare the bank's portfolio under a reference transition scenario (e.g., the orderly transition) to a baseline (business as usual) or to another transition scenario with different characteristics (e.g., the disorderly transition). Climate stress testing methodologies have also been developed by regulatory bodies (ACPR, 2020; Grippa, Mann, *et al.*, 2020; Schotten *et al.*, 2016), and some exercises are ongoing at this time (Alogoskoufis *et al.*, 2021; ECB, 2022). These initiatives generally use static scenarios; most often even the balance sheet of the bank is assumed to be static; when a dynamic balance sheet is allowed (ACPR, 2020) the scenario is still static and is assumed to be fully known to the financial institution when defining the dynamic balance sheet evolution.

However, the future climate, climate-related economic policies, and therefore also climate-related financial risks are subject to deep uncertainties (Bolton *et al.*, 2020; Chenet *et al.*, 2019; Monasterolo *et al.*, 2019; W. Nordhaus, 2018b). They are related, among other factors, to uncertainty about future availability of mitigation technologies and international cooperation (Edenhofer *et al.*, 2006); uncertainty of climate sensitivity and carbon budgets, which may have to be revised in the future (Cox *et al.*, 2018; Meehl *et al.*, 2020), uncertainty about tipping points, which may require bold immediate actions (Keen *et al.*, 2022; Weitzman, 2009), etc. In this context, perfect knowledge of the scenario corresponding to a fixed climate objective is clearly not a valid assumption. Although the deep uncertainty and unpredictability of climate-related financial risks is recognized by the literature, its impact on corporate debt, on banks' portfolios and on the resiliency of the financial system as a whole, is not sufficiently well understood.

In this context, Flora and Tankov (2022) developed a discrete time real options model for pricing energy assets, compatible with the NGFS scenarios and taking into account scenario uncertainty. These authors assume that the possible futures are described by the NGFS scenarios, but that the specific scenario is not known to the agent. Instead, the agent observes a signal (such as the global or regional CO2 emissions), whose distribution depends on the scenario, and may therefore use Bayesian filtering to compute posterior scenario probabilities. The present paper uses the Bayesian filtering approach in continuous time to account for scenario uncertainty in the context of corporate bond pricing.

Our model belongs to the literature on structural default modeling starting with the seminal papers of Black and Cox (1976) and Merton (1974) and more precisely to the field of *endogenous default models*, where the shareholders can optimally choose the default time to maximize the equity value. Endogenous default models were first proposed by Leland (1994) and Leland and Toft (1996) in the setting of diffusion processes and complete observation, and later extended to include jump risk by N. Chen and Kou (2009) and Hilberink and Rogers (2002) and to account for partial observation by Duffie and Lando (2001) and Palmowski *et al.* (2020), among other authors.

In the same vein but with an explicit focus on transition risks, Agliardi and Agliardi (2021) recently developed a model for defaultable perpetual bonds incorporating uncertainty due to

climate-related risks in addition to the uncertainty about corporate earnings, and similar to the one of Hilberink and Rogers (2002). In their specification, the random policy shocks and *degree of greenness* determine downward jumps in the firm value. Compared to this reference, our contribution is to quantify the impact of scenario uncertainty and progressive information discovery on bond prices. More precisely, we model explicit dependence of company revenues on carbon price, and explicit dependence of carbon price shocks on policy scenarios, which are discovered progressively by the agent through Bayesian learning.

4.2 The bond pricing model

Firm value dynamics We consider a company generating a stochastic continuous cash flow V_t per unit time, which is affected by the climate policy.[2] The climate policy is characterized by an increasing carbon price process $C_t = \sum_{i=1}^{N_t} \widetilde{Y}_i$, where N is a doubly stochastic Poisson process, whose intensity depends on the transition scenario, and $(\widetilde{Y}_i)_{i\geq 1}$ is a sequence of i.i.d. random variables, independent from N, representing the adjustments of the carbon price. One may assume, for example, that every time the process N jumps, the carbon price is adjusted upwards by a fixed value, say \$10, which corresponds to taking $\widetilde{Y}_i \equiv 10$. The carbon price is thus a piecewise constant process, which changes at unpredictable random dates. This may not be a fully realistic assumption, and in practice the carbon price trajectories will depend on the specific mechanisms in place: e.g., in an emission trading scheme the price evolves continuously, and when a carbon tax is in place, regulatory changes are announced well in advance. Nevertheless, our assumption allows to study the impact of the transition scenario uncertainty in a simple framework, which is the main point of this paper.

We assume that there are n scenarios with increasing environmental stringency, and denote by $\lambda_1, \dots, \lambda_n$ the respective price intensities, where $0 < \lambda_1 < \cdots < \lambda_n$. In other words, the adjustment values $\tilde{Y}^i$ have the same distribution in every scenario, but the frequency of adjustments will be higher in environmentally stringent scenarios. Let I be an unobservable random variable taking values $1, \dots, n$, which represents the true scenario unknown to the agent. Conditionally on I the process N is a Poisson process with intensity λ_I. The assumption of constant intensity in every scenario may appear restrictive, but it greatly simplifies the computations. More importantly, given that future carbon price adjustments are subject to multiple uncertainties, it seems preferable to have a parsimonious model accounting for the phenomenon of interest rather than a full-fledged model with time-dependent intensities, which will be very hard to calibrate.

The cash flow dynamics of the company under the risk-neutral probability measure is given by

$$\frac{dV_t}{V_{t-}} = \mu dt + \sigma dW_t - dL_t, \quad L_t = \sum_{i=1}^{N_t} Y_i, \tag{4.1}$$

where W is a standard Brownian motion independent from I and N, and $(Y_i)_{i\geq 1}$ is a sequence of i.i.d. random variables, independent from W, N and I, which determine how the carbon price affects the cash flow. Every jump in the carbon price corresponds to a jump in the cash flow, and the jump sizes $\widetilde{Y}_i$ and Y_i may be correlated to each other (but $\widetilde{Y}_i$ and Y_j with $i \neq j$ are independent).

2. Unlike some other papers on endogenous default, which model the firm value dynamics, we find it more convenient to model directly the cash flow (EBITDA).

For example, if the firm has constant emission intensity per unit of revenue, denoted by α, then $Y_i = \alpha\widetilde{Y}_i$. We let ν be the distribution of Y_1, $e := \mathbb{E}[Y_1]$ and assume that ν has bounded support belonging to $(-\infty, 1)$ and

$$r + e\lambda_i - \mu > 0 \tag{4.2}$$

for all i, where r is the risk-free rate. Condition (4.2) is the analogue in our setting of the assumption $\mu < r$ commonly made in the financial literature on corporate defaultable debt, and is needed to guarantee the non-explosion of the expected discounted future cash flows of the firm. The assumption (4.2) may once again appear restrictive, but recall that μ is the growth rate of revenues under the *risk-neutral* probability, which does not include the risk premium and is therefore expected to be lower than the historical growth rate.

Denote by $\mathcal{F}_t = \sigma(W_s, N_s, s \le t)$ the observation filtration, which contains the firm's revenues and the carbon price trajectory but does not contain the true scenario I, and let $\hat{p}_t^i = \mathbb{E}[I = i|\mathcal{F}_t]$ be the posterior probability of being in scenario i given the available observations at time t. Then (Brémaud, 1981, section VI.3), in $(\mathcal{F}_t)$, the intensity of N is given by $\hat{\lambda}_t = \sum_{i=1}^n \lambda_i \hat{p}_t^i$, and the filtered probabilities are given by

$$\hat{p}_t^i = \frac{e^{-\lambda_i t}\lambda_i^{N_t}\hat{p}_0^i}{\sum_j e^{-\lambda_j t}\lambda_j^{N_t}\hat{p}_0^j} \tag{4.3}$$

so that

$$\hat{\lambda}_t = \frac{\sum_i e^{-\lambda_i t}\lambda_i^{N_t+1}\hat{p}_0^i}{\sum_j e^{-\lambda_j t}\lambda_j^{N_t}\hat{p}_0^j},$$

which means that in the filtration $(\mathcal{F}_t)$, the couple (V_t, N_t) is a time-inhomogeneous Markov process. Thus, one does not need to keep track of all probabilities $\hat{p}_t^i$ to recover the Markov property in the observation filtration. [3] We also introduce the notation for the jump intensity and probabilities with explicit dependence on N:

$$\hat{\lambda}^N(t) := \frac{\sum_i e^{-\lambda_i t}\lambda_i^{N+1}\hat{p}_0^i}{\sum_j e^{-\lambda_j t}\lambda_j^{N}\hat{p}_0^j}, \qquad \hat{p}_t^{i,N} = \frac{e^{-\lambda_i t}\lambda_i^{N}\hat{p}_0^i}{\sum_j e^{-\lambda_j t}\lambda_j^{N}\hat{p}_0^j}$$

The jump times of the process (N_t), denoted by $\tau_1, \tau_2, \dots$ can then be simulated using the following formula:

$$\tau_0 = 0, \quad \text{and} \quad \tau_{N+1} = \inf\{t > \tau_N : \int_{\tau_N}^t \hat{\lambda}^N(s)ds > e_N\} \quad \text{for } N \ge 0, \tag{4.4}$$

where (e_n) is an sequence of i.i.d. exponential random variables with parameter 1. The integral is not available in explicit form for $n > 2$, but is easy to compute numerically. Figure 4.2.1 shows an example trajectory of the jump process (N_t), obtained with equation (4.4), together with the filtered probabilities. In this simulation there are three scenarios with intensities $\lambda_1 = 3$, $\lambda_2 = 5$, $\lambda_3 = 1$ and prior probabilities $\hat{p}_0^1 = 0.3$, $\hat{p}_0^2 = 0.3$, $\hat{p}_0^3 = 0.4$.

3. This simplification stems from the assumption that the intensity λ^i is constant within each scenario.

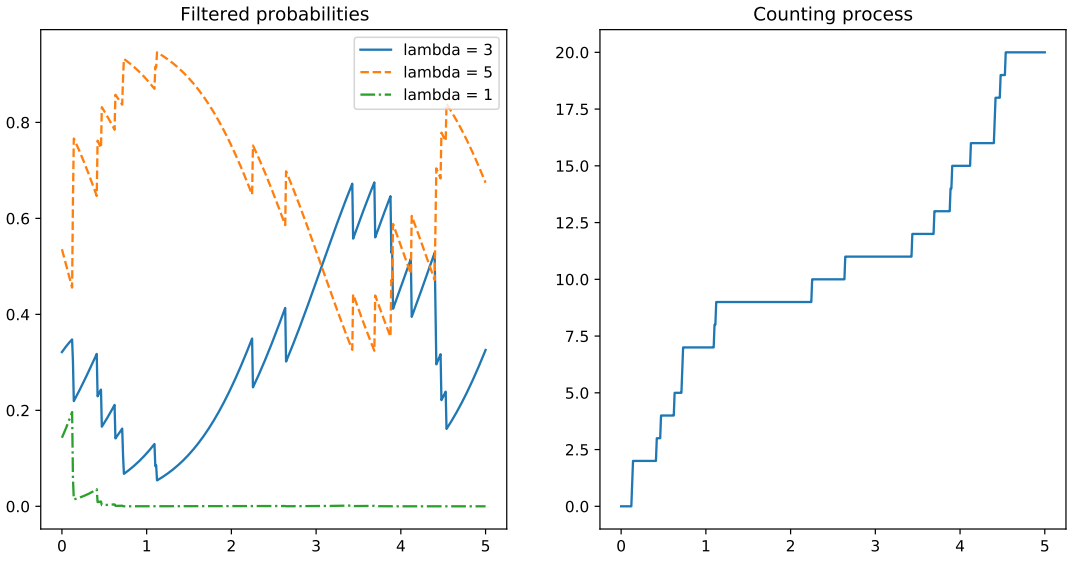

Figure 4.2.1 – Sample trajectory of the carbon price process (right) and the filtered scenario probabilities.

Computing the firm value and the bond price We consider a model with endogenous bankruptcy and optimal default/restructuring thresholds, inspired by Leland and Toft (1996), and subsequent literature on the topic. Unlike Leland and Toft (1996) and some other papers, we do not consider optimal capital structure but are only interested in determining the bond price and the optimal thresholds for a fixed capital structure. Also, while Leland and Toft (1996) and many others consider perpetual bonds to obtain explicit solutions, we model a finite-maturity bond with a given notional value and a given coupon. [4] The company pays a continuous coupon b corresponding to a debt with notional value K and maturity T. At any time $\tau < T$, the shareholders may make one of the following two decisions, depending on the value of the company's future cash flows:

— If the value of the future cash flows is greater than the notional value K of the debt, the shareholders may decide to redeem the debt at notional value (restructuring event).

— If the value of the future cash flows is smaller than the notional value K of the debt, the shareholders may decide to trigger the default event, in which case the bondholders receive the value of the future cash flows.

The default/restructuring date is determined by the company's owners to maximize equity

4. In our setting perpetual bonds do not bring any added tractability since the underlying Markov process is time-inhomogeneous due to its dependence on the filtered probabilities.

value. The value of the future cash flows at time t is given by

$$\begin{aligned}\widehat{V}_t &= \mathbb{E}\Big[\int_t^\infty e^{-r(s-t)}V_s\Big|\mathcal{F}_t\Big] = \sum_{i=1}^n \mathbb{P}[I=i|\mathcal{F}_t]\,\mathbb{E}\Big[\int_t^\infty e^{-r(s-t)}V_s\Big|\mathcal{F}_t, I=i\Big]\\ &= V_t\sum_{i=1}^n \frac{\hat{p}_t^i}{r+e\lambda_i-\mu} = V_t\,\alpha_t^{N_t},\end{aligned}$$

where we denote

$$\alpha_t^N := \sum_{i=1}^n \frac{1}{r+e\lambda_i-\mu}\,\frac{e^{-\lambda_i t}\lambda_i^N\hat{p}_0^i}{\sum_j e^{-\lambda_j t}\lambda_j^N\hat{p}_0^j}.$$

The equity value is then given by

$$\sup_{\tau\in\mathcal{T}([0,T])}\mathbb{E}\Big[\int_0^{\tau\wedge T} e^{-rt}(V_t-b)dt + e^{-r(T\wedge\tau)}(\widehat{V}_{T\wedge\tau}-K)^+\Big], \tag{4.5}$$

where $\mathcal{T}([0,T])$ is the set of $(\mathcal{F}_t)$-stopping times with values in $[0,T]$.

Define the associated value function which corresponds to the equity value at time t, provided that default/restructuring did not occur before this date:

$$U^N(t,V) = \sup_{\tau\in\mathcal{T}([t,T])}\mathbb{E}\Big[\int_t^{\tau\wedge T} e^{-r(s-t)}(V_s^{t,V,N}-b)ds + e^{-r(T\wedge\tau-t)}(\widehat{V}_{T\wedge\tau}^{t,V,N}-K)^+\Big], \tag{4.6}$$

where the superscript t,V,N means that the Markov process (V_s,N_s) is started at time t with initial value (V,N), and $\mathcal{T}([t,T])$ is the set of stopping times with values in $[t,T]$, with respect to the filtration of $(V_s^{t,V,N},N_s^{t,V,N})_{s\geq t}$.

The optimal default/restructuring time after time t can then be defined as follows:

$$\tau_t^* = \inf\{s\geq t : U^{N_s^{t,N}}(t,V_s^{t,V,N}) = (\widehat{V}_s^{t,V,N}-K)^+\}, \tag{4.7}$$

and the price of the bond is

$$B^N(t,V) = \mathbb{E}\Big[\int_t^{\tau_t^*\wedge T} e^{-r(s-t)}b\,ds + e^{-r(T\wedge\tau_t^*-t)}\widehat{V}_{T\wedge\tau_t^*}^{t,V,N}\wedge K\Big].$$

It is then easy to see that the sum of equity value and the bond price is equal to the value of the future cash flows:

$$\begin{aligned}U^N(t,V)+B^N(t,V) &= \mathbb{E}\Big[\int_t^{\tau_t^*\wedge T} e^{-r(s-t)}V_s^{t,V,N}ds + e^{-r(T\wedge\tau_t^*-t)}\widehat{V}_{T\wedge\tau_t^*}^{t,V,N}\Big]\\ &= \widehat{V}_t^{t,V,N} = V\alpha_t^N.\end{aligned}$$

Thus, the bond price can also be written as a solution to an optimization problem:

$$\begin{aligned}B^N(t,V) &= V\alpha_t^N - \sup_{\tau\in\mathcal{T}([t,T])}\mathbb{E}\Big[\int_t^{\tau\wedge T} e^{-r(s-t)}(V_s^{t,V,N}-b)ds + e^{-r(T\wedge\tau-t)}(\widehat{V}_{T\wedge\tau}^{t,V,N}-K)^+\Big]\\ &= \inf_{\tau\in\mathcal{T}([t,T])}\mathbb{E}\Big[\int_t^{\tau\wedge T} e^{-r(s-t)}b\,ds + e^{-r(T\wedge\tau-t)}\widehat{V}_{T\wedge\tau}^{t,V,N}\wedge K\Big].\end{aligned} \tag{4.8}$$

In the sequel, we will use Equation (4.8) rather than (4.6) to compute the bond price, because of its superior numerical performance.

For every $N \geq 0$, one can define the associated continuation region

$$\mathcal{C}^N = \{(t, V) : B^N(t, V) < \alpha_t^N V \wedge K\}$$

and exercise (default or restructuring) region

$$\mathcal{E}^N = \{(t, V) : B^N(t, V) = \alpha_t^N V \wedge K\}$$

The following proposition characterizes the behavior of these regions depending on model parameters.

Proposition 3.

i. Assume that $r \geq b/K$. Then the continuation region has the form $\mathcal{C}^N = \{(t, V) : t \in [0, T], V > V_D^N(t)\}$ for some default threshold function $V_D^N : [0, T] \to \mathbb{R}_+$, which satisfies $V_D^N(t) \leq b$ for all $t \in [0, T]$.

In other words, the default may only occur when the cash flow of the company is smaller than the coupon, and the restructuring never occurs in this case.

ii. Assume that $r < b/K$. Then the continuation region has the form $\mathcal{C}^N = \{(t, V) : t \in [0, T], V_U^N(t) > V > V_D^N(t)\}$, for some default threshold function $V_D^N : [0, T] \to \mathbb{R}_+$ which satisfies $V_D^N(t) \leq b$ and $\alpha^N(t) V_D^N(t) \leq K$ and some restructuring threshold function $V_U^N : [0, T] \to \mathbb{R}_+$, which satisfies $\alpha^N(t) V_U^N(t) \geq K$ for all $t \in [0, T]$.

In other words, the default may only occur when the cash flow of the company is smaller than the coupon and the value of the future cash flows is smaller than the notional of the debt, and the restructuring may occur only when the value of the future cash flows is greater than the notional of the debt.

Proof. From the expression (4.8), one easily deduces that for each t, $B^N(t, V)$ is concave and increasing in V. Since also $U^N(t, V)$ is increasing in V and $U^N(t, V) + B^N(t, V) = \alpha_t^N V$, it follows that $B^N(t, V)$ is Lipschitz with constant α_t^N.

Therefore, the set of points

$$\mathcal{C}_t^N = \{V : B^N(t, V) < \alpha^N(t) V \wedge K\}$$

necessarily has the form $(V_D^N(t), V_U^N(t))$ with $V_D^N(t) \in [0, K/\alpha^N(t)]$ and $V_U^N(t) \in [K/\alpha^N(t), +\infty]$. Moreover, from the definition (4.6), it is clear that if $\alpha^N(t) V \leq K$ and $V > b$, the value function is greater than zero and it is not optimal to stop immediately, so that $V_D^N(t) \leq b$.

Assume now that $r \geq b/K$. The bond price function can alternatively be written as follows:

$$B^N(t, V) = K - \sup_{\tau \in \mathcal{T}([t,T])} \mathbb{E}\left[\int_t^{\tau \wedge T} e^{-r(s-t)}(rK - b) dt + e^{-r(T \wedge \tau - t)}(K - \widehat{V}_{T \wedge \tau}^{t,V,N})^+ \right]. \tag{4.9}$$

If $\alpha^N(t) V > K$, the bond price is therefore smaller than the pay-off from immediate exercise and immediate stopping (for the shareholders) is not optimal, so that $V_U^N(t) = +\infty$. □

4.3 Numerical approximation of the bond price

The following proposition provides a method for the numerical approximation of the bond price $B^N(t,V)$. Its proof can be found in the appendix.

Proposition 4. *Let $B^{N,M}(t,V):[0,T]\times\mathbb{R}_+\mapsto\mathbb{R}$, for $N\le M$ be defined as follows:*

$$B^{M,M}(t,V) := G^M(t,V),$$

where for each M, G^M is bounded and Lipschitz continuous in V and and for $N<M$, $B^{N,M}(t,V)$ is the solution of the variational inequality

$$\min\{b - rB^{N,M} + \mathcal{L}^{N,M}B^{N,M}, \alpha_t^N V\wedge K - B^{N,M}\} = 0, \tag{4.10}$$

on $(t,V)\in[0,T]\times\mathbb{R}_+$ with $B^{N,M}(T,V)=\alpha_T^N V\wedge K$, where

$$\mathcal{L}^{N,M}f = \frac{\partial f}{\partial t} + \mu V\frac{\partial f}{\partial V} + \frac{1}{2}\sigma^2V^2\frac{\partial^2 f}{\partial V^2} + \hat{\lambda}^N(t)\int_{-\infty}^{1}\left\{B^{N+1,M}(t,V(1-x)) - f(t,V)\right\}\nu(dx). \tag{4.11}$$

Then,

$$\lim_{M\to\infty} B^{N,M}(t,V) = B^N(t,V)$$

for $N=0,1,\dots$ and $(t,V)\in[0,T]\times\mathbb{R}_+$, where the convergence takes place at faster than exponential rate, meaning that for any $\alpha>0$,

$$|B^{N,M}(t,V) - B^N(t,V)| \le e^{-\alpha M}$$

starting from sufficiently large M, for all t,V.

Furthermore, if $G^M(t,V)\le B^M(t,V)$, respectively, $G^M(t,V)\ge B^M(t,V)$ for all $t,V\in[0,T]\times\mathbb{R}_+$ then $B^{N,M}(t,V)\le B^N(t,V)$, respectively $B^{N,M}(t,V)\ge B^N(t,V)$ for all $t,V\in[0,T]\times\mathbb{R}_+$.

This proposition suggests the following algorithm for computing the bond price $B^N(t,V)$:

— Fix $M\ge N$ sufficiently large.

— Choose the functions $\overline{G}^M$ and $\underline{G}^M$ with

$$\underline{G}^M(t,V)\le B^M(t,V)\le\overline{G}(M)(t,V)$$

for all $t\in[0,T]$, $V>0$.

— Compute $\underline{B}^{N,M}$ and $\overline{B}^{N,M}$ by iterating (4.10) $M-N$ times with, respectively, $\underline{G}^M$ and $\overline{G}^M$ as starting values.

By Proposition 4, the unknown function $B^N(t,V)$ then satsfies

$$\underline{B}^{N,M}\le B^N(t,V)\le\overline{B}^{N,M},$$

so that the estimation error may be controlled. It remains to find an initial upper and lower bound to start the algorithm. Possible bounds are provided by the following result.

Proposition 5. *For all $t \in [0,T]$, $V > 0$ and $N = 0, 1 \dots$, the bond price function B^N satisfies*

$$B^N(t,V) \geq \sum_{i=1}^{n} \hat{p}_t^{i,N} B^{\lambda_i, \alpha^{\max_j \lambda_j}}(t,V).$$

In addition, if the support of the distribution ν of Y_i belongs to $[0,1)$, then

$$B^N(t,V) \leq B^{\min_j \lambda_j, \alpha^{\min_j \lambda_j}}(t,V).$$

where

$$B^{\lambda,\alpha}(t,V) = \inf_{\tau \in \mathcal{T}([t,T])} \mathbb{E}\Big[\int_t^{\tau \wedge T} e^{-r(s-t)} b \, dt + e^{-r(T \wedge \tau - t)} \alpha V_{T\wedge\tau}^{\lambda,t,V} \wedge K \Big], \tag{4.12}$$

where $V^{\lambda,t,V}$ has the dynamics

$$\frac{dV_s^{\lambda,t,V}}{V_s^{\lambda,t,V}} = \mu ds + \sigma dW_s - dL_s^{\lambda}, \quad s \geq t, \quad V^{\lambda,t,V} = V, \quad L_s^{\lambda} = \sum_{i=1}^{N_s^{\lambda}} Y_i,$$

N^{λ} is a Poisson process with intensity λ and $\alpha^{\lambda} = \frac{1}{r + e\lambda - \mu}$.

Proof. Let us first show the lower bound.

$$\begin{aligned}
B^N(t,V) &= \inf_{\tau \in \mathcal{T}([t,T])} \mathbb{E}\Big[\int_t^{\tau\wedge T} e^{-r(s-t)} b \, ds + e^{-r(T\wedge\tau - t)} \widehat{V}_{T\wedge\tau}^{t,V,N} \wedge K \Big] \\
&= \inf_{\tau \in \mathcal{T}([t,T])} \sum_{i=1}^{n} \hat{p}_t^{i,N} \mathbb{E}\Big[\int_t^{\tau\wedge T} e^{-r(s-t)} b \, ds \\
&\qquad + e^{-r(T\wedge\tau - t)} \left(V_{T\wedge\tau}^{t,V,N} \sum_{i=1}^{n} \alpha^{\lambda_i} \frac{e^{-\lambda_i \tau} \lambda_i^{N_\tau^{t,N}} \hat{p}_0^i}{\sum_j e^{-\lambda_j \tau} \lambda_j^{N_\tau^{t,N}} \hat{p}_0^j} \right) \wedge K \Big| I = i \Big] \\
&\geq \sum_{i=1}^{n} \hat{p}_t^{i,N} \inf_{\tau \in \mathcal{T}([t,T])} \mathbb{E}\Big[\int_t^{\tau\wedge T} e^{-r(s-t)} b \, ds \\
&\qquad + e^{-r(T\wedge\tau - t)} (\alpha^{\max_j \lambda_j} V_{T\wedge\tau}^{\lambda_i,t,V}) \wedge K \Big] = \sum_{i=1}^{n} \hat{p}_t^{i,N} B^{\lambda_i, \alpha^{\max_j \lambda_j}}(t,V).
\end{aligned}$$

For the upper bound, we can similarly write:

$$\begin{aligned}
&B^N(t,V) \\
&\leq \inf_{\tau \in \mathcal{T}([t,T])} \sum_{i=1}^{n} \hat{p}_t^{i,N} \mathbb{E}\Big[\int_t^{\tau\wedge T} e^{-r(s-t)} b \, ds + e^{-r(T\wedge\tau - t)} (V_{T\wedge\tau}^{\lambda_i,t,V} \alpha^{\min_j \lambda_j}) \wedge K \Big]
\end{aligned}$$

The upper bound then follows from the fact that under the support condition one can define the processes $(V_s^{\lambda_i,t,V})_{t \leq s \leq T}$ for $i = 1, \dots, n$ on the same probability space, such that

$$V_s^{\lambda_i,t,V} \leq V_s^{\lambda_j,t,V}$$

a.s. for all $s \in [t,T]$ whenever $\lambda_i > \lambda_j$. □

The problem (4.12) is a standard American option pricing problem in an exponential Lévy model, see e.g., (Cont & Tankov, 2003, Chapter 11). In particular, B^λ satisfies the integro-differential variational inequality

$$\min\{b - rB^\lambda + \mathcal{L}^\lambda B^\lambda, \alpha V \wedge K - B^\lambda\} = 0, \tag{4.13}$$

on $(t, V) \in [0, T] \times \mathbb{R}_+$ with $B^\lambda(T, V) = \alpha V \wedge K$, where

$$\mathcal{L}^\lambda f = \frac{\partial f}{\partial t} + \mu V \frac{\partial f}{\partial V} + \frac{1}{2}\sigma^2 V^2 \frac{\partial^2 f}{\partial V^2} + \lambda \int_{-\infty}^{1} \{f(t, V(1-x)) - f(t, V)\}\, \nu(dx).$$

The last result of this section establishes the boundary behavior of the bond price function B^N.

Proposition 6. *For all $t \in [0, T]$ and $N = 0, 1, \ldots,$*

$$\lim_{V \to 0} B^N(t, V) = 0$$
$$\lim_{V \to +\infty} \{B^N(t, V) - \widetilde{B}^N(t, V)\} = 0,$$

where

$$\widetilde{B}^N(t, V) = K - (rK - b)^+ \frac{1 - e^{-r(T-t)}}{r}.$$

Proof. From the representation (4.8)

$$\begin{aligned} B^N(t, V) &\le \inf_{\tau \in \mathcal{T}([t,T])} \mathbb{E}\Big[\int_t^{\tau \wedge T} e^{-r(s-t)} b\, dt + e^{-r(T \wedge \tau - t)} \alpha^N (T \wedge \tau) V_{T \wedge \tau}^{t,V,N} \Big] \\ &\le \inf_{\tau \in \mathcal{T}([t,T])} \mathbb{E}\Big[\int_t^{\tau \wedge T} e^{-r(s-t)} (b + V_t^{t,V,N})\, dt + e^{-r(T \wedge \tau - t)} \alpha^N (T \wedge \tau) V_{T \wedge \tau}^{t,V,N} \Big] \\ &= \alpha^N(t) V + \inf_{\tau \in \mathcal{T}([t,T])} \mathbb{E}\Big[\int_t^{\tau \wedge T} e^{-r(s-t)} b\, dt \Big] = \alpha^N(t) V. \end{aligned}$$

Since the right-hand side converges to zero as $V \to 0$ and $B^N(t, V) \ge 0$, it follows that $B^N(t, V) \to 0$ as $V \to 0$.

To prove the second limit, observe that from the representation (4.9),

$$\begin{aligned} B^N(t, V) &\ge K - \sup_{\tau \in \mathcal{T}([t,T])} \mathbb{E}\left[\int_t^{\tau \wedge T} e^{-r(s-t)} (rK - b) dt \right] - \sup_{\tau \in \mathcal{T}([t,T])} \mathbb{E}\left[e^{-r(T \wedge \tau - t)} (K - \widehat{V}_{T \wedge \tau}^{t,V,N})^+ \right] \\ &\ge K - (rK - b)^+ \frac{1 - e^{-r(T-t)}}{r} - \mathbb{E}\left[(K - \min_{s \in [t,T]} \widehat{V}_s^{t,V,N})^+ \right] \\ B^N(t, V) &\le K - \sup_{\tau \in \mathcal{T}([t,T])} \mathbb{E}\left[\int_t^{\tau \wedge T} e^{-r(s-t)} (rK - b) dt \right] \\ &= K - (rK - b)^+ \frac{1 - e^{-r(T-t)}}{r}. \end{aligned}$$

Since, by the dominated convergence theorem,

$$\lim_{V \to +\infty} \mathbb{E}\left[(K - \min_{s \in [t,T]} \widehat{V}_s^{t,V,N})^+ \right] = 0,$$

the proof is complete. □

4.4 Implementing the numerical algorithm

To implement the algorithm described in the previous section, we need to solve, repeatedly, the variational inequality (4.10). In addition, for the starting point of the algorithm, the integro-differential variational inequality (4.13) must be solved. The integro-differential variational inequality (4.13) is more complex due to the presence of the integral term, however it is well studied in the literature, see e.g., (Cont & Voltchkova, 2005; Toivanen, 2008). For completeness, we briefly review the numerical schemes in this section.

To start, we switch to logarithmic coordinates $x = \log V$, $u^{N,M}(t,x) = B^{N,M}(t,V)$ and $u^{\lambda}(t,x) = B^{\lambda}(t,V)$, and truncate the inequalities to the interval $[\underline{A}, \overline{A}]$, imposing the boundary conditions of Proposition 6. We then need to solve the following problems:

— Integro-differential variational inequality (4.13):

$$\min\{b - ru^{\lambda} + \overline{\mathcal{L}}^{\lambda} u^{\lambda}, \alpha^{\lambda} e^{x} \wedge K - u^{\lambda}\} = 0,$$

on $(t,x) \in [0,T] \times [\underline{A}, \overline{A}]$ with $u^{\lambda}(T,x) = \alpha^{\lambda} e^{x} \wedge K$, $u^{\lambda}(t,x) = 0$ for $x \le \underline{A}$, $u^{\lambda}(t,x) = \widetilde{B}^{\lambda}(t,e^{x})$ for $x \ge \overline{A}$ and

$$\overline{\mathcal{L}}^{\lambda} u = \frac{\partial u}{\partial t} - \lambda u + \mu \frac{\partial u}{\partial x} + \frac{1}{2}\sigma^2 \left(\frac{\partial^2 u}{\partial x^2} - \frac{\partial u}{\partial x} \right) + \lambda \int_{-\infty}^{1} u(t, x + \log(1-z)) \nu(dz), \tag{4.14}$$

where in the integral in the right-hand side, the function u is replaced by the boundary condition when the variable is outside the domain.

— Variational inequality (4.10):

$$\min\{b - ru^{N,M} + \overline{\mathcal{L}}^{N,M} u^{N,M}, \alpha_t^{N} e^{x} \wedge K - u^{N,M}\} = 0,$$

on $(t,x) \in [0,T] \times [\underline{A}, \overline{A}]$ with $u^{N,M}(T,x) = (\alpha_T^{N} e^{x} - K)^{+}$, $u^{N,M}(t,x) = 0$ for $x \le \underline{A}$, $u^{N,M}(t,x) = \widetilde{B}^{N}(t,e^{x})$ for $x \ge \overline{A}$ and

$$\overline{\mathcal{L}}^{N,M} u = \frac{\partial u}{\partial t} - \hat{\lambda}^{N}(t) u + \mu \frac{\partial u}{\partial x} + \frac{1}{2}\sigma^2 \frac{\partial^2 u}{\partial x^2} - \frac{1}{2}\sigma^2 \frac{\partial u}{\partial x} + \hat{\lambda}^{N}(t) \int_{-\infty}^{1} u^{N+1,M}(t, x + \log(1-z)) \nu(dz), \tag{4.15}$$

where once again in the integral in the right-hand side, the function u is replaced by the boundary condition when the variable is outside the domain. Notice that in this equation, the integral term does not depend on the unknown function, so it is a PDE with a source term rather than an integro-differential equation.

Discretization Introduce time and space grids: $x_j = \underline{A} + j\Delta x$, $j = 0, \dots, m$ and $t_i = i\Delta t$, $i = 0, \dots, n$, where $\Delta x = \frac{\overline{A} - \underline{A}}{m}$ and $\Delta t = \frac{T}{n}$. The value $\hat{u}_{i,j}$ (with appropriate superscript) will denote the approximation of the solution $u(t_i, x_j)$.

We set $\hat{u}_{n,j}^{N,M} = \alpha_T^{N} e^{x_j} \wedge K$ and $\hat{u}_{n,j}^{\lambda} = \alpha^{\lambda} e^{x_j} \wedge K$ for all j and use the following two-step algorithm for $i = N-1, \dots, 0$:

— Compute the continuation value $\tilde{u}_{i,j}$ for all $j = 0, \dots, M$ using the implicit scheme.

— Set $\hat{u}_{i,j}^{N,M} = \min\{\tilde{u}_{i,j}^{N,M}, \alpha_{t_i}^{N} e^{x_j} \wedge K\}$ and $\hat{u}_{i,j}^{\lambda} = \min\{\tilde{u}_{i,j}^{\lambda}, \alpha^{\lambda} e^{x_j} \wedge K\}$ for all $j = 0, \dots, M$.

The continuation value may be computed as follows:

— Integro-differential variational inequality (4.13). The implicit scheme writes:

$$b - r\tilde{u}^{\lambda}_{ij} + \frac{\hat{u}^{\lambda}_{i+1,j} - \tilde{u}^{\lambda}_{ij}}{\Delta t} + \left(\mu - \frac{\sigma^2}{2}\right)\frac{\tilde{u}^{\lambda}_{i,j+1} - \tilde{u}^{\lambda}_{i,j-1}}{2\Delta x} + \frac{\sigma^2}{2}\frac{\tilde{u}^{\lambda}_{i,j+1} - 2\tilde{u}^{\lambda}_{ij} + \tilde{u}^{\lambda}_{i,j-1}}{\Delta x^2} + \lambda\sum_k w_k\{\tilde{u}^{\lambda}_{i,j-k} - \tilde{u}^{\lambda}_{ij}\} = 0$$

This holds for $j = 0, \dots, M$, with additional constraints/conventions $\tilde{u}_{i,j} = 0$ for $j \le 0$ and $\tilde{u}_{i,j} = \widetilde{B}^{\lambda}(t_i, e^{x_j})$ for $j \ge M$. The weights w_k are defined by discretizing the Lévy measure:

$$w_k = \int_{(k-\frac{1}{2})\Delta x}^{(k+\frac{1}{2})\Delta x} \nu(dx).$$

This system can be written in the form $A\tilde{u}_{i,\cdot} + B = \hat{u}_{i+1,\cdot}$ and solved by matrix inversion for each step.

— Variational inequality (4.10). The implicit scheme writes:

$$b(t_i) - r\tilde{u}^{N,M}_{ij} + \frac{\hat{u}^{N,M}_{i+1,j} - \tilde{u}^{N,M}_{ij}}{\Delta t} + \left(\mu - \frac{\sigma^2}{2}\right)\frac{\tilde{u}^{N,M}_{i,j+1} - \tilde{u}^{N,M}_{i,j-1}}{2\Delta x} + \frac{\sigma^2}{2}\frac{\tilde{u}^{N,M}_{i,j+1} - 2\tilde{u}^{N,M}_{ij} + \tilde{u}^{N,M}_{i,j-1}}{\Delta x^2} + \hat{\lambda}^N(t_i)\sum_k w_k\{\tilde{u}^{N+1,M}_{i,j-k} - \tilde{u}^{N,M}_{ij}\} = 0$$

4.5 Model calibration and examples

In this section we aim to illustrate our model using a realistic data set.

Scenario intensities We first retrieve the global carbon prices suggested by the REMIND-MAgPIE 2.1 model, on a 5 year basis, from the NGFS scenario database. [5] The database contains 6 scenarios: Nationally Determined Contributions, Below $2°C$, Net Zero 2050, Current Policies, Delayed Transition and Divergent Net Zero. Among these scenarios, Current Policies implies very small carbon price levels, Delayed Transition implies a near-zero carbon price for the first 10 years followed by a quick growth, and divergent net zero is very similar to Net Zero 2050 in terms of carbon pricing. Since our model focuses on carbon prices and requires a constant intensity of carbon price increases, we concentrate on the first three scenarios, that is Nationally Determined Contributions (scenario 1), Below $2°C$ (scenario 2) and Net Zero 2050 (scenario 3). Carbon price trajectories in these scenarios for the period 2025-2050 are shown in Figure 4.5.1 (we start in 2025 since the scenarios start to diverge in earnest after this date).

The NGFS scenarios are, of course, deterministic, and the carbon price follows a known deterministic trajectory in each scenario. To match our stochastic carbon price model with the NGFS scenarios, we assume that the carbon price trajectory in each of the scenarios 1, 2, 3 of our model

5. Available at https://data.ene.iiasa.ac.at/ngfs/.

is given by a Lévy process with constant jump size ΔC and with jump intensity $\lambda_i, i = 1, 2, 3$, and we match the expected carbon price in each of our scenarios with the deterministic carbon price in the corresponding NGFS scenarios.

Since there is no a priori reason to attribute a higher probability to any of the scenarios, we choose uniform prior probabilities equal to 1/3. To estimate the intensities from the data, we need to choose a value for the carbon price increment ΔC. The estimated intensity for the period $[T_1, T_2]$ is then given by

$$\hat{\lambda} = \frac{C_{T_2} - C_{T_1}}{\Delta C(T_2 - T_1)}.$$

As we aim at pricing corporate bonds under medium-term transition scenario uncertainty we focus on a time period in line with bond maturities: $T_1 = 2025$ and $T_2 = 2050$. Choosing $\Delta C = 10$ USD, we get the following annualized intensities: $\hat{\lambda}_1 = 0.104$, $\hat{\lambda}_2 = 0.634$ and $\hat{\lambda}_3 = 2.234$. For other values of ΔC, the intensities will be proportionally different. These historical intensities will be used for computations under the risk-neutral measure in our model: this amounts to making an implicit assumption that there is no risk premium for carbon price risk.

The parameter ΔC measures the speed of information discovery in our model: for low jump sizes, the intensities will be large, and therefore easier to estimate, while for large jump sizes, intensities will be small, few jumps will be observed and it will therefore be more difficult to distinguish the scenarios. In most of our examples we choose $\Delta C = 10$ USD, but a sensitivity analysis for this parameter will be performed below.

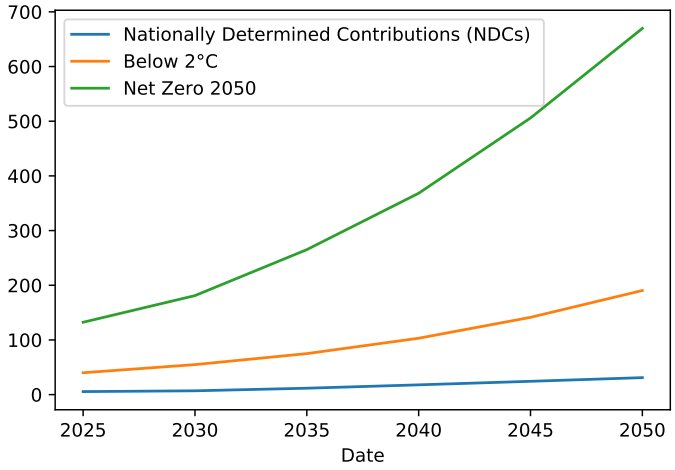

Figure 4.5.1 – Carbon price trajectories in selected NGFS scenarios.

The reference risk free-rate value generally used is the US 10 Year Treasury Rate, $r = 3.33\%$ (for Jun 15 2022), but since we are interested in a long-term analysis and historical rates have been much higher, we revise this value slightly upward and use $r = 4\%$.

Company dynamics and sensitivity to carbon price We extract Earnings Before Interest, Taxes, Depreciation, and Amortization (EBITDA) in USD billion from Facset, for several companies from carbon intensive sectors (Utilities or Materials) within the MSCI World Index between

2009 to 2021) and compute the historical annual returns. Table 4.5.1 shows the values of μ and σ estimated on this period. Recall that our model requires risk-neutral dynamics of earnings; the historical estimate is given for comparison only. The risk-neutral value could be estimated by comparing the model-derived firm value with the actual stock price, however this requires a much more detailed analysis of the capital structure and is out of scope of this paper. We then simply assume $\mu = r = 4\%$, so that assumption (4.2) is always satisfied.

To calibrate the firms' sensitivity to carbon price shocks α we use the following formula:

$$\alpha_{\Delta C} = \frac{\mathcal{CE}_1 \times \Delta C}{V}.$$

where $\mathcal{CE}_1$ are the direct scope 1 emissions from Trucost (reporting year 2019) and V is the company EBITDA in 2019. The estimated values are given in the last column of Table 4.5.1.

Table 4.5.1 – μ_P: EBITDA expected growth rate under the real-world measure; σ: EBITDA volatility; $\mathcal{CE}$: Carbon Emissions-Scope 1 (thousands of tons CO2e) in 2019; EBITDA in USD million (Factset) in 2019; DEBT in USD million (Orbis) in 2019.

Company	μ_P	σ	$\mathcal{CE}_1$	EBITDA	DEBT	α_{10}
C1	7.92%	13.47%	129	2 910	26598	0.04%
C2	6.96%	13.21%	5 217	4 314	43480	1.21%
C3	4.30%	30.03%	19 270	1 853	11830	10.40%
C4	4.15%	28.21%	121 404	6 061	30102	20.03%

In our numerical examples, in view of the above estimations, we choose the following parameter values: $r = 4\%$ (risk-free rate), $\mu = 4\%$ (risk-neutral earnings growth rate), $\sigma = 30\%$ (earnings volatility), $b = 1.5$ (annual coupon, USD billion or 5%), $K = 30$ (bond notional, USD billion), $T = 5$ (bond maturity in years). We use three different representative values of the coefficient α describing the sensitivity of earnings to a USD10 jump in carbon price: $\alpha_{10} = 2\%$, $\alpha_{10} = 5\%$ and $\alpha_{10} = 10\%$. For the first two values of α we take $\underline{A} = -3$, $\overline{A} = 4$ (truncation interval), $m = 700$ (space discretization), $n = 300$ (time discretization) and $M = 40$ (number of iterations). For the largest value of α, we take $\underline{A} = -3$, $\overline{A} = 5$, $m = 800$, $n = 300$ and $M = 40$. Figure 4.5.2 plots the maximum difference between the upper and lower bounds on the bond price $\sup_V |\overline{B}^{M-k,M}(0,V) - \underline{B}^{M-k,M}(0,V)|$ (in log scale) as function of the number of iterations of the scheme k. We observe faster than exponential convergence as expected from Proposition 4.

In the remainder of this section we discuss our numerical results, emphasizing the impact of scenario uncertainty on the results.

Impact of scenario uncertainty on bond prices and credit spreads The top graphs in Figure 4.5.3 show the bond price and credit spread at time $t = 0$ for the largest value of the carbon price sensitivity parameter $\alpha_{10} = 10\%$[6]. We plot the model-generated price and credit spread for carbon price increment $\Delta C = 10$, the model-generated price and spread obtained by taking $\Delta C = 20$ and dividing the scenario intensities by two, the model-generated price and spread

6. The graphs for other values of the carbon price sensitivity parameters ($\alpha_{10} = 2\%$ and $\alpha_{10} = 5\%$) are similar to Figure 4.5.3, with lower spread values, and are not shown to save space.

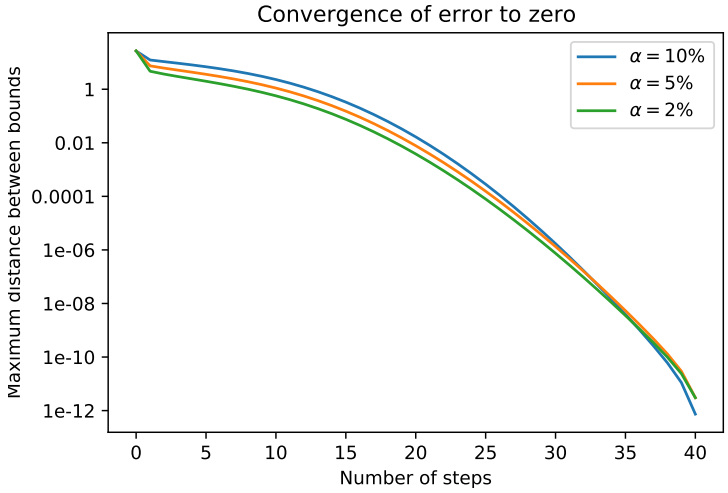

Figure 4.5.2 – Maximum difference between the upper and lower bounds on the bond price $\sup_V |\overline{B}^{M-k,M}(0,V) - \underline{B}^{M-k,M}(0,V)|$ as function of the number of iterations of the scheme k.

obtained by taking $\Delta C = 5$ and multiplying the intensities by two, and, finally, the model-generated price and spread without Bayesian learning, that is, when the price is given by the average of prices obtained in each of the three scenarios assuming perfect knowledge of the scenario from the start.

These four curves correspond to the same average carbon price in every scenario, but illustrate the impact of information discovery/dynamic scenario uncertainty on bond prices and the cost of capital: the curve with $\Delta C = 20$ corresponds to the situation where scenario uncertainty is resolved slowly (because carbon price updates are least frequent) and the 'Average' curve corresponds to the situation where the scenario information is fully revealed just after $t = 0$. We observe that the bond price is decreasing with the speed of information discovery, and consequently, the spread value is increasing. This happens because in our model, the shareholders have the option to default or restructure the debt; when the information they have about the scenario is more precise, their exercise decision will be closer to the optimal one: this increases the value of the default/restructuring option for the shareholders, and consequently decreases the bond price.

Note that the four curves discussed above correspond to the same level of initial scenario uncertainty since the initial scenario probabilities are the same and equal for the three scenarios: it is the speed at which the uncertainty resolves that is different for the four curves. On the other hand, the dashed lines λ_{min} and λ_{max} show the bond price and the credit spread in the case where the intensity is known (no scenario uncertainty), and equal to the minimum and maximum value among the three scenarios.

Impact of scenario uncertainty on default and restructuring thresholds The lower graphs in Figure 4.5.3 show the optimal default and restructuring thresholds, as function of time, for different values of N (number of carbon price adjustments). The optimal default threshold is below the coupon level b (as expected from Proposition 3), increases with N and exhibits an interesting non-monotonic behavior as function of time. This happens because, in the beginning, as time goes on, if N stays constant, the posterior probability of the scenario with the lowest

intensity increases, and it becomes advantageous to default at lower value of revenues. At the end of the time interval, however, the potential of future gains decreases and it becomes optimal to default earlier. The optimal restructuring threshold, on the other hand, is increasing in N and decreasing in time.

The observation that the default threshold increases with N implies that a carbon price adjustment is more likely to trigger a default under scenario uncertainty than when the scenario is known. Indeed, when the scenario is known the default threshold remains fixed, and a default happens when the carbon price adjustment shifts the revenue process below the threshold. By contrast, in the presence of scenario uncertainty, a carbon price adjustment shifts the revenue process downwards, and simultaneously shifts the default threshold upwards because a more environmentally stringent scenario becomes more likely.

Dynamic behavior of firm revenues and credit spreads Figure 4.5.4 shows two sample trajectories of the firm's revenues (together with the default and restructuring thresholds) and the credit spread for the highest value of the carbon price sensitivity parameter (α_{10} = 10%), Figure 4.5.5 shows two sample trajectories for the medium value of the carbon price sensitivity (α_{10} = 5%), and Figure 4.5.6 shows a sample trajectory for the lowest value of the carbon price sensitivity (α_{10} = 2%). The jump times of the carbon price and the default/restructuring time are highlighted with vertical bars in the graphs. The (potential) revenues are shown for the entire time period of 5 years, and the spread is shown up to the default time. We see that the credit spread evolves as function of time and the firm's revenues V, and exhibits upward jumps at the jump times of the carbon price. The default may occur in two ways: in a 'predictable' manner (as in the top graph of Figure 4.5.5) when the revenue process moves continuously below the default threshold for the current value of N, or in an 'unpredictable' manner (as in the top graph of Figure 4.5.4 or the bottom graph of Figure 4.5.5), when a jump in the carbon price triggers a downward jump in the firm's revenues and simultaneously shifts the optimal default threshold upwards in such way that it becomes optimal to default immediately. By contrast, restructuring only happens in a predictable manner (as in the bottom graph of Figure 4.5.4 or in Figure 4.5.6), because a jump in the carbon price may only move the threshold upwards, and will not therefore trigger a restructuring event.

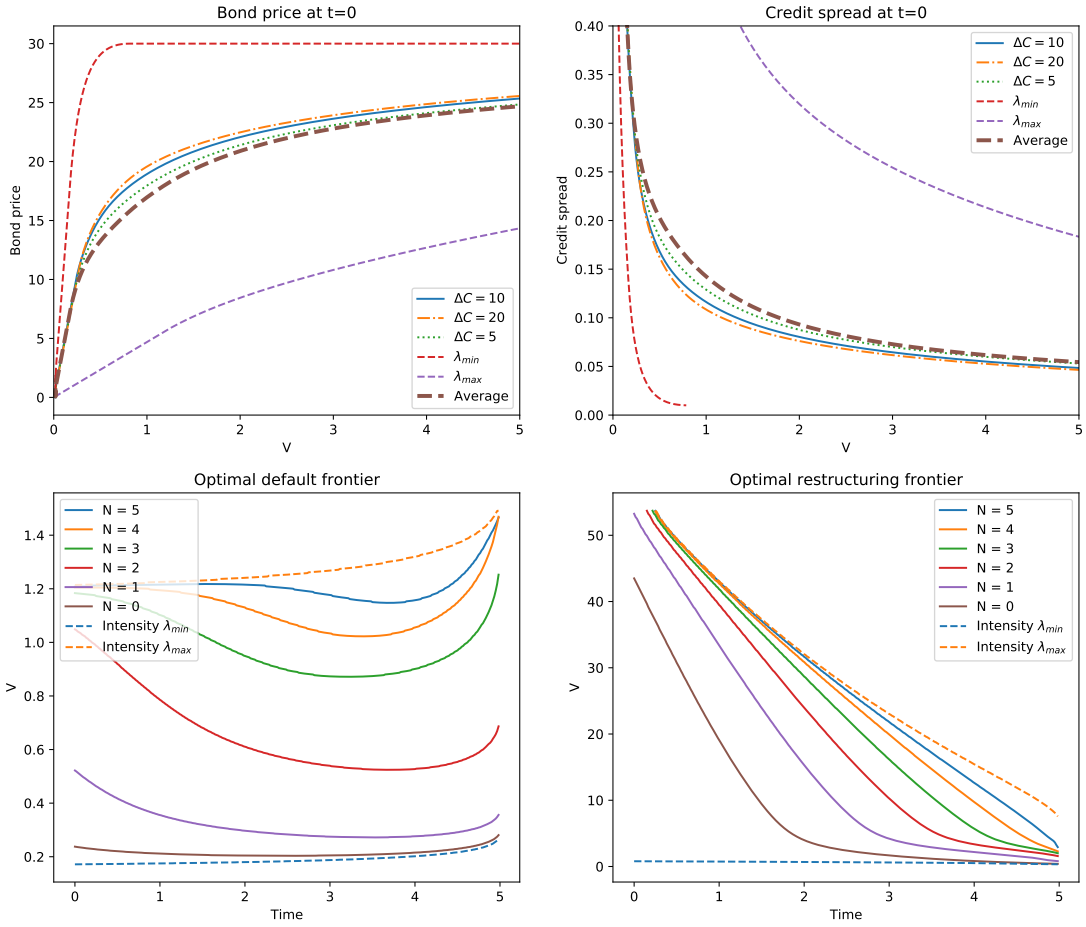

Figure 4.5.3 – Top: bond price and credit spread as function of annualized revenues V; bottom: default and restructuring thresholds as function of time. All financial quantities are in USD billion. Carbon price sensitivity parameter is $\alpha_{10} = 10\%$.

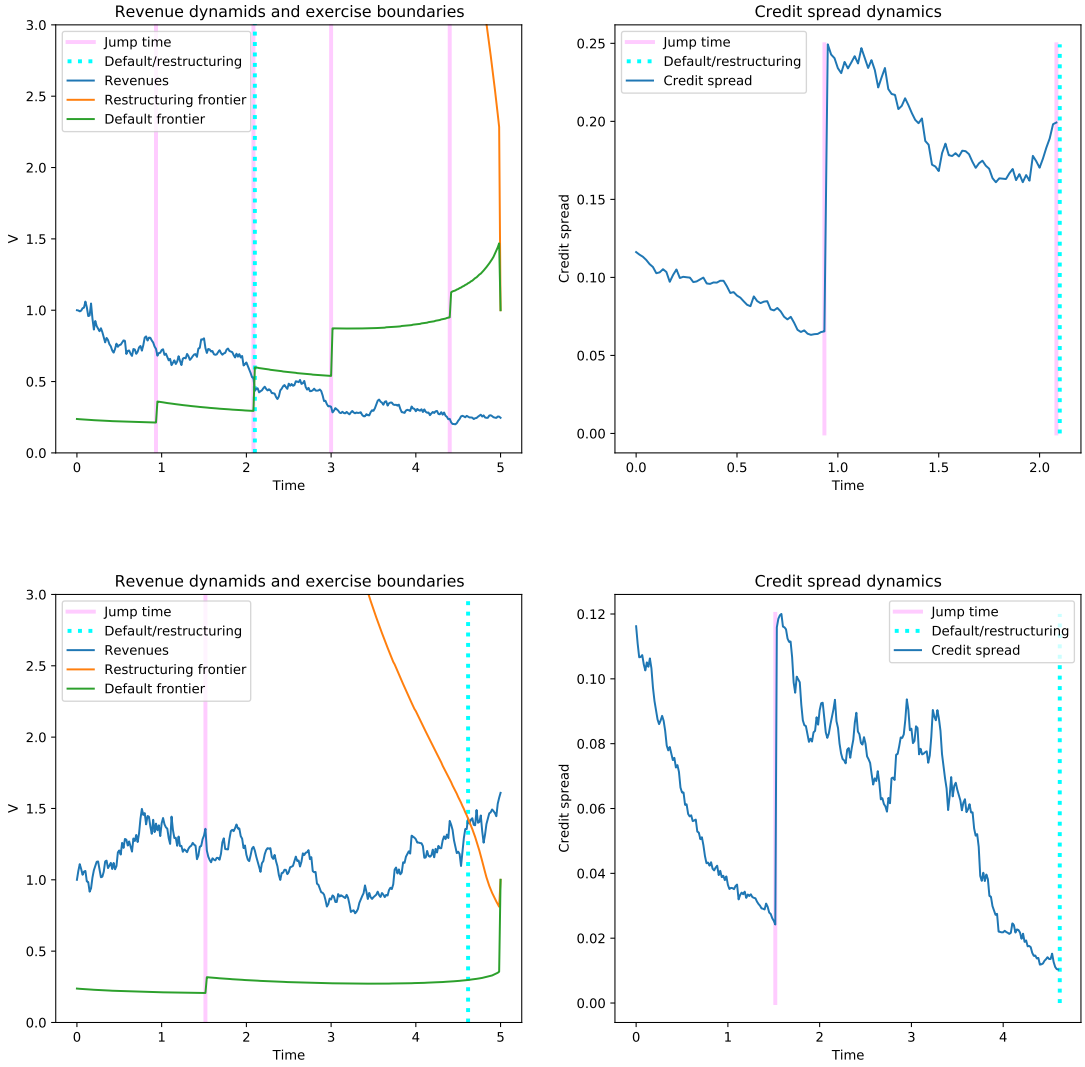

Figure 4.5.4 – Sample trajectories of the firm's annualized revenues (left) and credit spread (right). All financial quantities are in USD billion. Carbon price sensitivity parameter is $\alpha_{10} = 10\%$.

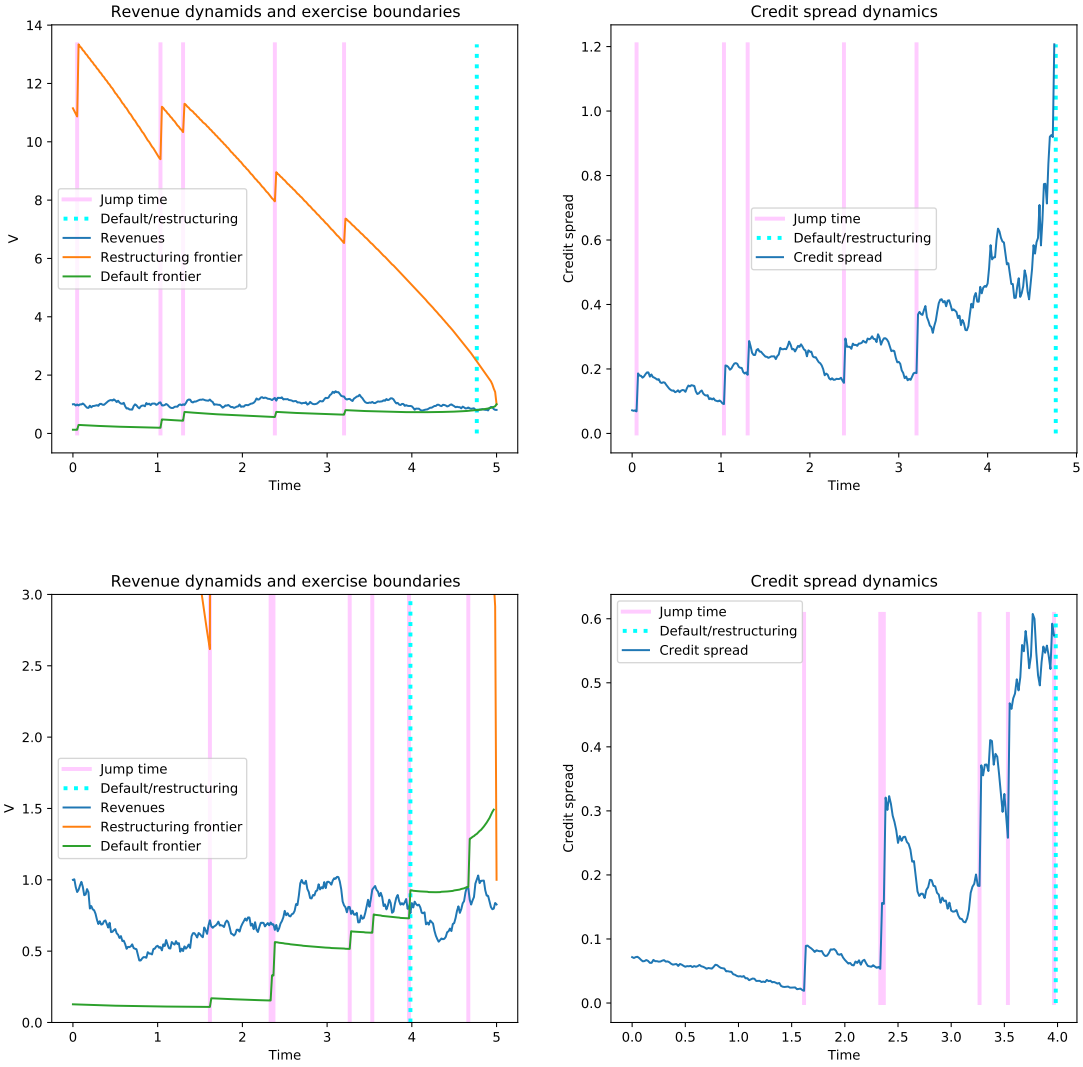

Figure 4.5.5 – Sample trajectories of the firm's annualized revenues (left) and credit spread (right). All financial quantities are in USD billion. Carbon price sensitivity parameter is $\alpha_{10} = 5\%$.

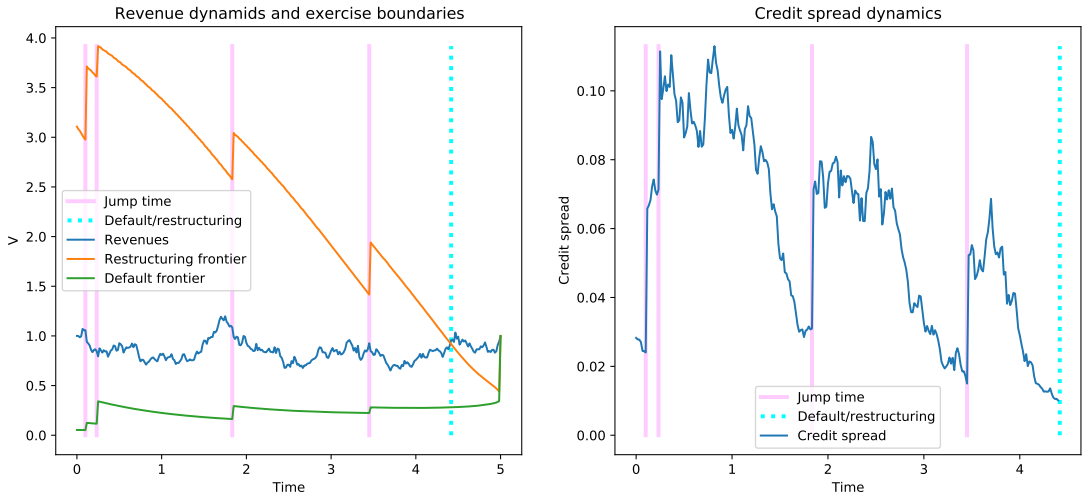

Figure 4.5.6 – Sample trajectory of the firm's annualized revenues (left) and credit spread (right). All financial quantities are in USD billion. Carbon price sensitivity parameter is $\alpha_{10} = 2\%$.

4.6 Conclusion

In this paper, we have presented a structural model for valuing corporate debt under transition scenario uncertainty and progressive learning of scenario information. The model allows to express the bond price and the credit spread as function of the carbon price level and firm's annualized revenue level.

From the practical point of view, our model allows to develop pricing and hedging procedures for bonds of carbon emitting companies taking into account transition risk and transition scenario uncertainty. In particular, the model explains simultaneous defaults triggered by carbon price shocks and higher correlation levels caused by systemic transition risk, which are an important transmission channel of climate transition risk to market risk. Besides, our findings show that under transition scenario uncertainty, carbon price adjustments are more likely to trigger defaults than when the true scenario is known.

From the more theoretical/regulatory viewpoint, our model emphasizes the importance of scenario information for bond pricing in the context of environmental transition: we find that insufficient information about future carbon prices and slow information discovery may lead to overpricing of defaultable bonds and potentially painful market-wide default or repricing events when information is finally discovered.

4.7 Data and code availability statement

This project did not produce any new data other than that contained in tables throughout the article. The code implementing the algorithms described in this article and used to produce the graphs is available for download at `github.com/petertankov/bond-pricing`

Appendix

4.A Proof of Proposition 4

For $M \geq 1$ and $N = 0, \dots, M$, let $\tau_M = \inf\{s > t : N_s^{t,N} = M\}$ and define the function

$$\widetilde{B}^{N,M}(t,V) = \inf_{\tau \in \mathcal{T}([t,T])} \mathbb{E}\Big[\int_t^{\tau \wedge T \wedge \tau_M} e^{-r(s-t)} b \, ds + e^{-r(T \wedge \tau - t)} \widehat{V}_{T \wedge \tau}^{t,V,N} \wedge K \mathbf{1}_{\tau_M > T \wedge \tau} + e^{-r(\tau_M - t)} G^M(\tau_M, V_{\tau_M}^{t,V,N}) \mathbf{1}_{\tau_M \leq T \wedge \tau} \Big].$$

Let us first show that

$$\lim_{M \to \infty} \widetilde{B}^{N,M}(t,V) = B^N(t,V).$$

Indeed, for any $\tau \in \mathcal{T}([t,T])$, the difference of expressions under the expectation sign in $\widetilde{B}^{N,M}$ and B^N admits the following upper bound:

$$\begin{aligned} &\mathbf{1}_{\tau_M \leq T \wedge \tau} \Big| \int_{\tau \wedge T \wedge \tau_M}^{\tau \wedge T} e^{-r(s-t)} b \, ds + e^{-r(T \wedge \tau - t)} \widehat{V}_{T \wedge \tau}^{t,V,N} \wedge K - G^M(\tau_M, V_{\tau_M}^{t,V,N}) \Big| \\ &\leq C \mathbf{1}_{\tau_M \leq T} \end{aligned}$$

for some constant $C < \infty$. Since the jump intensity of N is bounded from below by $\lambda_{min} := \min_i \lambda_i$,

$$\begin{aligned} \mathbb{P}[\tau_M \leq T] = \mathbb{P}[N_T^{t,N} - N \geq M - N] &\leq \sum_{k \geq M-N} \frac{(\lambda_{min}(T-t))^k}{k!} e^{-\lambda_{min}(T-t)} \\ &\leq \frac{(\lambda_{min}(T-t))^{M-N}}{(M-N)!} \end{aligned}$$

From Stirling formula it is then clear that this expression, or any positive power of it, converges to zero at faster than exponential rate.

Let us now prove that the function $\widetilde{B}^{N,M}$ defined above coincides with the function $B^{N,M}$ defined in the statement of the lemma. By standard arguments (see e.g., Bensoussan and Lions, 2011, Theorem 4.7, Chapter 3), $B^{N,M}$ has sufficient regularity to apply Itô's lemma and is Lipschitz

continuous in V. Then, omitting the subscript t, V, N to save space,

$$\begin{aligned}
&e^{-r(s\wedge\tau_M - t)} B^{N_s\wedge M, M}(s\wedge\tau_M, V_{s\wedge\tau_M}) - B^{N,M}(t,V) \\
&= \sum_{k=N}^{M-1} \int_{s\wedge\tau_k}^{s\wedge\tau_{k+1}} e^{-r(q-t)} \Big\{ \frac{\partial B^{k,M}}{\partial t} + \mu V_q \frac{\partial B^{k,M}}{\partial V} + \frac{\sigma^2}{2} V_q^2 \frac{\partial^2 B^{k,M}}{\partial V^2} - r B^{k,M} \Big\} dq \\
&+ \sum_{k=N}^{M-1} \int_{s\wedge\tau_k}^{s\wedge\tau_{k+1}} e^{-r(q-t)} \frac{\partial B^{k,M}}{\partial V} \sigma V_q dW_q \\
&+ \sum_{k=N}^{M-1} \mathbf{1}_{\tau_{k+1}\le s} e^{-r(\tau_{k+1}-s)} \Big\{ B^{k+1,M}(\tau_{k+1}, V_{\tau_{k+1}}) - B^{k,M}(\tau_{k+1}, V_{\tau_{k+1}-}) \Big\}
\end{aligned}$$

The last term can be alternatively written as follows:

$$\begin{aligned}
&\sum_{k=N}^{M-1} \mathbf{1}_{\tau_{k+1}\le s} e^{-r(\tau_{k+1}-s)} \Big\{ B^{k+1,M}(\tau_{k+1}, V_{\tau_{k+1}}) - B^{k,M}(\tau_{k+1}, V_{\tau_{k+1}-}) \Big\} \\
&= \int_t^{s\wedge\tau_M} \int_{-\infty}^1 e^{-r(q-t)} \Big\{ B^{N_{q-}+1,M}(q, V_{q-}(1-z)) - B^{N_{q-},M}(q, V_{q-}) \Big\} J(dq, dz) \\
&= \int_t^{s\wedge\tau_M} \int_{-\infty}^1 e^{-r(q-t)} \Big\{ B^{N_{q-}+1,M}(q, V_{q-}(1-z)) - B^{N_{q-},M}(q, V_{q-}) \Big\} \widetilde{J}(dq, dz) \\
&+ \int_t^{s\wedge\tau_M} \int_{-\infty}^1 e^{-r(q-t)} \Big\{ B^{N_q+1,M}(q, V_q(1-z)) - B^{N_q,M}(q, V_q) \Big\} \nu(dz) \hat{\lambda}^{N_q}(q)\, dq \\
&= \int_t^{s\wedge\tau_M} \int_{-\infty}^1 e^{-r(q-t)} \Big\{ B^{N_{q-}+1,M}(q, V_{q-}(1-z)) - B^{N_{q-},M}(q, V_{q-}) \Big\} \widetilde{J}(dq, dz) \\
&+ \sum_{k=N}^{M-1} \int_{s\wedge\tau_k}^{s\wedge\tau_{k+1}} \int_{-\infty}^1 e^{-r(q-t)} \Big\{ B^{k+1,M}(q, V_q(1-z)) - B^{k,M}(q, V_q) \Big\} \nu(dz) \hat{\lambda}^k(q)\, dq,
\end{aligned}$$

where J denotes the jump measure of the process L and $\widetilde{J}$ denotes its compensated jump measure.

Then, since $B^{k,M}$ is Lipschitz in V, it holds that

$$\begin{aligned}
&e^{-r(s\wedge\tau_M - t)} B^{N_s\wedge M, M}(s\wedge\tau_M, V_{s\wedge\tau_M}) - B^{N,M}(t,V) = M_s \\
&+ \sum_{k=N}^{M-1} \int_{s\wedge\tau_k}^{s\wedge\tau_{k+1}} e^{-r(q-t)} \Big\{ \frac{\partial B^{k,M}}{\partial t} + \mu V_q \frac{\partial B^{k,M}}{\partial V} + \frac{\sigma^2}{2} V_q^2 \frac{\partial^2 B^{k,M}}{\partial V^2} - r B^{k,M} \Big\} dq \\
&+ \sum_{k=N}^{M-1} \int_{s\wedge\tau_k}^{s\wedge\tau_{k+1}} e^{-r(q-t)} \hat{\lambda}^k(q)\, dq \int_{-\infty}^1 \Big\{ B^{k+1,M}(q, V_q(1-z)) - B^{k,M}(q, V_q) \Big\} \nu(dz),
\end{aligned}$$

where M is a martingale. Then, for any stopping time $\tau \in \mathcal{T}([0,T])$, using the variational inequality,

$$\begin{aligned}
B^{N,M}(t,V) &\le M_{s\wedge\tau} + \int_t^{s\wedge\tau_M\wedge\tau} e^{-r(q-t)} b\, dq \\
&+ e^{-r(s\wedge\tau - t)} \widehat{V}_{s\wedge\tau} \wedge K \mathbf{1}_{\tau_M > s\wedge\tau} + e^{-r(\tau_M - t)} G^M(\tau_M, V_{\tau_M}) \mathbf{1}_{\tau_M \le s\wedge\tau}
\end{aligned}$$

Taking the expectation, we then conclude that $B^{N,M}(t,V) \le \widetilde{B}^{N,M}(t,V)$. On the other hand, choosing

$$\tau^* = \inf\{ s > t : B^{N_s\wedge M, M}(s\wedge\tau_M, V_{s\wedge\tau_M}) = \widehat{V}_{s\wedge\tau_M} \wedge K \},$$

we see that the inequality above becomes an equality, showing that $B^{N,M}(t,V) = \widetilde{B}^{N,M}(t,V)$.

To prove the last estimate of the proposition, remark that we could have similarly shown, for $N \le K \le M$,

$$B^{N,M}(t,V) = \inf_{\tau \in \mathcal{T}([t,T])} \mathbb{E}\Big[\int_t^{\tau \wedge T \wedge \tau_K} e^{-r(s-t)} b \, ds + e^{-r(T\wedge\tau - t)} \widehat{V}^{t,V,N}_{T\wedge\tau} \wedge K \mathbf{1}_{\tau_K > T\wedge\tau} + e^{-r(\tau_K - t)} B^{K,M}(\tau_K, V^{t,V,N}_{\tau_K}) \mathbf{1}_{\tau_K \le T\wedge\tau} \Big].$$

Passing to the limit $M \to \infty$ (which can be justified in the right-hand side with the dominated convergence theorem) yields

$$B^{N}(t,V) = \inf_{\tau \in \mathcal{T}([t,T])} \mathbb{E}\Big[\int_t^{\tau \wedge T \wedge \tau_K} e^{-r(s-t)} b \, ds + e^{-r(T\wedge\tau - t)} \widehat{V}^{t,V,N}_{T\wedge\tau} \wedge K \mathbf{1}_{\tau_K > T\wedge\tau} + e^{-r(\tau_K - t)} B^{K}(\tau_K, V^{t,V,N}_{\tau_K}) \mathbf{1}_{\tau_K \le T\wedge\tau} \Big].$$

Since the right-hand side is monotone in B^K, the result follows.

Chapter 5

Measuring and Pricing Tropical Cyclone related Physical Risk under Climate Change [1]

The direct effects of global warming on the planet are unequivocal – melting of glaciers, rising sea levels, unstable climate conditions, expanding deserts – phenomena that have been comprehensively detailed by the Scientific Committee of the Intergovernmental Panel on Climate Change (IPCC) in their reports (Pachauri *et al.*, 2014; Solomon *et al.*, 2007). However, these environmental issues are only the tip of the iceberg of the consequences of climate change, which also encompass the effects of climate change on societies and economies.

The financial implications of climate change fall in two main categories. First, transition risks and opportunities are the financial consequences of the transition toward a low carbon economy. A large body of literature describes the transmission channels of transition risk to the financial markets (Battiston *et al.*, 2017; Battiston & Monasterolo, 2019). On the other hand, the second type of climate-related risk categorized as '*physical risk*' has been less addressed in the literature. Indeed, if the global effort is too late or insufficient (Jewell & Cherp, 2020), societies will be threatened by more intense disasters, and financial assets will suffer greater losses. These risks are particularly hard to apprehend as they will likely materialize in the long-term and are subject to deep uncertainty.

In this article, our aim is to quantify *physical risks at the country level, and assess their impact on financial markets*. We focus on tropical cyclones and model explicitly the four main dimensions of the problem: (*i*) the sensitivity of tropical cyclone intensity to climate change, (*ii*) the exposure level of the countries to the tropical cyclone risk, (*iii*) the vulnerability (amount of losses which may be caused by the tropical cyclone to the exposed assets) and (*iv*) pricing of the tropical cyclone risk by the financial markets.

To address the first dimension, we provide a reproducible methodology to generate future cyclones from climate data inspired by Bloemendaal *et al.* (2020). We define an integrated cyclone generator that can be launched on any climate projection from the Phase 5 Coupled Model Intercomparison Project (CMIP5). Regarding the second dimension, to define countries' exposure

1. A revised version of this chapter is published in the Geoscientific Model Development Journal (Le Guenedal, Drobinski, *et al.*, 2022).

while encompassing the diversity of scenarios proposed in the IPCC assessment framework, we use multiple sources. We define the current local downscaled physical asset value exposed to tropical cyclone risk as in Eberenz *et al.* (2020). Then, to determine the future physical asset value exposure we apply two correction factors to the current local physical asset value: a global macroeconomic GDP/population ratio based on the trajectory defined in Riahi *et al.* (2017), and a local scenario-based population distribution based on the grid defined in Jones and O'Neill (2020). The vulnerability dimension is determined as in Eberenz *et al.* (2021) who designed regional specific damage functions in the CLIMADA project. Finally, to address the market pricing issue, we channel the expected damages to emerging countries credit spreads by assuming that damage costs are financed by issuing new government debt and using an econometric model of Hilscher and Nosbusch (2010) to estimate the impact of debt to GDP ratio on bond spread. Combining open data sources and methodologies allows us to propose a complete integrated physical tropical cyclone damage assessment framework with a financial pricing module.

To quantify the model uncertainty of future climate projections, we use a multi-model ensemble consisting of 7 general circulation models developed by different climatological centers around the world. This approach allows us to quantify the main sources of uncertainty in our estimates, namely the natural climate variability (by simulating many years of synthetic cyclones), the model uncertainty and the socio-economic uncertainty taken into account through the use of RCP pathways and SSP scenarios.

The methodology of this paper is illustrated in Figure 5.0.1. We first construct a synthetic cyclone tracks database translating the relationship between the scenario-based sea-surface temperature rise and the change in cyclones intensity. To this end we first define a model of cyclone genesis, which describes the number of cyclones appearing each year in each basin (North Atlantic, East, West and South Pacific, North and South Indian). Once initiated, the cyclones start moving, following the dynamics defined using simple auto-regressive formulas. The local variables determining the genesis and evolution of cyclones are based on four statistical equations and one thermodynamic relationship, calibrated on climate data and historical cyclone tracks.

In the second step of our methodology, we define the geographical distribution of sovereign exposure, in each scenario. We use the framework of the shared-socioeconomic pathways (SSP) (Riahi *et al.*, 2017). These narratives are used in the IPCC development scenarios and provide a reference framework for risk assessment. To this end, we use the current downscaled physical asset value from Eberenz *et al.* (2020) and the vulnerability of each region from Eberenz *et al.* (2021). We then determine the projected exposure using local expansion factor from NASA Socioeconomic Data and Applications Center (SEDAC, Jones and O'Neill (2020)) and / or global GDP per capita variation factor from Riahi *et al.* (2017). We apply a localized damage function to the exposure and aggregate the losses along cyclone tracks to estimate the loss for each synthetic cyclone.

Finally, we integrate the future cyclones damage cost in the pricing of emerging sovereign debt. To price the financial consequences of climate change related to tropical cyclones, we consider that the costs are paid by issuing new government debt and use the sensitivity of the option adjusted spread to the debt ratio. We use the JP Morgan EMBI Index constituents to fit our relationship.

In the end, we construct a full financial risk model, based on thermodynamic and statistical relationships, calibrated on open source climate and socio-economic data. We find that socioeconomic factors are influential but that climate change has a major impact on the future potential damage. Using the projections currently available for the time horizon 2070-2100 and in absence

Figure 5.0.1 – Framework of cyclone physical risks assessment

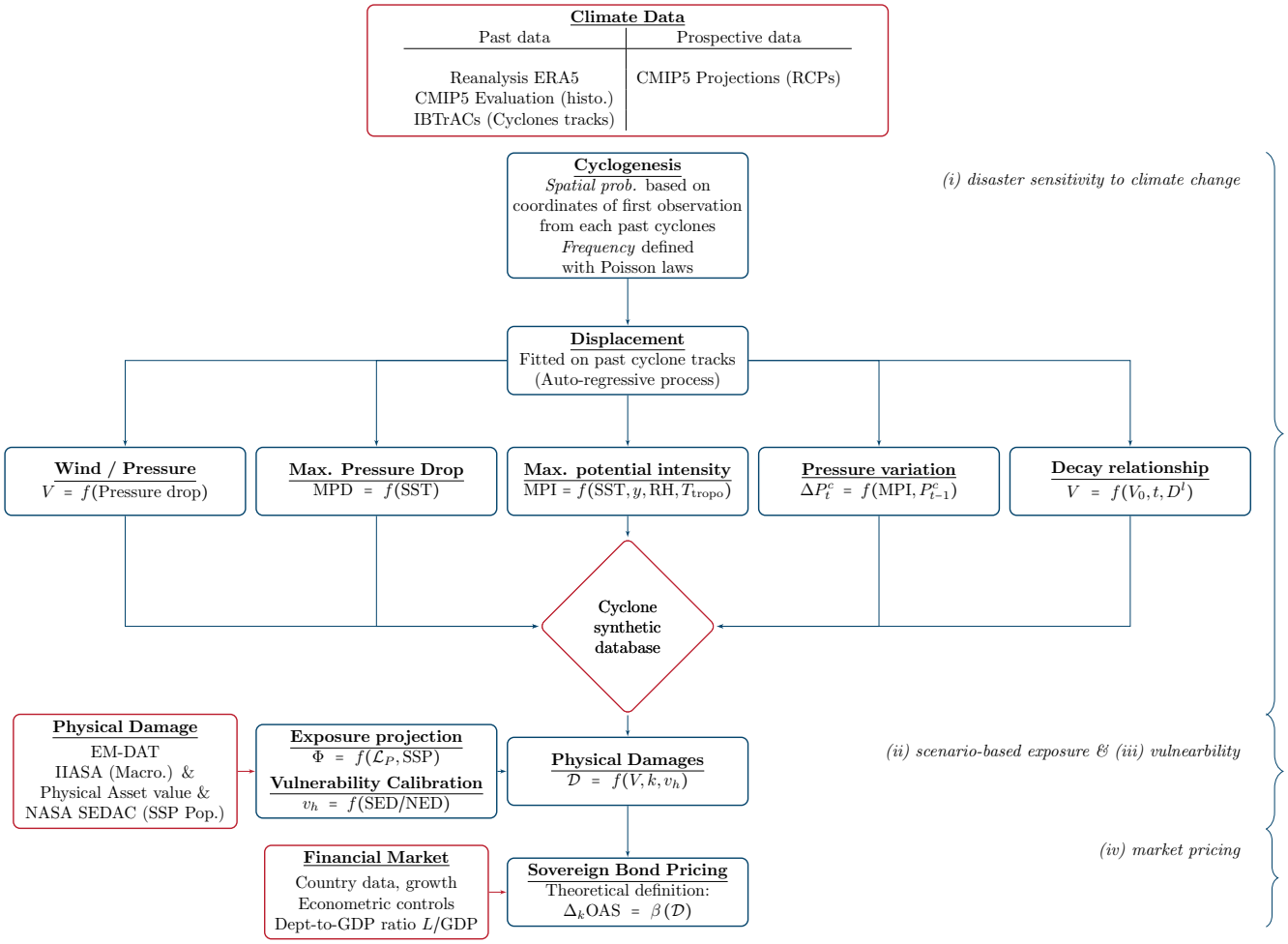

of adaptation, the RCP 2.6 scenario, which is in line with the Paris Agreement and keeps global warming below 2℃ by 2100, involves a growth of expected global annual financial losses from tropical cyclones by a factor of 4.84 on average compared to the last 40 years. In the case of RCP 4.5 (between 1.7 and 3.2℃ warming by 2100) and RCP 8.5 (between 3.2 and 5.4℃ warming by 2100), the average expected damage will be multiplied by 5.99 and 7.95 respectively. These results were obtained under the economic assumptions associated with the socio-economic pathway SSP2 (i.e. the '*Middle of the Road*' scenario in O'Neill *et al.* (2014)'s framework). The choice of the socio-economic scenario is also a determinant for damage estimation. In the case of the SSP5 socio-economic scenario (which assumes sustained exponential economic growth), with constant damage functions, the previous figures become 8.67, 11.1 and 15.22 respectively. In terms of emerging market impact,[2] and by 2070, we estimate that the maximum annual cyclone-related spread variation for countries within the JP Morgan EMBI Index could increase in high concentration pathways up to 200 bps for most vulnerable countries with respect to a 2℃ baseline.

2. Using the damage distribution without climate data bias-correction and country correction introduced in the revised version of Le Guenedal *et al.* (2021a).

This Chapter is organized as follows. Section 5.1.1 describes the datasets used to fit the model on ERA-5 and to generate synthetic cyclones based on both ERA-5 and CMIP5 models datasets. Section 5.1 describes the statistical calibration process and the details of the thermodynamic instrumental variables. Section 5.3 recalls the calibration methods implemented in the CLIMADA environment to fit the regional damage functions, defines the parameters of these functions using Eberenz *et al.* (2021) and applies them along the synthetic tracks produced to study the distribution of national annual damages. Section 5.4 explores the properties of the produced synthetic tracks, with ERA-5 and 7 CMIP models, assesses climate uncertainty and introduces the bias correction module in the context of changing climate conditions. To close this section, we present the global and regional projections of cyclone damage between 2070 and 2100 obtained with CATHERINA. Section 5.4.3 presents the implications of physical risks on emerging countries' bond spread.

5.1 Tropical cyclone intensity

Our model structure follows Bloemendaal *et al.* (2020) with three main modeling steps: genesis, displacement of the eye and calibration of the cyclone properties. The STORM model relies on statistical relationships (DeMaria & Kaplan, 1994; James & Mason, 2005; Kaplan & DeMaria, 1995). This simulation method differs from the purely thermodynamic approach developed by Kerry Emmanuel (K. A. Emanuel, 1999; K. Emanuel *et al.*, 2008).

The major change in our specification compared to Bloemendaal *et al.* (2020) is that we use the local definition of the available thermodynamic potential based on climate data. In particular, we use relative humidity (RH) and tropopause temperature (at 50 hPa, T_{tropo}), for better theoretical representation of the physics underlying the intensification process. In this section, we present the process of generating synthetics tracks, characterized by the maximum wind (V_t) and central pressure (P_t^c) at each time step, given the climate conditions extracted from climate models.

5.1.1 Input data

In the CATHERINA framework, we fit the properties of historical cyclones (IBTrACS database) on past climate reanalyses (ERA-5) in the perspective of describing future cyclones based on global climate models outputs (CMIP), having a lower spatial and temporal resolution. This perspective constrains us to use monthly data.

Climate model data (CMIP) CATHERINA aims at generating cyclone tracks with properties drawn from climate models to enable national damage assessments, bridging the gap between Atmosphere-Ocean General Circulation Models (AOGCM) outputs and damage assessments. To reduce the bias in the variables produced by climate models and evaluate the performance of CATHERINA on past data by comparing the simulated cyclone damages to the realized ones we use historical simulations (as opposed to future climate projections) from the Coupled Model Inter-comparison project (Phase 5) models (Taylor *et al.*, 2012). We use the historical climate simulations at the monthly frequency for the relative humidity (RH) at two meters, sea surface

temperature (SST), mean sea level pressure (MSLP) and tropauspose temperature (T_{tropo}) (at pressure level of 50 hPa) from Copernicus climate data store.[3] CMIP5 data are used in the 5th assessment report of the Intergovernmental Panel on Climate Change (IPCC). The latest synthesis Report in 2022 (IPCC AR6) uses CMIP6 datasets but in the present paper, we use CMIP5 data because of the broader availability of climate variables.

We use models from the following climate centers: NASA, Goddard Institute for Space Studies (GISS-E2-H, USA), Institut Pierre Simon Laplace (IPSL-CM5A-NR, France), Bureau of Meteorology - Commonwealth Scientific and Industrial Research Organisation (ACCESS1-0, BoM-CSIRO, Australia), Beijing Climate Center (bcc-csm1-1-m, China), Institute of Numerical Mathematics (inmcm4, Russia), Norwegian Climate Centre (NorESM1-ME, Norway), Canadian Centre for Climate Modelling and Analysis (CanESM2, Canada). The spatial resolution goes from 0.75° to 2.5° depending on the model (See Table 5.1.1). Each climate model produces a potentially biased estimate of multiple climate variables at the spatial resolution given in Table 5.1.1 and on a monthly basis. The choice of the CGMs was driven by the availability of the variables of interest in the Copernicus Climate data store (CDS) in the representative concentration pathways used in the exercise (RCP 2.6, 4.5 and 8.5 W/m2) in both single level and multiple pressure level monthly data in the same ensemble (r1i1p1). We also aimed at having multiple regions represented.

To reduce the influence of model bias, we use a large number of models and consider the distribution of results provided by all the models. Then we correct, variable by variable, and for each basin and each model, the biases with respect to the reanalysis along the same tracks.

Table 5.1.1 – Climate data resolution

	Resolution
ERA-5 (Reanalysis)	0.25 x 0.25
ACCESS1-0 (BoM-CSIRO, Australia)	1.88x 0.93
CanESM2 (CCCMA, Canada)	1.41x 0.94
GISS-E2-H (NASA, USA)	2.5 x 2
NorESM1-ME (NCC, Norway)	1 x 1
bcc-csm1-1-m (BCC, China)	1 x 0.74
IPSL-CM5A-MR (IPSL, France)	1 x 1
INMCM4 (INM, Russia)	2 x1.5

ERA-5 Reanalysis Climate reanalyses describe the historical climate conditions, obtained by assimilating all available observations into the models. They provide numerical estimates of atmospheric parameters (e.g. air temperature, pressure and wind) at different altitudes / pressure levels, and surface parameters (such as rainfall, soil moisture content, ocean-wave height and sea-surface temperature) on a single level. We use reanalyses to calibrate the cyclone generation algorithm based on the most realistic available estimates of climate variables.

We use ERA-5 reanalysis from the European Centre for Medium-Range Weather Forecasts (ECMWF) to fit the CATHERINA model (Hersbach *et al.*, 2020). This dataset covers the Earth

3. Climate data is available on the Copernicus Climate data store: https://cds.climate.copernicus.eu/.

on a 30 km grid (~ 0.25) and resolves the atmosphere using 137 levels from the surface up to a height of 80 km. In this paper, to ensure compatibility with CMIP5 models, we extract mean sea-level pressure (MSLP), sea-surface temperature (SST), sea-level relative humidity (RH), and tropopause temperature (T_{tropo}) at the monthly frequency. Because ERA-5 better resolves past tropical cyclones than climate models, the historical mean sea-level pressure values in ERA-5 are influenced by their presence. Consequently, we retrieve the mean sea-level pressure and environmental relative humidity 500 km (~ 5° longitude) away from the storm center to extract a value for P_{env}, that is meant to represent the pressure - at a given latitude and season - in normal environmental conditions. [4]

Historical cyclone tracks (IBTrACS) We use the International Best Track Archive for Climate Stewardship (IBTrACS) database (Knapp *et al.*, 2010). [5] This database provides information on past cyclone tracks at 3-hour frequency. We remove the events classified as disturbance or extra tropical, and do not consider the South Atlantic basin (see Figures 5.B.1 for more information). Climate reanalysis availability requires us to focus on post 1980 cyclones, which reduces the database to 4,574 cyclones. In the context of an integrated damage assessment, to focus on the events that have a potentially substantial impact on assets, we select only tropical cyclones with maximum wind speed exceeding 35 m.s^{-1} obtaining 2,966 on the full database and 1,451 focusing on tropical cyclones between 1980 and April 2020. In Figure 5.1.1, we plot the central pressure along each cyclone life. This graph suggests that the cyclone phases are fully represented in the database i.e. from the genesis to dissipation. The North Indian basin has the lowest number of reported events with wind speed above 35 m.s^{-1} (50 compared to 291 for East Pacific, 185 for North Atlantic, 305 for South Indian, 158 for South Pacific and 515 for West Pacific) with variable reporting quality, which explains the more erratic shapes of the central pressure. For example, the return to normal of some events does not seem to be completely reported for this basin as indicated in Figure 5.1.1. We extract the maximum wind speed, cyclone eye pressure and coordinate variations of the eye from this database.

5.1.2 Cyclone genesis

The scientific consensus is that climate change will induce a reduction in tropical cyclone frequency: "*Existing modeling studies also consistently project decreases in the globally averaged frequency of tropical cyclones, by 6 to 34%. Balanced against this, higher resolution modeling studies typically project substantial increases in the frequency of the most intense cyclones*" (T. Knutson *et al.*, 2020, p. 1). Although thermodynamic descriptions of cyclone genesis exist in the

4. We retrieve both pressure (MSLP) and humidity (RH) to define P^{env} and RH^{env} (Holland, 1997) away from the center in the reanalysis because tropical cyclone thermodynamic potential intensity - through thermodynamic efficiency and moist entropy (Equation (5.7) and (5.6))- arise from the deviations from the normal conditions. Monthly averaging may smooth values so that the data extracted along historical tracks may not represent the conditions at the time of cyclone passage. Therefore, using monthly means, this translation is mainly made for reasons of theoretical coherence. In future studies, this model will be applied with higher temporal resolution and performing this translation would be more important. In the present version of our paper, because the CMIP5 projections of the sea-level temperature were only available at monthly frequency in the CDS, we chose to perform the exercise using monthly data to illustrate our approach.

5. See http://ibtracs.unca.edu/ for a browser of the data and https://www.ncdc.noaa.gov/ibtracs/index.php?name=ib-v4-access for the full dataset.

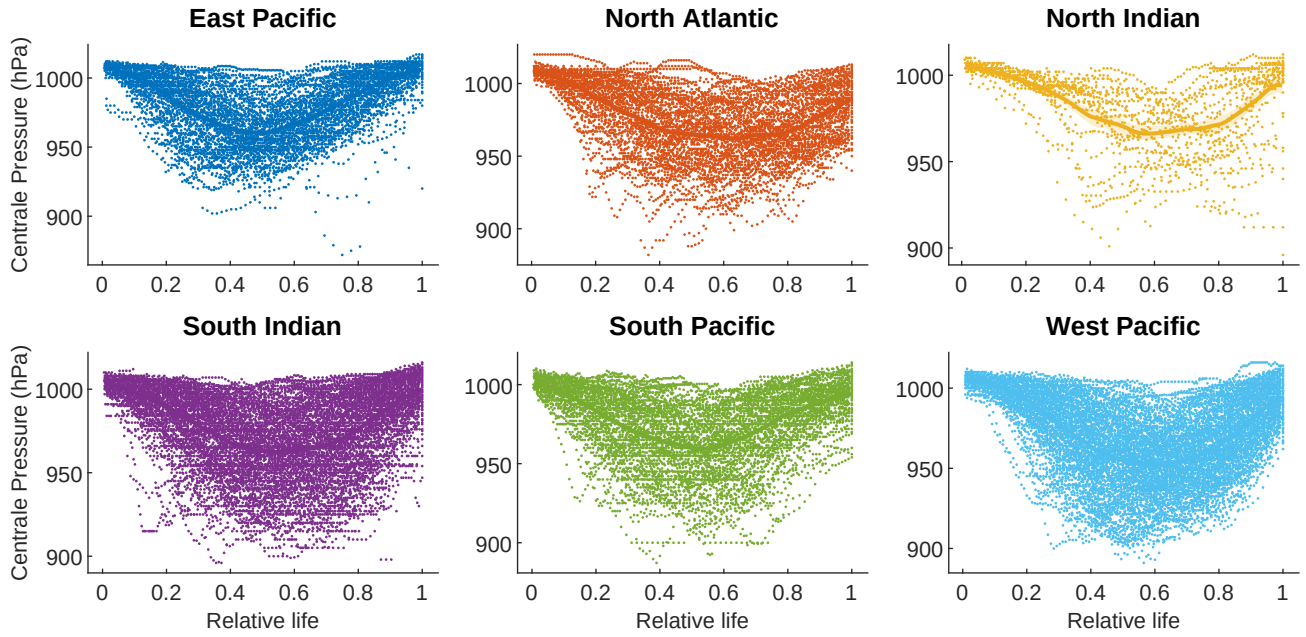

Figure 5.1.1 – Normalized evolution of the central pressure (in hPa) during cyclones life. The central pressure values are retrieved from IBTrACS. For the West Pacific we reduced the sample to events between 1995 and 2020 for visualisation purpose.

literature (DeMaria *et al.*, 2001; Gray, 1975) we choose to rely on a simple statistical model based on past frequencies for the genesis.

The number of synthetic cyclones each year is determined by the Poisson distribution in each basin, with intensity parameter defined as the average number of cyclones per year in the historical data. We use the parameters given in Bloemendaal *et al.* (2020) i.e. $\hat{\lambda}_{\text{EP}} = 14.5$ for the East Pacific, $\hat{\lambda}_{\text{NA}} = 10.8$ for the North Atlantic, $\hat{\lambda}_{\text{NI}} = 2.0$ for the North Indian, $\hat{\lambda}_{\text{SI}} = 12.3$ for the South Indian, $\hat{\lambda}_{\text{SP}} = 9.3$ for the South Pacific, and $\hat{\lambda}_{\text{WP}} = 22.5$ for the West Pacific. The parameters would have been smaller if estimated using our filtered database of tropical cyclones with wind speed above 35 m.s^{-1}: $\hat{\lambda}^{35}_{\text{EP}} = 7.31$, $\hat{\lambda}^{35}_{\text{NA}} = 4.43$, $\hat{\lambda}^{35}_{\text{NI}} = 1.6$, $\hat{\lambda}^{35}_{\text{SI}} = 6.81$, $\hat{\lambda}^{35}_{\text{SP}} = 4.00$ and $\hat{\lambda}^{35}_{\text{WP}} = 11.86$. However, we maintain the original parameters used in STORM to take into consideration the fact that some events will be generated in conditions not favorable for the development of cyclones and cleared out of the database. The number of cyclones making landfall being critical for damage estimation (Arthur, 2021; Hall & Jewson, 2007; Lee *et al.*, 2018), we ensured that the simulated landfall rates are in line with the observations over the historical period: Figure 5.1.2 shows that the parameters of Bloemendaal *et al.*, 2020 lead to approximately the same number of intense cyclones making landfall per year in each basin in the historical data, in our simulations based on reanalysis data and in simulations based on CGMs. We note however that the framework can be further improved by choosing the intensity parameter to match exactly the average historical number of cyclones making landfall.

Similarly, the temporal and spatial initial positions of synthetic future cyclones (longitude x, latitude y and starting month m) are generated by independent sampling from the historical distribution of these variables. Figure 5.1.3 shows the geographical distribution of cyclones retrieved

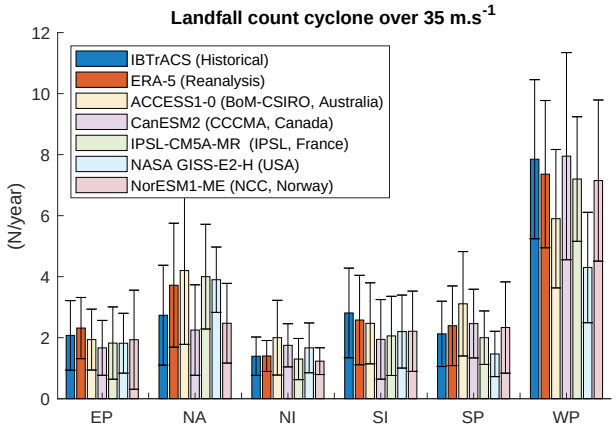

Figure 5.1.2 – Number of tropical cyclones over 35m.s^{-1} making landfall simulated using Bloemendaal *et al.* (2020) parameters over the historical period (1980-2010)

from IBTrACS (i.e. x_{obs}, y_{obs}) and the histograms in Figure 5.1.4 show the monthly distribution (m_{obs}) of cyclones in each basin.

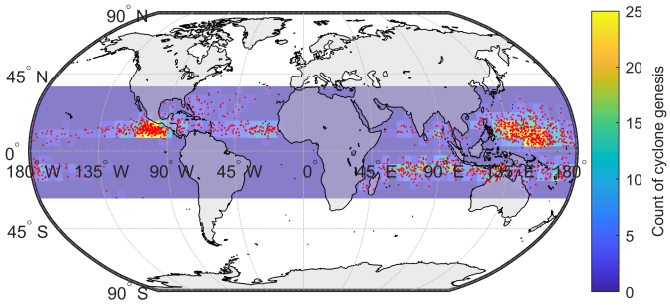

Figure 5.1.3 – Spatial distribution of genesis points (tropical cyclones over 35m.s^{-1} in IBTrACS). The color scale corresponds to the count of cyclone per 5x5° box (truncated to 25 for scaling reason). The genesis location corresponds to the first reported point of each track.

5.1.3 Cyclone trajectories

A rich literature focuses on cyclone tracking algorithms, see e.g., Neu *et al.* (2013) for a comprehensive review. Although more advanced definitions have been proposed (Fabregat *et al.*, 2016; Hall & Jewson, 2007), we choose, in line with Bloemendaal *et al.* (2020), to implement a simple auto-regressive model for cyclone coordinates. Following James and Mason (2005), the time evolution of the latitude and longitude of the cyclone center is described by the following stochastic dynamics:

$$\Delta x_t = a_0 + a_1 \Delta x_{t-1} + \varepsilon_t^x, \qquad \varepsilon_t^x \sim \mathcal{N}(0, \sigma_x), \tag{5.1}$$

$$\Delta y_t = b_0 + b_1 \Delta y_{t-1} + \frac{b_2}{y_t} + \varepsilon_t^y, \qquad \varepsilon_t^y \sim \mathcal{N}(0, \sigma_y). \tag{5.2}$$

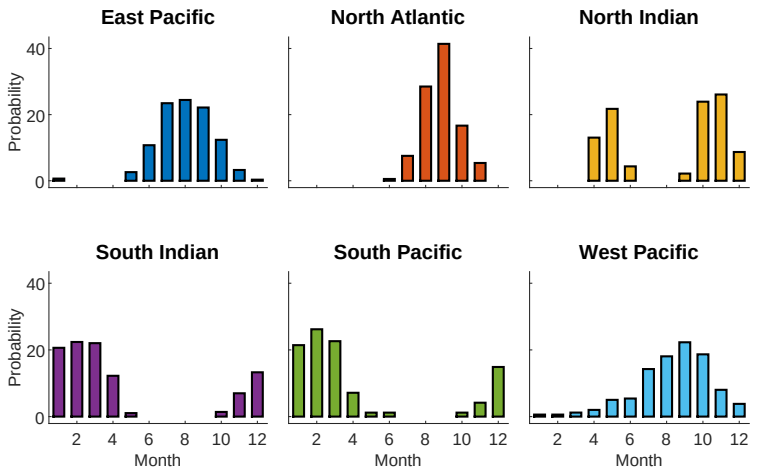

Figure 5.1.4 – Relative monthly distribution (%) of cyclones in each basin defined from potentially damaging cyclones (over 35m.s^{-1}) in IBTrACS. Each bar gives the probability for each cyclone to be allocated to a given month.

Here x_t and y_t are the latitude and longitude of the cyclone center sampled with a 3 hour time step; $\Delta x_t = x_t - x_{t-1}$, $\Delta y_t = y_t - y_{t-1}$, ε_t^x and ε_t^y are i.i.d. noises independent from one another, and the constants a_0, a_1, b_0, b_1, b_2, σ_x and σ_y are fitted on IBTrACS data independently for each basin by least squares regression. The non-linear term in the incremental variation of the latitude is justified by the tendency for cyclones to move away from the equator, especially at very low latitudes James and Mason, 2005, p. 183.

To take into account the dependency of the cyclone displacement on the location of the eye, and following Bloemendaal *et al.* (2020), we fitted these relationships locally using an additional grouping by 5 longitude and latitude sections and months. Figure 5.B.2 illustrates the parameters a_0 and a_1, the adjusted R^2 and the number of observation averaged over months used to fit the Equation (5.1). We note that the trajectories in North Indian basin are less well captured in some areas, particularly longitudinal movements near the coast from Yemen, Oman and the United Arab Emirates (see maps of adjusted R^2 in Figure 5.B.2).

This statistical definition of cyclone trajectories does not consider changes in track behaviour. For example, observed trends in tropical cyclone translation speed Kossin (2018) and poleward migration of maximum intensity Kossin *et al.*, 2014 could be considered to improve the projections of tropical activity. This indeed has potential implications for tropical cyclone-related risk in some areas where vulnerabilities are high and the present-day frequency of tropical cyclones is low Bruyère *et al.*, 2019.

5.1.4 Thermodynamic description of cyclone intensity

The intensity of cyclones in our model is defined through the following five steps described in detail in subsequent paragraphs. The wind-pressure relationship (WPR) links the central pressure to the maximum 10 minute-sustained wind speed. The local thermodynamic maximum potential intensity (MPI) is determined from local meteorological variables. The maximum pressure drop (MPD) is determined from historically observed pressures. The depression dynamics (DD) along

tracks is defined using an autoregressive stochastic equation. When the cyclone arrives on land, a statistical decay relationship (SDR) dictates the evolution.

Wind-pressure relationships (WPR)

We describe the cyclone intensity through its central pressure P_t^c, which is linked with the maximum wind through an empirical relationship. Let V_t be the maximum 10-min sustained wind speed (in m.s^{-1}) [6] of the cyclone at time t. This maximum wind is observed around 50 km away from the storm center on average [7] and reported in the IBTrACS dataset for historically observed cyclones.

The wind-pressure relationship (WPR) is calibrated separately for each basin and takes the following form:

$$V_t = a\,\left(P_{env}(x_t, y_t, t) - P_t^c\right)^b, \tag{5.3}$$

where $P_{env}(x, y, t)$ is the mean sea-level pressure (MSLP) extracted 500 km away from the eye location at this time in ERA-5 and P_t^c is the central pressure extracted from IBTrACS. This relationship is illustrated in Figure 5.1.5 and the parameters a and b are fitted on ERA-5 and IBTrACS data using nonlinear least squares.

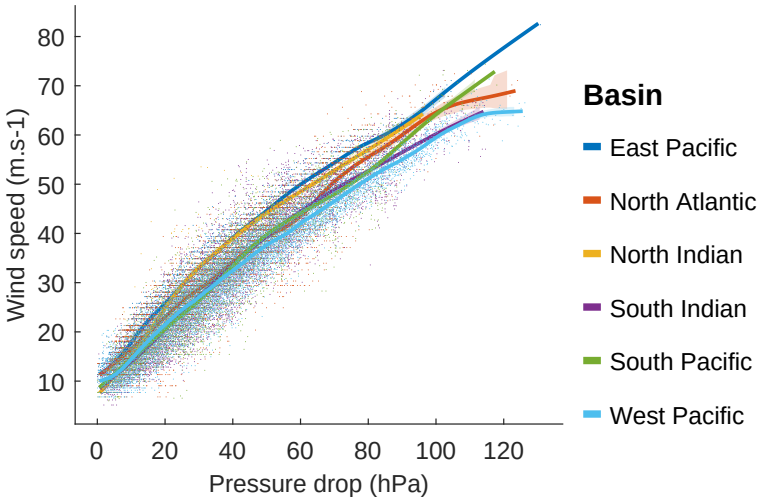

Figure 5.1.5 – Maximum wind and pressure drop values from IBTrACS together with the fit of Equation (5.3). The coefficients a and b fitted per basin are provided in Table 5.C.2.

We acknowledge that most cyclone track data use wind-pressure relations (WPRs) to determine P_c. The conversion back to wind speed from reported P_c using a basin-specific WPR still introduces errors, as different WPRs are used to operationally estimate P_c within each basin (J. Courtney, 2009; J. Courtney & Burton, 2018; J. B. Courtney *et al.*, 2021; Harper, 2002). However, given

6. For the data from the World Meteorological Organisation (WMO) and the agencies reporting 1 or 3-minutes sustained wind speed, we performed the conversion to 10-minutes sustained wind speed using the coefficients suggested by Knapp *et al.*, 2010. See Figure 5.B.1 in the Appendix for more details about the agencies and reporting bias.

7. Radii of maximum wind are also reported in IBTrACS but this information is not central for national level assessment.

the similarity of the relationships, we find that basin-level estimations are a sufficient proxy in the context of this illustration of the CATHERINA framework.

Local thermodynamic maximum potential intensity (MPI)

We compute the local thermodynamic maximum potential intensity (MPI) following the thermodynamic relationships defined in Holland (1997). This is particularly relevant in the context of a national damage assessment under a changing climate. Greenhouse gas emissions not only warm up the oceans but also cool down the lower stratosphere (Butchart *et al.*, 2000; Forster *et al.*, 2007; Ramaswamy *et al.*, 2006). Thus, the tropopause temperature - that is, the temperature corresponding to a pressure of 50 hPa or to an altitude of approximately 20 km available in multi-level CMIP dataset (T_{tropo}) must be included in the modeling of the intensification process. Indeed, the thermodynamic efficiency factor $\mathcal{E}_t$ proportional to the difference between tropopause and sea-surface temperatures plays an essential role in the determination of the central pressure of tropical cyclones. The relative humidity (RH) (which changes with climate change, see Sherwood *et al.* (2010)) is also an influential parameter allowing for a better description of thermodynamic potential enabling cyclone intensification. Adding these two climate variables enables the CATHERINA model to better take into account the additional energy potential due to the widening of temperature differences between the sea-surface and upper troposphere and variation in moist entropy.

Following the seminal formulation in K. A. Emanuel (1988) and integrating additional simplifications proposed in the subsequent paper (K. A. Emanuel, 1991), leads to the following framework summarized in Holland (1997).

$$\text{MPI}_t = \text{MSLP}(x_t, y_t, t) \cdot \exp^{-X_t}, \tag{5.4}$$

$$X_t = \frac{\mathcal{E}_t \cdot \text{SST}(x_t, y_t, t) \cdot \Delta S_t^m - \frac{f(y_t)^2 r_{env}^2}{4}}{R_d \cdot \text{SST}(x_t, y_t, t)}, \tag{5.5}$$

$$\mathcal{E}_t = \frac{\text{SST}(x_t, y_t, t) - T_{\text{tropo}}(x_t, y_t, t)}{\text{SST}(x_t, y_t, t)}, \tag{5.6}$$

$$\Delta S_t^m = R_d \ln\left(\frac{\text{MSLP}(x_t, y_t, t)}{P_{t-1}^c}\right) + \frac{L_v(q_{c\,t}^\star - q_t^{env})}{\text{SST}(x_t, y_t, t)}, \tag{5.7}$$

with moist entropy potential defined along track using specific humidity in the eye vs. at environmental conditions:

$$q_{c\,t}^\star = \frac{3.08}{P_{t-1}^c} \exp\left(\frac{(\text{SST}(x_t, y_t, t) - 273.15)}{\text{SST}(x_t, y_t, t) - 29.65}\right), \tag{5.8}$$

$$q_t^{env} = \frac{3.08 \cdot \text{RH}(x_t, y_t, t)}{\text{MSLP}(x_t, y_t, t)} \times \exp\left(\frac{17.67\,(\text{SST}(x_t, y_t, t) - 273.15)}{\text{SST}(x_t, y_t, t) - 29.65}\right). \tag{5.9}$$

where (x_t, y_t, t) are the coordinates of the eye defined in Equations (5.1) and (5.2), $\text{SST}(x_t, y_t, t)$ and $T_{\text{tropo}}(x_t, y_t, t)$ are respectively the sea-surface and tropopause temperatures, $R_d = 287.058$

$J.kg^{-1}.K^{-1}$ is the specific gas constant for dry air, $\mathrm{MSLP}(x_t, y_t, t)$ is the mean local sea-level pressure, $\mathrm{RH}(x_t, y_t, t)$ is the near surface relative humidity at 2 meters extracted from the monthly dataset of ERA-5 climate reanalysis or CMIP climate models. $f(y_t) = 2\omega \sin(y_t)$ is a Coriolis parameter depending on the latitude, r_{env} is the distance between the eye and the area under regular conditions (fixed at 500 km), q_{env} and q_c^* respectively are the specific humidity at environmental conditions and at saturation, i.e. for RH = 100%, in the eye. ΔS^m is the difference of moist entropy between the environment and the storm center and L_v is the latent heat of vaporization. The distributions of the climate variables and the instrumental indicators computed from ERA-5 climate variables along IBTrACS involved in this step are shown in Figure 5.1.6.

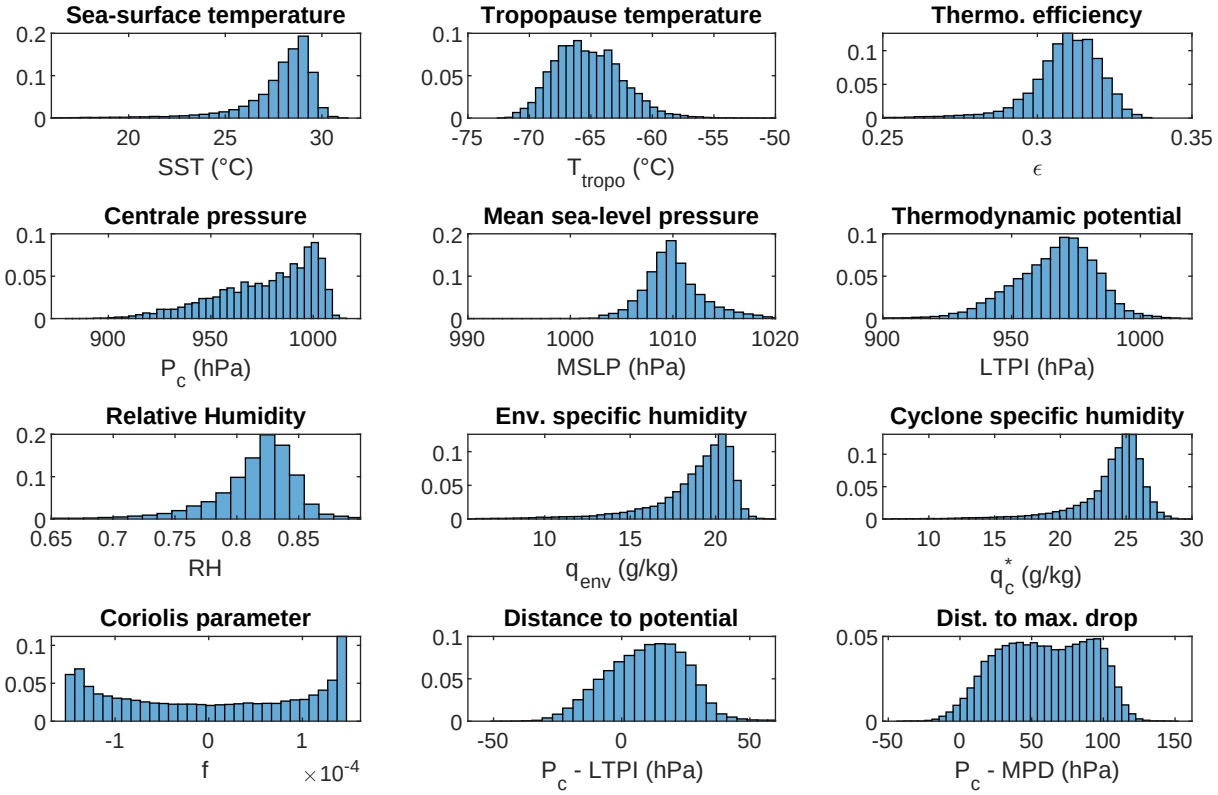

Figure 5.1.6 – Empirical distribution of physical properties along tracks (IBTrACS and ERA-5), and distribution of instrumental variables of CATHERINA

Maximum pressure drop (MPD)

Several papers, including Bloemendaal *et al.* (2020), link the sea-surface temperature directly to the pressure drop, or equivalently the wind speed, via a statistical relationship (DeMaria & Kaplan, 1994). Merrill (1987) suggests that this predictor alone does not provide a good indication of whether a given storm will intensify. However, in line with K. A. Emanuel (1988) and DeMaria and Kaplan (1994) the sea-surface temperature can be used to fix a limit for the pressure drop. Thus in CATHERINA, to prevent the pressure drop from diverging in the projection, we cap it by the maximum observed pressure drop for the corresponding sea-surface temperature:

$$P_t^c := \max(P_t^c, \mathrm{MSLP}(x_t, y_t, t) - \mathrm{MPD}(\mathrm{SST}(x_t, y_t, t))),$$

where the maximum pressure drop function is given by the following equation:

$$\text{MPD}(\text{SST}) = A + B \cdot e^{C(\text{SST}(x_t, y_t, t) - T_0)} \tag{5.10}$$

with $T_0 = 30^{\circ}$C. To fit this functional relationship, we first retrieve, for each basin, and for each value of the sea-surface temperature SST, rounded at 0.1, the maximum observed value of the pressure drop in the basin. These values are shown as crosses in Figure 5.1.7. The coefficients A, B and C from relationship (5.10) are then fitted to these values by nonlinear least squares. The resulting MPD functions for each basin are shown in Figure 5.1.7 as solid lines.

The definition of the MPD is identical in STORM and CATHERINA, but the role of this quantity differs in the two models. Figure 5.1.7 gives a misleading idea about the strength of correlation between the sea-surface temperature and the central pressure: indeed, fitting the distribution on the full sample (instead of just the maximum pressure drop for each temperature value) shows a much weaker influence of sea-surface temperature alone, even on a weekly basis (see Jien *et al.* (2017)). However, this instrumental variable is essential to prevent CATHERINA from producing unrealistically low central pressure. On the other hand, limiting the maximum pressure drop in simulations to the parametric function given by equation (5.10) fitted by non-linear least squares to the observed MPD leads to an excessively strong limitation on the intensity of the simulated cyclones, since many points in Figure 5.1.7 (lower graph) are above the red curve. Therefore, we shift this parametric function upward to the highest observed point to relax this limitation.

Depression dynamics (DD)

The evolution of the central pressure depending on the intensification factor Y_t (which is defined differently in our approach and in STORM, Bloemendaal *et al.*, 2020) is described by the following autoregressive stochastic equation (James & Mason, 2005):

$$\Delta P_t^c = c_0 + c_1 \Delta P_{t-1}^c + c_2 e^{-c_3[P_t^c - Y_t]} + \varepsilon_t^P, \tag{5.11}$$

$$\varepsilon_t^P \sim \mathcal{N}(0, \sigma_{P^c}), \tag{5.12}$$

This relationship channels the effect of global warming, affecting the thermodynamic potential constructed with climate projections, on the cyclone intensity. Thus, the incremental variation of the central depression of the cyclone is linked to the difference between the central pressure at time t and the potential available in the environment.

The intensification module of CATHERINA is inspired by STORM (Bloemendaal *et al.*, 2020). The main differences are the definition of the thermodynamic maximum potential intensity (MPI) used in Equation (5.11) and the role of played by the maximum pressure drop (MPD). In Bloemendaal *et al.* (2020), the MPI is defined subtracting the maximum pressure drop (MPD) from the normal environmental pressure (MSLP) where the MPD is defined as a function of the SST and Bister and Emanuel, 2002 values are used to bound their values. On the other hand, we define the thermodynamic intensification factor following Holland, 1997 with variables extracted along the synthetic tracks and use the SST-MPD relationship as a capping function (see Figure 5.1.7). Table 5.C.3 summarizes the main differences of the two approaches.

As illustrated in Figure 5.1.8, both methods produce a similar dependence of the intensitication function (5.11) on the distance to potential and maximum pressure drop. When P_c approaches the

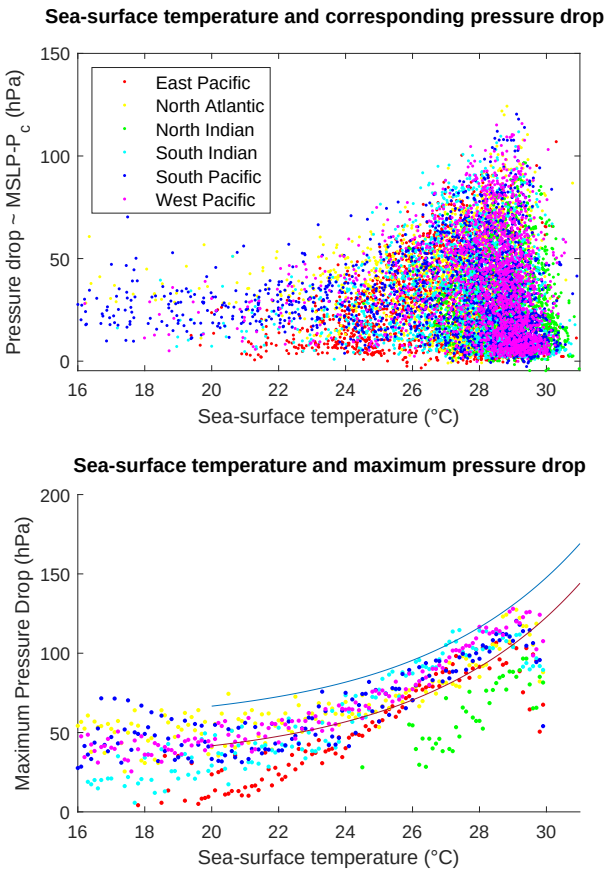

Figure 5.1.7 – Top: full distribution of observed pressure drop values for given SST. Bottom: maximum observed pressure drop values for given SST. The red line shows the least squares fit of Equation (5.10), which corresponds to parameter values $A = 30.6$, $B = 86.3$ and $C = 0.19$. The blue curve is the capping function used to prevent unrealistic pressure drops, obtained by shifting the red curve upwards.

local maximum potential intensity (or maximum pressure drop), ΔP^c is more likely to be positive and to decrease the storm intensity. In other words, we can distinguish two phases (see Figure 5.1.8, left graph): the intensification phase (in blue), when the central pressure is above the local MPI threshold, and a decay phase (in red) where the central pressure is below this local MPI.

In contrast to the MPD, the MPI does not represent the maximum achievable pressure and can be exceeded when accounting for additional external factors not reflected in climate data. For example, Y. Chen *et al.* (2021) suggest that rapid intensification also depends on dynamical factors (e.g. upper divergence and wind shear). While James and Mason (2005) formulation implicitly assumes that these factors are accounted for in the residual term of Equation (5.12), it does not consider that the distance to the maximum potential thus defined, can take negative values. Indeed, this specification originally suggests using the maximum achievable central pressure, therefore that $P_c - \text{MPI} > 0$. As a result, the two intensification factors are not defined on the same domain (see Figure 5.1.6). Using the local thermodynamic MPI, negative values, corresponding to a situation where the central pressure is below the MPI ($P_c < \text{MPI}$), are associated with a positive response of the pressure dynamic module, and an decrease in storm intensity. Using the MPD, the

response (is likely to) become positive when distance to MPD is below 40 to 60 hPa, depending on whether the function has been applied to the local sea-surface temperature or the maximum per grid box ($5° \times 5°$×month). Given the similar response provided, using the local MPI instead of MPD as the intensification factor offers a better theoretical representation of the conditions affecting cyclone intensification in the cyclone dynamic module. The central pressure dynamics used for the fitting and the dynamics of the synthetic tracks produced in the north Atlantic basin are illustrated in Figure 5.1.9. The intensification of synthetic cyclones is in line with historical observations.

Statistical decay relationship (SDR) over land

We model the evolution of the cyclone after landfall using an exponential decay function considering that tropical cyclone intensity decreases as a function of the time and distance the tropical cyclone has covered whilst being over land (Kaplan & DeMaria, 1995). Similarly to Bloemendaal *et al.* (2020), after three steps on land we suppose that the wind at time t_L follows:

$$\begin{aligned} V_{t_L} &= V_b + (R \cdot V_0 - V_b)e^{-\alpha t_L} - f_1(t_L)\left(\ln\frac{D^l}{D_0}\right) + f_2(t_L) \\ &= V(t_L, D^l, V_0). \end{aligned} \tag{5.13}$$

where D^l is the distance to coast computed using natural earth coastlines,[8] V_0 is the wind at landfall and t_L the time spent on land by the eye. This function was fitted on IBTrACS using nonlinear least squares. In our procedure, we use the global parameters: $R = 0.79$, $V_b = 15$ m.s^{-1}, $\alpha = 0.044$ h^{-1}, and $f_1(t_L) = \tilde{c}_1 t_L(t_{0,L} - t_L)$, $\tilde{c}_1 = 3.35.10^{-4}$ ms^{-1}h^{-2} , $t_{0,L} = 172$ h, $f_2(t_L) = d_1 t_L(t_{0,L} - t_L)$, $d_1 = -0.00186$ ms^{-1}h^{-2} and $D_0 = 1$ km. Kaplan and DeMaria (1995) introduced this function to model the decay of tropical cyclones over land in a simple way and showed that it provides an acceptable approximation for $t_L \geqslant 12$ h. As each time step is 3 hours, we let the TC intensity be driven by Eq. (5.11) the first three steps and apply the decay function after three steps, that is, for $t_L \geqslant 12$ h. A more sophisticated description could integrate for instance, cyclone physics, kinetic energy, and non-meteorological parameters such as ground topology. The SDR puts a strong constraint on the cyclone evolution after three steps. However, in the context of national damage assessment we reiterate that reported damage costs are the combination of a series of various impacts including storm surge and not only extreme wind and that the most exposed area is at landfall. We consider therefore that the hypothesis of a rapid decay is acceptable and in line with observations.

5.1.5 Cyclone generation algorithm

The full cyclone generation procedure is presented in Algorithm 1. The cyclone wind speed is initiated at 20 m.s^{-1} and the initial pressure is determined from the WPR (Equation (5.3)). While the cyclone is over sea, the pressure evolution ΔP_c is entirely determined from Equation (5.11) based on the local thermodynamic potential. To prevent the model from producing unrealistically low central pressure, we cap the maximum pressure drop (MPD) using Equation (5.10). With

8. Available at https://www.naturalearthdata.com/downloads/10m-physical-vectors/.

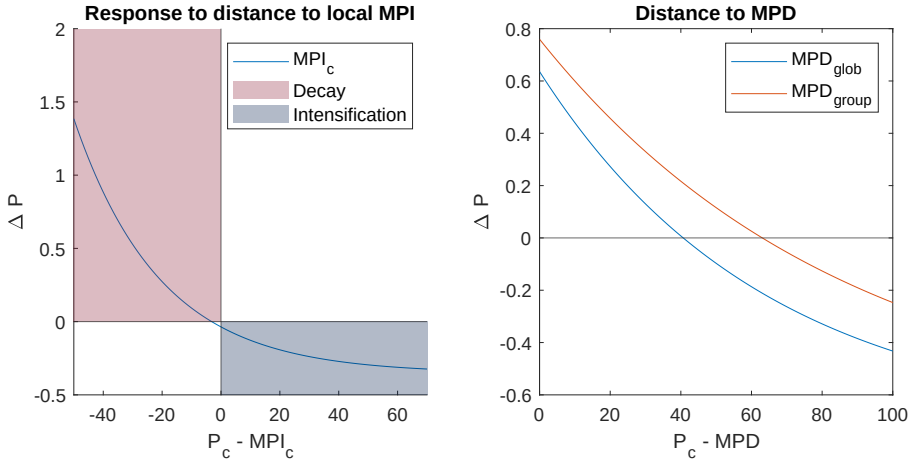

Figure 5.1.8 – Response of the depression dynamics model to distance to thermodynamic potentials over intensification factor domains

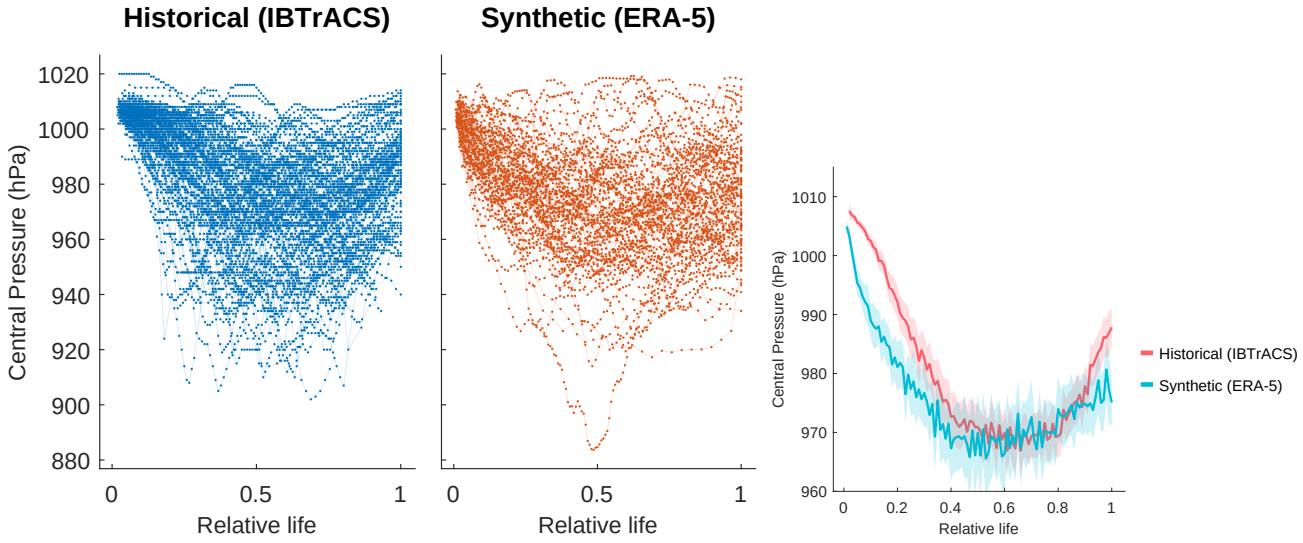

Figure 5.1.9 – Individual historical vs. Synthetic depression dynamics in North Atlantic Basin, and confidence interval.

this truncation the lower bound for the pressure is given by the observed low pressure values in similar sea-surface temperature conditions. While the cyclone is over sea, the wind is defined with the WPR (Equation (5.3)). When the cyclone arrives on land the MPI is computed from the last known climate variables for the first three steps and the pressure still follows the relationship (5.11). After three steps (9h) on land, we start applying the decay relationship (Equation (5.13)) to define the wind. The variations of longitude and latitude are always defined using Equation (5.1) and Equation (5.2). We force cyclones to remain in their genesis basins in this exercise. For example, running the algorithm on IPSL climate projections between 2075 and 2100, in the RCP85 produces the output plotted in Figure 5.1.10.

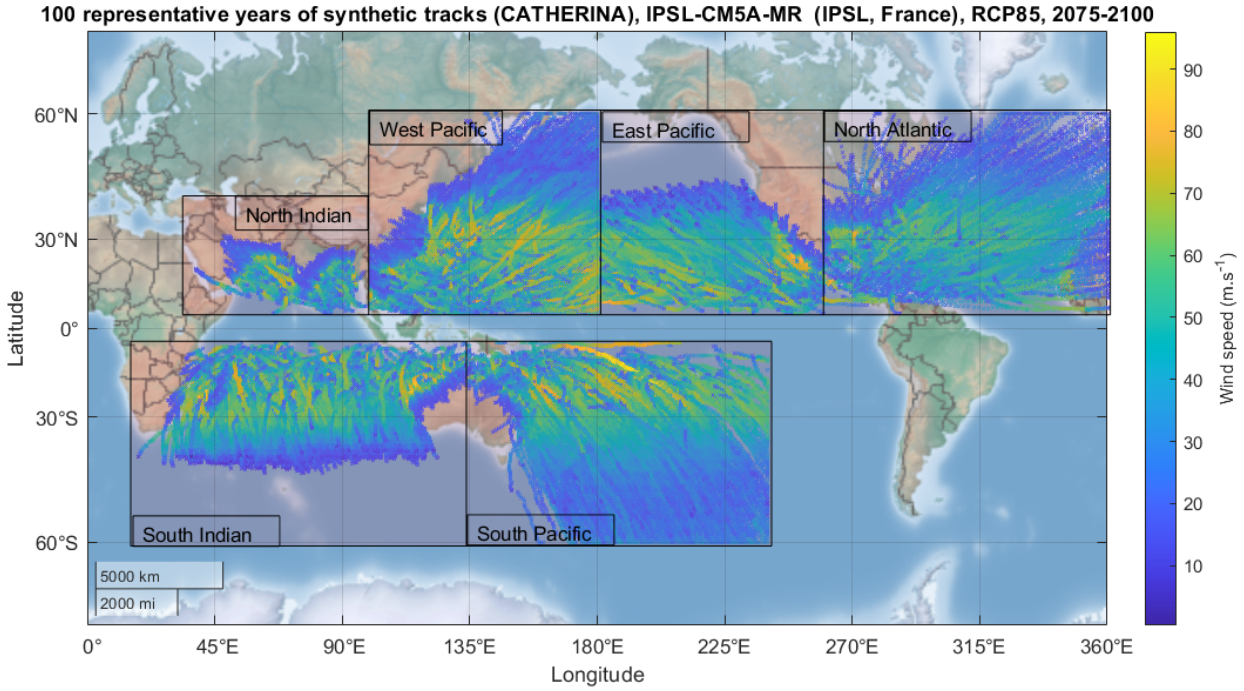

Figure 5.1.10 – Example of 100 representative years of synthetic tracks produced with CATHERINA on IPSL-CM5A-MR raw climate data in the RCP85 between 2075-2100 (i.e. four runs over the 25 years period)

The cyclone intensification process used is inspired by STORM model form Bloemendaal *et al.*, 2020, which includes a single climate variable, and extended following Holland, 1997 and K. A. Emanuel, 1988 to encompass 2 more variables. We found that this extension provides statistically significant instrumental variables in the description of tropical cyclone intensification, which is the aim of the algorithm. Consequently, even if some thermodynamic processes have been simplified in our approach, it is still a step forward with respect to the existing state-of-the-art in the field of integrated assessment modeling for climate impact analysis. Indeed, our approach is easy to implement, more sophisticated in terms of processes included than most existing IAM, has low bias due to our state of the art bias correction module described below, and can integrate any CMIP simulation with a limited set of available variables (only a few vertical levels, some only available at monthly time scale, with some variables not always available).

Algorithm 1: Cyclone Track Generator

Result: Definition of each cyclone trajectory and properties

$$
\begin{aligned}
V(s=0) &= 20 \text{ m/s} \\
\text{MSLP} - P_c(s=0) &= \left(\frac{V}{a}\right)^{1/b} \propto \text{Equation (5.3)} \\
&\sim 25 \text{ hPa} \\
P_c(s=0) &\sim 990 \text{ hPa}
\end{aligned}
$$

while $\text{MSLP} - P_c > 0$ *&* $V > v_m$ **do**

Extract $D(s)$ from naturalearth coastlines;

$$
\begin{aligned}
x(s) &= x(s-1) + \Delta x(s) + \mathcal{N}(\mu_{x,B}, \sigma_{x,B}) \\
\text{where} \quad & \Delta x(s) \propto \text{Equation (5.1)} \\
y(s) &= y(s-1) + \Delta y(s) + \mathcal{N}(\mu_{y,B}, \sigma_{y,B}) \\
\text{where} \quad & \Delta y_t \propto \text{Equation (5.2)} \\
\text{MPI}(s) &= \text{f}_{\text{MPI}}\left(y(s), P_c(s-1), \text{SST}(s), T_{tropo}(s), \text{MSLP}(s), \text{RH}(s)\right) \\
& \text{f}_{\text{MPI}} \propto \text{Equation (5.4)} \\
P_c(s) &= \max(P_c(s) + \Delta P_c(s), \text{MSLP}(s) - \text{MPD}(s)) \\
& \text{MPD} \propto \text{Equation (5.10) \&} \\
& \Delta P_c(s) \propto \text{Equation (5.11)} \\
V(s) &= a\left(\text{MSLP} - P_c(s)\right)^b
\end{aligned}
$$

if *on land* = TRUE **then**

$s_l = s_l + 1$

end

if $s_l > 4$ **then**

Compute distance to land $D(s)$ from naturalearth coastlines;

$$
\begin{aligned}
V(s) &= V_b + (R \cdot V_0 - V_b)e^{-\alpha s_l} - m(t_L)\left(\ln\frac{D}{D_0}\right) + b(t_L) \\
& V(s) \propto \text{Equation (5.13)}
\end{aligned}
$$

end

end

Note: This algorithm assumes step-wise extraction of climate data in the Monte-Carlo process. Another way, closer to the framework suggested in Bloemendaal *et al.* (2020) would be to (i) compute the tracks without properties, (ii) retrieve all climate variables, (iii) determine the properties using the extracted climate conditions in the last step.

5.2 Exposure in the shared-socioeconomic pathways

5.2.1 Physical asset exposure

Eberenz *et al.* (2019) present a methodology to downscale physical asset values on a high-resolution grid using a combination of nightlight intensity, population data, and global country indicators and make their dataset fully available (Eberenz *et al.*, 2020). These estimates of physical asset value are based on the light intensity L_i – from Nighttime lights of the Black Marble 2016 annual composite of the VIIRS day–night band (DNB) (Román *et al.*, 2018) in 2016 at the 15 arc-second resolution – and the population P_{pix} per pixel – from Gridded Population of the World (GPW) database (Center for International Earth Science Information Network (CIESIN), 2017) in 2015 at the 30 arc-sec resolution for 224 countries, and various additional sources [9] allowing to define the total asset (A_{tot}) for each country. This value is distributed to each grid cell proportionally to the light intensity L_i times the local population P_{pix}: [10]

$$A_{pix} = A_{tot} \frac{L_i \cdot P_{pix}}{\sum_{pix_i}^{N} (L_i \cdot P_{pix_i})}. \tag{5.14}$$

The physical asset value is expressed in USD as of 2014. Using this dataset in the future requires correcting (either simulated or reported damages) by inflation using, for instance, the consumer price index. [11]

This method for allocation of national assets has limitations. For example, the distribution of assets near the coast, industrial production sites or agricultural facilities may not be well represented. However, with this approach asset values are defined on a uniform grid across countries and can be projected by multiplication with appropriate dynamic factors.

5.2.2 The Shared Socioeconomic Pathways (SSPs) framework

Future exposure is sensitive to the scenarios of population growth and economic development. To take this into account, we use the framework of the shared socioeconomic pathways (SSP) introduced in O'Neill *et al.* (2014). These narratives are used in the IPCC development scenarios and provide a reference framework for risk assessment. A growing segment of the literature is dedicated to measuring the feasibility, costs and implications of achieving these scenarios (Riahi *et al.*, 2021; Riahi *et al.*, 2017) and multiple Integrated Assessment Models (IAMs) were launched on assumptions based on these narratives (Gidden *et al.*, 2019; Riahi *et al.*, 2017; Rogelj *et al.*, 2018). [12] Figure 5.2.1 displays the projections of the main features used by CATHERINA, the

9. Produced Capital, comprehensive global estimate of produced capital stock, i.e. the value of produced or manufactured assets per country (World Bank, 2018) – 2014 / 140 countries; the GDP to wealth ratio from Global Wealth Report (Credit Suisse, 2017) – 2017 / 84 countries; the gross domestic product (GDP) per country from World Bank Open Data portal (World Bank, 2019b) – 2014 / 224 countries and Subnational equivalent of GDP (GRP) from varying sources – 2012-2017 / 504 regions in 14 countries.

10. The values of A_{pix} on a 30 arc-second grid are available at https://www.research-collection.ethz.ch/handle/20.500.11850/331316.

11. Available at: https://fred.stlouisfed.org.

12. For example, for the variable of interest, the outputs of IIASA GDP, IIASA-WiC POP, NCAR, PIK GDP-32, OECD Env-Growth models are available.

global domestic production (GDP) and population in the five SSPs at the global level by the IIASA GDP model. [13] CATHERINA uses these two indicators at regional level (32 regions are available) to compute future local exposure (see section 5.2.3).

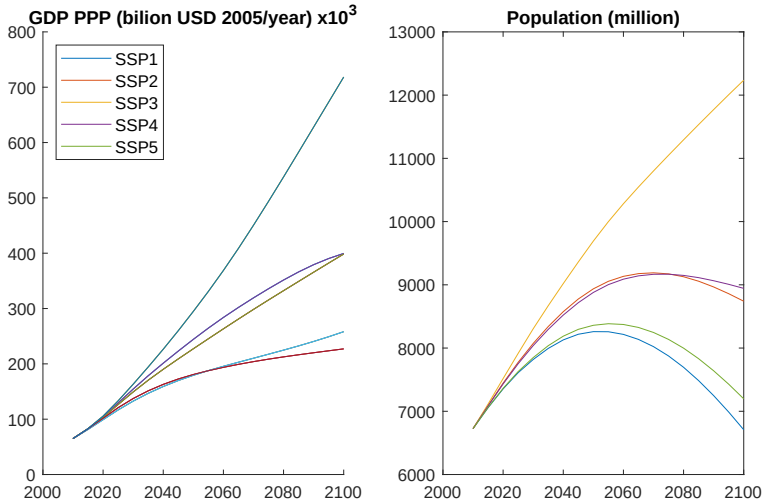

Figure 5.2.1 – SSP GDP and Population variation until 2100, at global scale, by the IIASA GDP model

We reiterate the main features underlying these narratives. The '*middle road*' pathway (SSP2) is used as the reference in most scenario analyses. It is a plausible baseline in terms of economic and social resiliency, in which the urbanization level is relatively high and GDP and population are constantly increasing following the observed historical trend. On the other hand, the '*rocky road*' or '*national-rivalry*' pathway (SSP3) presents totally different properties: relative stagnation of GDP with a strong increase of the population (See Figure 5.2.1). SSP4 corresponds to a scenario with the highest inequality and SSP5 is the most likely to lead to the higher concentration pathways (RCP8.5), with extensive use of fossil fuel reserves but higher economic development and global markets integration.

Based on these storylines, it is clear that the physical exposure to tropical cyclones will be driven by different factors in different SSP scenarios. Scenarios with steady growth of GDP are generally associated with an increase in urbanisation but a decrease in the global population by 2050. In general, all narratives, except the SSP3, present relatively similar population dynamics at the global level. On the other hand, the scenario with the lowest economic growth (SSP3) presents a sustained increase of the global population (cf. Figure 5.2.1), in particular in rural areas. We can therefore expect, in the former case, the physical asset value exposure to be driven by the increase of regional wealth, and mainly by the growth of the exposed population in the latter.

In this paper, we specify economic and climate parameters independently while the literature generally associates specific SSP and RCP, in particular in the CMIP6 exercise. Indeed, integrated assessment modeling demonstrates that specific temperature targets can only be reached under some socioeconomic conditions. The socioeconomic and representative concentration pathways

13. Variables relative to SSPs are available here: https://tntcat.iiasa.ac.at/SspDb/.

are therefore intrinsically linked at the global scale. For example, CMIP6 refers to the following scenarios: SSP1-1.9, SSP1-2.6, SSP2-4.5, SSP3-7.0, and SSP5-8.5. On the other hand, this pairing is not straightforward at the regional level. In particular, the SSP2 scenario is associated with regional heterogeneity in socioeconomic pathways. As a result, although we can expect a convergence in the long run, we considered it relevant to use economic development scenarios independently from RCP in this exercise. When looking at the aggregated level however, we consider only scenarios that are feasible (Rogelj *et al.*, 2018). For instance, the RCP85 exists only in the conditions of the SSP5.

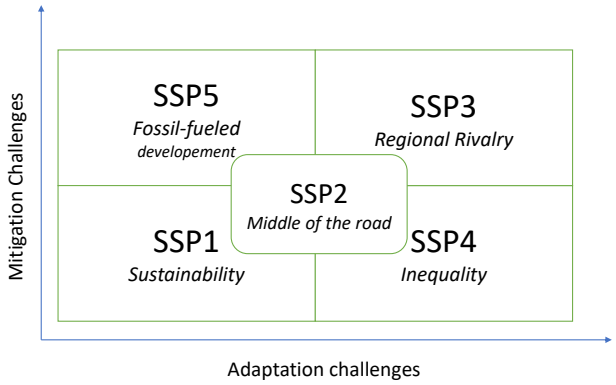

Figure 5.2.2 – SSP Matrix O'Neill *et al.* (2017) (based on O'Neill *et al.*, 2014 Figure 1, inspired by Kriegler *et al.*, 2012 Figure 3.)

Lastly, we acknowledge another limitation of our approach: The vulnerability parameter (represented by the damage function parameter v_h in our framework) does not depend on the SSP, while we could expect a reduction in the vulnerability parameter in the scenarios where the adaptation challenges are limited, such as SSP5 (cf. Figure 5.2.2). This question is left for further research.

5.2.3 Dynamic projection of local exposure in SSPs

To estimate future exposures along the cyclone tracks in each scenario, we use the downscaled estimation for the exposed wealth (Eberenz *et al.*, 2020) and the coefficients representing the change between the current state and the future scenario in the framework of the shared socioeconmic pathways (Jones & O'Neill, 2020; O'Neill *et al.*, 2017; O'Neill *et al.*, 2014). The local physical exposure at the coordinates (x, y) at time t in a region j in scenario k is defined as follows:

$$\Phi(x,y,j,k,t) = \underbrace{(F^{cap}_{\text{GDP}}(j,k,t))^{\alpha_1}}_{\text{Global macro factor}} \cdot \underbrace{(F_{pop}(x,y,k,t))^{\alpha_2} \cdot \mathcal{L}_P(x,y)}_{\text{Local factor}}. \tag{5.15}$$

where $\mathcal{L}_P(x,y)$ is the local population density from Eberenz *et al.* (2020), the factor F^{cap}_{GDP} is the projected GDP per capita growth for each region:

$$F^{cap}_{\text{GDP}}(j,k,t) = \frac{\text{GDP}(j,k,t)/\text{GDP}(j,t=2020)}{P(j,k,t)/P(j,t=2020)} \tag{5.16}$$

where P is the total population of the region retrieved from SSP database (Riahi *et al.*, 2017), [14] and F_{pop} is the population exposure growth factor:

$$F_{pop}(x, y, k, t) = \frac{p(x, y, k, t)}{p(x, y, t = 2020)} \tag{5.17}$$

where $p(x, y, k, t)$ represents the local projections of population (Jones & O'Neill, 2020) illustrated in Figure 5.2.4. Figure 5.2.3 displays the scenario-based projections of GDP and population in the five SSP, at the regional level by the IIASA model.

We introduce the exponents α_1 and α_2 to disentangle the effects of increased cyclone intensity, GDP growth and population growth on the future damages, as well as to account in a simple manner for possible future adaptation to tropical cyclone risk. Indeed, taking $\alpha_1 = \alpha_2 = 1$ amounts to assuming that damages from cyclones of similar intensity grow proportionally to local GDP, whereas newly accumulated wealth can be more resilient then the existing one and protected by additional adaptation measures. Indeed, Bakkensen and Mendelsohn, 2019 test for evidence of adaptation in past cyclone damages data and find that α_1 is statistically different from 1 in all countries except the USA. At the global level, they estimate α_1 to be equal to 0.364, with a standard error of 0.175, which is significant at the 95% confidence level.

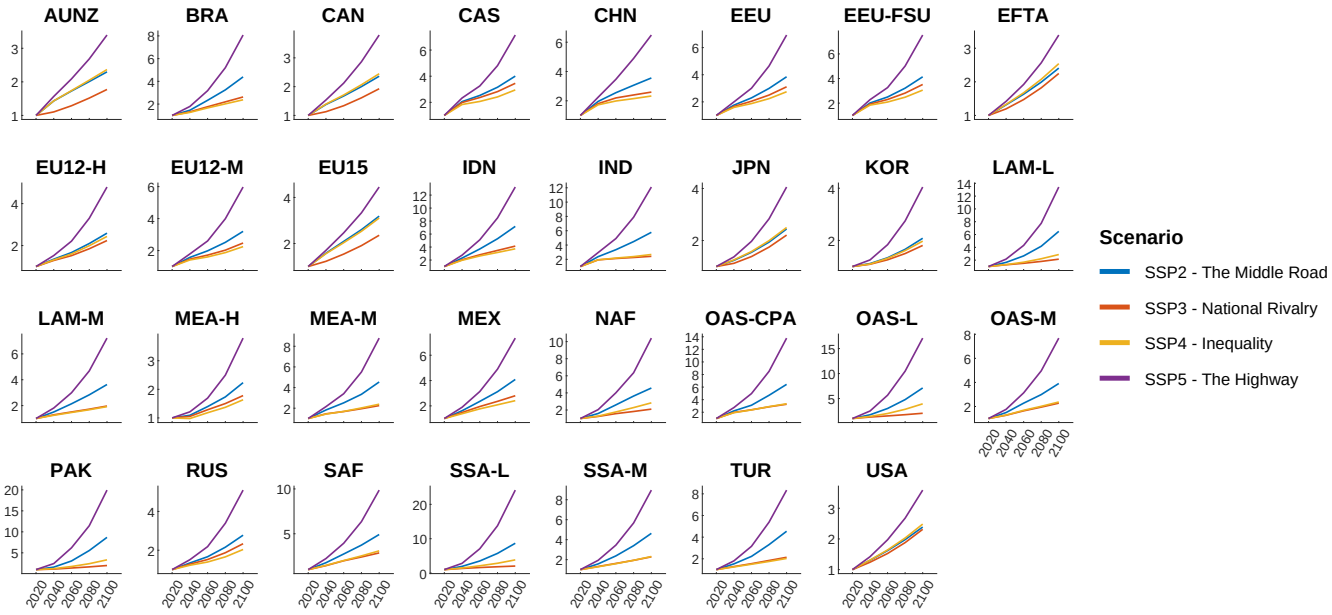

Figure 5.2.3 – Regional F^{cap}_{GDP} factor variation in SSPs IIASA database (R32). Source : https://tntcat.iiasa.ac.at/SspDb/. The country mapping is provided in Table 5.C.5.

14. https://tntcat.iiasa.ac.at/SspDb/.

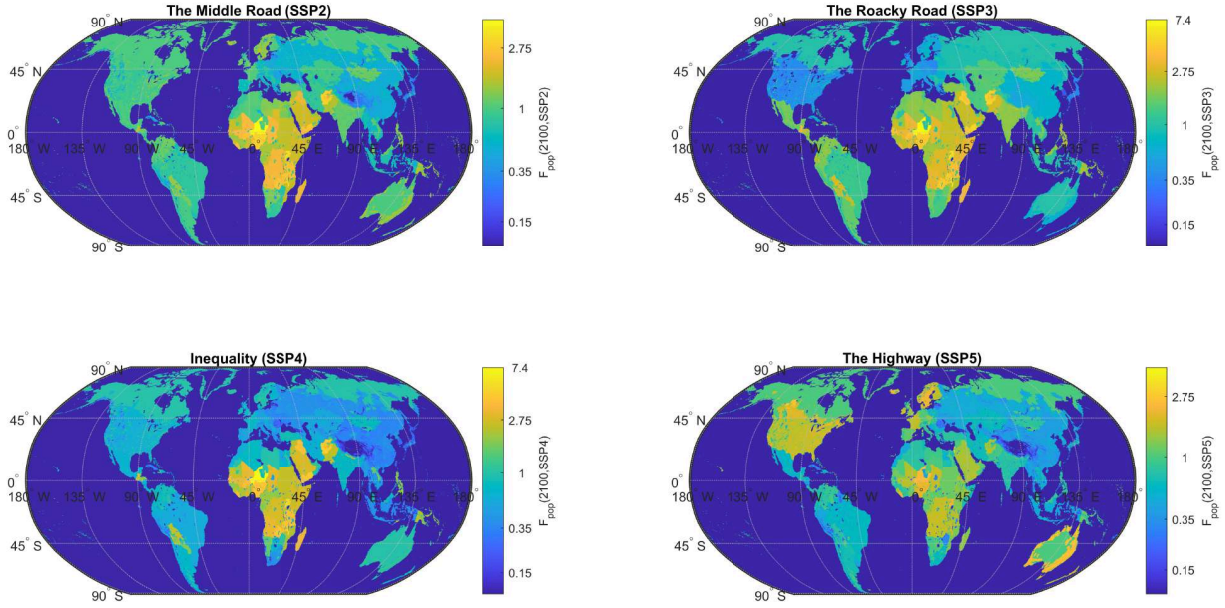

Figure 5.2.4 – Local F_{pop} factor variation in all SSPs in 20100 (source: Jones and O'Neill (2020), NASA Socio-Economic Data Application Center (SEDAC)). The scenario-based population grid generation methodology is detailed by Jones and O'Neill (2020) with a last version downscaled at 1 km following Gao (2020). This population grid is available every 10 years. CATHERINA uses the closest value in the definition of the exposure.

5.3 Damage assessment at the national level

Input data: Global disaster database (EM-DAT) The fitting of the damage functions was performed by Eberenz *et al.*, 2021 on reported damages in the EM-DAT database (Guha-Sapir *et al.*, 2018).[15] Filtering the database by sub-type 'tropial cyclone' allows us to extract 1 855 tropical cyclones in the period between 1980 and 2021, among which 1 101 events have a reported total damage cost in USD (See Figure 5.3.2). In terms of damage, tropical cyclones are, using the full set of observations from 1980 to 2021, the most damaging events reported (see Figure 5.3.1). This database includes a start date field (day, month and year) allowing us to map 455 events, with the events reported in IBTrACS using start year and month and country.[16] We use this database to validate our simplified estimation process.

15. Available at: www.emdat.be.
16. Eberenz *et al.* (2021) functions are fitted on a similar sample of 376 tropical cyclones used for calibration.

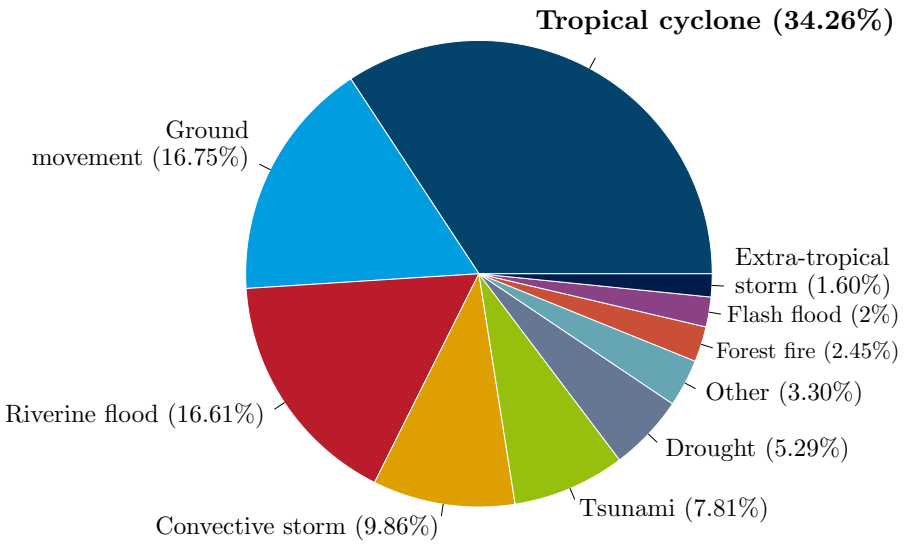

Figure 5.3.1 – Proportion of damage cost (total damage in USD) by disaster subtypes reported in EM-DAT. Using the number of people affected places tropical cyclones after riverine floods and droughts, and the number of deaths places ground movements in first position (see Table 5.C.1 for details).

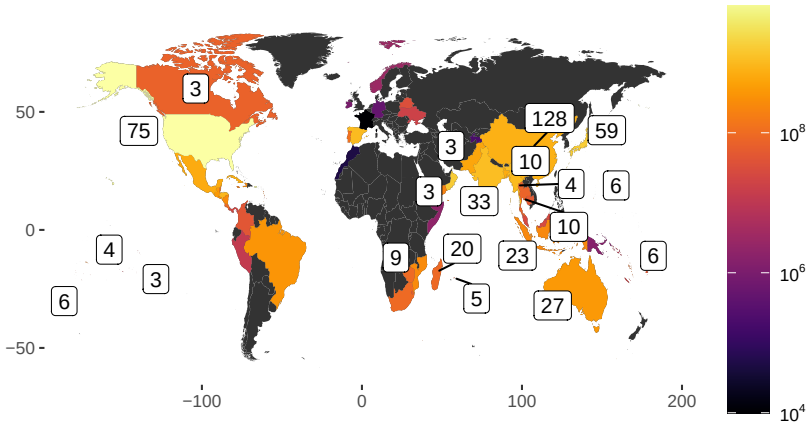

Figure 5.3.2 – Number of tropical cyclones with reported damage cost in EM-DAT database. The color scale indicates the average reported damage cost in USD in each country for each tropical cyclone.

5.3.1 Damage modeling

The percentage of asset value destroyed by a tropical cyclone depends on multiple parameters. For example, to assess the vulnerability of specific infrastructures to tropical cyclones, precise descriptions of building vulnerability are provided in the Federal Emergency Management Agency (FEMA) reports. Unanwa *et al.* (2000) propose a series of wind-damage bands depending on building types. The sensitivity is higher for commercial and institutional buildings than for residential and mid-rise buildings. Unanwa *et al.* (2000) reveals that generalized damages occur above 43-60 $m.s^{-1}$. A sustained wind regime above 73 $m.s^{-1}$ could lead to the destruction of the entire superstructure of most buildings (expect for mid- and low-rise ones). Damages provoked by winds between 60 and 81 $m.s^{-1}$ strongly depend on building components and connections. These bottom-up approaches allow us to set the limits of the potential damage functions, but their use requires a complete inventory of assets and up-to-date values of numerous parameters (age, height, materials, etc.). Therefore, CATHERINA relies on regional damage functions calibrated by Eberenz *et al.* (2021) on wind speed along cyclone track (IBTrACS) and reported damages in Guha-Sapir *et al.* (2018).

Damages provoked by tropical cyclones can be related to several sub-perils. While 40% of cyclone damages are directly wind-related, another 40% can generally be attributed to storm surge, and the rest of the damage is generated by heavy precipitation. However, CATHERINA does not distinguish these sub-perils, associated with key thermodynamical processes of cyclones (heavy precipitation, storm surge and associated flooding, strong winds) but uses a statistical relationship to estimate the regional global damage induced by a cyclone from a proxy variable given by the maximum wind speed. Indeed, the wind speed is the proxy used in the Saffir-Simpson Hurricane wind scale to define the intensity of a cyclone. The damage function is fitted on multiple events from the total damage reported in the global disaster database EM-DAT (Guha-Sapir *et al.*, 2018). This database, used in most studies on the topic, accounts for the total reported damage (sum of all sub-perils) and does not distinguish damages from sub-perils.

5.3.2 From an explicit damage function...

Damage functions can take several different forms (Prahl *et al.*, 2015) but the most common choice is a cubic functional of the wind speed. To estimate the fraction of loss from a storm with sustained wind speed V, K. A. Emanuel (2011) introduced the following formula:

$$f(V, v_h^j) = \frac{\left(\max(V - v_0, 0)\right)^3}{(v_h^j - v_0)^3 + \left(\max(V - v_0, 0)\right)^3}, \tag{5.18}$$

where f is the fraction of the property value lost, $v_0 = 25.7$ $m.s^{-1}$ and v_h^j a parameter that needs to be calibrated for each region j. Figure 5.3.3 illustrates the shape of the damage function for different values of this parameter.

To account for adaptation we could modify this function and introduce an additional threshold value. For instance, to account for local adaptation to the wind climate, Leckebusch *et al.* (2007) suggest to scale the wind value by the 98th percentile of the local wind speed distribution. However, the assumption that adaptation will always keep the damages from the 98-percentile wind at the same level is probably optimistic, and will prevent us from using the model to estimate the required investment to balance future damages and economic shocks.

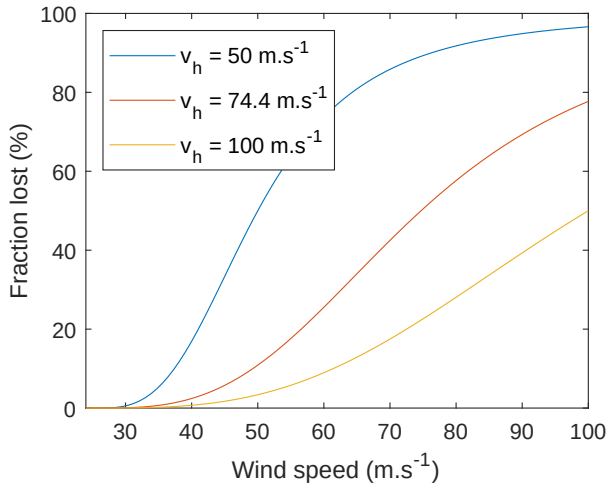

Figure 5.3.3 – Fraction of property value lost as a function of wind speed, obtained using Equation (5.18) with different values of v_h. Source: K. A. Emanuel (2011).

5.3.3 ... to a regional damage calibration

Using the reported damage estimates from the International Disaster Database (EM-DAT) crossed with cyclone tracks (IBTrACS), and geographical and socio-economic information along these tracks, Lüthi (2019) refined the damage function approach using machine learning techniques introducing region-specific damage functions.

We recall the main steps of the methodology presented in Eberenz *et al.* (2021) to define the regional damage functions. The authors first defined the event damage ratio (EDR) as a ratio of simulated damage (SED) to normalized reported damage (NRD) for each cyclone:

$$\mathrm{EDR}(i,j) = \frac{\mathrm{SED}(i, v_h(j))}{\mathrm{NRD}(i)}. \tag{5.19}$$

The total damage ratio (TDR) is then defined in each region summing over events:

$$\mathrm{TDR}(j) = \frac{\sum_i \mathrm{SED}(i, v_h(j))}{\sum_i \mathrm{NRD}(i)}. \tag{5.20}$$

For each event, there is a value for v_h allowing to optimally calibrate the explicit damage function given in Equation (5.18). The relatively wide distribution of v_h for the same country shows that there is a large uncertainty in the relationship between the wind speed and the corresponding fraction of losses. Figure 5.B.4 shows the uncertainty in regional damage functions depending on the optimization technique used and Figure 5.B.5 allows us to appreciate, for countries where more than 5 cyclones were reported, the spread of plausible damage functions.

Eberenz *et al.* (2021) propose two alternative optimization methodologies to find the value of $v_h^\star$ maximizing the prediction quality of the regional damages: root mean square fraction (RMSF), minimizing the spread of the event damage ratios (EDR):

$$v_{h\mathrm{RMSF}}^\star(j) = \mathrm{argmin}_j \exp\left(\sqrt{\frac{1}{N}\sum\left(\ln(\mathrm{EDR(i)})\right)^2}\right), \tag{5.21}$$

and total damage ratio (TDR), finding the value of $v_h^\star$, such that the ratio of total simulated damage – obtained summing over event damages – and total reported damage tends to 1.

$$v_{h^{\star}_{\mathrm{TDR}}}(j) = \mathrm{argmin}_j \, |\mathrm{TDR}(j) - 1| \tag{5.22}$$

The values of $v_h^\star$ obtained by Eberenz *et al.* (2021) with the two methods are given in Table 5.3.1. For most regions, the optimized curves are similar for the two optimization techniques, but the results diverge for the Philippines (WP2) and to a lesser extent for China Mainland (WP3) events. The case of the Philippines, for example, discussed in Eberenz *et al.* (2021), is explained by the large number of parameters involved in the damage estimation, and emphasizes two main limitations of the model: First, this framework lacks an explicit representation of sub-perils that disrupt and damage several sectors and services. Second, differences in exposure and vulnerability between urban and rural areas exposed to tropical cyclones are likely to contribute to the large spread in EDR.

5.3.4 Simplified damage estimation along tracks

In the context of our national level assessment, we propose a simplified damage module. The simulated damage for a given cyclone – in both IBTrACS and our synthetic tracks – is computed using the following procedure for each individual cyclone. First, a uniform grid of physical asset value with step given by the average cyclone radius is defined on the map of affected area. The cyclone track is linearly interpolated, and the tiles affected by the cyclone (containing a part of the interpolated path) are identified (see Figure 5.3.4). Second, for each tile identified in the

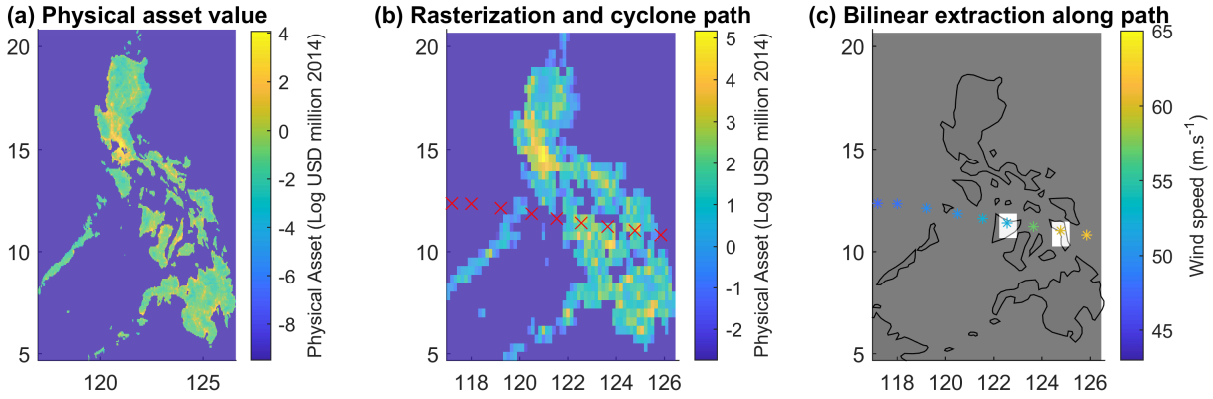

Figure 5.3.4 – Illustration of the high resolution asset data (a) original physical asset value resolution; (b) aggregation of asset value over 0.25° boxes to evaluate asset exposure along interpolated cyclone track (here corresponding to the 2013 Hayan cyclone); (c) Illustration of damage calculation: damage is aggregated over the white boxes which correspond to cyclone locations over land.

previous step, we retrieve the maximum wind speed V, and compute the proportion of wealth lost $f(V, v_h^j)$ using the relation (5.18) with the total damage ratio parameter given in Eberenz *et al.* (2021). Then, we compute the total simulated damage by aggregating the physical asset exposure multiplied by the proportion of wealth lost on each tile over all tiles affected by the cyclone.

Table 5.3.1 – Values of v_h obtained using TDR and RMSF methods for each region from the CLIMADA environment

Region	$v_{h\,\mathrm{TDR}}^{\star}$	$v_{h\,\mathrm{RMSF}}^{\star}$
Caribbean and Mexico (NA1)	58.8	59.6
China Mainland (WP3)	101.5	80.2
USA and Canada (NA2)	80.5	86
North Indian (NI)	63.7	58.7
South East Asia (WP1)	60.7	56.7
North West Pacific (WP4)	169.6	135.6
Philippines (WP2)	167.5	84.7
Oceania (OC)	56.8	49.7
South Indian (SI)	48.5	46.8
Global (GLB)	98.9	73.4

Coefficient from version 1.5 of the CLIMADA environment. Figure 5.B.4 also illustrates the shapes of the functions for the different optimization problems (RMSF vs. TDR) and version (1.0 vs 1.5).

As a result of this procedure, we obtain the total simulated damage $\mathrm{SED}_i(j,t)$ caused by the i-th cyclone in region j, simulated with climate variables for year t. Finally, the cyclone damage cost in region j and year t is simulated as follows:

$$\mathcal{D}(j,t) = \sum_i \mathrm{SED}_i(j,t), \tag{5.23}$$

where the sum is taken over all cyclones occurring in a given year. This procedure can then be repeated many times to obtain the distribution of annual cyclone damages and compute other statistics such as the mean and quantiles of this distribution.

The damage functions used in the second step are retrieved directly from the CLIMADA environment. These functions were fitted with the same physical asset value. However, in our case, we project these values on a coarser grid (first step), in such a way that the extraction is simplified for a large number of synthetic tracks in the context of the present global exercise. To ensure that the estimated damages produced with this simplification are consistent with the historical records, we computed simulated damages over the historical tracks and compared the results to EM-DAT. We aggregate asset values on 0.25 x 0.25 grid. The spread between SED and NRD distribution remains important. To further reduce the errors, we thus divide the simulated damage by the average estimated damage (SED) over realised damage (NRD) ratio in each region, which are computed using the RMSF damage function on IBTrACS and total reported damage from EM-DAT:

$$\hat{r}_j = \frac{\sum_i \mathrm{SED}(i, v_h^{\mathrm{RMSF}}(j))}{\sum_i \mathrm{NRD}} \tag{5.24}$$

Figure 5.3.5 presents the estimated versus actual damages computed using the RMSF damage function and the distribution of the re-scaled estimation by country using the intersection of IBTrACS with lands (762 events), crossed with EMDAT (606). Each dot represents the total damage over a year in a country (211 observations).

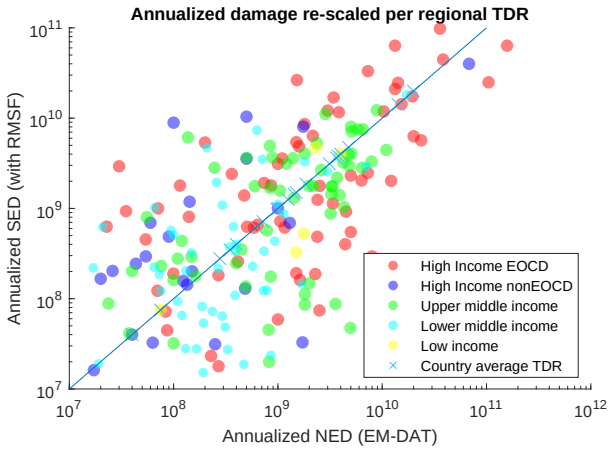

Figure 5.3.5 – Estimated (RMSF) vs. reported damage. The filled dots represent individual year/country pairs with reported damage in EM-DAT. This distribution is obtained using a 0.25 x 0.25 resolution projection. Crosses correspond to country average (over all years).

5.4 Application to representative concentration pathways (RCP)

5.4.1 Climate simulation bias correction for climate change application

The variables from climate model projections used by CATHERINA are subject to multiple biases. To reduce uncertainty caused by these biases, we use the *Cumulative Distribution Function-transform* (CDF-t) method developed in Michelangeli *et al.* (2009) and Vrac *et al.* (2012) to correct the distribution of each variable, in each basin. Our bias correction approach is the standard in the climate community (Navarro-Racines *et al.*, 2020). [17]

Consider a generic climate variable (denoted by χ) at a fixed location, which is available both from ERA5 reanalysis and from a given CMIP5 model. We are interested in two time periods: the historical period (covered both by the climate model and the reanalysis) and a future time period (covered only by the climate model). Let F^h_{ERA5} and F^h_{CMIP} be the distribution functions of χ under reanalysis and under climate model for the historical period, and F^f_{CMIP5} be the distribution function of χ under climate model for the future period. The distribution function under the climate model is subject to much stronger biases than that under the reanalysis. The CDF-t method constructs the distribution function for χ with reduced bias for the future time period, denoted by $\widehat{F}^f_{\text{CMIP}}$ and given by

$$\widehat{F}^f_{\text{CMIP}}(\cdot) = F^h_{\text{ERA5}}(F^{h,-1}_{\text{CMIP}}(F^f_{\text{CMIP}}(\cdot))),$$

where $F^{h,-1}_{\text{CMIP}}$ is the inverse function of F^h_{CMIP}. For a given value χ^f_{CMIP} of the variable χ obtained for the future period from the climate model, the corresponding bias-corrected value $\hat{\chi}^f_{CMIP}$ may

17. see http://ccafs-climate.org/bias_correction/.

then be computed via

$$\begin{aligned}\hat{\chi}^f_{CMIP} &= \widehat{F}^{f,-1}_{\text{CMIP}}(F^f_{\text{CMIP}}) \\ &= F^{f,-1}_{\text{CMIP}}(F^h_{\text{CMIP}}(F^{h,-1}_{\text{ERA5}}(F^f_{\text{CMIP}}(\chi^f_{CMIP})))).\end{aligned}$$

When the future period and the historical period coincide, the method reduces to the standard quantile transform:

$$\hat{\chi}^h_{CMIP} = F^{h,-1}_{\text{ERA5}}(F^h_{\text{CMIP}}(\chi^h_{CMIP})). \tag{5.25}$$

First, we use the method on the historical period to compare the description of the thermodynamic potential and wind speed with and without correction, so equation (5.25) may be used directly. To extract the CDFs of the variables of interest, we generate synthetic track candidates from 1980 (beginning of ERA-5) to 2010. We launch the simulation 10 times over these 30 years to obtain 300 representative years. By definition, for the genesis of the cyclones, the time of year and location are in line with historical cyclone data. However, in this module, the synthetic tracks are generated without climate constraints, i.e. cyclones are allowed to drift relatively far away from their genesis location (in the limits of their initial basin), and therefore can cover conditions which do not lead to the formation of tropical cyclones. At this stage, these tracks are not to be considered as 'tropical cyclone tracks' but as 'candidate' tracks. In the following stage, actual cyclone tracks will be generated from candidate tracks by filtering those ones where meteorological conditions for cyclone formation are satisfied. For each point in space and time along these synthetic tracks, we extract the values of the four climate variables from the reanalysis (ERA-5) and from the historical simulations of the 7 climate models. Then, by comparing the CDF of the climate variables estimated by the models with the reference CDF computed from the reanalysis, we determine the transformation allowing the values estimated by the models to better match those from ERA-5.

The sea-level pressure distributions are stable over basins and models. The tropospheric temperature and near surface relative humidity distributions depend largely on the basin and display evidence of non-negligible model uncertainty. The sea-surface temperature estimates along the same synthetic tracks in the historical period display much larger uncertainty. The North Indian basin presents the widest uncertainty for all climate variables, which adds further uncertainty concerning the impact of climate change on tropical cyclones in this area. [18]

Individual variables entering the MPI computation are correlated as shown in Table 5.4.1. For example, sea-surface temperature and tropopause temperature exhibit a negative correlation of 83%. Therefore, applying bias correction to individual variables may lead to unrealistic combinations when evaluating the thermodynamic potentials. For example, extremely low tropopause temperatures associated with very high SSTs lead to overemphasizing lapse rates therefore generating unrealistically large potentials. To overcome this issue we perform the bias correction on the MSLP, SST, thermodynamic efficiency factor $\mathcal{E}$, and relative humidity - which should not be correlated to other variable according to the level of correlation present in the reanalysis. Figure 5.4.1 shows that this correction leads to similar distribution of the thermodynamic potentials in the models and the reanalysis.

18. Figure 5.B.7 presents the CDF-t of climate data in the sub-sample. These important biases and uncertainties may be mitigated in the latest launch of the models at the occasion of the CMIP6 (Gusain *et al.*, 2020).

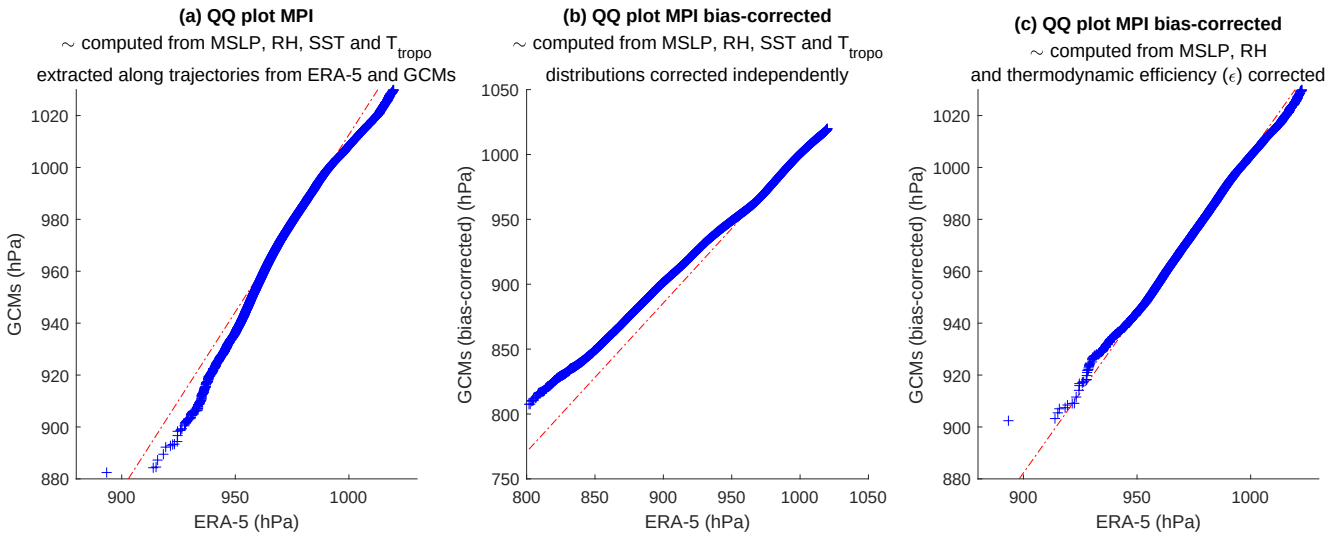

Figure 5.4.1 – Bias correction module QQplots

Table 5.4.1 – Correlation levels (global) of modeled variables affecting the MPI with their reference values in ERA5

	SST_{ERA5}	SST_{CGMs}	$MSLP_{ERA5}$	$MSLP_{CGMs}$	T^{tropo}_{ERA5}	T^{tropo}_{CGMs}	RH_{ERA5}	RH_{CGMs}
SST_{ERA5}	1							
SST_{CGMs}	0.95	1						
$MSLP_{ERA5}$	0.46	0.39	1					
$MSLP_{CGMs}$	0.45	0.38	0.86	1				
T^{tropo}_{ERA5}	-0.83	-0.82	-0.37	-0.33	1			
T^{tropo}_{CGMs}	-0.77	-0.79	-0.31	-0.27	0.85	1		
RH_{ERA5}	-0.07	-0.07	-0.12	-0.09	0.22	0.19	1	
RH_{CGMs}	-0.27	-0.30	-0.18	-0.14	0.33	0.37	0.47	1

We apply the CDF-t correction technique along our historical synthetic tracks and compute the maximum potential intensity following section 5.1.4. The pressure follows the dynamic process introduced in section 5.1.4 and the corresponding wind is derived from the WPR (see section 5.1.4). We define the model error as the relative error $(\frac{\chi_{CMIP}-\chi_{ERA5}}{\chi_{ERA5}})$ between the value produced by the model and the one produced by the reanalysis ERA-5. Figure 5.4.2 displays the average relative errors and shows that a 2% relative error in the description of the maximum potential intensity can lead to more than 20% error in the description of the implied wind compared to the result obtained with ERA-5. This figure illustrates the efficiency of bias correction in the historical period. Indeed, on average the CDF-t correction technique clearly reduces the error between the MPI estimated with climate reanalysis and the one computed from modeled climate data as well as (more importantly) the error in the description of the maximum wind speed. However, running CATHERINA on the different CGMs still produces a wide range of results in climate projections (c.f. Figure 5.4.3). Although the intensity of the storms increases with each model, underlying climate modeling uncertainty still strongly impacts the synthetic tracks produced.

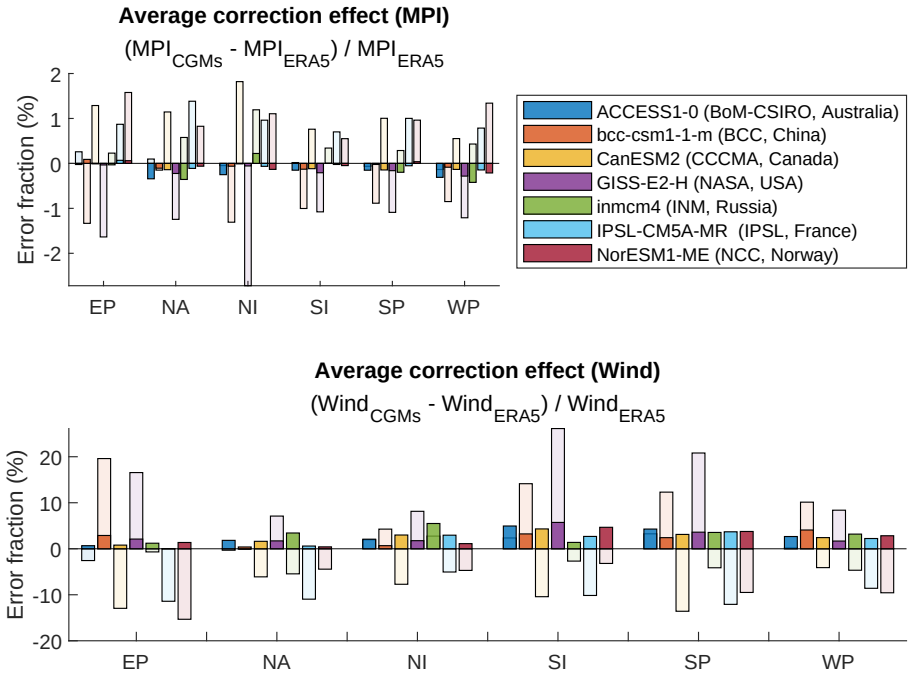

Figure 5.4.2 – Relative error at the level of maximum potential intensity (MPI) computed with ERA-5 and climate data produced by the 7 climate models for the historical period. The transparent bars represent original errors and the color parts represent the residual relative error after CDF-t correction averaged over 30 years of cyclones.

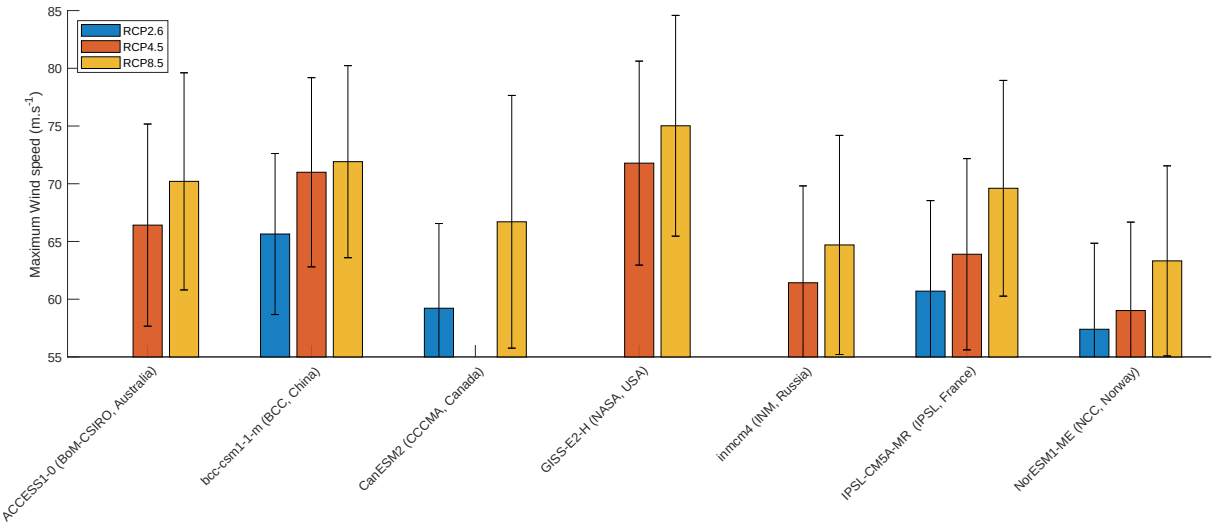

Figure 5.4.3 – Average and standard deviation of maximum wind speed of tropical cyclones generated with the CMIP5 models after correction. Table 5.C.4 provide average value of maximum wind speed.

5.4.2 Results in CMIP5 projections

The international climate modeling community introduced shared socioeconomic pathways (SSP) to translate varying narratives on the development of the society in the long-term. These projections impact the local physical asset value dynamics (G. Chen *et al.*, 2020; Jones & O'Neill, 2020), and global macroeconomic variables (O'Neill *et al.*, 2017; O'Neill *et al.*, 2014). Under the assumptions of constant cyclone genesis frequency and constant impact ratio (i.e. the damage functions remain the same), CATHERINA allows us to derive damage projections in varying climate and socio-economic scenarios. Using bias-corrected climate variable projections from the seven climate models over the period 2070-2100, we provide an example of the application of the CATHERINA framework. [19] As expected (cf. Mendelsohn *et al.* (2012), Figure 3 for example), socio-economic change leads to wider differences than climate change.

Figure 5.4.4 represents the expected value of future damage and Table 5.4.2 provides the expected values (together with standard errors) along with the 50, 66 and 95^{th} percentile of the global annual damage distribution in the simulations, under various assumptions on the future exposure growth (values of α_1 and α_2). In the discussion below, CATHERINA simulations of 300 representative years of synthetic tracks using using ERA-5 data over the period 1980-2010 are used as baseline.

The choice $\alpha_1 = \alpha_2 = 1$ assumes linear increase of exposure both with respect to GDP per capita and local exposed population. Using $\alpha_1 = 1/3$, which is close to the value estimated in (Bakkensen & Mendelsohn, 2019), allows to account for possible future adaptation . The configurations $\alpha_1 = 1, \alpha_2 = 0$ and $\alpha_1 = 0, \alpha_2 = 1$ allow to decompose the risk contribution between GDP and exposed population. Finally, the choice $\alpha_1 = 0, \alpha_2 = 0$ uses the current exposure value with no socioeconomic growth factor.

Assuming no future adaptation ($\alpha_1 = \alpha_2 = 1$), over the period 2070-2100, the RCP 2.6 scenario, which is in line with the Paris Agreement and keeps global warming below 2C by 2100, involves a growth of expected global annual financial losses from tropical cyclones by a factor of 4.2 on average. Ignoring socioeconomic and population growth factors ($\alpha_1 = 0$ and $\alpha_2 = 0$) our model suggest that the expected financial loss would grow by a factor of 1.6 due to increasing cyclone intensity. Taking into account adaptation, i.e. limiting the growth of damage with respect to GDP per capita ($\alpha_1 = 1/3$), the expected damage would grow by a factor 2.6. In the case of SSP2-RCP 4.5 (between 1.7 and 3.2°C warming by 2100) and SSP5-RCP 8.5 (between 3.2 and 5.4C warming by 2100), the average expected damage will be multiplied by 5.4 and 14.2 respectively without adaptation. In the RCP8.5 the expected damage will still grow by a factor 2.8 ignoring the change in GDP per capita and population ($\alpha_1 = 0$ and $\alpha_2 = 0$). Interestingly, in the SSP3, accounting for the population factor (that is, moving from $\alpha_2 = 0$ to $\alpha_2 = 1$) induces an decrease of global expected damage. This is due to a significant decrease of population in the USA, Australia, South Korea or Japan, in the regions subject to tropical cyclones in this scenario. As these countries represented a large share of tropical-cyclone related damages, the global expected damage is reduced.

Our expected damage estimates are subject to three types of uncertainty: internal climate

19. Because of the time slicing of the CMIP5 climate data available in the climate data store, we launch the models on 25 consecutive years over this period: 2070-2095 for IPSL, BCC, NCC, CCCMA, 2075-2100 for GISS and 2085-2095 for INM (only a 10 year slice of climate data is available on the CDS for this model). We repeat this process changing the seed 12 times to obtain 300 representative years in each model (except INM for which we only have 120 years).

variability, climate model uncertainty and socio-economic uncertainty related to future exposure growth, adaptation measures and concentration pathways. The first two types of uncertainty are quantified by the standard errors in Table 5.4.2, while the last one may be evaluated by performing simulations under different assumptions on adaptation, SSP narratives and representative concentration pathways as illustrated in Figure 5.4.4.

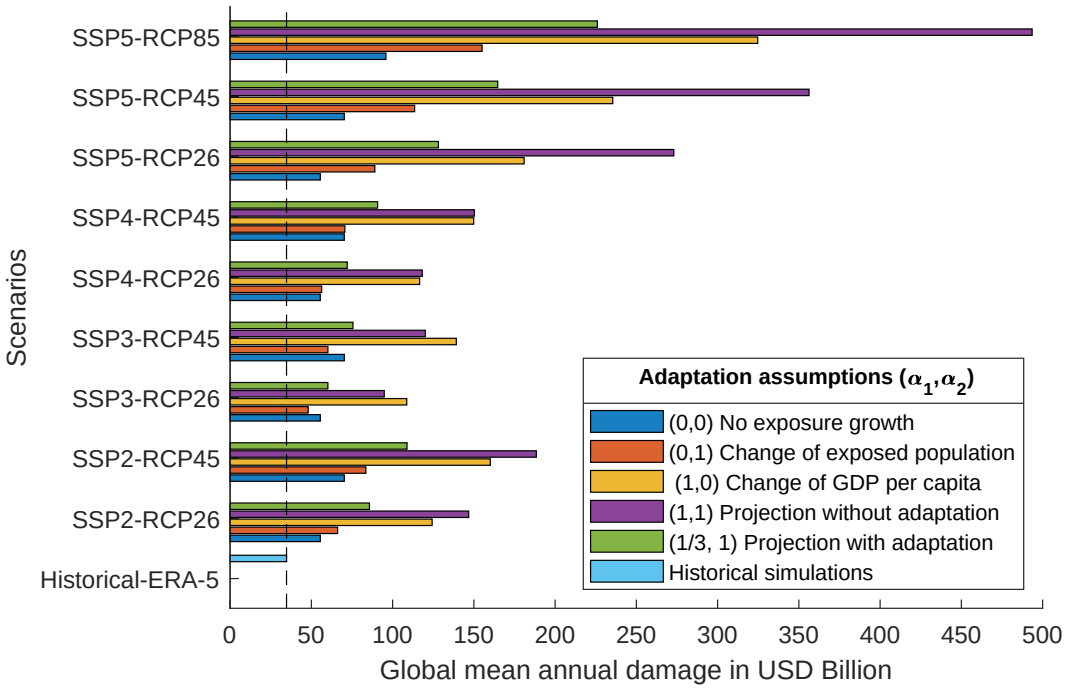

Figure 5.4.4 – Expected value of global annual damage (in USD billion) in different SSP-RCP and exposure projection hypothesis configurations. The vertical dotted line corresponds to historical simulations with ERA5 data.

Figures 5.4.5 displays the average annual damage per country, in the different shared socioeconomic pathways, assuming no future adaptation. We can see that the distributions across countries are slightly different from one SSP to another. Indeed, the distributions in SSP2 and SSP5 are similar, with a higher expected damage in SSP5 because of the growth hypothesis this scenario relies on. However, SSP3 (rocky road) or SSP4 (inequality) are distributed differently. The scenario emphasizing inequalities – and its interpretation by scientists in terms of (i) socioeconomic developments (Riahi *et al.*, 2017) and (ii) population distribution (Jones & O'Neill, 2017) – increases damage concentration in the United-States. On the other hand, the rocky-road scenario, linked to a larger and more rural population, lower GDP and national rivalry sees the damage more equally distributed among other nations.

Looking at the expected damage values is instructive, however, because the aim of the model was also to stress test the resiliency of the financial and economic systems, it is important to examine the risk of extreme events, corresponding to higher quantiles of the loss distribution. Figure 5.4.6 and Table 5.4.2 show that the 95% quantile of the loss distribution, correpsonding to losses which arise, on average, once in 20 years, may be as high as 4-5 times the expected loss. This observation is in line with Coronese *et al.* (2019) who show that the impact of climate change

Table 5.4.2 – Simulation statistics (in USD billion)

SSP	RCP	(α_1, α_2)	Mean	Standard Error	50^{th} perc.	66^{th} perc.	95^{th} perc.
	ERA-5		34.72	5.14	6.81	15.72	155.94
Historical	IBTrACS		47.59	N.R.	25.72	42.94	160.88
	Reported EM-DAT		21.1	N.R.	9.19	13.90	62.79
SSP2	RCP26	(1,1)	146.82	11.54	40.06	83.81	583.74
		(1/3,1)	85.74	7.14	21.14	45.38	362.46
		(0,1)	66.14	5.63	15.31	32.64	286.85
		(1,0)	124.31	8.82	39.61	78.72	492.96
		(0,0)	55.51	4.29	15.47	31.35	225.87
	RCP45	(1,1)	188.47	9.75	58.41	121.04	779.64
		(1/3,1)	108.87	5.94	30.81	63.41	483.78
		(0,1)	83.54	4.66	22.56	48.69	376.56
		(1,0)	160.12	7.64	57.59	112.31	637.80
		(0,0)	70.28	3.64	22.43	45.00	300.45
SSP3	RCP45	(1,1)	120.10	6.18	40.61	76.71	478.18
		(1/3,1)	75.60	3.95	25.26	46.68	315.38
		(0,1)	60.18	3.18	19.61	36.83	255.95
		(1,0)	139.20	7.10	46.09	93.13	580.09
		(0,0)	70.28	3.64	22.43	45.00	300.45
SSP4	RCP26	(1,1)	118.24	10.09	27.27	58.87	501.24
		(1/3,1)	72.07	6.18	16.29	35.57	313.51
		(0,1)	56.35	4.85	12.74	27.92	245.90
		(1,0)	116.63	8.96	32.90	67.65	483.69
		(0,0)	55.51	4.29	15.47	31.35	225.87
	RCP45	(1,1)	150.33	8.38	40.57	85.66	664.69
		(1/3,1)	90.75	5.10	24.13	52.11	413.71
		(0,1)	70.62	3.99	18.58	40.51	325.38
		(1,0)	149.90	7.68	47.48	98.81	622.79
		(0,0)	70.28	3.64	22.43	45.00	300.45
SSP5*	RCP45	(1,1)	356.26	18.92	104.58	219.89	1 478.45
		(1/3,1)	164.69	9.22	41.80	91.28	730.27
		(0,1)	113.56	6.48	27.15	60.71	530.05
		(1,0)	235.48	10.80	88.32	176.36	910.28
		(0,0)	70.28	3.64	22.43	45.00	300.45
	RCP85	(1,1)	493.56	27.04	140.69	281.66	2 290.21
		(1/3,1)	226.00	12.67	57.58	122.55	1 072.03
		(0,1)	155.05	8.76	36.95	81.72	737.30
		(1,0)	324.71	15.23	127.63	226.70	1 366.12
		(0,0)	95.89	4.81	30.70	59.48	445.36

Note: * The couple SSP5-RCP26 exists in the integrated assessment modeling literature (Rogelj *et al.*, 2018) but is not displayed because the SSP5 is more likely tied to high concentration scenarios.

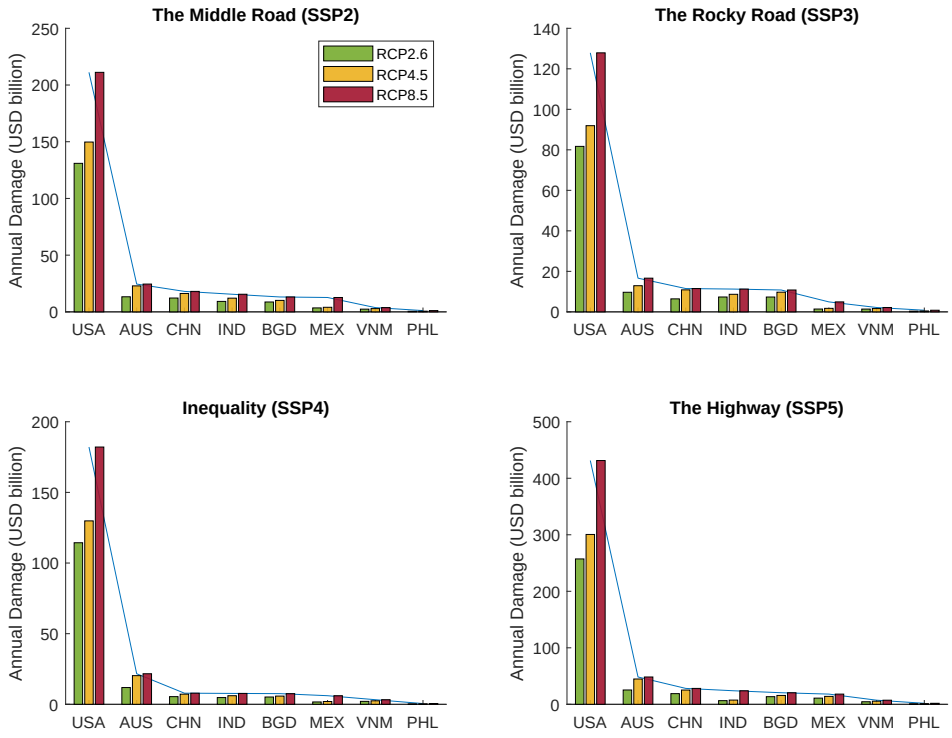

Figure 5.4.5 – Annualized regional expected damage in SSP and RCP between 2070 an 2100 based on synthetic tracks produced with 7 climate models (with bias correction) over 300 representative years launched independently. The scale differs between SSPs.

is particularly striking for extreme events (see for example, Figure 2A in this reference).

5.4.3 Impact on sovereign bond spreads in RCPs

In this section, we study the impact of cyclones on the exposed economies because of their higher vulnerability. A particular attention will be dedicated to emerging economies. We proceed in two steps. First we analyze how physical risks have affected the sovereign yields – bond returns and local currency valuation – of developing countries in the past. To this end, we study the behavior of financial variables around catastrophic events. In the second step, we use an econometric model to relate the spread of sovereign bonds to the scenario-based distributions of damage developed in previous sections.

Market integration of physical risks

Data To measure the impact of cyclones on the financial markets we extracted the bid prices of Treasury bonds (10 year and 3 months yields) and local currency valuation from Reuters Refinitiv and Bloomberg. We also tested the impact on 5 year credit default swaps (data source: Bloomberg). We use the dated disasters (when the start and end dates are known precisely) from EMDAT database [20]. To extend the database we use all types of natural disasters rather than

20. https://public.emdat.be/data.

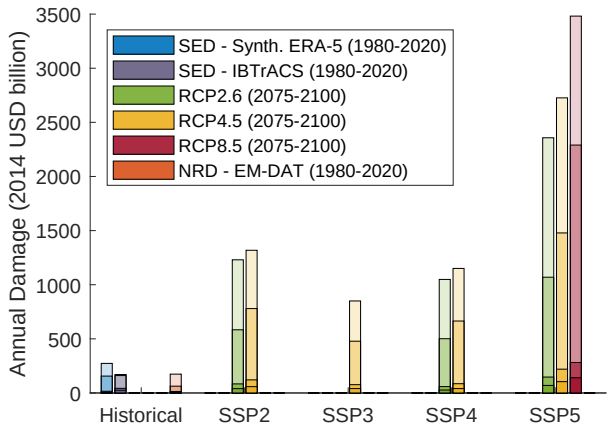

Figure 5.4.6 – Annualized global damage in shared socioeconomic pathways (SSP) and representative concentration pathways (RCP) between 2070 and 2100 based on synthetic tracks produced with 7 climate models (with bias correction) over 250 representative years launched independently, assuming no adaptation ($\alpha_1 = \alpha_2 = 1$). Top range: 95% – 98% (*extremely unlikely* losses), followed by 95% – 66%, 50% – 66% and 0% – 50%. Synthetic historical damages are computed with 300 representative years of synthetic tracks generated with ERA-5 between 1980-2010. The physical asset value is corrected by inflation between cyclone year and 2014 (GDP ref. year of Litpop). The global SSP-RCP configurations are presented as feasible in Rogelj *et al.* (2018).

just tropical storms. The database contains 496 dated events with costs above a USD 1 billion, 50 events with costs above USD 10 billion, 7 events with costs above USD 50 billion, and 2 events with costs above USD 100 billion from 1900 to 2021. Our aim is to quantify the impact of such events on financial markets, between 2000 and 2021.

Event study methodology Lanfear *et al.* (2019) showed that stock markets do respond to storm information using and event study approach. Recently, Dimov and Parsons (2021) analyzed the impact of historical cyclone landfall on the equity performance of manufacturers using a similar framework. From a sovereign perspective, in particular in emerging markets, low liquidity should mitigate market anticipation during cyclone formation (pre-landfall). The impact we seek to measure is the potential market meltdown after accounting for all the damages. Therefore, as a first approach to quantify the impact of natural catastrophes on sovereign markets, we perform an event study analysis on a 30 days window around the event end date, when total damage are observed. In absolute terms, for the given damage threshold value, for example USD 50 billion, we define the set of events affecting each country, in this case five events (see Figure 5.4.7). In relative terms, we normalized the events damage by the GDP of the country ($\mathcal{D}(t)$/GDP) and study the 100 most important events. For each event, we estimate abnormal the return it generates, using two approaches:

- With the constant mean approach, we compare the variation observed during the period with the averaged variation before the cyclone events:

$$\mathrm{AR}_{j,t} = r_{j,t\epsilon[\tau,\tau+w]} - \overline{r}_{j,t\epsilon[\tau-w,\tau]} \tag{5.26}$$

  where $\overline{r}_{j,t\epsilon[\tau-w,\tau]}$ is the average variation of the variable of interest (for instance yields or

currency variation) and $r_{j,t\in[\tau,\tau+w]}$ is the variation observed after the event.

- With the market model approach, we compare the returns observed during the periods with the estimated returns of the financial security based on a CAPM-like model:

$$\mathrm{AR}_{j,t} = r_{j,t\in[\tau,\tau+w]} - \widehat{\alpha}_{j,t\in[\tau-w,\tau]} - \widehat{\beta}_{j,t\in[\tau-w,\tau]} M_{r,t\in[\tau,\tau+w]} \tag{5.27}$$

where the r is the variation of market price variable (e.g. Treasury bonds price), $\widehat{\alpha}_{j,t\in[\tau-w,\tau]}$ and $\widehat{\beta}_{j,t\in[\tau-w,\tau]}$ are the coefficient of the CAPM model fitted on the period before the events and $M_{r,t\in[\tau,\tau+w]}$ is the time series of the market index variation after the event. Using a market model allows us to capture general fluctuations unrelated to country specific factors that can occur during the same period.

This methodology is very sensitive to the size of the estimation window and to the choice of the country. For yields or currency we will use the model based on constant mean correction (Equation 5.26). For bond price returns we will use the correction based on estimated returns (Equation 5.27), where the market returns are defined using 10 years U.S. bonds.

Impact on yields Over the 100 most damaging events relatively to the GDP of impacted countries, we find 55 matches with a series of daily 10 years yield variation suggesting an average 5 bps rise in emerging market bond yields (See Figure 5.B.8a on page 180). In absolute terms, the most extreme events are also the most impacting. For instance, considering dated events with cost over USD 50 billion restricts the database to the following five events: Tohoku, the Japanese earthquake and Tsunami (JP-2011-03-11) causing Fukushima, tropical cyclones Katrina (US-2005-09-19), Harvey (US-2017-08-29) and Maria (US-2017-09-28), and the Chinese Sichuan earthquake (CN-2008-05-12). The individual effects of these disasters on the cumulative variations of 10 year bond yields of the impacted countries are shown in Figure 5.4.7. This figure suggests that these events raised the cost of borrowing in the following months by 20 bps for affected countries [21].

When restricting the database to the five most impacting events by normalizing the damage by the GDP of the country impacted we only keep Tohoku and Sichuan earthquakes, together with tropical cyclone Amphan (IN-2020-05-20), Thailand floods during the 2011 monsoon season (TH-2011-08-05), or floods in India (IN-2019-09-30). Some catastrophic events – such as the floods in Pakistan (PK-2010-08-07) or cyclone Ivan passage through Cayman island (CY-2004-09-12) – could not be included because there are no matching yields in the database. However ,there is no significant effect for the top five events and the results obtained using different filtering thresholds are not consistent.

Discussion The procedure described above was performed using several different financial variables: 10 year Treasury bond yield and market price, 3 months yield, currency valuation, and 5 year credit default swap. The results found for different instruments are not fully consistent with each other and depend on the parameters of the algorithm, therefore one cannot draw robust and general conclusions. However, all results suggest that in the past, emerging markets reacted to natural disaster by a slight depreciation of local currency, increase of bond yields and underperformance of the bonds. We also reiterate that the impact of disasters on more liquid stock

21. The aggregated impact are given Figure 5.B.8b.

Figure 5.4.7 – Impact on 10 year sovereign yields

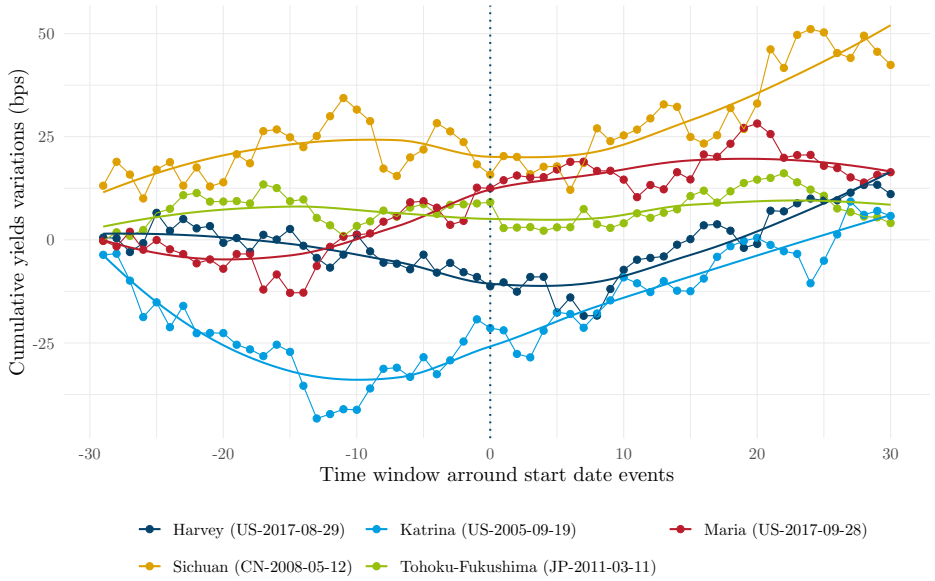

Top five most costly events. The event time is date end of the event reported by EMDAT the window is 30 days. The series are controlled using constant mean correction. Bid yield 10 years gov. from Reuters Refinitiv.

markets was demonstrated (Lanfear *et al.*, 2019), therefore physical risks are already priced by the equity markets.

Although in the past, bond market reactions to catastrophic events have been moderate, climate change is increasing event intensity, which may lead to higher impact in the future. We showed that with the advent of climate change, annualized damages will grow and may compromise ability of some countries to pay back their debt. Therefore, in the next section we focus on default risk and investigate this question using the spread of their USD dominated bonds with respect to U.S. treasury bonds.

Cyclones impact on sovereign spreads

In this section, we derive the scenario-based excess spread for each country impacted by tropical cyclones.

From direct damage to the sovereign debt The first step is to define the transmission channels from the cyclone damage to the costs of sovereign debt. The damages related to disasters fall in two categories: the direct physical losses, possibly insured, and the longer-term economic consequences of the event. For instance, the direct costs of hurricane Katrina are estimated to USD 125 billion (2005), among which USD 80 billion were covered by insurance (EMDAT and Swiss Re Group (2020)). The consequences of the cyclone on the U.S. economic growth, which went down from 4.1% in the third quarter of 2005 to 1.7% in the fourth quarter before bouncing back to 5.4%

in the first quarter of 2006, and on U.S. oil production (19% of which was damaged) [22] increased this cost further. It is sometimes hard to define long-term economic impact of the cyclone. For instance, cyclones often destroy agriculture and live stock, which affects the economy during a longer period. For instance, hurricanes Irma and Maria in 2017 in Dominica destroyed 100% of agricultural plantations, while Yassi in Australia in 2011 destroyed 75% of agricultural plantations in the affected areas.

In general, because of the propagation of damages in the economic system, the longer-term economic impacts are more complex to estimate. To address this difficulty, Hallegatte (2008) introduced an input-output framework and defined the economic amplification ratio (EAR) as the multiplier between direct cost and the total economic damage. For Katrina this coefficient was estimated to be 1.39. The author suggested that the economic outcomes of events with direct losses exceeding USD 200 billion could imply total cost twice as large. In this case, the increase of the cost because of climate change (cf. Table 5.4.2) may overwhelm reconstruction capacity of poorest countries. In our estimation we do not apply an economic amplification ratio because we consider that the damage reported already takes this effect into account.

In this section, we develop a simplified approach for assessing the effect of cyclone damage on sovereign credit spread, assuming that the cost of damages is paid by issuing new government debt. We build a structural econometric model for sovereign spread, including the debt to GDP ratio as an explanatory variable (Hilscher & Nosbusch, 2010). Assuming stationarity of model parameters then allows us to evaluate the effect of cyclone damages on spreads under various climate and economic scenarios.

Sovereign spread model The spread is the difference of yield between a given security and the risk-free asset i.e. AAA rated bond. In practice, we use the option-adjusted spread with respect to the U.S. 10 year Treasury bond. The option-adjusted spread (OAS) is the measurement of the spread adjusted to take into account specific options embedded in some fixed-income securities. Following Hilscher and Nosbusch (2010), we calibrate a cross-sectional econometric model for the option-adjusted spread based on annual end-of-year data:

$$\begin{aligned} \mathrm{OAS}_t = \alpha \quad &+ \quad \beta_1 \Delta \mathcal{C}_t + \beta_2 D_t + \beta_3 \mathrm{VIX}_t + \beta_4 r_t^{10Y} \\ &+ \quad \beta_5 \mathrm{TED}_t + \beta_6 \frac{L_t}{\mathrm{GDP}_t} + \beta_7 \frac{\mathrm{reserves}_t}{\mathrm{GDP}_t} + \beta_8 \mathcal{R}_t + \beta_9 \mathcal{K}_t + \varepsilon_t. \end{aligned} \tag{5.28}$$

OAS is the end-of-year option adjusted spread, from from JP Morgan EMBI position report in BarraOne;

$\mathcal{C}$ is the commodity price index, from Reuters Refinitiv;

D is the average duration of the bonds, from JP Morgan EMBI position report in BarraOne;

VIX is the CBOE volatility index, from Reuters Refinitiv;

r^{10Y} is the 10 year U.S. Treasury bonds rate, from Reuters Refinitiv;

TED is the difference between the three-month Treasury bill and the three-month LIBOR, from Reuters Refinitiv;

22. https://www.thebalance.com/hurricane-katrina-facts-damage-and-economic-effects-3306023.

L refers to the total external debt stocks in USD, from World Bank;

GDP refers to the end-of-year GDP, from World Bank;

reserves are the total reserves including gold, in USD;

$\mathcal{R}$ is the credit rating dummy variable (described below);

$\mathcal{K}$ is the country dummy variable, described below.

The model covers 74 countries between 2010 and 2020.

We chose to use all the bonds constituting the index, i.e. including multiple bonds per country per date. Rather that using Hilscher and Nosbusch (2010) fixed effect approach with our unbalanced panel, we chose to fit a simple ordinary least squares regression including dummies for ratings and country effects. Table 5.4.3 shows the sensitivity of the option adjusted spread of each bond belonging to the JP Morgan EMBI to macroeconomic and financial factors following Hilscher and Nosbusch (2010). The model (1) assesses the effect of a variation of debt/GDP ratio only, the model (2) introduces one rating dummy (splitting bellow B-), the model (3) introduces additional macro variables and (4) adds country effect dummies and bond duration [23].

Table 5.4.3 – Simple Option-Adjusted-Spread model

	Dependent variable:			
	OAS (bp)			
	(1)	(2)	(3)	(4)
$\Delta\mathcal{C}_T$			-486.681^{***}	-467.219^{***}
			(114.675)	(91.876)
Duration				8.639^{***}
				(1.659)
VIX			17.094^{***}	15.377^{***}
			(2.510)	(2.120)
TED			−13.753	−7.395
			(113.318)	(91.791)
$r_{US,10Y}$			-9.809^{***}	-8.478^{***}
			(2.199)	(1.756)
$\frac{L}{GDP}$	367.461^{***}	229.629^{***}	336.718^{***}	377.035^{***}
	(26.060)	(21.319)	(25.809)	(79.759)
$\frac{\text{reserves}}{GDP}$			-244.949^{***}	$-1{,}176.650^{***}$
			(41.034)	(185.851)
Rating <B-		$1{,}692.843^{***}$	$1{,}697.096^{***}$	$1{,}391.009^{***}$
		(42.121)	(41.011)	(36.858)
Countries				X
Constant	207.254^{***}	222.600^{***}	$1{,}410.488^{***}$	$1{,}521.181^{***}$
	(15.583)	(12.732)	(330.158)	(269.092)
Observations	2,212	1,860	1,832	1,832
R^2	0.083	0.509	0.542	0.723
Adjusted R^2	0.082	0.509	0.541	0.715
Residual Std. Error	411.571 (df = 2210)	316.591 (df = 1857)	308.258 (df = 1824)	242.855 (df = 1778)
F Statistic	198.832^{***} (df = 1; 2210)	962.874^{***} (df = 2; 1857)	308.792^{***} (df = 7; 1824)	87.609^{***} (df = 53; 1778)

Note: *p<0.1; **p<0.05; ***p<0.01

Dropping Argentina in constant in (4)

In line with Edwards (1986), we find that the debt ratio is significant. More importantly, we note that β_6 is relatively stable over the modeling frameworks implying that the sensitivity of the

23. Including bond duration is significant only when controlling by country effect.

spread to a sudden increase of debt ratio does not strongly depend on external nor idiosyncratic parameters. We find a positive effect of the VIX, and a hardly significant effect from TED spread. The duration of the bonds is of the expected sign and significant. The U.S. 10 years return has a negative effect on emerging country spread. This could be linked to two reasons. First, when the U.S. bond yield increases, investors may be less interested in emerging markets. Another reason is the positive correlation between Treasury returns and the dollar index [24], and negative correlation between the dollar index and emerging markets debt. In other words, the USD denominated debt of these countries grows when their local currency depreciates. Most of these countries are commodity exporters. A positive change in commodity price index, implies that a country's exports have become more expensive relative to its imports (Hilscher & Nosbusch, 2010). Therefore, we expect commodity price index to reduce sovereign spreads. This is an important channel of diffusion of the risks towards developing countries less exposed to tropical cyclones. The coefficients of models (3) and (4) are of the expected sign. Including country effects in (4) we obtain a model reaching 71.5% of adjusted R^2.

Cyclone impact on sovereign spreads under representative concentration pathways

We now use the econometric model developed in the previous paragraph to assess the impact of tropical cyclones on emerging country bond spreads under relative concentration pathways. To this end, we make the following simplifying assumptions:

— We assume that the bond spread model parameters remain stable over time;

— We assume that the cyclone damages are financed directly by the government by issuing new debt, and that other variables of the model are not affected by cyclones;

— We take into account only direct impact of cyclones and not the total economic costs.

For each country j in the JP Morgan EMBI index, we assess the annual bond spread variation due to cyclone damage, in scenario k for the year t using the following formula:

$$\Delta_{k,t}\mathrm{OAS}(j,k,t) = \beta_6 \times \frac{\mathcal{D}(j,k,t)}{F_{\mathrm{GDP}}(j,k,t)\mathrm{GDP}(j,2020)}, \tag{5.29}$$

where we recall that $\mathcal{D}$ stands for annualized cyclone damage, and F_{GDP} is the GDP growth factor for the specified country/scenario. For example, an event simulated in 2077 with GISS-E2-H (NASA, USA) in the RCP85, generated USD 158 billion damage in Australia. Normalised by the future projected domestic product in the scenario (e.g. reference value USD 1.3 trillion with growth coefficient 3.1, leading to 4.4 trillion), this damage represent about 7% of the country GDP in the year concerned. This would lead to a shock in Australian sovereign bond yield of 27 basis points (one basis points equal 0.01%), implying a considerable increase of financing cost.

We compare the spread variation defined from damages of the RCP26 baseline, RCP45 and RCP85 to obtain an annualized financial valuation of the cyclone-related physical climate risk. The impact of average annual cyclone damage on the spread of sovereign bonds of larger emerging countries, channeled by the impact on debt-to-GDP ratio, is small. This is consistent with the historical data, as countries are not equally affected each year by tropical cyclones, and when they

24. The U.S. Dollar Index (USDX) is an index of the value of the United States dollar relative to a basket of foreign currencies.

Figure 5.4.8 – Damage cost channeled to excess spread (cost of debt) of different countries, basis points.

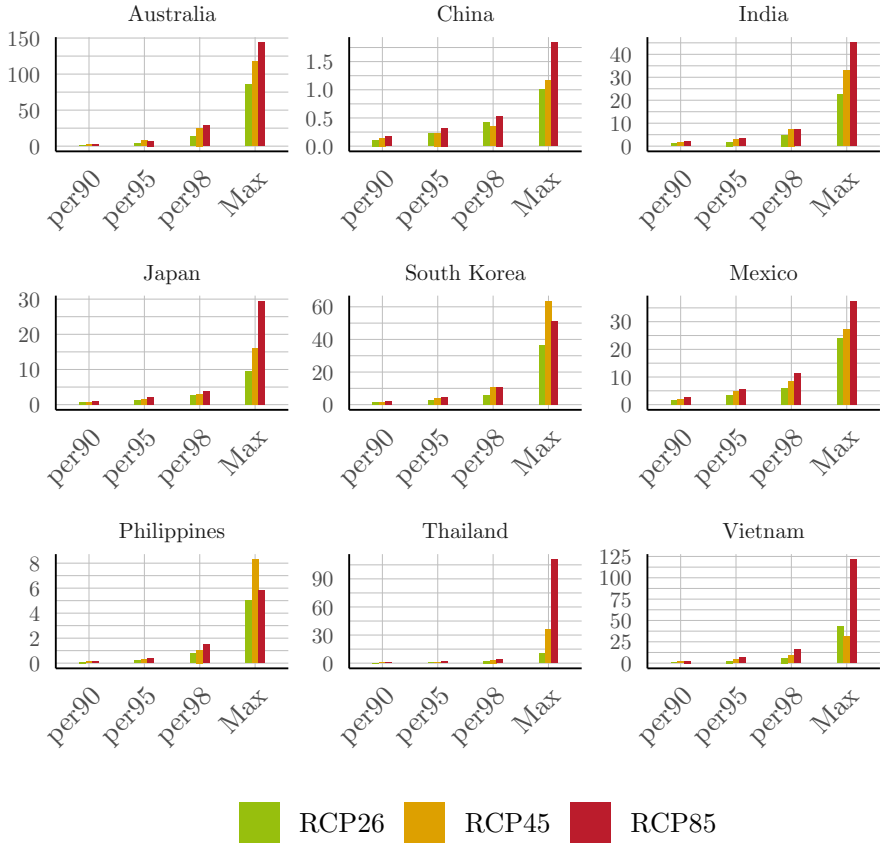

are, they develop a resiliency that is reflected in their damage functions. Therefore, we focus on the tail risk, that is on the extreme event quantiles. Figure 5.4.8 represents the annual excess spread for a sample of countries, when the annual cyclone damages are given by 90^{th}, 95^{th}, 98^{th} percentiles of the distribution as well as by the maximum cyclone related shock observed in the simulations. Recall that we have drawn 250 representative years from 7 models with independent launches to increase the number of cyclone trajectories. On average, larger countries' excess spreads remain limited, but the maximum observed damages induce a significant excess cost of debt.

Appendix

5.A Notation

	Indices	
B	Basin	
i	Cyclone	
j	Country (or region)	
k	Scenario	
s	Generative algorithm step $s \sim (x, y, t)$	
t	Date	
s_l, t_L	Step on land	
x	Longitude	
y	Latitude	
env	Environmental standard season/location variable	
	Variables	
$\mathcal{C}$	is the commodity price index	
D	Bond duration land	
$D^l(x_t, y_t, t)$	Distance to land	km
$\mathcal{D}(j, k, t)$	Simulated cyclone annualized damage	USD
$f(y)$	Coriolis parameter $(2\omega sin(y))$	
f_j	Fraction damage ratio	
$F_{pop}(x, y, k, t)$	Population variation (local level)	
$F_{GDP}(j, k, t)$	GDP variation (country level)	
$F^{cap}_{GDP}(j, k, t)$	GDP per capita (country level)	
$\text{GDP}(j, k, t)$	Global Domestic Product	USD
$\mathcal{L}(x, y)$	Local physical asset value	USD
$L(j, k, t)$	Total debt (external)	USD
$\text{MSLP}(x_t, y_t, t)$	Mean sea surface pressure	Pa (or hPa)
$\text{MPD}(\text{SST}_b)$	Max pressure drop observed for a given SST	Pa (or hPa)
OAS	option adjusted spread	dbs
P^c_t	Central pressure	Pa (or hPa)
$P(j, k, t)$	Population (country level)	number of people
$p(x, y, t)$	local population estimate	number of people
$q(x_t, y_t, t)$	Specific humidity	
$r_{env}(i, t)$	Radius to environmental conditions	km
$\text{RH}(x_t, y_t, t)$	Relative humidity	%
SED_i	Simulated damage per cyclone	USD
$\text{SST}(x_t, y_t, t)$	Sea surface temperature	K
SST_b	Temperature rounded to 0.1°C	K
$T_{\text{tropo}}(x_t, y_t, t)$	Tropopause temperature	K
V_t	Wind speed	m/s
$\Phi_c(i, j, k, t)$	Sovereign physical asset exposure	USD
x_t	Longitude along track	
y_t	Latitude along track	

Functions and operators	
Δ_t	Variation over time operator (X(t)/X(t-1))
Δ_k	Variation over scenario operator (X(k)/X(k=0))
Parameter	
a, b	Wind-pressure relationship coefficients
A, B, C	SST-MPD coefficients
a_n	AR longitude parameters
b_n	AR latitude parameters
c_n	Dynamic pressure variation
μ_X	Mean of the normal distribution fitted on variable X
d_n	Physical damage parameters
R_d	Dry air constant
t_0	Year 2020
L_v	Latent heat constant
ρ	Surface air density
σ_X	Standard deviation of the normal distribution fitted on variable X
v_t	Wind threshold (25.7m/s)
v_h	Wind function hyper parameter calibrated

5.B Supplementary Figures

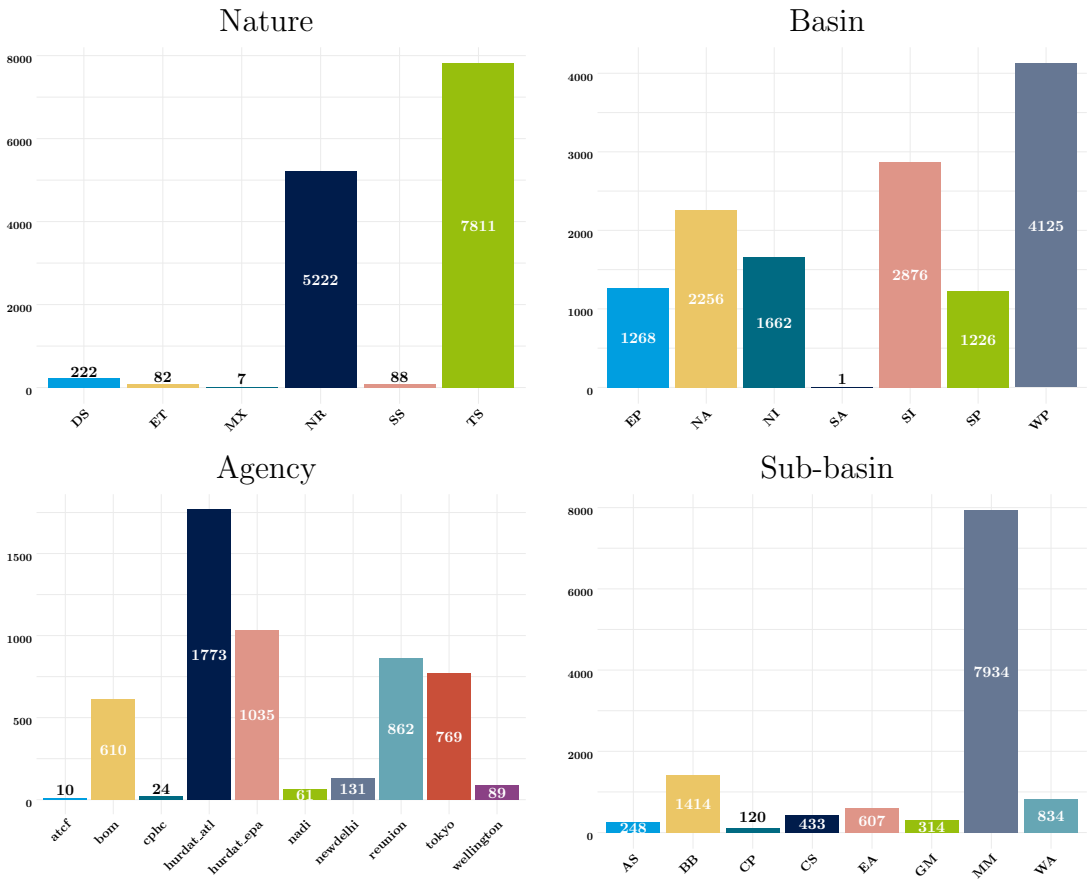

Figure 5.B.1 – Information in IBTrACS.

Notes: The cyclones are split by nature (DS: Disturbance; TS: Tropical; TE: Extratropical; ST: Subtropical; NR: Not reported; MX: Mixture or contradicting nature reports from different agencies). We remove Extratropical cyclones (75) and Disturbance (205). The cyclones are reported in the following basins: East Pacific (EP); North America (NA); North India (NI); South Atlantic (SA); South India (SI); South Pacific (SP); Western Pacific (WP). One can also explore sub-basin decomposition Eberenz *et al.* (2021) (MM : missing - no sub basin for this basin (no sub-basins provided for WP, SI); CS : Caribbean Sea; GM : Gulf of Mexico; CP : Central Pacific; BB : Bay of Bengal; AS : Arabian Sea; WA : Western Australia; EA : Eastern Australia) but we chose to use basins. The different agencies worldwide report central pressure and maximum wind speed but use sometimes different standards. In particular, the reporting can vary in terms of sustained wind speed. According to the dataset documentation the North Atlantic - U.S. Miami (NOAA NHC) bureau (hurdat/atcf) gives the 1-minute winds speed while Tokyo i.e. RSMC Tokyo (JMA) provides dirrectly the 10-minute sustained wind speed (Similarly, newdelhi corresponding to RSMC New Delhi (IMD) gives the 3-minute wind speed; reunion - RSMC La Reunion (MFLR), the Australian TCWCs (TCWC Perth, Darwin, Brisbane) (BOM), the RSMC Nadi (FMS); TCWC Wellington (NZMS) provide the 10 minute sustained wind speed and (CMA) 2-minute sustained wind). The lack of reporting standards between agencies is a source of uncertainty in the input data.

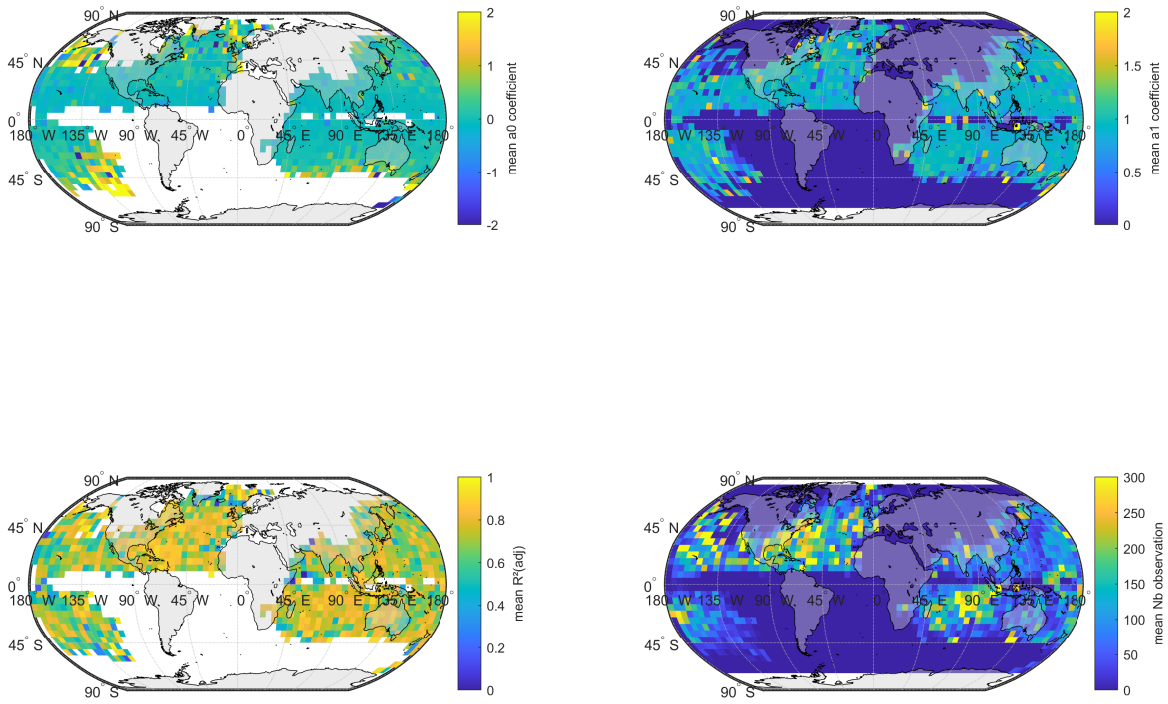

Figure 5.B.2 – Map of longitude variation mean coefficients fitted on a 5x5 grid grouped per month

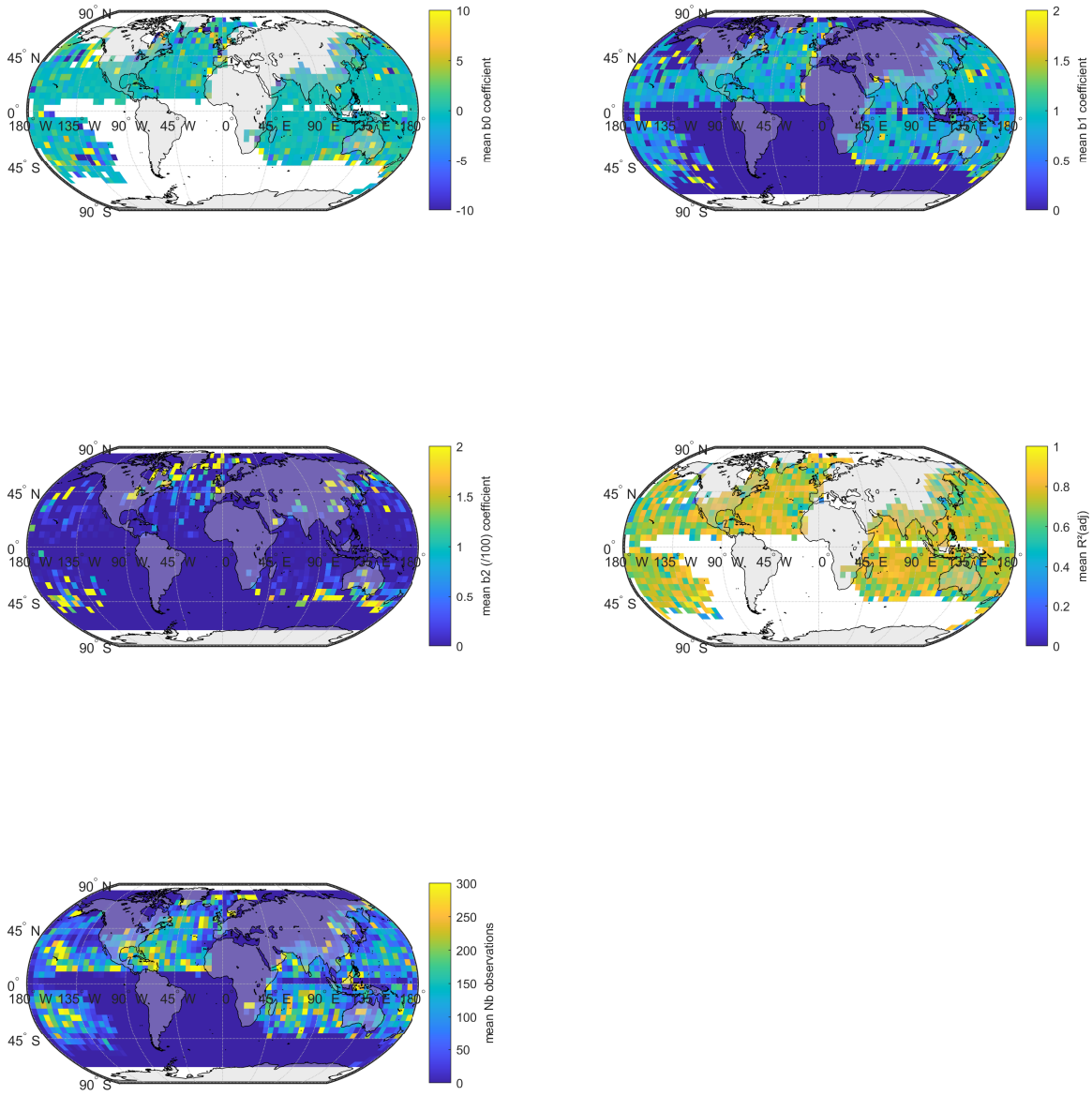

Figure 5.B.3 – Map of latitude variation mean coefficients fitted on a 5x5 grid grouped per month

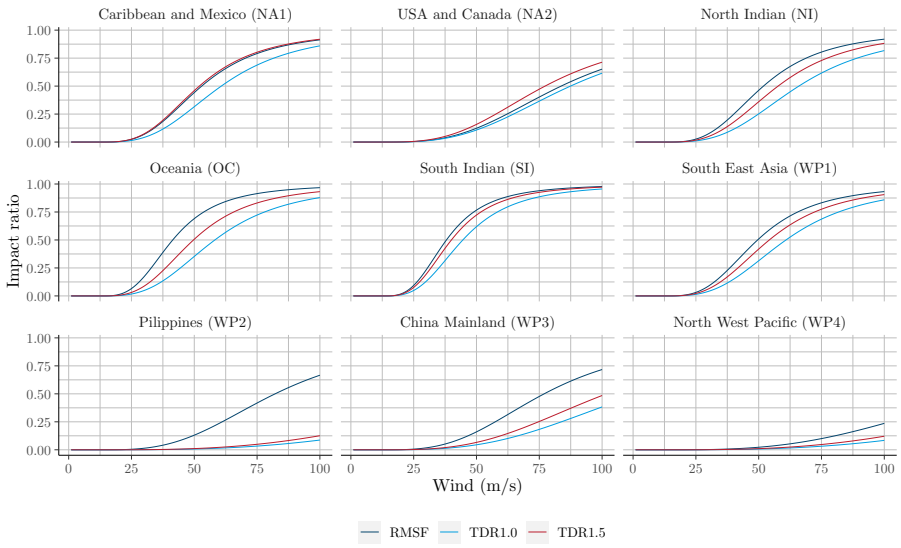

Figure 5.B.4 – Regional Optimal Damage Functions of the CLIMADA package (Eberenz *et al.*, 2021)

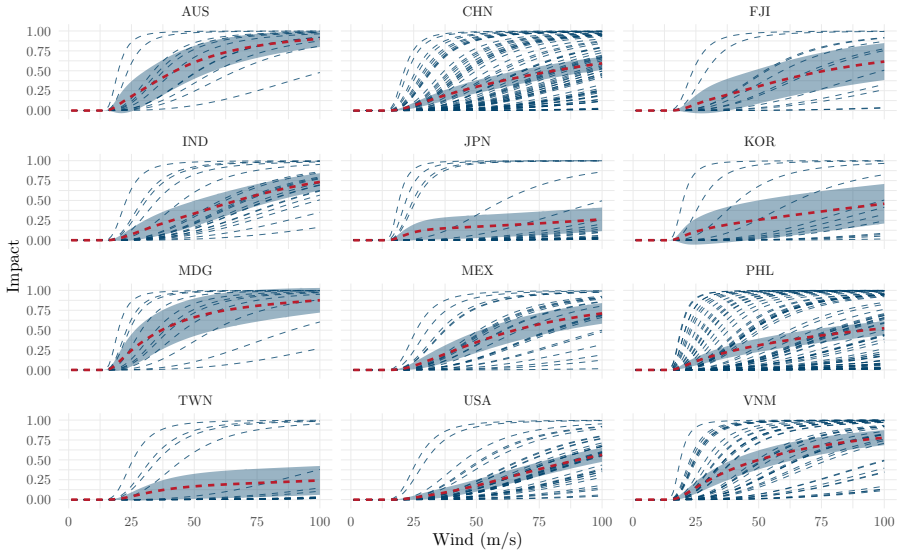

Figure 5.B.5 – Country calibration of damage function (when the countries has been hit more than 5 times)

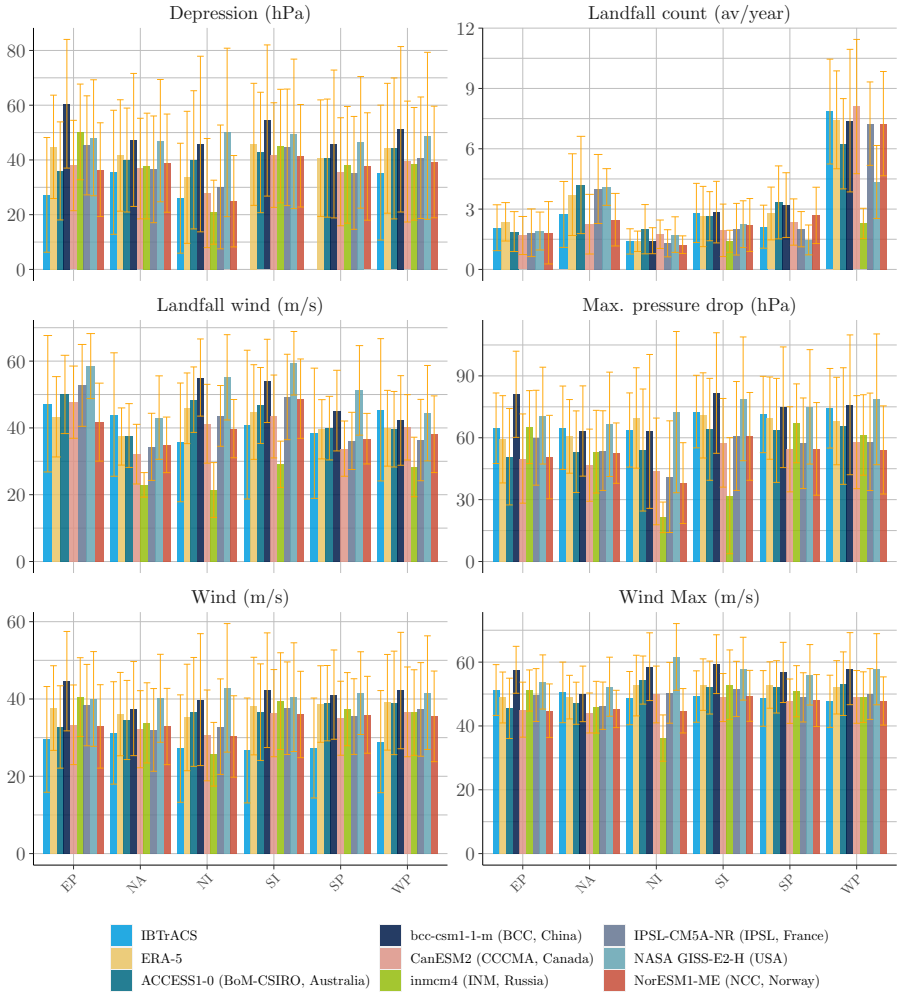

Figure 5.B.6 – Evidence of models uncertainty.

Note: A comparison of the properties obtained generating 30 years of tropical cyclones with different models from the CMIP5 raw climate data versus ERA-5. The average number of cyclone making landfall is computed averaging the number of event with a number of steps on land positive ($s_l > 0$). Maximum pressure drop and wind are respectively computed extracting the maximum value for the corresponding variables of the cyclone tracks.The light blue bars represent the mean of the variable of interest among IBTrACS filtered dataset (with the confidence interval drawn from the standard deviation of the distribution). The yellow bars represent the same variable extracted from the synthetic data generated by the algorithm 1 using ERA-5 data. In terms of average values the models produce consistent tracks on every basins. Then, we compare the output of this algorithm with different climate data produced on the historical by the climate models taking part of the 5^{th} phase of the CMIP. A general observation is the poorer performance of the model in the North Indian basin. This could be due to the smaller number of intense cyclones remaining in the sample after the filtration by intensity (1.6 storms per year with wind exceeding 35 m.s^{-1}).

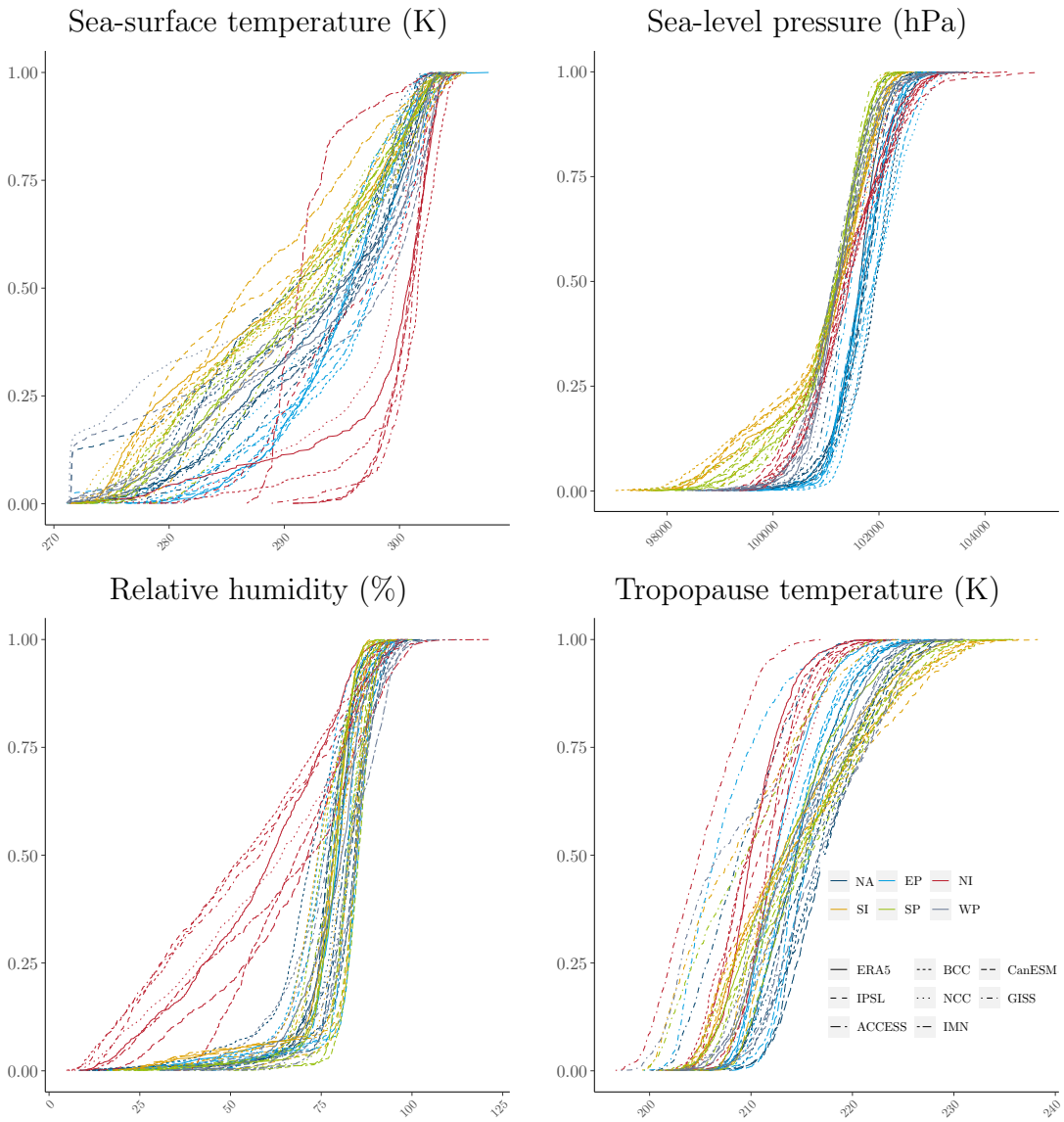

Figure 5.B.7 – Cumulative distribution functions per basin for the variables of interest along synthetic tracks produced with ERA-5 and extracted (at the same location) from climate data produced by the 7 climate models.

Note: NA: North America, EP: East Pacific, NI: North Indian, SI: South Indian, SP: South Pacific, WP: West Pacific. The bias-correction module is indeed fitted on a larger range of climate conditions. By definition, for the genesis of the cyclones, the time of year and location are in line with historical cyclone data. However, in the bias-correction module, the synthetic tracks are generated without climate constraints, i.e. cyclones are allowed to drift relatively far away from their genesis location (in the limits of their initial basin), and therefore can cover conditions which do not lead to the formation of tropical cyclones. At this stage, these tracks are not to be considered as 'TCs tracks' but as 'candidate' tracks. In the following stage, TC tracks will be generated from candidate tracks by filtering those ones where meteorologiocal conditions for cyclone formation are satisfied.

Figure 5.B.8 – Average impact on 10 year sovereign yields

(a) Top 55 most damaging events (relative) (b) Top 5 events (absolute)

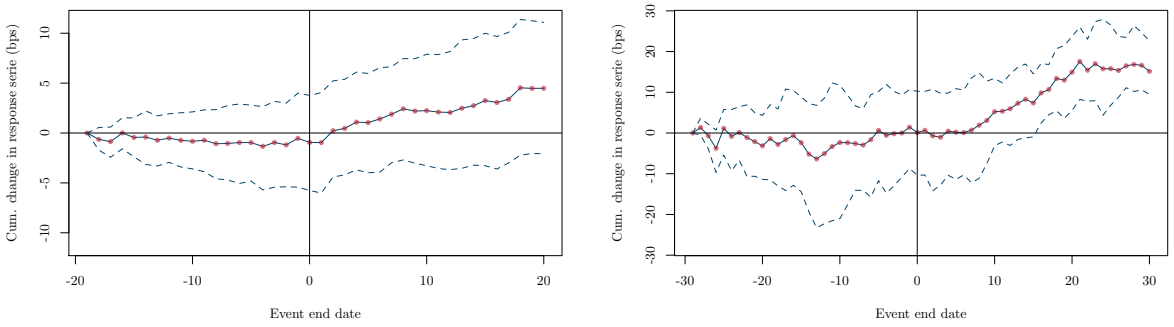

Top 100 most costly events matching 55 series. The event time is date end of the event reported by EMDAT the window is 30 days. The series are controlled using constant mean correction.

5.C Supplementary Tables

Table 5.C.1 – EM-DAT reporting proportions*

	Total Damages (US$)	Total Deaths	Insured (US$)	Total Affected	RCs** (US$)
Ash fall	0,12%	1,09%	0,00%	0,09%	0,00%
Avalanche	0,02%	0,20%	0,02%	0,00%	0,00%
Coastal flood	0,30%	0,14%	0,14%	0,32%	0,00%
Cold wave	0,37%	0,70%	0,51%	0,25%	0,00%
Convective storm	9,86%	0,68%	21,78%	4,51%	0,00%
Drought	5,29%	24,75%	2,58%	36,35%	0,00%
Extra-tropical storm	1,60%	0,02%	3,09%	0,06%	3,31%
Flash flood	2,07%	2,58%	1,18%	3,03%	0,00%
Forest fire	2,45%	0,08%	3,86%	0,09%	0,76%
Ground movement	16,75%	26,78%	6,59%	2,61%	87,07%
Heat wave	0,68%	7,09%	0,03%	0,08%	0,00%
Land fire***	0,80%	0,03%	1,76%	0,02%	0,00%
Landslide	0,14%	1,04%	0,01%	0,15%	0,00%
Lava flow	0,02%	0,00%	0,00%	0,01%	0,00%
Mudslide	0,10%	0,21%	0,00%	0,02%	0,00%
Pyroclastic flow	0,01%	0,02%	0,00%	0,03%	0,00%
Riverine flood	16,61%	5,20%	6,59%	38,68%	4,46%
Rockfall	0,00%	0,02%	0,00%	0,00%	0,00%
Severe winter cond.	0,74%	0,16%	0,20%	1,27%	0,00%
Subsidence	0,00%	0,01%	0,00%	0,00%	0,00%
Tropical cyclone	**34,26%**	**18,33%**	**45,64%**	**12,34%**	2,23%
Tsunami	7,81%	10,87%	6,01%	0,11%	2,16%

Notes:
* Proportion exclude damages which sub types are not reported.
** RC: Reconstruction costs are not well reported over disaster subtypes.
*** Brush, Bush, Pasture
Among disasters subtypes, tropical cyclones present an higher quality in reporting and represent a large share of total damages.

Table 5.C.2 – Wind pressure relationships coefficients

Basin	Coefficient	estimate	std error
EP	a	5.181	0.023
EP	b	0.550	0.001
NA	a	4.020	0.037
NA	b	0.589	0.002
NI	a	3.707	0.065
NI	b	0.632	0.005
SI	a	3.012	0.016
SI	b	0.653	0.001
SP	a	2.935	0.025
SP	b	0.660	0.002
WP	a	3.652	0.011
WP	b	0.598	0.001

Table 5.C.3 – Comparison STORM-CATHERINA cyclone intensification module

	STORM	CATHERINA
Nb of variables	2	4
MDP definition	SST-MPD relationship - Eq. (4) 0.25x0.25 0.1°C bins	SST-MPD relationship - Eq. (4) basin 0.1°C bins
MDP use	Infer MPI	Cap basin pres. drop
MPI definition	MPI = P^{env} – MPD	Holland (1997)
Unrealistic values	Bister and Emanuel (2002)	MPD

Table 5.C.4 – Mean of the maximum wind speed of synthetic cyclones in representative representation pathways

	RCP26	RCP45	RCP85
ACCESS1-0 (BoM-CSIRO, Australia)		66.42	70.21
bcc-csm1-1-m (BCC, China)	65.65	71.00	71.91
CanESM2 (CCCMA, Canada)	59.22		66.70
GISS-E2-H (NASA, USA)		71.79	75.02
inmcm4 (INM, Russia)		61.42	64.70
IPSL-CM5A-MR (IPSL, France)	60.70	63.89	69.61
NorESM1-ME (NCC, Norway)	57.40	59.02	63.32
Mean	60.74	65.59	68.78

Table 5.C.5 – Mapping countries to IIASA regions

admin	REGION	admin	REGION
Mexico	R32MEX	Australia	R32ANUZ
United States of America	R32USA	Madagascar	R32SSA-L
Canada	R32CAN	Mozambique	R32SSA-L
Cuba	R32LAM-M	South Africa	R32SSA-L
Haiti	R32LAM-L	United Republic of Tanzania	R32SSA-L
Dominican Republic	R32LAM-M	Indonesia	R32IDN
Mauritania	R32LAM-M	Mauritius	R32SSA-M
Nicaragua	R32LAM-L	France	R32EU15
Guatemala	R32LAM-L	Malawi	R32SSA-L
Belize	R32LAM-L	Zimbabwe	R32SSA-L
Venezuela	R32LAM-M	Swaziland	R32SSA-L
Honduras	R32LAM-L	Lesotho	R32SSA-L
Jamaica	R32LAM-M	Zambia	R32SSA-L
Puerto Rico	R32LAM-M	Comoros	R32SSA-L
Costa Rica	R32LAM-M	New Zealand	R32ANUZ
The Bahamas	R32LAM-M	Vanuatu	R32OAS-L
El Salvador	R32LAM-M	Fiji	R32OAS-L
Panama	R32LAM-M	Solomon Islands	R32OAS-L
Colombia	R32LAM-M	New Caledonia	R32EU15
Grenada	R32LAM-M	French Polynesia	R32EU15
Antigua and Barbuda	R32LAM-M	Papua New Guinea	R32OAS-L
Barbados	R32LAM-M	Wallis and Futuna	R32EU15
Cape Verde	R32SSA-L	Cambodia	R32OAS-CPA
India	R32IND	Thailand	R32OAS-L
Pakistan	R32PAK	Laos	R32OAS-CPA
Bangladesh	R32OAS-L	Vietnam	R32OAS-CPA
Oman	R32MEA-H	South Korea	R32KOR
United Arab Emirates	R32MEA-H	Japan	R32JPN
Iran	R32MEA-M	Russia	R32RUS
Myanmar	R32OAS-L	Philippines	R32OAS-L
Nepal	R32OAS-L	Taiwan	R32TWN
Yemen	R32MEA-M	North Korea	R32OAS-L
Saudi Arabia	R32MEA-H	United States of America	R32USA
Qatar	R32MEA-H	Mongolia	R32OAS-CPA
Kuwait	R32MEA-H	Hong Kong S.A.R.	R32CHN
Iraq	R32MEA-M	Federated States of Micronesia	R32OAS-L
Sri Lanka	R32OAS-M	Macao S.A.R	R32CHN
Afghanistan	R32PAK	Guam	R32OAS-M
China	R32CHN	Malaysia	R32OAS-M

Table 5.C.6 – Example of Country statistics ($\alpha_1 = 1$, $\alpha_2 = 1$)

	SSP	Config	Mean	Std. error	per50	per66	per75	per95
AUS	SSP2	RCP26	13.19	2.46	0.01	0.24	1.26	41.36
		RCP45	22.88	3.10	0.07	0.88	3.35	99.62
		RCP85	24.57	3.51	0.06	0.95	3.59	85.48
	SSP3	RCP26	6.37	1.21	0.01	0.11	0.59	19.47
		RCP45	10.85	1.47	0.04	0.40	1.46	46.30
		RCP85	11.55	1.68	0.03	0.44	1.55	36.53
	SSP4	RCP26	11.79	2.21	0.01	0.21	1.12	36.01
		RCP45	20.27	2.74	0.06	0.77	2.83	87.33
		RCP85	21.71	3.12	0.05	0.85	3.11	73.63
	SSP5	RCP26	25.14	4.66	0.02	0.49	2.62	79.28
		RCP45	44.76	6.17	0.15	1.83	7.12	202.33
		RCP85	48.46	6.82	0.13	2.04	7.42	170.75
CHN	SSP2	RCP26	8.67	0.73	1.42	3.19	5.70	46.16
		RCP45	10.12	0.56	2.32	6.08	10.25	46.55
		RCP85	13.14	0.79	3.06	7.52	12.48	64.57
	SSP3	RCP26	7.31	0.60	1.27	2.87	4.71	39.87
		RCP45	8.68	0.48	2.10	5.40	9.06	39.45
		RCP85	11.26	0.67	2.82	6.77	11.17	53.47
	SSP4	RCP26	5.15	0.44	0.81	1.84	3.17	26.53
		RCP45	5.84	0.33	1.29	3.43	5.71	27.61
		RCP85	7.56	0.46	1.67	4.35	7.05	38.88
	SSP5	RCP26	13.48	1.16	2.07	4.84	8.52	73.92
		RCP45	15.75	0.89	3.46	9.17	15.86	72.24
		RCP85	20.51	1.26	4.63	11.28	19.06	100.22
JPN	SSP2	RCP26	2.40	0.22	0.28	0.87	1.48	12.27
		RCP45	2.87	0.23	0.33	1.03	2.01	14.08
		RCP85	3.78	0.34	0.54	1.44	2.80	18.06
	SSP3	RCP26	1.38	0.12	0.19	0.57	0.91	7.08
		RCP45	1.63	0.13	0.23	0.66	1.22	7.77
		RCP85	2.16	0.18	0.37	0.96	1.70	10.13
	SSP4	RCP26	2.10	0.19	0.24	0.76	1.29	10.54
		RCP45	2.50	0.21	0.29	0.90	1.70	12.36
		RCP85	3.28	0.29	0.47	1.24	2.37	15.52
	SSP5	RCP26	4.57	0.43	0.51	1.63	2.85	21.28
		RCP45	5.55	0.44	0.64	1.99	4.02	27.04
		RCP85	7.32	0.68	1.02	2.87	5.49	33.72
MEX	SSP2	RCP26	9.18	0.91	0.52	2.41	5.26	50.38
		RCP45	12.11	0.92	1.19	4.30	8.29	71.05
		RCP85	15.54	1.15	2.06	6.47	11.93	80.18
	SSP3	RCP26	9.63	0.96	0.56	2.68	5.68	53.54
		RCP45	12.94	0.98	1.32	4.74	9.07	72.48
		RCP85	16.65	1.23	2.25	7.10	12.32	87.09
	SSP4	RCP26	4.76	0.48	0.27	1.23	2.67	28.14
		RCP45	6.11	0.46	0.62	2.04	4.29	34.82
		RCP85	7.72	0.59	1.00	3.07	5.77	38.43
	SSP5	RCP26	10.91	1.09	0.56	2.66	5.86	61.01
		RCP45	14.08	1.09	1.30	4.69	9.41	81.86
		RCP85	18.09	1.36	2.24	7.07	13.52	93.66
USA	SSP2	RCP26	131.80	13.76	17.99	51.49	88.19	588.12
		RCP45	150.20	10.45	26.06	64.81	120.59	747.43
		RCP85	210.89	14.22	39.68	93.71	176.39	1 078.51
	SSP3	RCP26	82.27	8.83	10.46	31.31	52.37	372.94
		RCP45	92.22	6.61	14.40	39.85	72.11	455.65
		RCP85	127.71	8.73	22.04	53.80	101.54	661.06
	SSP4	RCP26	115.13	12.16	15.28	44.81	76.52	512.94
		RCP45	130.25	9.18	21.91	56.20	103.88	649.04
		RCP85	181.86	12.32	32.58	79.12	148.01	944.76
	SSP5	RCP26	258.84	26.45	38.70	102.77	183.70	1 085.39
		RCP45	301.50	20.48	51.24	133.52	249.84	1 450.39
		RCP85	430.81	29.13	81.24	197.55	386.07	2 107.37

General Conclusion

This work attempts to bring quantitative bottom-up and structural methodologies to an issue that requires urgent immediate action backed by academic research at different levels. This project was conducted with the hope of having a positive impact on these different aspects, by working in parallel on different time horizons. First, it is urgent to reduce greenhouse gases emissions implied by our activity. To this end, the (immediate) implementation of a system of control of absolute emission and intensity trajectories is a possibility that has been explored during this research project in related work, i.e., Le Guenedal *et al.* (2020) and Le Guenedal, Lombard, *et al.* (2022). Second, our society must adapt to the warmer (and more variable climate) we can no longer avoid, and understand the financial risk related to the transition towards a greener economy in the medium-term. At this horizon, we focused solely on the transition dimension, through different angles. Finally, it is also urgent to measure the climate risk that can still be avoided in the long-term (to support the implementation of immediate action). The chapters of this thesis therefore bring elements of answers to the research questions presented in the introduction in order to better apprehend and quantify the transition and physical risks on the basis of explicit methodologies.

In this thesis, the transition is approached through the exposure of companies while the physical risks are measured at the state level. Beyond the operational constraints of data availability of the production sites, value-chain information and other, it is a question of putting the right agents in front of the right issues. Companies will have to reduce their GHG emissions or face a (transition-related) business risk in the relatively short or medium term if governments implement carbon regulation. Due to their nature, companies are (relatively) incapable of integrating (very) long term projections, it is therefore difficult to transpose scenario-based physical risks to them, given that substantial divergences between representative concentration scenarios are only observed over horizons of at least twenty years. The physical risks encountered by companies in the next decade are growing '*meteorological*' risks,[25] whose likelihood and intensity will increase regardless of the action undertaken because of climate inertia. Companies can therefore measure their exposure to natural disasters on a 'meteorological' level, but it is more difficult to include the time horizons necessary to integrate a 'climatic' sensitivity in their business plan. Concerning corporate physical risk, it would make sense to concentrate the effort on asset specific expertise, allowing companies to adapt to the rapidly changing conditions, rather than introducing a systematic explicit methodology. The first three questions are therefore dedicated to improving the understanding of companies' transition risks and their financial implications.

On the other hand, imposing transition risks on countries would be counterproductive, since

25. Strictly speaking, in climate science, it is more correct to speak about meteorology rather than climatology for shorter time periods (< 20 years).

they are already not doing enough to reduce global warming. Nevertheless, states are supposed to be able to integrate a slower signal, especially if it implies important costs which are not extremely far away, but may materialize already for the next generation. Therefore, it seems appropriate to measure the physical damage that will be incurred at the level of individual countries, if they do not put in place the necessary mitigation and adaptation measures, in order to push them to do so. However, there is a lack of standards in physical risks assessment methodologies applicable to all countries. Each country, if not region or city, compute their sensitivity to climate change using different events and asset inventories, providing inhomogeneous signals hardly usable in decision making or pricing models. The last question therefore aims at harmonizing physical risk assessment modeling by first defining extreme event intensity, then computing and projecting asset exposure and finally designing region-specific damage functions to draw Monte-Carlo simulation of future losses.

Question 1 ***How to compute a structural measure of firms' idiosyncratic credit risk sensitivity to transition risk, that does not use expert opinions but rather carbon price trajectories suggested by integrated assessment models?*** The first chapter, aims at providing an answer to this first question which arose in a context where little was known about climate risk. We show that transition risk can be simply modeled as any other financial risk, using essentially the same tools (i.e. Merton, 1974 model). This first work shows that a large number of Utilities companies are not profitable in the most ambitious transition context (1.5°C), and implies that it is necessary to support them in the conversion to greener technology. However, we also show that the rest of the economy could sustain carbon prices suggested by the integrated assessment models to reach the 1.8°C scenario with credit risk level below the global financial crisis level. On the other hand, the lack of diffusion of the risk among other sectors in the real economy is the main limitation of this paper, which therefore raises the second question.

Question 2 ***How to compute the transition risk contributions among sectors with a better consideration of cascading effects through supply-chain but also firm-level direct carbon emissions?*** Financial studies focus on economic sensitivities (top-down) and interbank dependencies. However, it seems crucial to integrate the real economy supply-chain more explicitly to model transition risk. Developing research on this axis has several objectives. First, the accounting of carbon scopes is still not mature. As a result, the data (in particular scope 3) remains highly uncertain, which raises questions about the risk of numerical machine learning methodologies based on input of uneven quality. It is therefore essential to introduce structural methods as much as possible to identify sector-country risk carbon contributions in a more transparent manner. The integrated calculation method used here has the advantage of identifying the indirect upstream emissions in a relatively clear and precise manner given the granularity of the database (despite the residual updating or mapping problems). To go further, it is possible to improve this diffusion matrix with real supply-chain data, at company level. Second, the direct shock measure introduced in Chapter 2 and the one introduced in Chapter 3 are complementary because they represent two extreme cases of carbon cost pass-trough (0 and 1). Therefore, in the context of this project, we shed light on tow complementary dimensions of the transition risk: direct exposure and credit risk sensibility and supply-chain effect.

Question 3 ***How to account for scenario uncertainty, gradually lifted by the observation of jumps in carbon price, in the pricing of the corporate debt?*** Uncertainty around the possible materiality of transition risks is growing given the inconsistent signals from

the states. For example, the *withdrawal and reacceptance of the Paris Agreement by the US; the introduction and repeal of the Australian carbon tax; the EU rapid withdrawal from clean energy subsidies* (Campiglio *et al.*, 2022) or the canceling of the scheduled jump from EUR 44.6 to 55 per ton of CO_2e in France following the yellow vest movement in 2019. On the other hand, current approaches to transition risk assessment are limited to univariate stress tests introducing a carbon price (possibly at a given time horizon), without taking into account the probability of this scenario occurring. Based on Agliardi and Agliardi (2021), Leland (1994), and Leland and Toft (1996) and classical bond pricing literature, we show the importance of scenario information for bond pricing in the context of environmental transition: we find that insufficient information about future carbon prices and slow information discovery may lead to overpricing of defaultable bonds and potentially painful market-wide default or repricing events when information is finally discovered.

Question 4.a ***How to built database of depressions (tropical-cyclones 'candidate') that would be compatible with Monte-Carlo financial risk assessment from broadly available climate data?*** The main method lies on probability maps and assumptions on the impact of global warming on changes in return periods of each category in the Saffir–Simpson wind scale. To better integrate the output of general circulation models (GCMs), one could use machine learning to determine the probability of extreme events occurring in a set a given climate conditions in the reanalysis, then apply the algorithm in climate projections. However, in order to capture cyclone sensitivity to climate change in a transparent manner, we decided to introduce a thermodynamic instrumental variable in our description of cyclone intensification. Based on a rich literature, we build a model generating synthetic tracks directly from the output of the climate models participating the Couple Model Intecomparison Project (CMIP).

Question 4.b ***How to define physical asset exposure in such a way that (i) it represents sufficiently well real local asset value (ii) it can be projected in shared-socioeconomic scenarios?*** The two requirements are in fact incompatible. A good representation of assets requires the introduction of geolocated infrastructures. On the other hand, these infrastructure values cannot be projected into the representative concentration scenarios because in practice most of them will no longer exist within 30 years (which is the minimum time horizon required to study various climate scenarios due to climate inertia). We therefore chose to use a dataset constructed during the CLIMADA project based on light intensity and the other macroeconomic and population indicators. This dataset has the advantage of being compatible with projections in socio-economic scenarios, taking into account several assumptions about adaptation.

Question 4.c/d ***How to compute damage related to tropical cyclone along synthetic tracks? What might be the impact of the annualized tropical cyclone-related damages on emerging countries spread?*** Regarding damages, the CLIMADA project allows to answer this question. However, the inclusion in a pricing model is more complex. Whereas equity markets, which are more liquid, do price extreme events, sovereign debt markets have historically been less reactive. We have therefore chosen to focus on a forward-looking measure by assimilating the costs of future damages to potential debt to channel the impact of cyclones to the debt of countries.

Bibliography

2 Investing Initiative. (2018). *Insurance Companies Operating in California*. 2 Investing Initiative.

ACPR. (2020). *Scenarios and main assumptions of the ACPR pilot climate exercise*. Autorité de contrôle prudentiel et de résolution.

ACPR-AMF. (2020). *Les engagements climatiques des institutions financières françaises*. Autorité de contrôle prudentiel et de résolution, Autorité des marchés financiers.

Adenot, T., Briere, M., Counathe, P., Jouanneau, M., Le Berthe, T., & Le Guenedal, T. (2022). *Cascading Effects of Carbon Price Through the Value Chain: Impact on Firm's Valuation. Available at SSRN*.

Aerts, J. C., Botzen, W. W., Emanuel, K., Lin, N., De Moel, H., & Michel-Kerjan, E. O. (2014). *Evaluating flood resilience strategies for coastal megacities. Science*, *344*(6183), 473–475.

Agliardi, E., & Agliardi, R. (2021). *Pricing climate-related risks in the bond market. Journal of Financial Stability*, *54*, 100868.

Albert, R., Albert, I., & Nakarado, G. L. (2004). *Structural vulnerability of the North American power grid. Physical review E*, *69*(2), 025103.

Alessi, L., & Battiston, S. (2022). *Two sides of the same coin: Green Taxonomy alignment versus transition risk in financial portfolios. International Review of Financial Analysis*, 102319.

Alessi, L., Battiston, S., & Kvedaras, V. (2021). *Over with carbon? Investors' reaction to the Paris Agreement and the US withdrawal*. JRC Working Papers in Economics and Finance.

Allen, T., Dees, S., Caicedo Graciano, C. M., Chouard, V., Clerc, L., de Gaye, A., Devulder, A., Diot, S., Lisack, N., Pegoraro, F., et al. (2020). *Climate-related scenarios for financial stability assessment: An application to France*.

Alogoskoufis, S., Dunz, N., Emambakhsh, T., Hennig, T., Kaijser, M., Kouratzoglou, C., Muñoz, M. A., Parisi, L., Salleo, C., et al. (2021). *ECB's economy-wide climate stress test*. European Central Bank.

Andersson, M., Bolton, P., & Samama, F. (2016). *Hedging climate risk. Financial Analysts Journal*, *72*(3), 13–32.

Apergis, N., Poufinas, T., & Antonopoulos, A. (2022). *ESG scores and cost of debt. Energy Economics*, 106186.

Arthur, W. C. (2021). *A statistical–parametric model of tropical cyclones for hazard assessment. Natural Hazards and Earth System Sciences*, *21*(3), 893–916.

Aubert, M., William, B., Sébastien, D., Vernet, L., et al. (2019). *Les groupes bancaires français face au risque climatique*. Banque de France.

Auffhammer, M. (2018). *Quantifying economic damages from climate change. Journal of Economic Perspectives*, *32*(4), 33–52.

Aznar Siguan, G., & Bresch, D. N. (2019). *CLIMADA v1: a global weather and climate risk assessment platform. Geoscientific Model Development*, *12*, 3085–3097.

Babiker, M. H., Reilly, J. M., Mayer, M., Eckaus, R. S., Sue Wing, I., & Hyman, R. C. (2001). *The MIT emissions prediction and policy analysis (EPPA) model: revisions, sensitivities, and comparisons of results.*

Bachmair, S., Svensson, C., Prosdocimi, I., Hannaford, J., & Stahl, K. (2017). *Developing drought impact functions for drought risk management. Natural Hazards and Earth System Sciences*, *17*(11), 1947–1960.

Baker, M., Bergstresser, D., Serafeim, G., & Wurgler, J. (2018). *Financing the response to climate change: The pricing and ownership of US green bonds.* National Bureau of Economic Research.

Baker, M., Bradley, B., & Wurgler, J. (2011). *Benchmarks as limits to arbitrage: Understanding the low-volatility anomaly. Financial Analysts Journal*, *67*(1), 40–54.

Bakkensen, L. A., & Mendelsohn, R. O. (2019). *Global tropical cyclone damages and fatalities under climate change: An updated assessment. Hurricane risk* (pp. 179–197). Springer.

Bank of England. (2015). *The impact of climate change on the UK insurance sector.* Bank of England.

Bank of England. (2017). *The Bank of England's response to climate change.* Bank of England.

Bantwal, V. J., & Kunreuther, H. C. (2000). *A cat bond premium puzzle? The Journal of Psychology and Financial Markets*, *1*(1), 76–91.

Barradale, M. J. (2014). *Investment under uncertain climate policy: A practitioners' perspective on carbon risk. Energy policy*, *69*, 520–535.

Basel Committee on Banking Supervision. (2021). *Climate-Related Risk Drivers and Their Transmission Channels.*

Basel Committee on Banking Supervision. (2022). *Principles for the effective management and supervision of climate-related financial risks.*

Batten, S., Sowerbutts, R., & Tanaka, M. (2016). *Let's talk about the weather: the impact of climate change on central banks.*

Battiston, S., Jakubik, P., Monasterolo, I., Riahi, K., & van Ruijven, B. (2019). *Climate risk assessment of the sovereign bond portfolio of European insurers. Financial Stability Report.*

Battiston, S., Mandel, A., Monasterolo, I., Schütze, F., & Visentin, G. (2017). *A climate stress-test of the financial system. Nature Climate Change*, *7*(4), 283–288.

Battiston, S., & Monasterolo, I. (2019). *A climate risk assessment of sovereign bonds' portfolio. University of Milan Bicocca Department of Economics, Management and Statistics Working Paper*, (420).

Beirne, J., Renzhi, N., & Volz, U. (2020). *Feeling the heat: Climate risks and the cost of sovereign borrowing.*

Ben Slimane, M., Brard, E., Le Guenedal, T., Roncalli, T., & Sekine, T. (2019a). *ESG Investing in Fixed Income: It's Time to Cross the Rubicon. Eric and Le Guenedal, Théo and Roncalli, Thierry and Sekine, Takaya, ESG Investing in Fixed Income: It's Time to Cross the Rubicon (November 30, 2019).*

Ben Slimane, M., Da Fonseca, D., & Mahtani, V. (2020). *Facts and fantasies about the green bond premium*. Working Paper 102-2020. Amundi. https://research-center. amundi. com/files ...

Ben Slimane, M., Le Guenedal, T., Roncalli, T., & Sekine, T. (2019b). *ESG Investing in Corporate Bonds: Mind the Gap. Amundi Working Paper, WP-94*.

Bennani, L., Le Guenedal, T., Lepetit, F., Ly, L., Mortier, V., & Sekine, T. (2018). *The alpha and beta of ESG investing. URL: http://research-center. amundi. com. Amundi working paper, 76*.

Bensoussan, A., & Lions, J.-L. (2011). Applications Of Variational Inequalities In Stochastic Control. Elsevier.

Berner, R., Engle, R., Jung, H., et al. (2021). *Climate Stress Testing*.

Bister, M., & Emanuel, K. A. (2002). *Low frequency variability of tropical cyclone potential intensity 1. Interannual to interdecadal variability. Journal of Geophysical Research: Atmospheres, 107*(D24), ACL–26.

Black, F., & Cox, J. C. (1976). *Valuing corporate securities: Some effects of bond indenture provisions. The Journal of Finance, 31*(2), 351–367.

Bloemendaal, N., Haigh, I. D., de Moel, H., Muis, S., Haarsma, R. J., & Aerts, J. C. (2020). *Generation of a global synthetic tropical cyclone hazard dataset using STORM. Scientific Data, 7*(1), 1–12.

Bolton, P., Despres, M., Da Silva, L. A. P., Samama, F., Svartzman, R., et al. (2020). *The green swan. BIS Books*.

Bolton, P., & Kacperczyk, M. (2021). *Do investors care about carbon risk? Journal of financial economics, 142*(2), 517–549.

Bouchet, V., Dayan, H., & Contoux, C. (2022). *Finance and climate science: worlds apart? Journal of Risk Research, 25*(2), 176–197.

Bouchet, V., & Le Guenedal, T. (2020a). *Carbon Price sensitivity and Credit Risk*.

Bouchet, V., & Le Guenedal, T. (2022). *Sensibilité du risque de crédit au prix du carbone. Revue économique, 73*(2), 151–172.

Bouchet, V., & Le Guenedal, T. (2020b). *Credit Risk Sensitivity to Carbon Price. Available at SSRN 3574486*.

Brémaud, P. (1981). Point Processes And Queues: Martingale Dynamics. Springer.

Bresch, D. N. (2017). *CLIMADA-the open-source and-access global probabilistic risk modelling platform*.

Bressan, G., Duranovic, A., Monasterolo, I., & Battiston, S. (2022). *Asset-level climate physical risk assessment and cascading financial losses. Available at SSRN*.

Bretz, L. (2017). *Climate Change and Homes: Who Would Lose the Most to a Rising Tide? Zillow Research*.

Brooks, H. E. (2013). *Severe thunderstorms and climate change. Atmospheric research, 123*, 129–138.

Bruyère, C., Holland, G., Prein, A., Done, J., Buckley, B., Chan, P., Leplastrier, M., & Dyer, A. (2019). *Severe weather in a changing climate. Insurance Australia Group and National Center for Atmospheric Research, November*. https://www.iag.com.au/sites/default/files/documents/Severe-weather-in-a-changing-climate-report-011119.pdf

Butchart, N., Austin, J., Knight, J. R., Scaife, A. A., & Gallani, M. L. (2000). *The response of the stratospheric climate to projected changes in the concentrations of well-mixed greenhouse gases from 1992 to 2051. Journal of climate*, *13*(13), 2142–2159.

Byers, L., Friedrich, J., Hennig, R., Kressig, A., Li, X., McCormick, C., & Valeri, L. M. (2018). *A global database of power plants. World Resour. Inst*, *18*.

Cahen-Fourot, L., Campiglio, E., Dawkins, E., Godin, A., & Kemp-Benedict, E. (2019). *Capital stranding cascades: The impact of decarbonisation on productive asset utilisation*.

Caldecott, B. (2017). *Introduction to special issue: stranded assets and the environment. Journal of Sustainable Finance & Investment*, *7*(1), 1–13. https://doi.org/10.1080/20430795.2016.1266748

Caldecott, B., Harnett, E., Cojoianu, T., Kok, I., & Pfeiffer, A. (2016). *Stranded assets: a climate risk challenge*.

Caldecott, B., Howarth, N., & McSharry, P. (2013). *Stranded assets in agriculture: Protecting value from environment-related risks*.

Caldecott, B., Kruitwagen, L., Dericks, G., Tulloch, D. J., Kok, I., & Mitchell, J. (2016). *Stranded Assets and Thermal Coal: An analysis of environment-related risk exposure. Stranded Assets Programme, SSEE, University of Oxford*.

Calvet, L., & Marical, F. (2012). *Consommation de carburant : effets des prix à court et à long terme par type de population. INSEE*. https://www.insee.fr/fr/statistiques/1377454?sommaire=1377458

Cambridge Econometrics. (2019). *E3ME technical manual v6. 1. Version March*.

Campiglio, E. (2016). *Beyond carbon pricing: The role of banking and monetary policy in financing the transition to a low-carbon economy. Ecological economics*, *121*, 220–230.

Campiglio, E., Dafermos, Y., Monnin, P., Ryan-Collins, J., Schotten, G., & Tanaka, M. (2018). *Climate change challenges for central banks and financial regulators. Nature Climate Change*, *8*(6), 462.

Campiglio, E., Lamperti, F., & Terranova, R. (2022). *Believe me when I say green! Heterogeneous expectations and climate policy uncertainty. GRASFI 2022, Zurich*.

Carhart, M. M. (1997). *On persistence in mutual fund performance. The Journal of finance*, *52*(1), 57–82.

Carney, M. (2015). *Breaking the Tragedy of the Horizon–climate change and financial stability. Speech given at Lloyd's of London*, *29*, 220–230.

Cartellier, F. (2022). *Climate Stress Testing, an answer to the challenge of assessing climate-related risks to the financial system ? Available at SSRN*.

Center for International Earth Science Information Network (CIESIN). (2017). *Documentation for the gridded population of the world, Version 4 (GPWv4), Revision 10 Data Sets*.

Chen, G., Li, X., Liu, X., Chen, Y., Liang, X., Leng, J., Xu, X., Liao, W., Wu, Q., Huang, K., et al. (2020). *Global projections of future urban land expansion under shared socioeconomic pathways. Nature communications*, *11*(1), 1–12.

Chen, N., & Kou, S. G. (2009). *Credit spreads, optimal capital structure, and implied volatility with endogenous default and jump risk. Mathematical Finance: An International Journal of Mathematics, Statistics and Financial Economics*, *19*(3), 343–378.

Chen, Y., Gao, S., Li, X., & Shen, X. (2021). *Key Environmental Factors for Rapid Intensification of the South China Sea Tropical Cyclones. Frontiers in Earth Science*, *8*, 727.

Chen, Y.-H. H., Paltsev, S., Gurgel, A., Reilly, J., & Morris, J. (2022). *The MIT EPPA7: A Multisectoral Dynamic Model for Climate Policy Analysis*.

Chen, Y.-H., Paltsev, S., Reilly, J. M., Morris, J. F., & Babiker, M. H. (2015). *The MIT EPPA6 model: Economic growth, energy use, and food consumption*. MIT Joint Program on the Science and Policy of Global Change.

Chenet, H., Ryan-Collins, J., & Van Lerven, F. (2019). *Climate-related financial policy in a world of radical uncertainty: Towards a precautionary approach. UCL Institute for Innovation and Public Purpose WP*, *13*.

Colas, J., Khaykin, I., Pyanet, A., & Westheim, J. (2018). *Extending our horizons. Assessing credit risk and opportunity in a changing climate: Outputs of a working group of 16 banks piloting the TCFD Recommendations*. UNEP Finance Initiative - Oliver Wyman.

Cont, R., & Tankov, P. (2003). Financial Modelling With Jump Processes. Chapman; Hall/CRC.

Cont, R., & Voltchkova, E. (2005). *A finite difference scheme for option pricing in jump diffusion and exponential Lévy models. SIAM Journal on Numerical Analysis*, *43*(4), 1596–1626.

Coronese, M., Lamperti, F., Keller, K., Chiaromonte, F., & Roventini, A. (2019). *Evidence for sharp increase in the economic damages of extreme natural disasters. Proceedings of the National Academy of Sciences*, *116*(43), 21450–21455.

Courtney, J. (2009). *Adapting the Knaff and Zehr wind-pressure relationship for operational use in Tropical Cyclone Warning Centres. Australian Meteorological and Oceanographic Journal*, *58*(3), 167.

Courtney, J., & Burton, A. (2018). *Joint Industry Project for Objective Tropical Cyclone Reanalysis: Final Report. Bureau of Meteorology, 87pp*.

Courtney, J. B., Foley, G. R., van Burgel, J. L., Trewin, B., Burton, A. D., Callaghan, J., & Davidson, N. E. (2021). *Revisions to the Australian tropical cyclone best track database. Journal of Southern Hemisphere Earth Systems Science*, *71*(2), 203–227.

Cox, P. M., Huntingford, C., & Williamson, M. S. (2018). *Emergent constraint on equilibrium climate sensitivity from global temperature variability. Nature*, *553*(7688), 319–322.

Credit Suisse. (2017). *Credit Suisse Research Institute: Global Wealth Report 2017*. https://www.credit-suisse.com/about-us-news/en/articles/news-and-expertise/global-wealth-report-2017-201711.html

Crompton, R. P., & McAneney, K. J. (2008). *Normalised Australian insured losses from meteorological hazards: 1967–2006. Environmental Science & Policy*, *11*(5), 371–378.

Crowther, T. W., Glick, H. B., Covey, K. R., Bettigole, C., Maynard, D. S., Thomas, S. M., Smith, J. R., Hintler, G., Duguid, M. C., Amatulli, G., et al. (2015). *Mapping tree density at a global scale. Nature*, *525*(7568), 201–205.

Daniel, K. D., Litterman, R. B., & Wagner, G. (2019). *Declining CO2 price paths. Proceedings of the National Academy of Sciences*, *116*(42), 20886–20891.

Delis, M. D., De Greiff, K., & Ongena, S. (2019). *Being stranded with fossil fuel reserves? Climate policy risk and the pricing of bank loans. Climate Policy Risk and the Pricing of Bank loans (September 10, 2019). EBRD Working Paper*, (231).

DeMaria, M., & Kaplan, J. (1994). *A statistical hurricane intensity prediction scheme (SHIPS) for the Atlantic basin. Weather and Forecasting*, *9*(2), 209–220.

DeMaria, M., Knaff, J. A., & Connell, B. H. (2001). *A tropical cyclone genesis parameter for the tropical Atlantic. Weather and Forecasting*, *16*(2), 219–233.

Dey, A. (2022). *Surging Sovereign Spreads: The Impact of Coastal Flooding on Sovereign Risk. Available at SSRN 4058301.*

Dietz, S., Bowen, A., Dixon, C., & Gradwell, P. (2016). *'Climate value at risk' of global financial assets. Nature Climate Change*, *6*(7), 676.

Dimov, I., & Parsons, T. (2021). *Quantifying the impact of cyclones on equity returns of manufacturers. Bloomberg whitepaper.*

Donat, M., Leckebusch, G., Wild, S., & Ulbrich, U. (2011). *Future changes in European winter storm losses and extreme wind speeds inferred from GCM and RCM multi-model simulations. Natural Hazards and Earth System Sciences*, *11*(5), 1351–1370.

Drei, A., Le Guenedal, T., Lepetit, F., Mortier, V., Roncalli, T., & Sekine, T. (2019). *ESG investing in recent years: New insights from old challenges. Available at SSRN 3683469.*

Duan, T., Li, F. W., & Wen, Q. (2021). *Is carbon risk priced in the cross-section of corporate bond returns? Available at SSRN 3709572.*

Duenas-Osorio, L., & Vemuru, S. M. (2009). *Cascading failures in complex infrastructure systems. Structural safety*, *31*(2), 157–167.

Duffie, D., & Lando, D. (2001). *Term structures of credit spreads with incomplete accounting information. Econometrica*, *69*(3), 633–664.

Dunz, N., Emambakhsh, T., Hennig, T., Kaijser, M., Kouratzoglou, C., & Salleo, C. (2021). *ECB's Economy-Wide Climate Stress Test. ECB Occasional Paper*, (2021/281).

Eaton, J., & Gersovitz, M. (1981). *Debt with potential repudiation: Theoretical and empirical analysis. The Review of Economic Studies*, *48*(2), 289–309.

Eberenz, S., Lüthi, S., & Bresch, D. N. (2021). *Regional tropical cyclone impact functions for globally consistent risk assessments. Natural Hazards and Earth System Sciences*, *21*(1), 393–415.

Eberenz, S., Stocker, D., Röösli, T., & Bresch, D. N. (2019). *LitPop: Global Exposure Data for Disaster Risk Assessment.*

Eberenz, S., Stocker, D., Röösli, T., & Bresch, D. N. (2020). *Asset exposure data for global physical risk assessment. Earth Syst*, *12*. https://doi.org/10.5194/essd-12-817-2020

ECB. (2022). *Macro-financial scenarios for the 2022 climate risk stress test.* European Central Bank.

Edenhofer, O., Lessmann, K., Kemfert, C., Grubb, M., & Kohler, J. (2006). *Induced technological change: Exploring its implications for the economics of atmospheric stabilization: Synthesis report from the innovation modeling comparison project. The Energy Journal*, (Special Issue# 1).

Edwards, S. (1986). *The pricing of bonds and bank loans in international markets: An empirical analysis of developing countries' foreign borrowing. European Economic Review*, *30*(3), 565–589.

EIOPA. (2018). *Financial Stability Report.* European Insurance and Occupational Pensions Authority.

EIOPA. (2022). *Methodological principles of insurance stress testing - climate change component*. European Insurance and Occupational Pensions Authority.

Eliwa, Y., Aboud, A., & Saleh, A. (2021). *ESG practices and the cost of debt: Evidence from EU countries. Critical Perspectives on Accounting*, *79*, 102097.

Elsner, J., & Guishard, M. (2014). *Understanding How Climate Change Could Affect Tornadoes: First International Summit on Tornadoes and Climate Change; Crete, Greece, 25–30 May 2014*.

Elsner, J. B., Kossin, J. P., & Jagger, T. H. (2008). *The increasing intensity of the strongest tropical cyclones. Nature*, *455*(7209), 92–95.

Emanuel, K. A. (1988). *The maximum intensity of hurricanes. Journal of the Atmospheric Sciences*, *45*(7), 1143–1155.

Emanuel, K. A. (1991). *The theory of hurricanes. Annual Review of Fluid Mechanics*, *23*(1), 179–196.

Emanuel, K. A. (1999). *Thermodynamic control of hurricane intensity. Nature*, *401*(6754), 665–669.

Emanuel, K. A. (2005). *Increasing destructiveness of tropical cyclones over the past 30 years. Nature*, *436*(7051), 686–688.

Emanuel, K. A. (2011). *Global warming effects on US hurricane damage. Weather, Climate, and Society*, *3*(4), 261–268.

Emanuel, K., Sundararajan, R., & Williams, J. (2008). *Hurricanes and global warming: Results from downscaling IPCC AR4 simulations. Bulletin of the American Meteorological Society*, *89*(3), 347–368.

Engle, R. F., Giglio, S., Kelly, B., Lee, H., & Stroebel, J. (2020). *Hedging climate change news. The Review of Financial Studies*, *33*(3), 1184–1216.

ESMA. (2022). *Sustainable Finance Roadmap 2022-2024*. European Securities and Markets Authority.

Fabregat, A., Mezic, I., & Poje, A. C. (2016). *Finite-time partitions for lagrangian structure identification in Gulf Stream eddy transport. arXiv preprint arXiv:1606.07382*.

Faccini, R., Matin, R., & Skiadopoulos, G. S. (2021). *Dissecting Climate Risks: Are they Reflected in Stock Prices? Available at SSRN 3795964*.

Fama, E. F., & French, K. R. (1993). *Common risk factors in the returns on stocks and bonds. Journal of financial economics*, *33*(1), 3–56.

Fankhauser, S., Smith, S. M., Allen, M., Axelsson, K., Hale, T., Hepburn, C., Kendall, J. M., Khosla, R., Lezaun, J., Mitchell-Larson, E., et al. (2022). *The meaning of net zero and how to get it right. Nature Climate Change*, *12*(1), 15–21.

FEMA. (2009). *Multi-hazard loss estimation methodology: Flood model*.

Flora, M., & Tankov, P. (2022). *Green investment and asset stranding under transition scenario uncertainty. Available at SSRN 4006304*.

Forster, P. M., Bodeker, G., Schofield, R., Solomon, S., & Thompson, D. (2007). *Effects of ozone cooling in the tropical lower stratosphere and upper troposphere. Geophysical Research Letters*, *34*(23).

Gao, J. (2020). *Downscaling global spatial population projections from 1/8-degree to 1-km grid cells. Technical Notes NCAR, National Center for Atmospheric Researcher, Boulder, CO., USA*. https://doi.org/10.7927/q7z9-9r69

Geiger, T., Gütschow, J., Bresch, D. N., Emanuel, K., & Frieler, K. (2021). *Double benefit of limiting global warming for tropical cyclone exposure. Nature Climate Change*, *11*(10), 861–866.

Gemechu, E. D., Butnar, I., Llop, M., & Castells, F. (2014). *Economic and environmental effects of CO2 taxation: an input-output analysis for Spain. Journal of Environmental Planning and Management*, *57*(5), 751–768.

Gidden, M. J., Riahi, K., Smith, S. J., Fujimori, S., Luderer, G., Kriegler, E., van Vuuren, D. P., van den Berg, M., Feng, L., Klein, D., Calvin, K., Doelman, J. C., Frank, S., Fricko, O., Harmsen, M., Hasegawa, T., Havlik, P., Hilaire, J., Hoesly, R., ... Takahashi, K. (2019). *Global emissions pathways under different socioeconomic scenarios for use in CMIP6: a dataset of harmonized emissions trajectories through the end of the century. Geoscientific Model Development*, *12*(4), 1443–1475. https://doi.org/10.5194/gmd-12-1443-2019

Ginger, J., Henderson, D., Edwards, M., & Holmes, J. (2010). *Housing damage in windstorms and mitigation for Australia.*

Giraud, G., Isaac, F., Bovari, E., & Zatsepina, E. (2016). *Coping With The Collapse: A Stock-Flow Consistent, Monetary Macro-dynamics of Global Warming. AIEE Energy Symposium.*

Giuzio, M., Krušec, D., Levels, A., Melo, A. S., Mikkonen, K., Radulova, P., et al. (2019). *Climate change and financial stability. Financial Stability Review*, *1*.

Görgen, M., Jacob, A., Nerlinger, M., Riordan, R., Rohleder, M., & Wilkens, M. (2019). *Carbon risk. Available at SSRN 2930897.*

Gostlow, G. (2019). *Pricing climate risk. Available at SSRN 3501013.*

Gourdel, R., & Sydow, M. (2021). *Bi-layer stress contagion across investment funds: a climate application.*

Gray, W. M. (1975). *Tropical cyclone genesis. Atmospheric science paper; no. 234.*

Grippa, P., Mann, S. et al. (2020). *Climate-Related Stress Testing: Transition Risks in Norway.* International Monetary Fund.

Guha-Sapir, D., Below, R., & Hoyois, P. (2018). *EM-DAT: the CRED/OFDA international disaster database.*

Guo, Z., Zhang, X., Zheng, Y., & Rao, R. (2014). *Exploring the impacts of a carbon tax on the Chinese economy using a CGE model with a detailed disaggregation of energy sectors. Energy Economics*, *45*, 455–462.

Gurran, N., Norman, B., & Hamin, E. (2013). *Climate change adaptation in coastal Australia: an audit of planning practice. Ocean & coastal management*, *86*, 100–109.

Gurvich, A., & Creamer, G. G. (2021). *Carbon Risk Factor Framework. Available at SSRN 3901956.*

Gusain, A., Ghosh, S., & Karmakar, S. (2020). *Added value of CMIP6 over CMIP5 models in simulating Indian summer monsoon rainfall. Atmospheric Research*, *232*, 104680.

Hall, T. M., & Jewson, S. (2007). *Statistical modelling of North Atlantic tropical cyclone tracks. Tellus A: Dynamic Meteorology and Oceanography*, *59*(4), 486–498.

Hallegatte, S. (2008). *An adaptive regional input-output model and its application to the assessment of the economic cost of Katrina. Risk Analysis: An International Journal*, *28*(3), 779–799.

Hallegatte, S., Green, C., Nicholls, R. J., & Corfee-Morlot, J. (2013). *Future flood losses in major coastal cities. Nature climate change*, *3*(9), 802.

Hallegatte, S., Ranger, N., Mestre, O., Dumas, P., Corfee-Morlot, J., Herweijer, C., & Wood, R. M. (2011). *Assessing climate change impacts, sea level rise and storm surge risk in port cities: a case study on Copenhagen. Climatic change*, *104*(1), 113–137.

Hanemann, W. M. (2008). *What is the economic cost of climate change?*

Harper, B. (2002). *Tropical cyclone parameter estimation in the Australian Region. Systems Engineering Australia Pty Ltd for Woodside Energy Ltd, Perth*, *83*.

Harris, J. (2015). *The Carbon Risk Factor (EMI-'Efficient Minus Intensive'). Available at SSRN 2666757*.

Hart, G. (1976). *Estimation of structural damage due to tornadoes. Symposium on Tornadoes: Assessment of Knowledge and Implications for Man*, 645–65.

Helm, D., Hepburn, C., & Mash, R. (2003). *Credible carbon policy. Oxford Review of Economic Policy*, *19*(3), 438–450.

Hersbach, H., Bell, B., Berrisford, P., Hirahara, S., Horányi, A., Muñoz-Sabater, J., Nicolas, J., Peubey, C., Radu, R., Schepers, D., et al. (2020). *The ERA5 global reanalysis. Quarterly Journal of the Royal Meteorological Society*, *146*(730), 1999–2049.

Hilberink, B., & Rogers, L. C. (2002). *Optimal capital structure and endogenous default. Finance and Stochastics*, *6*(2), 237–263.

Hilscher, J., & Nosbusch, Y. (2010). *Determinants of sovereign risk: Macroeconomic fundamentals and the pricing of sovereign debt. Review of Finance*, *14*(2), 235–262.

Hinkel, J., & Klein, R. J. (2009). *Integrating knowledge to assess coastal vulnerability to sea-level rise: The development of the DIVA tool. Global Environmental Change*, *19*(3), 384–395.

Hoepner, A. G., Oikonomou, I., Sautner, Z., Starks, L. T., & Zhou, X. (2018). *ESG shareholder engagement and downside risk*.

Holland, G. J. (1997). *The maximum potential intensity of tropical cyclones. Journal of the atmospheric sciences*, *54*(21), 2519–2541.

Hong, H., Li, F. W., & Xu, J. (2019). *Climate risks and market efficiency. Journal of econometrics*, *208*(1), 265–281.

Hourcade, J. C., Frédéric, G., Grandjean, R., Lefèvre, J., Tankov, P., & Voisin, S. (2021). *Climate-economic scenarios and models: a reading guide for sustainable finance*.

Hourcade, J. C., Sassi, O., Crassous, R., Gitz, V., Waisman, H., & Guivarch, C. (2010). *IMACLIM-R: a modelling framework to simulate sustainable development pathways. International Journal of Global Environmental Issues*, *10*(1/2), 5–24.

Howard, A., & Patrascu, O. (2017). *Climate change : redefining the risks*. Schroders.

Huizinga, J., Moel, H. D., & Szewczyk, W. (2017). *Global flood depth-damage functions: Methodology and the database with guidelines*, (KJ-NA-28552-EN-N). https://doi.org/10.2760/16510

Huppmann, D., Kriegler, E., Krey, V., Riahi, K., Rogelj, J., Rose, S. K., Weyant, J., Bauer, N., Bertram, C., Bosetti, V., Calvin, K., Doelman, J., Drouet, L., Emmerling, J., Frank, S., Fujimori, S., Gernaat, D., Grubler, A., Guivarch, C., ... Zhang, R. (2018). *IAMC 1.5°C Scenario Explorer and Data hosted by IIASA*. https://doi.org/10.22022/SR15/08-2018.15429

Ilhan, E., Sautner, Z., & Vilkov, G. (2019). *Carbon Tail Risk. Available at SSRN 3204420.*

Ilhan, E., Sautner, Z., & Vilkov, G. (2021). *Carbon tail risk. The Review of Financial Studies*, *34*(3), 1540–1571.

In, S. Y., Park, K. Y., & Monk, A. H. (2018). *Is' Being Green'Rewarded in the Market?: An Empirical Investigation of Decarbonization and Stock Returns.*

Intergovernmental Panel on Climate Change. (2018). Global Warming Of 1.5° C: An IPCC Special Report On The Impacts Of Global Warming Of 1.5° C Above Pre-industrial Levels And Related Global Greenhouse Gas Emission Pathways, In The Context Of Strengthening The Global Response To The Threat Of Climate Change, Sustainable Development, And Efforts To Eradicate Poverty. Intergovernmental Panel on Climate Change.

James, M., & Mason, L. (2005). *Synthetic tropical cyclone database. Journal of waterway, port, coastal, and ocean engineering*, *131*(4), 181–192.

Jewell, J., & Cherp, A. (2020). *On the political feasibility of climate change mitigation pathways: Is it too late to keep warming below 1.5° C? Wiley Interdisciplinary Reviews: Climate Change*, *11*(1), e621.

Jien, J. Y., Gough, W. A., Butler, K., Cheng, V., & Arhonditsis, G. (2017). *Near-Time Sea Surface Temperature and Tropical Cyclone Intensity in the Eastern North Pacific Basin. Hurricanes and climate change* (pp. 55–89). Springer.

Jones, B., & O'Neill, B. C. (2020). *Global One-Eighth Degree Population Base Year and Projection Grids Based on the Shared Socioeconomic Pathways. Palisades*, (Revision 01).

Jones, B., & O'Neill, B. (2017). *Global Population Projection Grids Based on Shared Socioeconomic Pathways (SSPs), 2010-2100. Socioecon. Data Appl.*

Jongman, B., Ward, P. J., & Aerts, J. C. (2012). *Global exposure to river and coastal flooding: Long term trends and changes. Global Environmental Change*, *22*(4), 823–835.

Jung, H., Engle, R. F., & Berner, R. (2021). *Climate Stress Testing. FRB of New York Staff Report*, (977).

Jung, J., Herbohn, K., & Clarkson, P. (2018). *Carbon risk, carbon risk awareness and the cost of debt financing. Journal of Business Ethics*, *150*(4), 1151–1171.

Kaplan, J., & DeMaria, M. (1995). *A simple empirical model for predicting the decay of tropical cyclone winds after landfall. Journal of applied meteorology*, *34*(11), 2499–2512.

Karydas, C., & Xepapadeas, A. (2019). *Pricing climate change risks: CAPM with rare disasters and stochastic probabilities. CER-ETH Working Paper Series Working Paper*, *19*, 311.

Karydas, C., & Xepapadeas, A. (2021). *Climate change nancial risks: implications for asset pricing and interest rates.*

Keen, S., Lenton, T. M., Garrett, T. J., Rae, J. W., Hanley, B. P., & Grasselli, M. (2022). *Estimates of economic and environmental damages from tipping points cannot be reconciled with the scientific literature. Proceedings of the National Academy of Sciences*, *119*(21), e2117308119.

Kharin, V. V., Zwiers, F. W., Zhang, X., & Wehner, M. (2013). *Changes in temperature and precipitation extremes in the CMIP5 ensemble. Climatic change*, *119*(2), 345–357.

Klusak, P., Agarwala, M., Burke, M., Kraemer, M., & Mohaddes, K. (2021). *Rising Temperatures, Falling Ratings: The Effect of Climate Change on Sovereign Creditworthiness.* Faculty of Economics, University of Cambridge.

Knapp, K. R., Kruk, M. C., Levinson, D. H., Diamond, H. J., & Neumann, C. J. (2010). *The international best track archive for climate stewardship (IBTrACS) unifying tropical cyclone data. Bulletin of the American Meteorological Society*, *91*(3), 363–376.

Knutson, T., Camargo, S. J., Chan, J. C., Emanuel, K., Ho, C.-H., Kossin, J., Mohapatra, M., Satoh, M., Sugi, M., Walsh, K., et al. (2020). *Tropical cyclones and climate change assessment: Part II: Projected response to anthropogenic warming. Bulletin of the American Meteorological Society*, *101*(3), E303–E322.

Knutson, T. R., McBride, J. L., Chan, J., Emanuel, K., Holland, G., Landsea, C., Held, I., Kossin, J. P., Srivastava, A., & Sugi, M. (2010). *Tropical cyclones and climate change. Nature geoscience*, *3*(3), 157–163.

Kohler, J., Grubb, M., Popp, D., & Edenhofer, O. (2006). *The transition to endogenous technical change in climate-economy models: a technical overview to the innovation modeling comparison project. The Energy Journal*, (Special Issue# 1).

Koks, E. E., Rozenberg, J., Zorn, C., Tariverdi, M., Vousdoukas, M., Fraser, S. A., Hall, J. W., & Hallegatte, S. (2019). *A global multi-hazard risk analysis of road and railway infrastructure assets. Road & Transport Research: A Journal of Australian and New Zealand Research and Practice*, *10*(2677).

Kossin, J. P. (2018). *A global slowdown of tropical-cyclone translation speed. Nature*, *558*(7708), 104–107.

Kossin, J. P., Emanuel, K. A., & Vecchi, G. A. (2014). *The poleward migration of the location of tropical cyclone maximum intensity. Nature*, *509*(7500), 349–352.

Kossin, J. P., Knapp, K. R., Olander, T. L., & Velden, C. S. (2020). *Global increase in major tropical cyclone exceedance probability over the past four decades. Proceedings of the National Academy of Sciences*, *117*(22), 11975–11980.

Kousky, C., Kunreuther, H., LaCour-Little, M., & Wachter, S. (2020). *Flood risk and the US housing market. Journal of Housing Research*, *29*(sup1), S3–S24.

Kriegler, E., O'Neill, B. C., Hallegatte, S., Kram, T., Lempert, R. J., Moss, R. H., & Wilbanks, T. (2012). *The need for and use of socio-economic scenarios for climate change analysis: a new approach based on shared socio-economic pathways. Global Environmental Change*, *22*(4), 807–822.

Kumar, L., & Taylor, S. (2015). *Exposure of coastal built assets in the South Pacific to climate risks. Nature Climate Change*, *5*(11), 992.

Lanfear, M. G., Lioui, A., & Siebert, M. G. (2019). *Market anomalies and disaster risk: Evidence from extreme weather events. Journal of Financial Markets*, *46*, 100477.

Le Guenedal, T., Drobinski, P., & Tankov, P. (2022). *Cyclone generation Algorithm including a THERmodynamic module for Integrated National damage Assessment (CATHERINA 1.0) compatible with Coupled Model Intercomparison Project (CMIP) climate data. Geoscientific Model Development*, *15*(21), 8001–8039. https://doi.org/10.5194/gmd-15-8001-2022

Le Guenedal, T. (2019a). *Economic Modeling of Climate Risks. Available at SSRN 3693661*.

Le Guenedal, T. (2019b). *Economic Modeling of Climate Risks. Amundi Working Paper*, *WP-83*.

Le Guenedal, T., Drobinski, P., & Tankov, P. (2021a). *Cyclone generation Algorithm including a THERmodynamic module for Integrated National damage Assessment (CATHERINA*

1.0) compatible with CMIP climate data. Geoscientific Model Development Discussions, 1–43.

Le Guenedal, T., Drobinski, P., & Tankov, P. (2021b). *Measuring and Pricing Cyclone-Related Physical Risk Under Changing Climate. Proceedings of Paris December 2021 Finance Meeting EUROFIDAI-ESSEC*.

Le Guenedal, T., Girault, J., Jouanneau, M., Lepetit, F., & Sekine, T. (2020). *Trajectory Monitoring in Portfolio Management and Issuer Intentionality Scoring. Available at SSRN 3630302*.

Le Guenedal, T., Lombard, F., Roncalli, T., & Sekine, T. (2022). *Net Zero Carbon Metrics. Available at SSRN 4033686*.

Le Guenedal, T., & Roncalli, T. (2022). *Portfolio Construction with Climate Risk Measures. Available at SSRN 3999971*.

Le Guenedal, T., & Tankov, P. (2022). *Corporate Debt Value under Transition Scenario Uncertainty. Available at SSRN 4152325*.

Leckebusch, G. C., Ulbrich, U., Fröhlich, L., & Pinto, J. G. (2007). *Property loss potentials for European midlatitude storms in a changing climate. Geophysical Research Letters*, *34*(5).

Lee, C.-Y., Tippett, M. K., Sobel, A. H., & Camargo, S. J. (2018). *An environmentally forced tropical cyclone hazard model. Journal of Advances in Modeling Earth Systems*, *10*(1), 223–241.

Leland, H. E. (1994). *Corporate debt value, bond covenants, and optimal capital structure. The journal of finance*, *49*(4), 1213–1252.

Leland, H. E., & Toft, K. B. (1996). *Optimal capital structure, endogenous bankruptcy, and the term structure of credit spreads. The Journal of Finance*, *51*(3), 987–1019.

Leontief, W. (1970). *Environmental repercussions and the economic structure: an input-output approach. The review of economics and statistics*, 262–271.

Lepetit, F., Cherief, A., Ly, Y., & Sekine, T. (2021). *Revisiting Quality Investing. Available at SSRN 3877161*.

Lepetit, F., Le Guenedal, T., Ben Slimane, M., Cherief, A., Mortier, V., Sekine, T., & Stagnol, L. (2021). *The Recent Performance of ESG Investing, the Covid-19 Catalyst and the Biden Effect. Available at SSRN 3946483*.

Linnerud, K., Mideksa, T. K., & Eskeland, G. S. (2011). *The impact of climate change on nuclear power supply. The Energy Journal*, *32*(1).

Lüthi, S. (2019). *Applying Machine Learning Methods to the Assessment of Tropical Cyclone Impacts. Master thesis, ETH Zurich*.

Mallucci, E. (2020). *Natural Disasters, Climate Change, and Sovereign Risk. International Finance Discussion Papers 1291*.

Mandel, A., Tiggeloven, T., Lincke, D., Koks, E., Ward, P., & Hinkel, J. (2021). *Risks on global financial stability induced by climate change: the case of flood risks. Climatic Change*, *166*(1), 1–24.

Mardones, C., & Mena, C. (2020). *Economic, environmental and distributive analysis of the taxes to global and local air pollutants in Chile. Journal of Cleaner Production*, *259*, 120893. https://doi.org/https://doi.org/10.1016/j.jclepro.2020.120893

Mardones, C., & Muñoz, T. (2018). *Environmental taxation for reducing greenhouse gases emissions in Chile: an input–output analysis. Environment, Development and Sustainability*, *20*(6), 2545–2563.

McGranahan, G., Balk, D., & Anderson, B. (2007). *The rising tide: assessing the risks of climate change and human settlements in low elevation coastal zones. Environment and urbanization*, *19*(1), 17–37.

McKee, T. B., Doesken, N. J., Kleist, J., et al. (1993). *The relationship of drought frequency and duration to time scales. Proceedings of the 8th Conference on Applied Climatology*, *17*(22), 179–183.

Meehl, G. A., Senior, C. A., Eyring, V., Flato, G., Lamarque, J.-F., Stouffer, R. J., Taylor, K. E., & Schlund, M. (2020). *Context for interpreting equilibrium climate sensitivity and transient climate response from the CMIP6 Earth system models. Science Advances*, *6*(26), eaba1981.

Meijer, J. R., Huijbregts, M. A., Schotten, K. C., & Schipper, A. M. (2018). *Global patterns of current and future road infrastructure. Environmental Research Letters*, *13*(6), 064006.

Mendelsohn, R., Emanuel, K., Chonabayashi, S., & Bakkensen, L. (2012). *The impact of climate change on global tropical cyclone damage. Nature climate change*, *2*(3), 205–209.

Merrill, R. T. (1987). An Experiment In Statistical Prediction Of Tropical Cyclone Intensity Change. US Department of Commerce, National Oceanic; Atmospheric Administration.

Merton, R. C. (1974). *On the pricing of corporate debt: The risk structure of interest rates. The Journal of finance*, *29*(2), 449–470.

Merz, B., Blöschl, G., Vorogushyn, S., Dottori, F., Aerts, J. C., Bates, P., Bertola, M., Kemter, M., Kreibich, H., Lall, U., et al. (2021). *Causes, impacts and patterns of disastrous river floods. Nature Reviews Earth & Environment*, *2*(9), 592–609.

Merz, B., Kreibich, H., Schwarze, R., & Thieken, A. (2010). *Review article" Assessment of economic flood damage". Natural Hazards and Earth System Sciences*, *10*(8), 1697–1724.

Michelangeli, P.-A., Vrac, M., & Loukos, H. (2009). *Probabilistic downscaling approaches: Application to wind cumulative distribution functions. Geophysical Research Letters*, *36*(11).

Monasterolo, I., Roventini, A., & Foxon, T. J. (2019). *Uncertainty of climate policies and implications for economics and finance: An evolutionary economics approach. Ecological Economics*, *163*, 177–182.

Monnin, P. (2018). *Integrating climate risks into credit risk assessment - current methodologies and the case of central banks corporate bond purchases.* Council on Economic Policies.

Morana, C., & Sbrana, G. (2019). *Climate change implications for the catastrophe bonds market: An empirical analysis. Economic Modelling*, *81*, 274–294.

Muñoz-Zamponi, T. B., & Mardones-Poblete, C. A. (2016). *Simulation of a CO2 e tax to mitigate impacts from Chilean agriculture and livestock sector on climate change. Agrociencia*, *50*(3), 271–285. http://www.scielo.org.mx/scielo.php?script=sci_abstract&pid=S1405-31952016000300271&lng=es&nrm=iso&tlng=en

Naqvi, A., & Monasterolo, I. (2021). *Assessing the cascading impacts of natural disasters in a multi-layer behavioral network framework. Scientific reports*, *11*(1), 1–14.

Navarro-Racines, C., Tarapues, J., Thornton, P., Jarvis, A., & Ramirez-Villegas, J. (2020). *High-resolution and bias-corrected CMIP5 projections for climate change impact assessments. Scientific data*, *7*(1), 1–14.

Nemet, G. F., Braden, P., Cubero, E., & Rimal, B. (2014). *Four decades of multiyear targets in energy policy: aspirations or credible commitments? Wiley Interdisciplinary Reviews: Energy and Environment*, *3*(5), 522–533.

Nemry, F., Demirel, H. et al. (2012). *Impacts of Climate Change on Transport: A focus on road and rail transport infrastructures. European Commission, Joint Research Centre (JRC), Institute for Prospective Technological Studies (IPTS)*.

Neu, U., Akperov, M. G., Bellenbaum, N., Benestad, R., Blender, R., Caballero, R., Cocozza, A., Dacre, H. F., Feng, Y., Fraedrich, K., et al. (2013). *IMILAST: A community effort to intercompare extratropical cyclone detection and tracking algorithms. Bulletin of the American Meteorological Society*, *94*(4), 529–547.

Neumann, B., Vafeidis, A. T., Zimmermann, J., & Nicholls, R. J. (2015). *Future coastal population growth and exposure to sea-level rise and coastal flooding-a global assessment. PloS one*, *10*(3), e0118571.

NGFS. (2018). *NGFS, First Progress Report*. Network for Greening the Financial System.

Nguyen, Q., Diaz-Rainey, I., Kuruppuarachchi, D., McCarten, M., & Tan, E. K. (2020). *Climate Transition Risk in US Loan Portfolios: Are All Banks the Same? Available at SSRN 3766592*.

Niu, G.-Y., Yang, Z.-L., Mitchell, K. E., Chen, F., Ek, M. B., Barlage, M., Kumar, A., Manning, K., Niyogi, D., Rosero, E., et al. (2011). *The community Noah land surface model with multiparameterization options (Noah-MP): 1. Model description and evaluation with local-scale measurements. Journal of Geophysical Research: Atmospheres*, *116*(D12).

Nordhaus, W. (1993). *Optimal greenhouse-gas reductions and tax policy in the "DICE" model. The American Economic Review*, *83*(2), 313–317.

Nordhaus, W. (2018a). *Evolution of modeling of the economics of global warming: changes in the DICE model, 1992–2017. Climatic change*, *148*(4), 623–640.

Nordhaus, W. (2018b). *Projections and uncertainties about climate change in an era of minimal climate policies. American economic journal: economic policy*, *10*(3), 333–60.

Nordhaus, W. D. et al. (1992). *The'dice' model: Background and structure of a dynamic integrated climate-economy model of the economics of global warming*. Cowles Foundation for Research in Economics, Yale University.

Novy-Marx, R. (2013). *The other side of value: The gross profitability premium. Journal of financial economics*, *108*(1), 1–28.

Noy, I. (2016). *The socio-economics of cyclones. Nature Climate Change*, *6*(4), 343–345.

OCDE. (2018). Effective Carbon Rates 2018. https://doi.org/https://doi.org/https://doi.org/10.1787/9789264305304-en

Oestreich, A. M., & Tsiakas, I. (2015). *Carbon emissions and stock returns: Evidence from the EU Emissions Trading Scheme. Journal of Banking & Finance*, *58*, 294–308.

O'Neill, B. C., Kriegler, E., Ebi, K. L., Kemp-Benedict, E., Riahi, K., Rothman, D. S., van Ruijven, B. J., van Vuuren, D. P., Birkmann, J., Kok, K., et al. (2017). *The roads ahead: Narratives for shared socioeconomic pathways describing world futures in the 21st century. Global environmental change*, *42*, 169–180.

O'Neill, B. C., Kriegler, E., Riahi, K., Ebi, K. L., Hallegatte, S., Carter, T. R., Mathur, R., & van Vuuren, D. P. (2014). *A new scenario framework for climate change research: the concept of shared socioeconomic pathways. Climatic change*, *122*(3), 387–400.

Pachauri, R. K., Allen, M. R., Barros, V. R., Broome, J., Cramer, W., Christ, R., Church, J. A., Clarke, L., Dahe, Q., Dasgupta, P., et al. (2014). *Climate change 2014: synthesis report. Contribution of Working Groups I, II and III to the fifth assessment report of the Intergovernmental Panel on Climate Change*.

Palmowski, Z., Pérez, J. L., Surya, B. A., & Yamazaki, K. (2020). *The Leland–Toft optimal capital structure model under Poisson observations. Finance and Stochastics*, *24*(4), 1035–1082.

Pástor, L., Stambaugh, R. F., & Taylor, L. A. (2021). *Sustainable investing in equilibrium. Journal of Financial Economics*, *142*(2), 550–571.

Pedersen, L. H., Fitzgibbons, S., & Pomorski, L. (2021). *Responsible investing: The ESG-efficient frontier. Journal of Financial Economics*, *142*(2), 572–597.

Pérez-Zanón, N., Caron, L.-P., Terzago, S., Van Schaeybroeck, B., Lledó, L., Manubens, N., Roulin, E., Alvarez-Castro, M. C., Batté, L., Delgado-Torres, C., et al. (2021). *The CSTools (v4. 0) Toolbox: from Climate Forecasts to Climate Forecast Information. Geoscientific Model Development Discussions*, 1–32.

Petrakopoulou, F., Robinson, A., & Olmeda-Delgado, M. (2020). *Impact of climate change on fossil fuel power-plant efficiency and water use. Journal of Cleaner Production*, *273*, 122816.

Pielke Jr, R. A., Gratz, J., Landsea, C. W., Collins, D., Saunders, M. A., & Musulin, R. (2008). *Normalized hurricane damage in the United States: 1900–2005. Natural Hazards Review*, *9*(1), 29–42.

Pindyck, R. S. (2017). *The use and misuse of models for climate policy. Review of Environmental Economics and Policy*, *11*(1), 100–114.

Pineau, E., ESTRAN, R., & Delzant, L. (2022). *Sensibilité du risque de crédit au prix du carbone. Available at SSRN 4064036*.

Pita, G., Pinelli, J.-P., Gurley, K., & Mitrani-Reiser, J. (2015). *State of the art of hurricane vulnerability estimation methods: a review. Natural Hazards Review*, *16*(2), 04014022.

Postic, S., & Fetet, M. (2021). *Global carbon accounts in 2021*. I4CE Institute for Climate Economics.

Postic, S., & Métivier, C. (2019). *Global Carbon Account 2019*. Institute for Climate Economics, Paris.

Prahl, B. F., Boettle, M., Costa, L., Kropp, J. P., & Rybski, D. (2018). *Damage and protection cost curves for coastal floods within the 600 largest European cities. Scientific data*, *5*(1), 1–18.

Prahl, B. F., Rybski, D., Boettle, M., & Kropp, J. P. (2016). *Damage functions for climate-related hazards: unification and uncertainty analysis. Natural Hazards and Earth System Sciences*, *16*(5), 1189–1203.

Prahl, B. F., Rybski, D., Burghoff, O., & Kropp, J. P. (2015). *Comparison of storm damage functions and their performance. Nat. Hazards Earth Syst. Sci.*, *15*, 769–788.

Raimo, N., Caragnano, A., Zito, M., Vitolla, F., & Mariani, M. (2021). *Extending the benefits of ESG disclosure: The effect on the cost of debt financing. Corporate Social Responsibility and Environmental Management*, *28*(4), 1412–1421.

Ramaswamy, V., Schwarzkopf, M., Randel, W., Santer, B., Soden, B. J., & Stenchikov, G. (2006). *Anthropogenic and natural influences in the evolution of lower stratospheric cooling. Science*, *311*(5764), 1138–1141.

Ramstein, C., Dominioni, G., Ettehad, S., Lam, L., Quant, M., Zhang, J., Mark, L., Nierop, S., Berg, T., Leuschner, P., et al. (2019). State And Trends Of Carbon Pricing 2019. The World Bank.

Raymond, C., Horton, R. M., Zscheischler, J., Martius, O., AghaKouchak, A., Balch, J., Bowen, S. G., Camargo, S. J., Hess, J., Kornhuber, K., et al. (2020). *Understanding and managing connected extreme events. Nature climate change*, *10*(7), 611–621.

Reinders, H. J., Schoenmaker, D., & Van Dijk, M. A. (2020a). *A finance approach to climate stress testing. Available at SSRN 3573107.*

Reinders, H. J., Schoenmaker, D., & Van Dijk, M. A. (2020b). *A finance approach to climate stress testing.*

Riahi, K., Bertram, C., Huppmann, D., Rogelj, J., Bosetti, V., Cabardos, A.-M., Deppermann, A., Drouet, L., Frank, S., Fricko, O., et al. (2021). *Cost and attainability of meeting stringent climate targets without overshoot. Nature Climate Change*, *11*(12), 1063–1069.

Riahi, K., van Vuuren, D. P., Kriegler, E., Edmonds, J., O'Neill, B. C., Fujimori, S., Bauer, N., Calvin, K., Dellink, R., Fricko, O., Lutz, W., Popp, A., Cuaresma, J. C., KC, S., Leimbach, M., Jiang, L., Kram, T., Rao, S., Emmerling, J., ... Tavoni, M. (2017). *The Shared Socioeconomic Pathways and their energy, land use, and greenhouse gas emissions implications: An overview. Global Environmental Change*, *42*, 153–168. https://doi.org/10.1016/j.gloenvcha.2016.05.009

Rizzi, C. (2022). *Nature as a Defense from Disasters: Natural Capital and Municipal Bond Yields. Available at SSRN.*

Rogelj, J., Popp, A., Calvin, K. V., Luderer, G., Emmerling, J., Gernaat, D., Fujimori, S., Strefler, J., Hasegawa, T., Marangoni, G., et al. (2018). *Scenarios towards limiting global mean temperature increase below 1.5 C. Nature Climate Change*, *8*(4), 325.

Román, M. O., Wang, Z., Sun, Q., Kalb, V., Miller, S. D., Molthan, A., Schultz, L., Bell, J., Stokes, E. C., Pandey, B., et al. (2018). *NASA's Black Marble nighttime lights product suite. Remote Sensing of Environment*, *210*, 113–143.

Roncalli, T., Guenedal, T. L., Lepetit, F., Roncalli, T., & Sekine, T. (2020). *Measuring and Managing Carbon Risk in Investment Portfolios. arXiv preprint arXiv:2008.13198.*

Roncalli, T., Le Guenedal, T., Lepetit, F., Roncalli, T., & Sekine, T. (2021). *The Market Measure of Carbon Risk and its Impact on the Minimum Variance Portfolio. The Journal of Portfolio Management*, *47*(9), 54–68.

Roncoroni, A., Battiston, S., Escobar-Farfán, L. O., & Martinez-Jaramillo, S. (2021). *Climate risk and financial stability in the network of banks and investment funds. Journal of Financial Stability*, *54*, 100870.

Rozenberg, J., Espinet Alegre, X., Avner, P., Fox, C., Hallegatte, S., Koks, E., Rentschler, J., & Tariverdi, M. (2019). *From A Rocky Road to Smooth Sailing.*

Rozenberg, J., & Fay, M. (2019). Beyond The Gap: How Countries Can Afford The Infrastructure They Need While Protecting The Planet. World Bank Publications.

Rübbelke, D., & Vögele, S. (2011). *Impacts of climate change on European critical infrastructures: The case of the power sector. Environmental science & policy*, *14*(1), 53–63.

Sathaye, J., Dale, L., Larsen, P., Fitts, G., Koy, K., Lewis, S., & Lucena, A. (2012). *Estimating risk to California energy infrastructure from projected climate change.*

Scholtens, B., & van der Goot, F. (2014). *Carbon prices and firms' financial performance: an industry perspective. Carbon Management*, *5*(5-6), 491–505.

Schotten, G., van Ewijk, S., Regelink, M., Dicou, D., & Kakes, J. (2016). *Time for transition: An exploratory study of the transition to a carbon-neutral economy.* Netherlands Central Bank, Research Department.

Sharpe, W. F. (1964). *Capital asset prices: A theory of market equilibrium under conditions of risk. The journal of finance*, *19*(3), 425–442.

Sherwood, S. C., Ingram, W., Tsushima, Y., Satoh, M., Roberts, M., Vidale, P. L., & O'Gorman, P. A. (2010). *Relative humidity changes in a warmer climate. Journal of Geophysical Research: Atmospheres*, *115*(D9).

Siriwardana, M., Meng, S., & McNeill, J. (2011). *The impact of a carbon tax on the Australian economy: Results from a CGE model. Business, Economics and Public Policy Working Papers*, *2*.

Solomon, S., Manning, M., Marquis, M., Qin, D., et al. (2007). Climate Change 2007-the Physical Science Basis: Working Group I Contribution To The Fourth Assessment Report Of The IPCC. Cambridge university press.

Sosa, J., Sampson, C., Smith, A., Neal, J., & Bates, P. (2020). *A toolbox to quickly prepare flood inundation models for LISFLOOD-FP simulations. Environmental Modelling & Software*, *123*, 104561.

Stadler, K., Wood, R., Bulavskaya, T., Södersten, C.-J., Simas, M., Schmidt, S., Usubiaga, A., Acosta-Fernández, J., Kuenen, J., Bruckner, M., et al. (2018). *EXIOBASE 3: Developing a time series of detailed environmentally extended multi-regional input-output tables. Journal of Industrial Ecology*, *22*(3), 502–515.

Sutanudjaja, E. H., Van Beek, R., Wanders, N., Wada, Y., Bosmans, J. H., Drost, N., Van Der Ent, R. J., De Graaf, I. E., Hoch, J. M., De Jong, K., et al. (2018). *PCR-GLOBWB 2: a 5 arcmin global hydrological and water resources model. Geoscientific Model Development*, *11*(6), 2429–2453.

Swiss Re Group. (2020). *Ten Years After Katrina.*

Tabari, H. (2020). *Climate change impact on flood and extreme precipitation increases with water availability. Scientific reports*, *10*(1), 1–10.

Taleb, W., Le Guenedal, T., Lepetit, F., Mortier, V., Sekine, T., & Stagnol, L. (2020). *Corporate ESG news and the stock market. Available at SSRN 3723799.*

Tankov, P., & Tantet, A. (2019). *Climate data for physical risk assessment in finance. Available at SSRN 3480156.*

Taylor, K. E., Stouffer, R. J., & Meehl, G. A. (2012). *An overview of CMIP5 and the experiment design. Bulletin of the American meteorological Society*, *93*(4), 485–498.

TCFD. (2017). *The Use of Scenario Analysis in Disclosure of Climate-Related Risks and Opportunities.* Task Force on Climate-Related Financial Disclosures.

Thom, J., & Ralite, S. (2019). *Storm ahead, a proposal for a climate stress-test scenario*. 2° Investing Initiative.

Timmer, M. P., Dietzenbacher, E., Los, B., Stehrer, R., & De Vries, G. J. (2015). *An illustrated user guide to the world input–output database: the case of global automotive production. Review of International Economics*, *23*(3), 575–605.

Timmer, M. P., Erumban, A. A., Los, B., Stehrer, R., & De Vries, G. J. (2014). *Slicing up global value chains. Journal of economic perspectives*, *28*(2), 99–118.

Toivanen, J. (2008). *Numerical valuation of European and American options under Kou's jump-diffusion model. SIAM Journal on Scientific Computing*, *30*(4), 1949–1970.

Tol, R. S. (2018). *The economic impacts of climate change. Review of Environmental Economics and Policy*, *12*(1), 4–25.

Tsai, J., & Wachter, J. A. (2015). *Disaster risk and its implications for asset pricing. Annual Review of Financial Economics*, *7*, 219–252.

Unanwa, C., McDonald, J., Mehta, K., & Smith, D. (2000). *The development of wind damage bands for buildings. Journal of Wind Engineering and Industrial Aerodynamics*, *84*(1), 119–149.

UNEP. (2018). *The Emissions Gap Report 2018*. United Nations Environment Programme, Nairobi.

UNEP. (2019). *Changing Course. A comprehensive investor guide to scenario-based methods for climate risk assessment, in response to the TCFD*. UNEP Finance Initiative.

Van Der Knijff, J., Younis, J., & De Roo, A. (2010). *LISFLOOD: a GIS-based distributed model for river basin scale water balance and flood simulation. International Journal of Geographical Information Science*, *24*(2), 189–212.

Van Vliet, M. T., Yearsley, J. R., Ludwig, F., Vögele, S., Lettenmaier, D. P., & Kabat, P. (2012). *Vulnerability of US and European electricity supply to climate change. Nature Climate Change*, *2*(9), 676–681.

Vermeulen, R., Schets, E., Lohuis, M., Kolbl, B., Jansen, D.-J., Heeringa, W., et al. (2018a). *An energy transition risk stress test for the financial system of the Netherlands*. Netherlands Central Bank, Research Department.

Vermeulen, R., Schets, E., Lohuis, M., Kolbl, B., Jansen, D.-J., Heeringa, W., et al. (2018b). *An energy transition risk stress test for the financial system of the Netherlands*. Netherlands Central Bank, Research Department.

Vermeulen, R., Schets, E., Lohuis, M., Kölbl, B., Jansen, D.-J., & Heeringa, W. (2019). *The Heat is on: A framework measuring financial stress under disruptive energy transition scenarios*. Netherlands Central Bank, Research Department.

Vermeulen, R., Schets, E., Lohuis, M., Kölbl, B., Jansen, D.-J., & Heeringa, W. (2021). *The heat is on: A framework for measuring financial stress under disruptive energy transition scenarios. Ecological Economics*, *190*, 107205.

Verschuur, J., Koks, E., & Hall, J. (2020). *Port disruptions due to natural disasters: Insights into port and logistics resilience. Transportation research part D: transport and environment*, *85*, 102393.

Vicente Serrano, S., Begueria, S., & Lopez Moreno, J. (2010). *A multiscalar drought index sensitive to global warming: the standardized precipitation evapotranspiration index. Journal of climate*, *23*(7), 1696–1718.

Virot, E., Ponomarenko, A., Dehandschoewercker, É., Quéré, D., & Clanet, C. (2016). *Critical wind speed at which trees break. Physical Review E*, *93*(2), 023001.

Volz, U., Beirne, J., Ambrosio Preudhomme, N., Fenton, A., Mazzacurati, E., Renzhi, N., & Stampe, J. (2020). *Climate change and sovereign risk*.

Vousdoukas, M. I., Mentaschi, L., Voukouvalas, E., Bianchi, A., Dottori, F., & Feyen, L. (2018). *Climatic and socioeconomic controls of future coastal flood risk in Europe. Nature Climate Change*, *8*(9), 776–780.

Vrac, M., Drobinski, P., Merlo, A., Herrmann, M., Lavaysse, C., Li, L., & Somot, S. (2012). *Dynamical and statistical downscaling of the French Mediterranean climate: uncertainty assessment. Natural Hazards and Earth System Sciences*, *12*(9), 2769–2784.

Wachter, J. A. (2013). *Can time-varying risk of rare disasters explain aggregate stock market volatility? The Journal of Finance*, *68*(3), 987–1035.

Wang, Z., Wei, S.-J., & Zhu, K. (2013). *Quantifying international production sharing at the bilateral and sector levels*. National Bureau of Economic Research.

Weinkle, J., Landsea, C., Collins, D., Musulin, R., Crompton, R. P., Klotzbach, P. J., & Pielke, R. (2018). *Normalized hurricane damage in the continental United States 1900–2017. Nature Sustainability*, *1*(12), 808–813.

Weinkle, J., Maue, R., & Pielke Jr, R. (2012). *Historical global tropical cyclone landfalls. Journal of Climate*, *25*(13), 4729–4735.

Weitzman, M. L. (2009). *On modeling and interpreting the economics of catastrophic climate change. The review of economics and statistics*, *91*(1), 1–19.

Weitzman, M. L. (2010). *What Is The" Damages Function" For Global Warming—And What Difference Might It Make? Climate Change Economics*, *1*(01), 57–69.

Weitzman, M. L. (2012). *GHG targets as insurance against catastrophic climate damages. Journal of Public Economic Theory*, *14*(2), 221–244.

Weyzig, F., Kuepper, B., Van Gelder, J. W., & Van Tilburg, R. (2014). *The price of doing too little too late; the impact of the carbon bubble on the European financial system. Green New Deal Series*, *11*.

World Bank. (2018). *Building the World Bank's Wealth Accounts: Methods and Data*. https://development-data-hub-s3-public.s3.amazonaws.com/ddhfiles/94641/wealth-methodology-january-30-2018_4_0.pdf

World Bank. (2019a). *State and Trends of Carbon Pricing 2019*. World Bank Group, Washington DC.

World Bank. (2019b). *World Bank Open Data, available at*. https://data.%20worldbank.org/

Xie, J. (2000). *An environmentally extended social accounting matrix. Environmental and Resource Economics*, *16*(4), 391–406.

Yang, Z.-L., Niu, G.-Y., Mitchell, K. E., Chen, F., Ek, M. B., Barlage, M., Longuevergne, L., Manning, K., Niyogi, D., Tewari, M., et al. (2011). *The community Noah land surface model with multiparameterization options (Noah-MP): 2. Evaluation over global river basins. Journal of Geophysical Research: Atmospheres*, *116*(D12).

Ye, M., Wu, J., Liu, W., He, X., & Wang, C. (2020). *Dependence of tropical cyclone damage on maximum wind speed and socioeconomic factors. Environmental Research Letters*, *15*(9), 094061.

Zerbib, O. D. (2019). *The effect of pro-environmental preferences on bond prices: Evidence from green bonds. Journal of Banking & Finance*, *98*, 39–60.

Zhang, R. L. (2021). ESG And Cost Of Debt. Stanford University.

Zhang, Y.-X., Chao, Q.-C., Zheng, Q.-H., & Huang, L. (2017). *The withdrawal of the US from the Paris Agreement and its impact on global climate change governance. Advances in Climate Change Research*, *8*(4), 213–219.

ECOLE
DOCTORALE
DE MATHEMATIQUES
HADAMARD

Titre : Modélisation financière des risques liés au changement climatique

Mots clés : Transition, risque de credit, risque physique, chaine d'approvisionnement, incertitude du scenario, changement climatique

Résumé : Ce projet de recherche est consacré à l'estimation des risques financiers liés au changement climatique. Au-delà des applications et des résultats quantitatifs, les chapitres de cette thèse ont pour principal objectif d'apporter des méthodologies générales utilisables par les praticiens. Le premier chapitre propose une méthode d'évaluation bottom-up du risque de transition adjointe aux modèles de risque classiques. Cette approche du risque opérationnel par les coûts engendrés par une taxe potentielle limite l'impact aux secteurs directement polluants, ce qui amène au deuxième chapitre, introduisant les tables d'entrée-sorties pour appréhender les effets indirects du risque de transition dans la chaîne d'approvisionnement. Ces approches offrent une structure statique permettant d'évaluer le risque dans un scénario donné, mais pas de déterminer le prix des obligations en considérant des scénarios hétérogènes et leur probabilité de réalisation. Pour ce faire, le troisième chapitre propose un modèle de pricing intégrant une approche bayésienne dans la mise à jours des probabilités de scénarios sur la base des sauts observés dans les mécanismes de tarification du carbone. Enfin, le dernier chapitre propose une méthodologie Monte-Carlo de simulation de dommages annuels causées par des cyclones tropicaux. La conversion des données climatiques brutes en base de données synthétique de sinistres est réalisée en couplant des relations statistiques et thermodynamiques. L'exposition des actifs physiques, les dynamiques des facteurs socio-économiques, les densités de populations locales et les vulnérabilités spécifiques aux différentes régions du monde sont empruntés à différents segments de la littérature. Ils sont combinés afin d'obtenir un modèle complet du triptyque classique nécessaire à l'étude des risques physiques : *intensité* x *exposition* x *vulnérabilité* généralisable et homogène sur l'ensemble des pays. Le signal résultant peut ensuite être inclus simplement dans des modèles de risque de crédit assimilant les dommages annualisés à de la dette additionnelle.

Title : Financial modeling of climate-related risks

Keywords : Transition risk, Credit risk, Physical risk, supply-chain, scenario uncertainty, climate change

Abstract : This research project aims at estimating financial risks related to climate change. Beyond the applications and quantitative findings, the main objective of the chapters of this thesis is to provide a structural and methodological framework that is generalizable, in order to facilitate their integration by practitioners. The first chapter proposes a bottom-up measure of transition risk, which can be incorporated with classical risk models (Merton or credit risk model). This *cost-based* approach is limited to the directly polluting sectors, which leads to the second chapter, which allows for the diffusion of transition risk through the value chain. These approaches offer a static structure that allows for a fixed scenario stress-test but not for pricing the bonds by considering heterogeneous scenarios and the probability of realization. To this end, chapter three proposes a pricing model that integrates a Bayesian approach in updating scenario probabilities based on observed jumps in carbon pricing mechanisms. Finally, the last chapter proposes a Monte-Carlo methodology for simulating annual damages caused by tropical cyclones. The conversion of raw climatic data into a synthetic database of losses is achieved by coupling statistical and thermodynamic relationships. The exposure of physical assets, the dynamics of socio-economic factors, local population densities and specific vulnerabilities in different regions of the world are borrowed from different segments of the literature, and combined to obtain a complete model of the classical triptych necessary for the study of physical hazards: hazard intensity x exposure x vulnerability generalizable and homogeneous across countries. The resulting signal can then be simply included in credit risk models equating annualized damages with additional debt.

Institut Polytechnique de Paris
91120 Palaiseau, France